

**A DESIGN APPROACH FOR RC PANELS (SHELLS) IN INDUSTRIAL  
FACILITIES BASED ON THE ACI CODES**

by

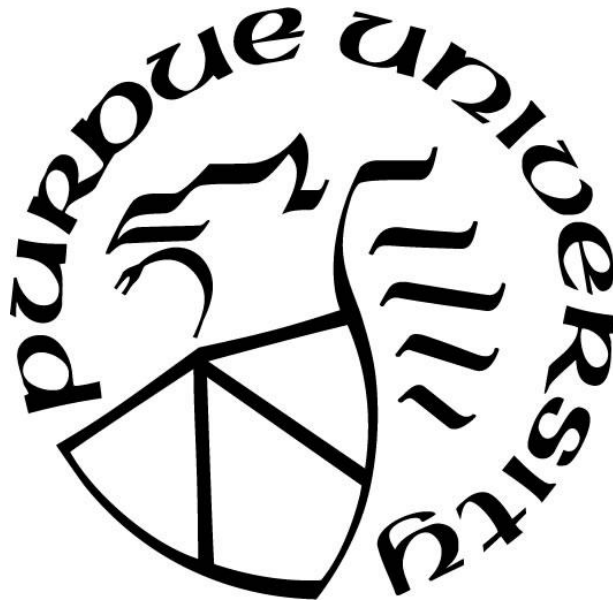
**Carlos Alberto Madera Sierra**

**A Dissertation**

*Submitted to the Faculty of Purdue University*

*In Partial Fulfillment of the Requirements for the degree of*

**Doctor of Philosophy**



Lyles School of Civil Engineering

West Lafayette, Indiana

December 2020

**THE PURDUE UNIVERSITY GRADUATE SCHOOL**  
**STATEMENT OF COMMITTEE APPROVAL**

**Dr. Amit Varma, Chair**

Lyles School of Civil Engineering

**Dr. Ayhan Irfanoglu**

Lyles School of Civil Engineering

**Dr. Arun Prakash**

Lyles School of Civil Engineering

**Dr. Samy Tindel**

Department of Mathematics

**Approved by:**

Dr. Dulcy Abraham

*Dedicated to the God of my salvation.*

## ACKNOWLEDGMENTS

To my **God** and Father in heaven, to **Jesus Christ** my Lord and savior, and to the **Holy Spirit** my helper who has always been faithful to me and my family. He is the one who *trains my hands for battle; my arms can bend a bow of bronze*. He is the one who *goes before me and levels the mountains: I will break down gates of bronze and cut through bars of Iron*. Because although all the doors were closed for almost 1 year, He opened a door for me that never was closed again; and because He moved the hearts of the people into my favor. *I love you God with all my heart*.

To my wife **Stephany** who was my companion even during the most difficult moments when we did not see any hope while pursuing this goal and everything seemed lost. Because she had the courage to come here, and more importantly to stay with me during this long and challenging journey. *I love you, and I always will*. Her love and care were an essential source of courage and strength to wake up every day and keep walking. She supported me and took care of my kids so I could focus on this much less important matter. Our **God** continues blessing us.

To my kids, **Juan-Jo and Daniel**, who gave me the necessary happiness to momentarily forget the difficulties and recharge my mind and my soul to continue fighting. Juan-Jo was there when everything looked fine, and then everything turned dark; then, Daniel came, and with him, God took darkness away. To my sister **Ingrid**, who always believed in me as well and supported me from a distance. To my dad **Alberto**, with whom I had the chance to get closer to in this far land. Finally, to my mom **Elizabeth**, who in 2016 departed to the Lord's presence, and who always believed in me, encouraged me to pursue not only this goal, but also every goal in my life. With her prayers and intercessions, I know the Lord was moved to help me and smoothed my path.

To my advisor **Amit Varma**, who was the only one willing to give me a shot again here at Purdue. He was one of the few professors who did not shut the door immediately without listening my history first. Professor Varma showed me how it is possible to be one of the best in academia without forgetting how to be an easy going, humble and a fair person. With his support, I regained confidence in myself when I had almost none. He helped me to exploit the best of my knowledge, and to put it into practice. Thanks a lot, professor.

To my friends and brothers in West Lafayette Christian Church, who always supported me and my family in this country and made us feel at home. Jason and Kristy, Shae and Evans, Lonnie and Jen, thanks for every weekend and for every trip you gave us. For letting me, my wife, and my kids have fun at your places, we won't forget. To Pastor John and Drew, who supported me with their prayers and advice. To all the elders in the Church who beyond the prayers, at some point were willing to support me financially; and although it was not necessary because God took care of that, it meant a lot to me, and I came to realize the love you had for me and my family. Finally, a very, very special dedication to our and friends and brothers in faith, Chuck and Brandi Moeschberger who not only opened their hearts but also their home for us, allowing us to live with them during the crazy pandemic time. As the bible says, "*Do not forget to show hospitality to strangers, for by so doing some people have shown hospitality to angels without knowing it.*"

To other friends from Varma's team who I will always remember as Kadir, Saahas and Jungil who had the patience to teach me ABAQUS. Also, to give me the chance to share some adventures in Utah and in France, where I felt I was part of a first world class academic research team.

To these three governmental agencies: *Colciencias*, *Colfuturo* and the *Universidad del Valle*, who supported me financially during this challenging PhD. To Juan Diego Velasquez who took my case personally and helped me when I was running out of funding. To Professor John Haddock, Patrick Corner, and Richard Domonkos who gave me the chance to work in LTAP, where I learned more administrative related functions and who supported with funding for more about three years.

# TABLE OF CONTENTS

LIST OF TABLES .....	10
LIST OF FIGURES .....	12
ABSTRACT.....	16
1. INTRODUCTION .....	17
1.1 Statement.....	17
1.2 Motivation and Research Need.....	22
1.2.1 Development of the ACI-Panel-Based-Design-Approach (PACI).....	22
1.2.2 Exploration of the Eurocode “Sandwich” Model Approach (EC2) in industrial facilities.....	24
1.2.3 Development of numerical models of RC panels in Abaqus.....	24
1.3 Goal.....	27
1.4 Objectives .....	27
1.5 Hypothesis.....	28
2. LITERATURE REVIEW .....	29
2.1 The Eurocode “Sandwich Model” Approach (EC2).....	29
2.1.1 Historical Notes about the development of the Sandwich Models.....	29
2.1.2 General Description.....	31
2.1.3 Design Stage 1: Out-of-plane shear design/verification of the Inner Layer .....	34
2.1.4 Estimate the in-plane reinforcement for the outer layers, and the inner layer.....	40
2.2 Theoretical concepts for the non-linear analysis and modeling of RC members .....	49
2.2.1 Uniaxial Behavior of Concrete in Compression.....	49
2.2.2 Behavior of Concrete in Tension.....	50
2.2.3 Modeling of Steel Reinforcement.....	57
2.2.4 Basic concepts of plasticity for concrete materials.....	62
2.2.5 The modified Compression Field Theory.....	67
2.3 Software for the Non-linear analysis and modelling of RC members .....	70
2.3.1 Abaqus .....	70

2.3.2	Shell-2000.....	79
2.3.3	Membrane-2000.....	81
3.	THE ACI-BASED DESIGN PANEL APPROACH .....	82
3.1	General Description .....	82
3.1.1	Existing Design Recommendations.....	83
3.1.2	Additional Design Recommendations .....	84
3.2	Computation of the Transverse Shear Reinforcement (TSHR) if needed .....	85
3.3	Computation of the in-plane (longitudinal and/or Transverse) Reinforcement.....	88
3.3.1	Analysis for when N is in tension.....	89
3.3.2	Analysis for when N is in compression and less than or equal to $N_{bal}$ .....	93
3.4	Analysis for when N is in compression and greater than or equal to $N_{bal}$ .....	94
3.5	Analysis for when N is in compression and greater than or equal to $N_{bal}$ .....	95
3.6	Conceptual comparison between the EC2 and the PACI design Approaches .....	97
4.	METHODOLOGY .....	99
4.1	Development Phase.....	101
4.1.1	Development of the PACI design approach .....	101
4.1.2	Explanation and exploration of the Eurocode (EC2) design approach.....	101
4.1.3	Development of a spreadsheet for the estimation of the steel reinforcement.....	102
4.2	Validation Phase .....	102
4.2.1	Selected RC panel tests.....	103
4.2.2	Estimation of the reinforcement areas suggested by the PACI and the EC2 approaches. .....	103
4.2.3	Estimation of the Numerical capacities of the Panels .....	105
4.3	Implementation Phase.....	106
4.3.1	Selection of the Analytical data.....	106
4.3.2	Estimation of the Capacity-to-Demand ratios for the analytical data.....	106
5.	MODELING AND CALIBRATION OF THE EXPERIMENTAL DATA .....	108
5.1	Modeling and Calibration of the SE series panels .....	108
5.1.1	Description of the SE series panels tests .....	108
5.1.2	Modeling details of the SE series panel Tests .....	109

5.1.3	Calibrated or Adjusted Responses for the SE series panels .....	111
5.2	Modeling and Calibration of the SM series panels.....	112
5.2.1	Description of the SM series panels tests .....	112
5.2.2	Modeling details for the SM series panels.....	113
5.2.3	Adjusted Responses for the SM series panels .....	118
5.3	Analysis and results for the PV series panels. ....	120
5.3.1	Description of the PV series panels tests.....	120
5.3.2	Modeling details and calibration of the PV series panels.....	120
5.3.3	Calibrated or adjusted Responses for the PV series Panels.....	125
5.3.4	Modeling and Calibration of the F series panels Description of the F series panels tests .....	126
5.3.5	Modeling details and calibration of the F series panels tests.....	127
5.3.6	Adjusted or Calibrated numerical curves for the F-series panels .....	128
5.4	Modeling and calibration of the ML series panels.....	129
5.4.1	Description of the tests .....	129
5.4.2	Modeling details for the ML series panel.....	130
5.4.3	Calibrated or Adjusted Responses for the ML series panels .....	131
5.5	Modeling and Calibration of the SP series panels. ....	132
5.5.1	Description of the SP series panel Tests.....	132
5.5.2	Modeling details of the SP series panel Tests .....	133
5.5.3	Calibrated or adjusted responses for the SP series panels .....	136
6.	VALIDATION of the approaches by using EXPERIMENTal Data.....	139
6.1	Validation of results using Experimental data .....	139
6.1.1	Validation of results using the SE series panels .....	139
6.1.2	Validation of results using the SM series panels.....	145
6.1.3	Validation of results using the PV series panels.....	148
6.1.4	Validation of results using the F series panels.....	152
6.1.5	Validation of results using the ML series panels.....	155
6.1.6	Validation of results using the SP series panels .....	158
6.1.7	Summary of results for the experimental data. ....	163

7. IMPEMETATION OF THE DESIGN APPROACHES USING ANALYTICAL DATA.....	171
7.1 Description of the analytical data. ....	171
7.2 Estimation of the required reinforcement areas. ....	172
7.3 Modeling and non-linear analysis of the Analytical cases.....	173
7.4 Estimation of the numerical capacities of the panels.....	175
7.4.1 Numerical Capacity curves for the analytical cases .....	175
7.4.2 Comparison between the PACI and the EC2 numerical capacities .....	177
8. CONCLUSIONS .....	179
9. LIMITATIONS.....	190
10. FUTURE RESEARCH .....	193
11. REFERENCES.....	194
APPENDIX A. SPREADSHEET IN MATHCAD.....	202
PUBLICATIONS.....	221

## LIST OF TABLES

Table 3.1. Summary of Equations to obtain the required reinforcement areas in the PACI approach .....	96
Table 5.1. Material constitutive data for modeling of the SE series panels.....	110
Table 5.2. Material constitutive data for modeling of the SM1 and SM2 panels .....	115
Table 5.3. Material constitutive data for modeling of the SM3 panel using BFC model in Abaqus .....	117
Table 5.4. Material constitutive data for modeling of the PV series panels using the SMC model in Abaqus .....	124
Table 5.5. Material constitutive data for modeling of the F series panels in Shell 2000.....	128
Table 5.6. Material constitutive data for modeling of the ML series in Shell 2000 .....	131
Table 5.7. Material constitutive data for modeling of the SE series panels.....	134
Table 6.1. Comparison between the suggested reinforcement areas by the PACI and EC2 design approach, and against the reinforcement area provided in the experiment.....	140
Table 6.2. Comparison between the estimated numerical capacities, and the reported experimental capacities for the SE series panels .....	144
Table 6.3. Comparison between the suggested reinforcement areas by the PACI and EC2 design approach, and against the reinforcement area provided in the experiment.....	145
Table 6.4. Experimental reported capacities vs estimated numerical capacities .....	147
Table 6.5. Comparison between the suggested reinforcement areas by the PACI and EC2 design approach, and against the reinforcement area provided in the experiment.....	149
Table 6.6. Experimental reported capacities vs estimated numerical capacities for the PV series. ....	151
Table 6.7. Comparison between the suggested reinforcement areas by the PACI and EC2 design approach against the reinforcement area provided in the experiment. ....	152
Table 6.8. Experimental reported capacities vs estimated numerical capacities for the F series. ....	155
Table 6.9. Comparison between the suggested reinforcement areas by the PACI and EC2 design approach, and against the reinforcement area provided in the experiment.....	156
Table 6.10. Experimental reported capacities vs estimated numerical capacities. ....	158
Table 6.11. Comparison between the suggested reinforcement areas by the PACI and EC2 design approach, and against the reinforcement area provided in the experiment.....	159
Table 6.12. Experimental reported capacities vs estimated numerical capacities .....	163

Table 6.13. Experimental vs suggested reinforcement areas by the EC2 approach. ....	164
Table 6.14. Comparison between experimental vs estimated reinforcement areas suggested by the PACI design approach. ....	165
Table 6.15. Comparison between experimental and numerical capacities .....	169
Table 7.1. Required reinforcement areas suggested for both Analytical cases. ....	173
Table 7.2. Capacity-to Demand-Ratios (CDRs) for the analytical case 1. ....	177
Table 7.3. Capacity-to Demand-Ratios (CDRs) for the analytical case 2. ....	177

## LIST OF FIGURES

Figure 1.1. Example of a “Labyrinth” Industrial Facility and internal demands of RC shells.....	17
Figure 2.1. Design Stages in the Eurocode Sandwich Model Approach .....	32
Figure 2.2. Flowchart Design for the Eurocode Sandwich Model Approach.....	33
Figure 2.3. Variation and relationship between the external out-of-plane shear ( $vEd_x$ and $vEd_y$ ) and the principal out-of-plane shear ( $vEd_o$ ).....	35
Figure 2.4. Computation of the axial membrane Force over the outer Layers. ....	40
Figure 2.5. Computation of the in-plane shear membrane forces over the outer layers. ....	41
Figure 2.6. Assumption of the Unique Lever arm distance and Identification of the Reinforcement Curtains (or layers). ....	42
Figure 2.7. Determination of the principal stresses and principal angles. ....	44
Figure 2.8. Yield Surface 3D-view, represented in the Haigh-Westergaard space. Taken from Chen (1993).....	46
Figure 2.9. Representation of Ottosen Cracking criteria (or failure surface) for the PV series panels in the special bi-axial case .....	46
Figure 2.10. Orthonormal position of the Reinforcement Curtains in any of the faces.....	47
Figure 2.11. Hognestad parabola model for concrete in compression.....	50
Figure 2.12. Rotating vs Fixed Crack Model. Kupfer and Bulicek (1991) .....	52
Figure 2.13. Modified Stress vs strain of material constitutive models to account for the tension stiffening effect. (Taken from Eleneas et al 2006). ....	53
Figure 2.14. Comparison of Tension Softening curves for a 20 MPa compressive strength concrete. ....	54
Figure 2.15. Shima et al (1987) Tension Stiffening curve for a 2.0 MPa tensile strength concrete. ....	56
Figure 2.16. Variation of the stress along an embedded bar between two cracks. (taken from Belarbi and Hsu (1994).....	58
Figure 2.17. Models for “Naked” mild steel reinforcement bars.....	59
Figure 2.18. Models for “Embedded” mild steel reinforcement bars .....	60
Figure 2.19. Hydrostatic and Deviatoric part of the Stress tensor.Taken from Chen and Han (2007) .....	63
Figure 2.20. Hydrostatic and Deviatoric part of the Stress tensor. ....	64

Figure 2.21. Hardening Rules Representations in bi-dimensional stress. Taken from Chen and Han (2007).....	65
Figure 2.22. Biaxial and Triaxial state of Hardening with non-associated flow rule for concrete applications. ....	66
Figure 2.23. Average Stress of the concrete between two cracks and Average stress on a crack surface. Taken from Menin et al (2009) .....	68
Figure 2.24. Internal Forces and principal stresses. Taken from Menin et al (2009) .....	70
Figure 2.25. The Layer Composite Shell (LCS) SR4 finite element for the 2D Models in Abaqus. ....	72
Figure 2.26. The continuum C3D8R and the B31 finite elements for the 3D models in Abaqus.	73
Figure 2.27. The Durcker & Pragger flow rule on a Meridian plane of the yield surface.....	75
Figure 2.28. Definition of the Shear Retention according to power law in Abaqus.....	77
Figure 2.29. Approximate Yield surface used in the Smeared Crack Model in Abaqus .....	78
Figure 2.30. Input for the Loading combination in Shell-2000 .....	80
Figure 2.31. Input for the Loading combination in Shell-2000.....	81
Figure 3.1. Force Convention for the application of the “PACI” Design Approach. ....	82
Figure 3.2. Out-of-plane shears .....	86
Figure 3.3. Computation of the Balanced Force for a RC panel.....	88
Figure 3.4. Obtention of the In-plane axial and shear forces to be resisted by the reinforcement layer.....	90
Figure 4.1. Flowchart methodology.....	100
Figure 4.2. Loading Pattern for the Experimental data.....	103
Figure 4.3. Identification of the Reinforcement Curtains (or layers). ....	104
Figure 5.1. Loading Application Pattern and Reinforcement details for the SE series panels. ..	109
Figure 5.2. Modeling details for the SE7 panel .....	110
Figure 5.3. Comparison Between experimental and numerical load vs deformation curves for the SE series panels.....	111
Figure 5.4. Loading Application Pattern and Reinforcement details for the SM series Panels..	113
Figure 5.5. Modeling details for the SM2 panel. ....	114
Figure 5.6. Comparison Between experimental and numerical load vs deformation curves for the SM series panels. ....	119
Figure 5.7. Loading Application Pattern and Reinforcement details for the PV series panel. ....	120

Figure 5.8. Modeling details for the PV28 panel.....	122
Figure 5.9. Main Modeling Inputs in Membrane 2000 for the PV28 Panel .....	123
Figure 5.10. Comparison between experimental and numerical load vs deformation curves for the PV series panels. ....	125
Figure 5.11. Loading Application Pattern and Reinforcement details for the PV series panel. .	127
Figure 5.12. Example of general input data for the modeling of the F-series panels. ....	128
Figure 5.13. Comparison between experimental and numerical load vs deformation curves for the PV series panels .....	129
Figure 5.14. Loading application pattern and reinforcement detail for the F series panels.....	130
Figure 5.15. General input data for the modeling of the ML2 panel. ....	131
Figure 5.16. Comparison Between experimental and numerical load vs deformation curves for the ML series panels. ....	132
Figure 5.17. Loading application pattern and reinforcement details for the SE series panels....	133
Figure 5.18. Modeling details for the SP7 panel. ....	134
Figure 5.19. Comparison Between experimental and numerical load vs deformation curves for the SP series panels. ....	137
Figure 6.1. Comparison between experimental and numerical load vs deformation curves for the SE series panels.....	141
Figure 6.2. Comparison Between experimental and numerical load vs deformation curves for the SM series panels. ....	146
Figure 6.3. Comparison between experimental and numerical load vs deformation curves for the PV series panels. ....	150
Figure 6.4. Comparison between experimental and numerical load vs deformation curves for the F series panels. ....	154
Figure 6.5. Comparison Between experimental and numerical load vs deformation curves for the ML series panels. ....	157
Figure 6.6. Comparison Between experimental and numerical load vs deformation curves for the SP series panels.....	161
Figure 6.7. Comparison between the experimental provided in-plane reinforcement areas against the in-plane reinforcement areas suggested by the PACI and the EC2 approaches. ....	166
Figure 6.8. Comparison between the EC2 and the PACI Capacity-to-Demand Ratios for all the panels. ....	170
Figure 7.1. Analytical cases .....	172

Figure 7.2. Modeling details for analytical case 1. Reinforcement suggested by the PACI approach. .... 174

Figure 7.3. Modeling details for analytical case 2. Reinforcement suggested by the PACI approach. .... 174

Figure 7.4. PACI and EC2 Numerical Capacity curves for analytical case 1 ..... 175

Figure 7.5. PACI and EC2 Numerical Capacity curves for analytical case 2 ..... 176

## ABSTRACT

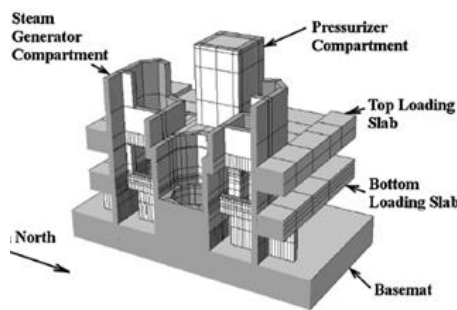
Currently, the design of Reinforced Concrete (RC) walled type structures such as RC containments in nuclear power plants (NPPs), offshore oil platforms, and other industrial facilities are designed following the Element-by-Element Level (ELD) technique. In this technique, the walls are not considered as single isolated units, and different portions (or sections) of the walls, which will be referred in this document as RC panels, need to be designed. As commonly accepted, the design demands of RC panels are a combination of in-plane and out-of-plane forces/moments, which interact simultaneously. The ACI 349 and the ACI 318.2-19, do not provide a clear design guideline for the design of RC panels, and for this reason, a new design approach based on the design concepts and formulations of these ACI codes will be proposed and developed in this thesis. The results of this ACI-Panel-Based-Design-Approach (PACI) will be verified by using experimental data of twenty-one RC panels subjected to different combinations of in-plane and out-of-plane forces. The results from the PACI approach –represented in the suggested reinforcement areas, and in the estimated nominal capacities of the panels resulting after introducing those suggested reinforcement areas into calibrated numerical models developed in Abaqus and/or Shell 2000– will be compared against the experimental results. These results will also be compared against the results of the more sophisticated “sandwich” model approach applicable for RC shells (or panels) proposed by the Eurocode. Finally, after designing a critical panel of a typical Steel Composite (SC) RP-1000 power plant, the applicability of the PACI design approach will be verified for use in industrial applications.

**Keywords:** RC panels, Industrial facilities, non-linear analysis, in-plane and out-of-plane forces interaction, ABAQUS.

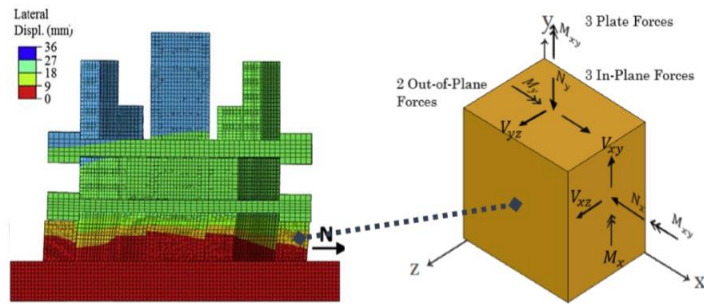
# 1. INTRODUCTION

## 1.1 Statement

Industrial facilities, such as nuclear power plants and offshore oil platforms among others, are characterized as having interconnected Reinforced Concrete (RC) walls forming a labyrinth shape as show in figure 1.1a. According to Coronado C. et al. (2014), the most accurate technique for the design of these facilities is known as the Element Level Technique with Membrane force Interaction (ELE-MFI). In this technique, the walls are not treated as single and/or isolated structural entities as usually done in conventional buildings. Instead, different sections (or portions) of the walls are designed according to the variations of the internal design demands (or stresses) displayed by a 2D or 3D finite element shell numerical model as shown in Figure 1.1b. In 2D or 3D models with shell elements, the internal design demands for the design of the panels is a set of eight internal demands which act simultaneously as shown in Figure 1.1b. These internal demands are classified as: three in-plane or membrane forces ( $N_x$ ,  $N_y$  and  $N_{xy}$ ); three out-of-plate forces or bending moments ( $M_x$ ,  $M_y$  and  $M_{xy}$ ); and two out-of-plate shear forces ( $v_{xz}$  and  $v_{yz}$ ). One of the virtues of the ELE-MFI technique is that it considers the interaction between the in-plane and the out-of-plate forces.



1.1a Example of a “Labyrinth” Industrial Facility.



1.1b Set of Internal design demand for RC panels or shells extracted from a 3D finite element model.

Figure 1.1. Example of a “Labyrinth” Industrial Facility and internal demands of RC shells

The American Concrete Institute (ACI) codes (the ACI-318.2-19 and the ACI-349) provide very clear design guidelines either for the design of “stick” reinforced concrete (RC) members

such as beam and columns or for RC walls in residential buildings. ***However, these codes do not provide a clear design guideline for RC shells or panels, in which the interaction between the in-plane and the out-of-plane forces must be considered.*** Even the ACI-349 code, which is devoted to the design of safety-related facilities in which the use of RC shells is more frequent than in conventional buildings, does not present an explicit design procedure for these types of elements. In fact, the first commentary of chapter 19 of the ACI-349 immediately refers to the ACI-318.2-19 code, which is devoted to the design of thin RC shells applicable in conventional buildings. In turn, the ACI-318.2-19 alludes to chapters 10 and 11 of the generic ACI 318-19 for the design of RC members subjected to bending moments and axial forces, and shear and torsion, respectively. In other words, both, the ACI 318.2 and the ACI 349 are dependent codes of the generic ACI 318-19 code. It must be stressed, however, that the design procedures in chapters 10 and 11 of the ACI 318-19 code are mainly intended for “stick” elements, which are subjected to no more than two or three internal demands, but not for shells, which are subjected to eight internal demands as previously explained. It is important to clarify that the ACI 318.2-19 used to be part of the generic ACI 318-19 codes until the ACI-318-11 version, and it was located in chapter 19. From the ACI 318-14 version onwards, the ACI committee removed this chapter and created the dependent ACI 318.2-19 code, which is devoted to the design of thin RC shells for conventional buildings.

Some previous researchers have also emphasized the need of a design guideline for RC shells in the American codes. For example, Coronado et al. (2009), who estimated the required reinforcement ratios for a heat sink reservoir tank in a nuclear facility by considering different seismic analysis and different design methods for RC walls, declared that the ACI-349 does not advise how to consider the interaction between the in-plane and the out-of-plane forces/moments during the design stage. Coronado et al (2009), explained the three more popular design methods followed by the designers used in the consulting field (in absence of a clear design guideline) for the design of RC walls.

- The first method is the *Standard Method*, which is the simpler but has two very coarse considerations. First, the walls are treated as global (or isolated) structural members disconnected from other walls, which is far from reality, especially in industrial facilities.

Second, only the in-plane axial and bending moment interaction (P-M) is considered, neglecting thus, the effect of the out-of-plane forces are during the design.

- The second is the *Element Level Design method* (ELM) in which the walls are not treated as global units as in the case for “stick” elements. In the ELM method, different sections (or portions) of the walls are designed using section cuts. In addition of the conventional P-M interaction, some interaction between the axial forces and the out-of-plate forces is considered.
- The third method, the *Element Level Design Method with Membrane force Interaction* (ELE-MFI) is deemed the most accurate because it considers all the internal force as displayed by the FEM similar to shells. Full interaction between the in-plane forces and the out-of-plane forces is considered in this method.

It is important to highlight that either due to ignorance, or for the sake of simplicity, there is an imminent risk of unsafe designs if the interaction between the in-plane and the out-of-plane forces is not considered during the design of the shells. According to Adebar and Collins (1994), disregarding the effect of the out-of-plane shear during the design of RC shells could lead either to conservative or unsafe results. Coronado et al. (2009), used the Shell-2000 software, which was developed by Bentz (2000), to estimate the required reinforcement areas in the that critical panel of the reservoir tank. The Shell-2000 software is based on the Modified Compression Field Theory (MCFT) proposed by Vecchio and Collins (1986). Bentz (2000) showed the capability of Shell-2000 by reproducing numerically the capacities (load vs deformation) curves of the RC panels tested by Kirschner (1986) and Kirschner and Collins (1986) and by Adebar and Collins (1994) as well. ***It must be highlighted that the reinforcement in Shell-2000 must be estimated by a trial and error process, until the set of the eight nominal capacities of the panels become equal to or greater than the eight internal demands.*** Shell-2000 will be extensively used in this thesis.

While Coronado et al. (2009) condemned the lack of a design approach for the design of RC walls in industrial facilities (in which if properly designed walls must be treated as shells) Rahimian (2017) did the same for the ACI 318-14. It is significant to recall that the procedure for the design of RC thin shells used to be included in the ACI-318-14 and previous versions. Starting from the ACI 318-19 version, the ACI committee removed the design procedure for RC thins shells from the generic ACI 318-14 and created the dependent ACI 318.2-19 code. This ACI 318.2-19

code, it is important to clarify, only deals with the design of RC thin shells. Rahimian (2017) said that the ACI-318-14, currently referring to the ACI 318.2-19, does not present any design criteria for the design of RC shells subjected to membrane actions. It is worthy to mention that a membrane element, which is subjected to only three internal in-plane forces, is a special case of a shell element. Rahimian (2017) developed a method to design RC membranes using the familiar concepts of the Modified Compression Field Theory (MCFT) proposed by Vecchio and Collins (1986) and the rotating angle field theory (RA-STM). The Rahimian method consists of building a capacity stress interaction diagram in function of the principal stresses ( $\sigma_1$  and  $\sigma_2$ ) of the panels. If the principal stress demand acting on the RC membrane element, represented by the two principal stresses remains inside this capacity principal stress diagram, the design will be considered satisfactory. This method, like the Shell-2000 software, requires of an initial guess of the amount of reinforcement in the panels in order to generate the capacity interaction diagram. ***Also, it is important to highlight that the Rahimiain method is only applicable for membrane elements, which are only subjected to in-plane forces, and not for shell elements which are subjected to in-plane and out-of-plane forces simultaneously.***

The British Standards Institution (2004) or Eurocode-2 (2004), contrary to the ACI codes, does provide a very complete design approach for the design of RC shells. This approach, known as the “Sandwich” model, follows a very rigorous design procedure based on mechanics and plasticity concepts of reinforced concrete. This sandwich model approach will be referred in this document as the EC2 design approach. One of the main features of the EC2 approach is that it considers the interaction between the in-plane and the out-of-plane forces for the estimation of the reinforcement of the panels. Nevertheless, such rigorous design procedure can be complicated, and therefore, difficult to implement at industrial level. Blaauwendraad (2010) used the experiments of Kirscher and Collins (1986) and Marti et al (1987) to validate the results of the EC2 approach with satisfactory results, ***although he also warned about its limitations.***

This thesis, therefore, will present a simplified approach (or guideline) for the design of RC shells which will be entirely based in the ACI 318.2-19 and the ACI 349 codes. This approach will be referred in here as the ACI-Panel-Based-Design (PACI) approach. The three main features of this PACI approach are:

1. It will meet the requirements for the estimation of steel reinforcement in RC shells stipulated in chapter 6 of the ACI 318.2-19, and in chapter 19 of the ACI 349 codes;
2. It will consider the interaction between the in-plane and the out-of-plane forces/moments similarly to the “sandwich” model approach proposed by the Eurocode-2, although in a more simplified way;
3. Contrary to the Rahimian method and to the Shell-2000 software as well, it will not require an initial guess (or assumption) of the amount of required reinforcement. Instead, it will directly compute the required reinforcement areas of the panels as a function of the internal design demands.

The PACI approach is intended for daily design applications in the consulting field. The results of the PACI approach will be validated by comparing them against experimental data and against the results of the more rigorous EC2 sandwich model approach. Specifically, the results to validate are: (a) the areas of reinforcement (or reinforcement ratios) suggested by the approach; and (b) the estimated numerical capacities of the panels after introducing those suggested reinforcement areas. These capacities are calculated using calibrated numerical models developed in Membrane-2000, Shell-2000 and/or Abaqus. In addition, the applicability of the PACI approach will be evaluated by designing a panel using actual design demands from a typical RP-1000 nuclear power plant model.

To provide an overall view of this research, this document has been organized into eight chapters as follows: Chapter 1 introduces the research along with its motivation and primary goals; chapter 2 provides the theoretical background of the research such the explanation of the EC2 sandwich model approach, and the theoretical development of the non-linear numerical models; chapter 3 is devoted to the development and explanation of the PACI design approach, which is the main intellectual contribution of this thesis; chapter 4 gives the methodology of this research, which explains how the main the goal and the objectives of this investigation were reached; chapter 5 deals with the simulation and calibration of the numerical models developed in Shell-2000, Membrane-2000 and Abaqus (Dassault Systemes Simulia Corp. 2013); chapter 6 focuses on the validation of the PACI approach against experimental data and the results of the EC2 design approach; chapter 7 is devoted to the application of the PACI and the EC2 design approaches in

industrial applications; and finally, chapter 8 summarizes the most important contributions and conclusions of this research.

## **1.2 Motivation and Research Need**

The motivation behind this research can be explained by highlighting the three main contributions associated with it:

(1) The development of a simplified yet safe design approach for RC panels based on the concepts and formulations of the ACI 349 and/or the ACI 318.2-19;

(2) The exploration of the more rigorous “Sandwich” model design approach for RC panels proposed by the Eurocode for industrial applications;

(3) The development and calibration of non-linear models of RC panels subjected to in-plane and out-of-plane demand forces in finite element analysis software (like Abaqus), which are limited in the literature.

### **1.2.1 Development of the ACI-Panel-Based-Design-Approach (PACI)**

The lack of a design approach for RC walls (or panels) in industrial facilities, usually produces non-optimal or conservative designs, which in turn, not only generate elevated and unnecessary costs, but also construction issues such as reinforcement congestion. The conservatism in these facilities can be demonstrated by both experimental evidence, and in-field-background evidence. Regarding experimental evidence, early, Farrar et al., (1993) confirms this conservatism by arguing that as a consequence of their heavy (massive) construction, RC walls in nuclear facilities typically have very large seismic capacities regarding its seismic demands. More recently, Prabir et al (2013) also confirmed this perception after analyzing the results from the CAMUS experiment in 1990 in which a five-story 1/3 scale RC shear building was subjected to near-field ground motions. Labbé et al. (2016) also pointed out the seismic margin design of squat walls, which have similar features to walls existing in nuclear facilities. They found that this margin in design is highly dependent of the frequency content of the signal; and they conclude that when the frequency content of the input is relatively higher than the natural frequency of the wall, the seismic margin increases.

With respect to in-field feedback, the conservatism in the design can also be corroborated with the good seismic performance of the TEPCO Kashiwazaki-Kariwa Nuclear plant in Japan. This nuclear facility only experienced minor cracks in the structural walls, even when the actual seismic demand (in terms of acceleration) was almost 5 times the expected acceleration design demands (IAEA 2011). Similarly, the apparent good performance of the Fukushima Daiichi Nuclear Power Plant, after the great East Japan Earthquake in 2010, also demonstrate this excess of conservatism. This same feedback of conservatism has been also experienced in the US. In 2011, the North Anna Power plant (VA) was struck by an earthquake that exceeded its design capacity. Despite this, the plant did not suffer structural damage. Reitenbach and Hylko (2015) stated that according to engineering analysis: “the structure could have withstood a quake well above that experienced”. It is also important to highlight that the lack of design guideline (or of a design approach) for RC panels might not only produce conservative but also un-conservative designs. Adebar and Collins (1994), referring to the design of RC shells in offshore platforms, stated for example that not considering the effect of the out-of-plane shear for the design of RC panels can lead either conservative or un-safe results.

Therefore, the statement of this project can be condensed to the following question: *Would it be possible to improve and optimize the design of RC panels in industrial facilities by developing a consistent design approach capable of accounting for the interaction between the in-plane and out-of-plane force demands, while remaining rooted in the ACI 349 and/or the ACI 318.2-19 concepts and formulations?* One way to tackle this problem, and a possible answer to the statement question, is to develop a more consistent and efficient design approach capable of accounting for the effects of simultaneous in-plane and out-of-plane forces on the capacity of the panels. The main contribution of this research project is the development of a design approach based on the ACI 349-13 and the ACI 318.2-19 assumptions and recommendations. This design approach will be named in this document as the American Concrete Institute Panel-Based-Design-Approach (PACI).

### **1.2.2 Exploration of the Eurocode “Sandwich” Model Approach (EC2) in industrial facilities.**

Another motivation of this research is to evaluate the safety of the EC2 sandwich model design approach when it is applied in industrial facilities. It must be mentioned that the EC2 design approach was developed for bridge applications and not for industrial facilities. In addition, being aware that applying the design methodology of this sandwich model can be difficult to implement in a day-to-day design basis; this thesis will develop an easy flow-chart design guideline, and provide explanations to help understand some concepts and assumptions behind the approach. This flow-chart will facilitate the implementation of the EC2 approach in the consulting field. The reliability of the PACI design approach will be compared against this more rigorous shell mechanics-based design approach proposed by the Eurocode, which will be referred in this document as the EC2 sandwich model approach. The results of this sandwich model approach, which applies cracking criteria, and accounts for the principal stresses and directions to estimate the in-plane reinforcement of the panels, will be taken as the reference values to validate the results the proposed PACI design approach.

The development of the PACI design approach and the exploration of the EC2 design approach will be useful to reduce the level of conservatism in the design of RC panels in industrial facilities, helping thus, to mitigate the environmental impact. Reduction in the consumption of concrete, as the primary material in industrial facilities, and steel reinforcement are vital in order to keep the competitiveness in the sector, and to mitigate the carbon dioxide (CO<sub>2</sub>) gas emission to the environment. According to Yazdani et al. (2017), concrete is the most utilized construction material and the second most consumed material after water. Yazdani et al. (2017) also states that by optimizing the design of RC structures, the environmental impact could be mitigated, and it will also promote environmental sustainability.

### **1.2.3 Development of numerical models of RC panels in Abaqus**

Finally, as an important activity to validate the simplified design approach, non-linear numerical models of RC panels will be developed in this thesis. Three software programs will be used for the development of the numerical models: Membrane-2000, Shell 2000 and Abaqus. Shell-2000 and Membrane-2000 are sectional analysis (not finite

element) software programs which have been widely implemented for the design and verification of RC shells. In contrast, there are limited studies using Abaqus for the modeling of RC panels. The numerical models are calibrated against experimental responses of RC tests panels subjected to in-plane and out-of-plane forces. These numerical models should be able to reproduce the capacity curves as well as to predict the damage progression and failure mode of the panels. The development of these calibrated numerical models will be essential to corroborate if the areas of reinforcement suggested by the PACI and the EC2 design approaches are enough to satisfy the corresponding design demands of the panels.

Abaqus has gained a lot of popularity for the modeling of RC members. Just in this last decade, several works devoted to the modeling of columns, beams, walls and slabs of reinforced concrete members can be found in the literature. For example, Charalambidi et al. (2012) analyzed the response of RC columns for different levels of confinement provided with FRP jacketing. Zeng (2017) also developed numerical models in Abaqus to analyze the response of RC columns with different levels of conventional transverse confinement. Xu and Zhang (2017) simulated the response of RC columns subjected to axial and cyclic lateral load proposing an axial-shear-flexural interaction scheme by which they successfully captured the pinching effect in the hysteresis loops during the test. Khani et al. (2018) also modeled the response of RC columns strengthened with Steel Fiber Reinforced Polymer (SFRP) but subjected to earthquake records.

Like for columns, there are also several studies focused on the modeling of RC beams in Abaqus. Ahmed (2014), for instance, simulated the response of RC beams subjected to impact loads. Demir et al (2016) modeled the non-linear static behavior (push over) of RC deep beams. Alrazi et al (2017) simulated the loading-unloading-reloading pattern for two flexural RC beams loaded at four points along its length. Emtiaz et al (2017), on the other hand, simulated the response of a typical slab-column connection in order to predict their seismic capacity and propose design recommendations. Regarding RC walls, Raseta et al (2018) performed a comparative analysis in the non-linear static response (or pushover) of RC walls using Abaqus and Open Sees. Gebreyohannes et al (2012) simulated the response of non-ductile RC walls with low reinforcement ratio with boundary elements. Li et al (2017) simulated the dynamic response in terms of peak accelerations and maximum displacement for different records of a three-story superimposed shear RC wall. Kezmane et al (2016) simulated the response of a RC squat wall

strengthened with FRP composite material. Finally, Sengupta and Li (2016), who developed seismic fragility curves for the assessment of light reinforced concrete walls, also used Abaqus to predict the hysteretic behavior of the walls.

As can be seen, at least to the best knowledge of the author of this thesis, there is not much research focused on the modeling of RC shells, or more specifically RC panels in Abaqus. Perhaps one of the few works involving RC panels is the recent research of Ren et al (2015), who tested six RC hybrid panels reinforced with CFRP tendons and uncoated steel tendons, subjected to quasi-static linear load applied along the panels. Ren et al (2015) modeled the experimental response of their panels (force vs displacement) also using the CDP model in Abaqus. Therefore, one of the main contributions of this research is the development of numerical models in Abaqus capable of reproducing and/or predicting the non-linear static response of RC panels subjected to different load combinations. Moreover, all the research briefly described had two features in common. First, all of them used 3D solid finite elements, and second, they only used the well-known Concrete Damage Plasticity (CDP) model. The numerical models in this research will be developed using Layers Composite Shell (LCS), instead of the conventional 3D solid models, in order to demonstrate their accuracy and efficiency in computational cost. In addition, not only the CDP concrete model will be explored in this thesis, but also the other concrete models available in Abaqus which are the Smeared Cracked (SMC) model, and the Brittle Failure Cracking (BFC) model.

In contrast to the small amount of research available in the literature devoted to the modeling of RC panels -especially in Abaqus- there is a significant amount of experimental work devoted to the testing of RC panels. Among those experimental research that will be analyzed in here, which will be vital for the fulfilment of the main goal of this thesis are: the research of Kirscher (1986) and Kirscher and Collins (1986), who tested RC subjected to in-plane shear and/or bending moment; the research of Vecchio and Collins (1982) who tested RC panels subjected to in-plane shear and in-plane tensile forces; the research of Polack and Vecchio (1994) who tested RC panels subjected to axial loads and out-of-plate bending moment; the research of Belarbi and Hsu (1995) who tested panels subjected to axial tension and compression forces; the research of Marti et al. (1987) who tested panels subjected to twisting moment only; and the research of Adebar (1989) and Adebar and Collins (1994) who tested RC panels subjected to the combined actions of out-of-

plate shear and its associated bending moments plus in-plane shear. These experimental works are crucial for the development of this thesis, and the modeling and calibration of the panels are one of the main objectives of this research. The calibration on the experimental response of these RC panels will be used to validate the results, not only of the PACI approach, but also of the EC2 approach. There has been other research that is worthy to mention such as Mansour and Hsu (2005) and Ohmori et al (1989) who tested RC panels subjected to cyclic in-plane shear, although they will not be included in the panels to analyze.

### **1.3 Goal**

The primary goal of this research is to develop a comprehensive design approach for reinforced concrete (RC) panels or walls (used in industrial facilities) that account for the fundamental behavior / mechanics of RC wall panels subjected to combined in-plane and out-of-plane forces / moments. This is a fundamental contribution because the current ACI codes do not include design approaches or methods that directly account for the fundamental behavior and effects of combined in-plane and out-of-plane forces. The design approach will be expressed in terms of the modifications to the traditional reinforced concrete design methods and approaches expressed in ACI 349, and used extensively in the United States and abroad, and therefore will be referred to in this study as the ACI-Panel-Based-Design Approach (PACI). The comprehensive design method / approach is expected to optimize the design of RC walls in safety-related nuclear facilities; however, this remains to be evaluated as part of the research.

### **1.4 Objectives**

To develop a comprehensive design approach for reinforced concrete (RC) wall panels subjected to combined in-plane (membrane) and out-of-plane (plate) forces/moment demands while accounting for fundamental behavior, mechanics, prior research, and the traditional RC design approaches (for individual force demands) provided in ACI 349. It will be referred to in this study as the ACI-Panel-Based -Design-Approach (PACI).

To validate the results of the PACI approach by analyzing experimental results from twenty-one RC panels tested under combine in-plane and out-of-plane forces. The results (in terms of amount of reinforcement) obtained by the PACI approach will be compared against those provided

during the experiment in order to evaluate the safety of the approach. The limitation of this verification is that in most tests the whole set of eight (8) (in-plane and out-of-plane) demand forces cannot be applied simultaneously because of set-up limitations.

To validate the results of the PACI design approach by comparing them against the results of a more “rigorous” design approach proposed by the Eurocode 2, which is referred to in this study as the Eurocode Design Approach (“EC2”). This comparison / evaluation will focus on the amount of reinforcement required in the RC wall panels, when subjected to membrane and plate forces. More optimized designs are expected from the “EC2” given the assumptions and design simplifications used in the PACI approach, which will be rooted in the traditional RC design approaches that are used for daily (regular) design in the industry.

To implement the PACI approach by using it in a more realistic design scenario using analytical data. Analytical data here refers to the estimated design demands (including combined in-plane and out-of-plane force / moment demands) obtained from the detailed finite element analysis of a real nuclear power plant model. These sets of combined demands will be obtained from the Design Control Document DCDs for NPPs (for example, AP1000(R), US-APWR(R), etc.) published in the public domain. In contrast to experimental data, this analytical data will provide the complete set of eight demands in wall panels. The RC wall panels (or simply panels) will be designed for those analytical demands following the PACI approach as well as the EC2 approach. In this case, since there is no experimental data to compare with, the safety of the approaches will be evaluated by conducting non-linear finite element analysis of those RC panels using numerical models and tools such as Abaqus and/or Shell-2000.

## **1.5 Hypothesis**

(1) A simple and safe design approach can be developed for RC wall panels subjected to combinations of in-plane and out-of-plane force/moment demands. (2) Such a design approach can be based on the current ACI design code principles and assumptions, while accounting for the fundamental behavior and mechanics of RC wall panels subjected to combinations of force demands. (3) The resulting design approach will be conservative with respect to results from representative experiments, numerical simulations, and more complex / comprehensive design approaches based on sandwich plate theory.

## 2. LITERATURE REVIEW

This chapter focuses in the literature review of this thesis. The literature review has been breaking down into three parts: a) the description and explanation of the Eurocode Sandwich model approach (EC2) for the design of the RC panels; b) the theory required for the modeling and non-linear analysis of the RC panels; and c) the description and limitations of the software utilized for the modelling of the RC panels, Abaqus, Shell-2000 and Membrane-2000.

### 2.1 The Eurocode “Sandwich Model” Approach (EC2)

Sandwich model approaches for RC panels are not new, and they have been proposed before over almost four decades ago. But before going into the history and development of the sandwich models, it is convenient to have a global description of the approach and at least to understand their basic assumptions. In the sandwich models, the RC panel is virtually divided in three layers: Two outer layers, (top and bottom layers), and one inner (or central) layer as shown in Figure 2.1. The main assumption for these models is that the outer layers will be only designed to resist membrane forces produced by the combined action of the in-plane forces and the plate forces (moments), while the inner layer will resist the out-of-plane shear forces only. Now, a brief history about the development of the sandwich model methods can be given.

#### 2.1.1 Historical Notes about the development of the Sandwich Models

One of the first sandwich models can be attributed to Gupta (1986). This model only considered the actions of the in-plane forces ( $n_x, n_y, n_{xy}$ ) and the plate forces ( $m_x, m_y$  and  $m_{xy}$ ), whereas the and the out-of-plane shear forces ( $v_{yz}, v_{yz}$ ) were left out. Some years later, Marti (1991) made possible the inclusion of these out-plane shears demands. Then, the work of Gupta (1986) and Marti (1991) were compiled into the MC90 (1993) -CEB-FIP model code 1990 for concrete structures- giving arising to the first standardized sandwich model procedure applicable for RC panels. In spite that the MC90 sandwich dealt with both, the in-plane and the out-of-plane forces, it had two remarkable two limitations: First, the model assumes an unique and averaged lever arm for all reinforcement layers inside the panel. Second, Blaauwendraad (2010) stated that when assembling the equilibrium equations, in order to estimate the required reinforcement areas, some

terms were missing -perhaps referring to the additional membrane forces that rises because of the presence of transverse shear reinforcement when provided-. Because of these two limitations, Blaauwendraad (2010) classified this model as basic sandwich model. Years later, the International Federation for structural concrete, fib (2008), in its bulletin 45, also proposed other sandwich model approach, capable of accounting with the additional membrane forces produced by the presence of transverse shear reinforcement. Nevertheless, the approximation of a unique and/or averaged lever arm between the reinforcement layers continued.

A more accurate three layer sandwich model was proposed by Lourenco and Figueiras (1993) and (1995). This model was considered by Blaauwendraad (2010) as an advanced three-layer sandwich model because the two limitations contained in the MC90 model, were considered and removed. In contrast to the MC90 sandwich model approach, the Lourenco and Figueiras model does not assume that the resultant internal forces in the concrete and in the reinforcement coincides, eliminating the assumption of an unique lever arm. After setting internal equilibriums equations the different lever arm distances are found through a iterative process, in which different cases for reinforcement placement are considered: a) Reinforcement required in both faces, top and bottom; b) reinforcement required in the top face only; c) reinforcement required in the bottom face only; and d) reinforcement not required in either of the two faces. Each case follows its own formulation to compute the amount of required reinforcement. Although finding in which case the RC panels falls requires of the iterative process, the first iteration is usually enough to reach this end. The detailed explanation about the implementation of this sandwich model is found in the work of Lourenco and Figueiras (1993).

Recently, the Eurocode (EN 1992-2:2005) also proposed a three-layer sandwich model. This sandwich model will be named in here as the EC2 design sandwich model approach. The EC2 approach is based on principal stress and cracking criteria. As an advantage of the EC2 approach regarding the Lourenco and Figueiras (1993) model, is that the EC2 approach does not required any iteration to find out in what faces (or layers) the panels require reinforcement or not. For this aim, the EC2 dictate if the layers require reinforcement by applying the cracking criteria based on plasticity theory for concrete materials. Blaauwendraad (2010), classified the EC2 sandwich model approach as basic sandwich model. However, it must be noticed that in this sandwich model, the designer defines the level of sophistication for the design by choosing either a single averaged

lever arm, or different lever arms for the typically four reinforcement layers. Similarly, this model also provides a procedure to estimate the additional membrane forces acting in the outer layers, when transverse shear reinforcement has been provided. In other words, the Eurocode Sandwich model could be classified either as basic or advanced, depending on the desired level of sophistication and/or accuracy required/preferred by the designer.

In this paper, it will be shown that even under the assumption of a unique lever arm for all reinforcement layers inside the panel, the Eurocode Sandwich Model provides very satisfactory results when compared against experimental data and after verifying with non-linear analysis. The authors believe that the implementation of this approach will help to reduce the currently existing high level in conservatism in the design of RC walls in industrial facilities. The conservatism, mainly represented in elevated and unnecessary reinforcement ratios in RC walls, is good from a safety perspective, but also haul problems such as congestion of reinforcement, and waste of economic resources. In the author's opinion, the Eurocode Sandwich model, despite its theoretical consistency and sophistication level, has not received been widely/fairly explored for industrial applications, include those non-safety related nuclear facilities. For this reason and being one of the main motivations of this paper, it intends to evaluate the suitability and accuracy of the Eurocode sandwich model for RC panels in industrial/nuclear facilities.

### **2.1.2 General Description**

The procedure of the Eurocode Design Approach (“EC2”) is described in the appendix LL of the Eurocode 2 (2005). As shown in figure 2.1, the EC2 approach is known as the “Sandwich Model”, because it divides the RC panel into three layers: the inner layer with thickness  $t_c$ , and two outer layers identified as the superior layer and the inferior layers with thicknesses  $t_s$  and  $t_i$ , respectively. A flowchart for the application of the EC2 design approach is provided in Figure 2.2. As shown in Figure 2.2, the design procedure can be described in two design stages: stage 1, in where the out-of-plane shear capacity of the inner layer is verified; and stage 2, in where the in-plane reinforcement for the outer layers, as wells as for the inner layer when apply, is estimated

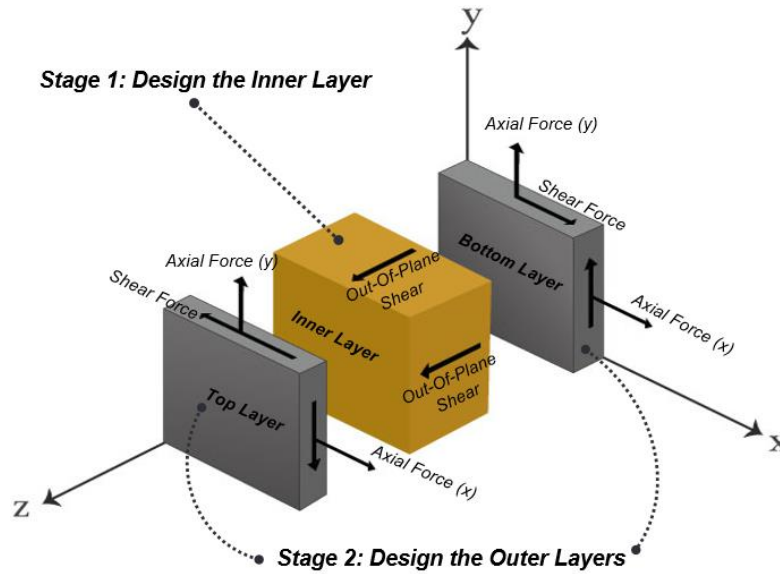


Figure 2.1. Design Stages in the Eurocode Sandwich Model Approach

The flowchart in Figure 2.2 shows the step-by-step procedure to complete the two design stages. In the first stage, the inner layer will be designed assuming that it will only resist the *out-of-plane shears* forces ( $v_{xz}$  and  $v_{yz}$ ). The main objective in this first stage consist in verify if the inner layer is capable to resist the maximum out-of-plane shear demand ( $v_{Edo}$ ) by only considering the contribution of the concrete. If the shear capacity of the inner layer, after only considering the contribution of the concrete is not enough to resist the out-of-plane shear demand, then (TSHR) needs to be provided. The procedure and explanation about how to estimate the required out-of-plane shear reinforcement will be given in detail later.

In the second stage, the two outer layers will be designed as *membrane elements*, assuming they will only resist *membrane* or in-plane forces. The in-plane forces are divided in *in-plane axial forces* and in *in-plane shear forces*, which result from the combined effect of the six remaining internal forces ( $n_{Edx}$ ,  $n_{Edy}$ ,  $n_{Edxy}$ ,  $m_{Edx}$ ,  $m_{Edy}$  and  $m_{Edxy}$ ). One of the main features of this EC2 sandwich model approach is the estimation of an effective thickness for the outer layers and for the inner layer. The estimation of the thicknesses layers follow an iterative process that will be described in detail in the next paragraphs. It is important to highlight that in that case where Transverse Shear Reinforcement (TSHR) is required for the inner layer, it will produce in-plane forces in the same inner layer, and therefore, it will have to be designed in the same way as the

outer layers. In other words, when TSHR have been required, the inner layer will probably also require in-plane reinforcement, just as the outer layers. An explanation for each design step in both design stages as shown in the flowchart in figure 2.2 will be given next.

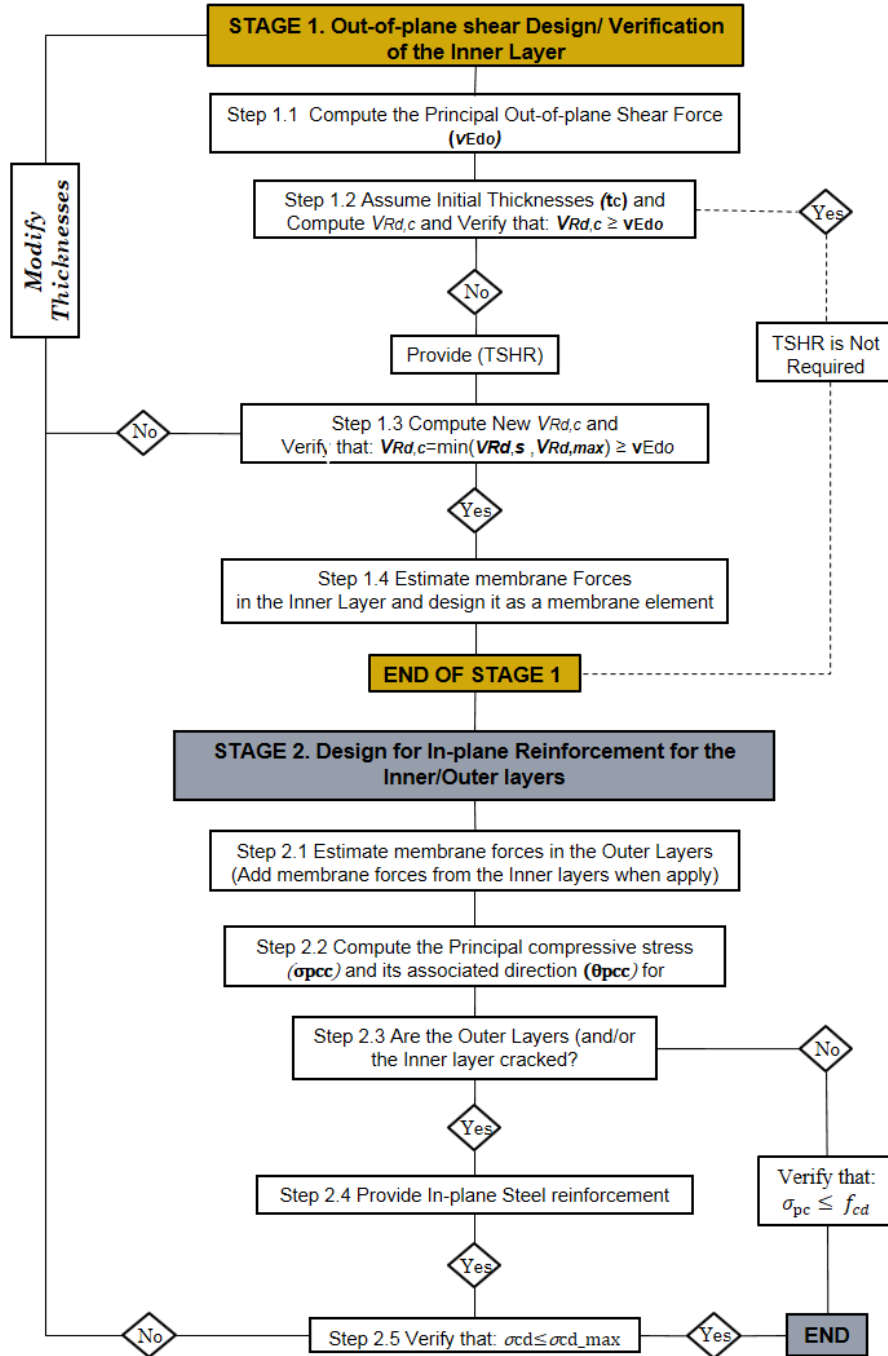


Figure 2.2. Flowchart Design for the Eurocode Sandwich Model Approach.

### 2.1.3 Design Stage 1: Out-of-plane shear design/verification of the Inner Layer

From the flowchart in Figure 2.2, it can be appreciated that the design of the inner layer can be completed in either two or four steps, depending on whether Transverse Shear Reinforcement (TSHR) is required or not. When the contribution of the concrete in the out-of-plane shear capacity of the panel ( $V_{R,dc}$ ), is equal to, or greater than the principal out-of-plane shear ( $v_{Edo}$ ), the design of the inner layer will be completed in just two steps (steps 1.1 through 1.2), because TSHR will not be required. On the contrary, if  $V_{R,dc}$  is less than the principal out-of-plane shear ( $v_{Edo}$ ), two additional steps (steps 1.3 and 1.4) are needed to complete the design of the inner layer since TSHR have been required.

#### *Step 1-1. Compute the Principal out-of-plane Shear Force ( $v_{Edo}$ )*

Although the computation of the  $v_{Edo}$  is very simple (if the designer is just limited to apply the formulas as they appear in the Eurocode), a detailed explanation about the assumptions and the procedure to compute it will be given in here. First, it is important to highlight that the  $v_{Edo}$  will be acting in a plane defined by the principal out-of-plane direction or angle ( $\varphi_o$ ), which can be given at any angle ( $\varphi$ ) that varies from 0 rad to  $\pi/2$  as shown in Figure 2.3a. In order to find the principal angle  $\varphi_o$ , at which the principal out-of-plane shear demand ( $v_{Edo}$ ) is associated, it is important to understand how the magnitudes of the normal and tangential out-of-plane shears  $v_{nz}$  and  $v_{tz}$ , respectively, vary as a function of the angle ( $\varphi$ ) and of the coordinated out-of-planes shear demands  $v_{Edx}$  and  $v_{Edy}$ . This variation can be investigated by doing equilibrium of the out-of-plane forces in the free diagram bodies in figures 2.3b and/or 2.3c. From the free body diagram in figure 3b, it can be seen that an internal out-of-plane shear ( $v_{nz}$ ) must appear to maintain equilibrium. This  $v_{nz}$  will be acting parallel to the plane that is perpendicular to the n-direction and along the z-axis ( $v_{nz}$ ). In the same way, from the free body diagram in figure 2.3c, it must be clear that an out-of-plane internal shear ( $v_{tz}$ ) must also appear in order to maintain equilibrium. This  $v_{tz}$  will be acting parallel to the plane that is perpendicular to the t-direction and along the z-axis. The variation between the internal out-of-plane shears  $v_{nz}$ , and  $v_{tz}$ , in function of  $v_{Edx}$ ,  $v_{Edy}$  and the angle  $\varphi$  are given in Equations 1 and 2, respectively.

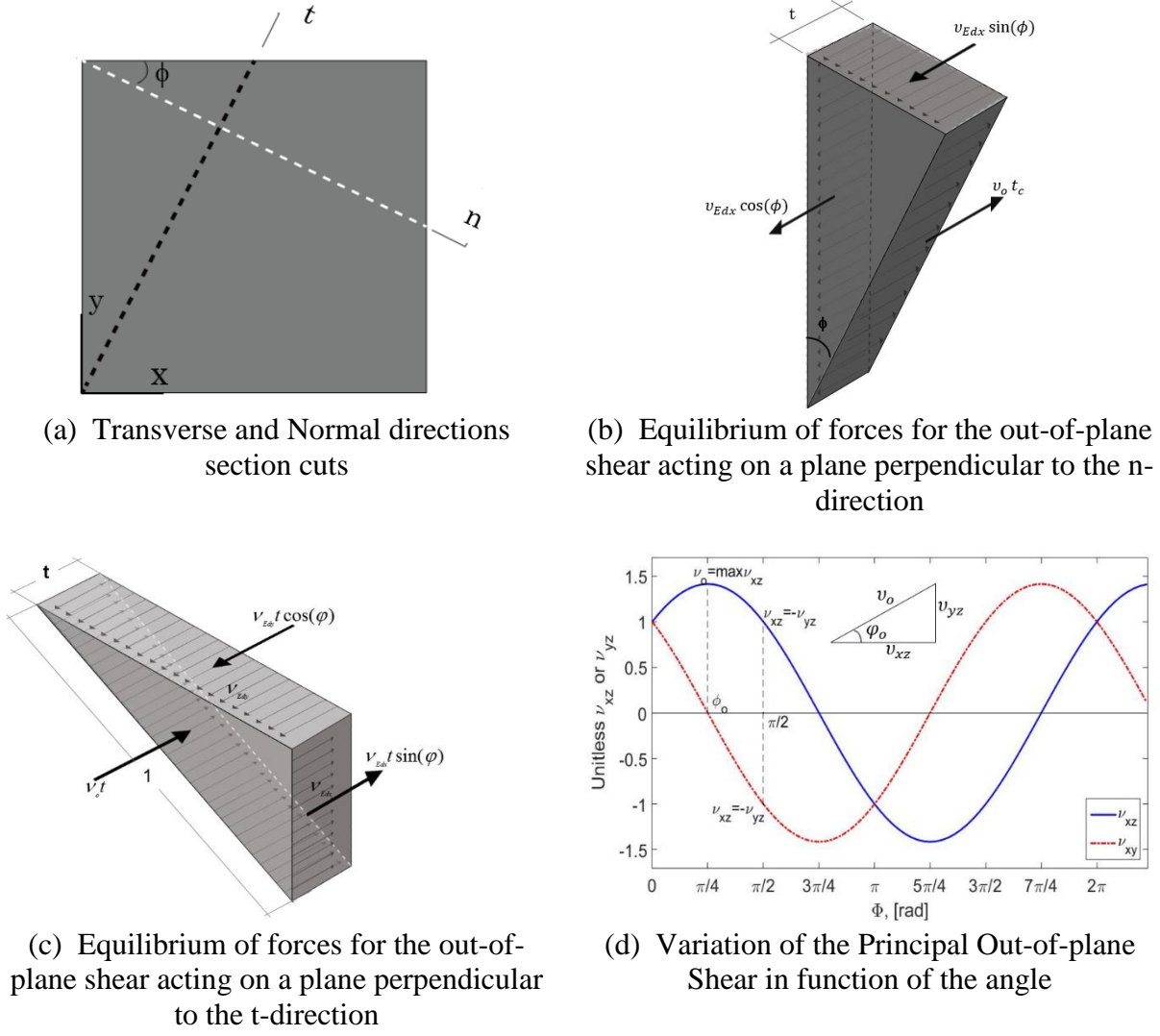


Figure 2.3. Variation and relationship between the external out-of-plane shear ( $v_{Edx}$  and  $v_{Edy}$ ) and the principal out-of-plane shear ( $v_{Edo}$ ).

The equilibrium for the out-of-plane forces in the panel were done assuming that the length of any of the two oblique planes in figures 2.3b or 2.3c have an unit value. Thus, considering for example figure 3b, the length of the plane parallel to the x-axis, will be  $1 \sin \phi$ , while the length of the plane parallel to the y-axis will be  $1 \cos \phi$ . Therefore, the out-of-plane forces acting on the xz-plane will be the product between the out-of-plane and its corresponding length,  $v_{Edx} \sin \phi$ . On the other hand, the out-of-plane shear acting on the yz-plane will be the product between the out-of-plane and its corresponding length, ( $v_{Edy} \cos \phi$ ). Finally, after doing summation of forces in

the z-direction for the out-of-plane forces, equation 1 gives the variation of the out-of-plane ( $v_n$ ) in function of the initial out-f-plane shears ( $v_{Edx}$  and  $v_{Edy}$ ) and of the angle ( $\varphi$ ). Similarly, after doing equilibrium of forces in Figure 2.3c, equation 2 gives the variation of the out-plane transverse shear ( $v_n$ ).

$$v_{nz} = v_{Edx} \cos \varphi + v_{Edy} \sin \varphi \quad \text{Eq (1)}$$

$$v_{tz} = v_{Edx} \sin \varphi + v_{Edy} \cos \varphi \quad \text{Eq (2)}$$

Knowing the relation between the  $v_{nz}$ ,  $v_{tz}$ ,  $v_{Edx}$ , and  $v_{Edy}$  in function of the angle ( $\varphi$ ), the next step consists in find out what will be the principal angle  $\varphi$  (where  $\varphi = \varphi_o$ ) which is associated to the maximum or principal out-of-plane shear ( $V_{Edo}$ ). Since both,  $v_{nz}$  and  $v_{tz}$ , are sinusoidal functions, their maximum values are found after derivating them with respect to the angle  $\varphi$  and equating them to zero. Moreover, when derivating  $v_{nz}$  in equation 1, it became the exact same expression of  $v_{tz}$ , in equation 2. In simpler words ( $\frac{dv_{nz}}{d\varphi} = v_{tz}$ ). It means, that when  $v_{nz}$  reaches its maximum values,  $v_{tz}$  reaches its minimums, and vice versa, which is demonstrated in Figure 2.3d. Consequently, after equating equation 2 -which gives the maximum values for equation 1( $v_{nz}$ )- to zero, the principal angle ( $\varphi_o$ ) is found through equation 4. Finally, the maximum out-of-plane shear ( $V_{Edo}$ ), associated with the principal angle ( $\varphi_o$ ), can be found after replacing the  $\cos(\varphi_o)$  and the  $\sin(\varphi_o)$ , in equation 1. From figure 2.3b it is clear that the  $\cos(\varphi_o) = v_{Edx}/v_{Edo}$ , and that the  $\sin(\varphi_o) = v_{Edy}/v_{Edo}$ , and thus, the maximum out-of-plane shear ( $v_{Edo}$ ), can be found as shown in equation 5. This ends the explanation about how the formulas to compute  $\varphi_o$  and  $v_{Edo}$  came up in the EC2 approach.

$$\varphi_o = \arctan\left(\frac{v_{Edx}}{v_{Edy}}\right) \quad (4)$$

$$v_{Edo} = \sqrt{v_{Edx}^2 + v_{Edy}^2} \quad (5)$$

***Step 1-2: Assume an initial thickness and estimate the out-of-plane shear capacity of the RC panel without considering TSHR.***

For this step, an initial thickness of the inner layer must be assumed. According to Blaauwendraad (2010), a good starting point is to assume that the thickness of the outer layers will be 20% of the total thickness of the wall ( $0.2t_w$ ). Thus, the thickness of the inner layer can be initially assumed as  $0.6 t_w$ . With an assumed thickness ( $t_c$ ), the next step is to compute an initial out-of-plane shear capacity of the panel assuming that there is no need of TSHR. This means that only the out-of-plane shear capacity that is only provided by the concrete ( $V_{Rd,c}$ ) will be considered. To compute  $V_{Rd,c}$ , the EC2 sandwich model assumes that along the direction of the principal out-of-plane shear ( $\varphi_o$ ), which is computed with equation 5, the panel behaves like a beam, and it can be estimated with equation 6. In equation 6,  $C_{Rd,c}$  is taken as 0.18 and  $\gamma_c$  is the safety factor that can be taken as 1.0.

$$v_{Rd,c} = \left[ \frac{C_{Rd,c}}{\gamma_c} k_v (100\rho_l f_{ck})^{1/3} + k_1 \sigma_{cp} \right] t_c d \geq (v_{\min} + k_1 \sigma_{cp}) t_c d$$

where,

$$\rho_l = \rho_x \cos^2 \varphi_o + \rho_y \sin^2 \varphi_o \quad (6)$$

$$k = 1 + \sqrt{200/d} \leq 2.0$$

$$\sigma_{cp} = N_{Ed} / A_c$$

Equation 6 accounts for the effects of the longitudinal reinforcement ( $\rho_l$ ) and the axial stress ( $\sigma_{cp}$ ) on the shear capacity of the panel. Both effects are a function of the principal out-of-plane shear angle  $\varphi_o$ .  $\sigma_{cp}$  is the axial stress produced by the force  $N_{Ed}$  which acts perpendicular to the plane of the maximum out-of-plane shear. Although the Eurocode 2 does not advise how to estimate this  $N_{Ed}$  force, a possible option is given through equation 7. As shown in equation 7, the  $N_{Ed}$  force is also a function of the angle  $\varphi_o$ , and it can be found by doing equilibrium of in-plane axial forces as shown in Figure 2.3b. The  $N_{Ed}$  force can be positive or negative, meaning tensile and compressive force, respectively. If positive, the sign of the axial force ( $N_{Ed}$ ) must be introduced as negative in equation 7 to capture the reduction in the shear capacity of the panel. If negative, on the contrary, the sign of the axial force ( $N_{Ed}$ ) will have to be introduced as positive to capture the increment in the shear capacity of the panel. Since it is not clear how to estimate this

Ned force, its contribution in the out-of-plane shear capacity of the panel will be neglected when applying the EC2 approach in this thesis.

$$N_{Ed} = \frac{\eta_{Edx} + \eta_{Edx}}{2} + \frac{\eta_{Edx} + \eta_{Edx}}{2} \cos(\varphi) \quad (7)$$

It is important to point out that in this step, it is dictated whether TSHR is or not required. If the shear capacity provided uniquely by the concrete is greater than the principal out-of-plane shear, ( $V_{R,dc} > V_{Edo}$ ), then, TSHR is not required, and the design of the inner layer will be completed. On the other hand, if  $V_{R,dc} < V_{Edo}$ , then, TSHR is required, and the two additional steps, step 1.3 and step 1.4, are required to complete the design of the inner layer.

***Step 1-3: Estimate and verify the out-of-plane shear Capacity of the RC panel considering TSHR.***

This step is only necessary if the out-of-plane shear capacity only provided by the concrete ( $V_{R,dc}$ ) is not enough to resist the principal out-of-plane shear ( $V_{Edo}$ ); or in other words, when  $V_{R,dc}$  is less than  $V_{Edo}$ . In this the case, the out-of-plane shear capacity of the panel will only depend upon the TSHR, and the contribution of the concrete will be neglected. The new out-of-plane shear capacity of the panel, now only provided by the TSHR, is estimated as the minimum value between the shear capacity provided only by the THRS ( $V_{Rd,s}$ ) and an upper shear capacity limit ( $V_{Rd,max}$ ). Equation 8 shows how to compute  $V_{Rd,s}$  and  $V_{Rd,max}$ .

$$V_{Rd,c} = \min of \begin{cases} V_{Rd,c} = \frac{A_{sw}}{s} f_{ywd} \cot \theta \\ V_{Rd,max} = \frac{\alpha_{sw} b_w z v_1 f_{cd}}{\cot \theta + \tan \theta} f_{ywd} \cot \theta \end{cases} \quad \text{Eq (8)}$$

It is clear from Equation 8 that  $V_{Rd,s}$  and  $V_{Rd,max}$ , are both dependent of the angle ( $\theta$ ), which is an approximate angle that define the direction of the concrete compressive struts in a strut and tie model for the panel. A typical way to estimate this angle is by equating the principal out-of-plane shear ( $V_{Edo}$ ) to the value of ( $V_{R,dc}$ ) in the same Equation 8. This will imply an iterative

process in which a certain amount of shear reinforcement must be first assumed in terms of spacing (s) and bar area ( $A_{sw}$ ). The final consideration is that this angle  $\theta$  must remain inside the range when its  $\cot(\theta)$  is limited by 1.0 and 2.5. The new out-of-plane shear capacity of the panel, which only accounts for the contribution of the TSHR, is now verified against the principal out-of-plane shear. If the new  $V_{R,dc}$  is less than  $V_{Edo}$  means that the design is not satisfied, one of the next two options must be followed. First, provide additional Transverse shear Reinforcement, and/or second, increase the thickness of the Panel. Blaauwendraad (2010) and the bulletin 45 of the (fib 2008) suggests that in practice, it is better to increase the thickness of the panel instead of providing TSHR. The design is satisfied when  $V_{R,dc}$  became equal to or greater than  $V_{Edo}$ .

***Step 1-4: Compute the additional membrane forces after TSHR has been provided.***

As said before, this step is only necessary if transverse TSHR have been required in the inner layer. The presence of THSR, will rise membranes forces in the inner layer. The magnitude of these membrane forces, resulting from the presence of the THRS, are found using Equations 9a to 9c. The inner layer will be then subjected to an in-plane axial force acting on the x-direction ( $n_{Edxc}$ ), an in-plane axial force acting on the y-direction ( $n_{Edyc}$ ), and to an in-plane shear force ( $n_{Edxyc}$ ), as well. With these membrane forces acting in the inner, it will need to be designed as membrane elements similarly to the outer layers. The procedure about how to design the outer layer will be explained later. It is convenient to anticipate that to maintain equilibrium, the outer layers of the panels will take half of those membrane forces raised in the inner layer.

$$\eta_{Edxc} = \frac{V_{Edx}^2}{V_{Edx}} \cot \theta \quad \text{Eq (9a)}$$

$$\eta_{Edyc} = \frac{V_{Edy}^2}{V_{Edx}} \cot \theta \quad \text{Eq (9b)}$$

$$\eta_{Edxyc} = \frac{V_{Edx} V_{Edy}}{V_{Edx}} \cot \theta \quad \text{Eq (9c)}$$

#### 2.1.4 Estimate the in-plane reinforcement for the outer layers, and the inner layer.

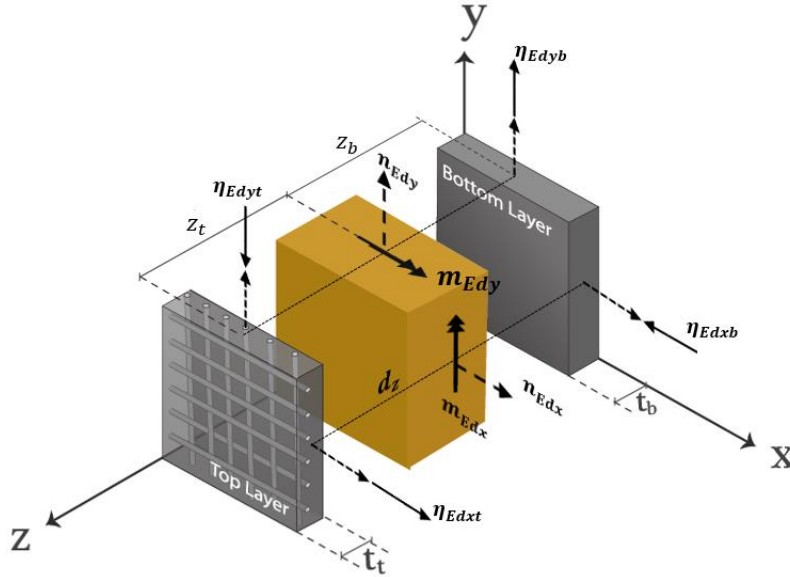


Figure 2.4. Computation of the axial membrane Force over the outer Layers.

The outer layers will be designed as membrane elements. It means that they will only resist in-plane forces. Figure 1 shows the in-plane axial forces and the in-plane shear forces, by which the outer layers will be designed for. Following the flowchart in figure 2.2, five steps are required to design the outer layers: 1. computation of the in-plane forces; 2. determination of the principal stresses and principal directions; 3. evaluation of the cracking condition of the layer; 4. estimation of the amount of reinforcement if needed; and 5. verification of the compressive stress capacity. Again, it is important to recall that in the case in which TSHR has been provided, these five steps will not only apply for the design of the outer layers, but for the inner layer as well. These five steps will be explained more in deep in below.

##### ***Step 2-1: Estimate the in-plane forces over the outer layers and in the inner Layers.***

The membrane forces acting on the outer layers are divided into axial membrane forces and shear membrane forces. The magnitude of those membrane force depend upon: the magnitude of the internal membrane forces ( $n_{Edx}$ ,  $n_{Edy}$ ,  $n_{Edxy}$ ), the magnitude of the internal plate forces ( $m_{Edx}$ ,  $m_{Edy}$  and  $m_{Edxy}$ ) and the lever arm distance ( $d_z$ ). The lever arm distance ( $d_z$ ) is the distance between the centroid of the bars from one reinforcement layer to another, as shown in figures 2.4 and 2.5.

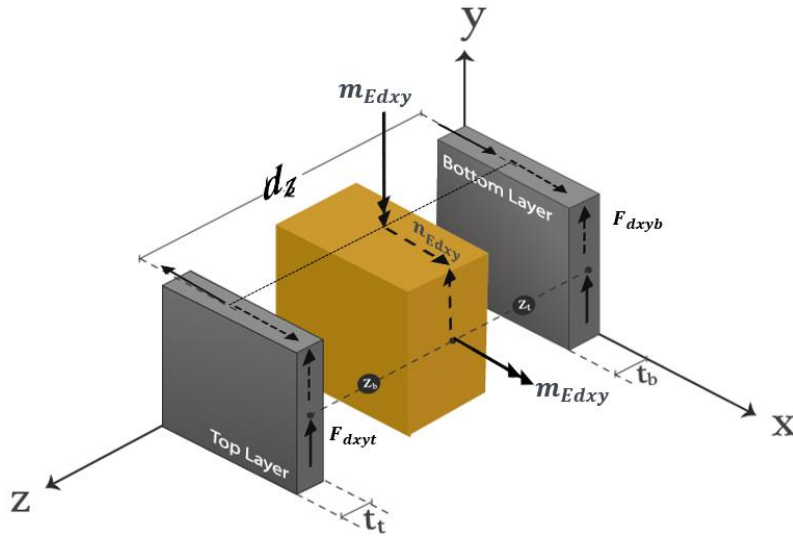


Figure 2.5. Computation of the in-plane shear membrane forces over the outer layers.

There were two very important considerations before computing the forces acting on the outer layers. First, it was assumed that there is only an unique averaged lever arm distance between the four reinforcement curtains as shown in Figure 2.6. This unique averaged lever arm distance ( $d_z$ ) goes from the middle line between the vertical and the horizontal reinforcement curtains in the top face, to the middle line of the vertical and the horizontal reinforcement in the bottom face. In reality, there will be two lever arm distances: one lever arm distance ( $d_{xz}$ ) between the reinforcement curtains running in the x-direction, and another lever arm distance between the reinforcement curtain running in the y-direction ( $d_{yz}$ ). However, the authors believe that the effect of this assumption, considering the thickness of the panels in industrial facilities, will be negligible for design purposes. In addition, this assumption will considerably simplify the computations.

The second assumption is that the centroid of the vertical and horizontal reinforcement curtains in both faces will always be forced to coincide with the centroid of the outer layers, as indicated in Figure 2.6 as well. If the centroid of reinforcement curtains does not coincide with the centroid of the outer layers, there will be an eccentricity between the reaction forces taken by the outer layers, and the forces that will be taken by the reinforcement curtains. This eccentricity, therefore, will produce an internal bending moment in the outer layers, and the computation of the forces taken by the reinforcement curtains will become a little trickier, which will be in opposition to the purpose of this paper. Nevertheless, it is worthy to mention that by increasing the thickness of the outer layers and leaving the reinforcement with eccentricity is a good option to reduce the

compressive stresses of the concrete in the outer layers, but without increasing the total thickness of the wall. In such a case where eccentric reinforcement is needed, the Appendix LL of the Eurocode gives the formulas to compute the forces that will resisted for the reinforcement. The author believes, however, that for practical design applications this level of accuracy might not be worthy.

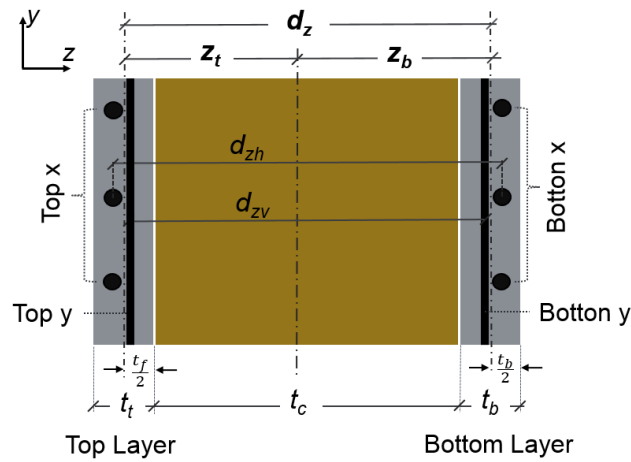


Figure 2.6. Assumption of the Unique Lever arm distance and Identification of the Reinforcement Curtains (or layers).

Following the previous two assumptions, the membrane forces over the outer layers are computed by doing simple statics as shown in Figure 2.4. From Figure 2.4, it can be seen that the design membrane forces over the outer layers are the summation of the decomposition (or resulting) of the internal axial forces ( $n_{Edx}$  or  $n_{Edy}$ ), plus the decomposition of the out-of-plate bending moments ( $m_{Edx}$  or  $m_{Edy}$ ). For example, the in-plane design axial force for the bottom layer ( $n_{Edxb}$ ) and the in-plane design axial force for the top layer ( $n_{Edxt}$ ), both acting along the x-direction are computed using equations 10a and 10b, respectively. Similarly, the in-plane design axial bottom force ( $n_{Edyb}$ ) and the in-plane design axial top force ( $n_{Edyt}$ ), both acting along the y-direction are computed using equations 10c and 10d, respectively. In the set of equations 10, the first term represents the action of the total internal axial demand forces ( $n_{Edx}$  or  $n_{Edy}$ ), the second term represents the effect of the out-of-plate bending moments ( $m_{Edx}$  or  $m_{Edy}$ ), and the third term in the formulas accounts for the presence of TSHR. If no TSHR is provided this third term will be canceled off.

$$\eta_{Edxb} = \eta_{Edx} \frac{(d_z - z_b)}{d_z} + \frac{m_{Edx}}{d_z} + \frac{1}{2} \frac{v_{Edx}^2}{v_{Edo}} \cot \theta \quad \text{Eq (10a)}$$

$$\eta_{Edxt} = \eta_{Edx} \frac{(d_z - z_t)}{d_z} - \frac{m_{Edx}}{d_z} + \frac{1}{2} \frac{v_{Edx}^2}{v_{Edo}} \cot \theta \quad \text{Eq (10b)}$$

$$\eta_{Edyb} = \eta_{Edy} \frac{(d_z - z_b)}{d_z} - \frac{m_{Edy}}{d_z} + \frac{1}{2} \frac{v_{Edy}^2}{v_{Edo}} \cot \theta \quad \text{Eq (10c)}$$

$$\eta_{Edyt} = \eta_{Edy} \frac{(d_z - z_t)}{d_z} - \frac{m_{Edy}}{d_z} + \frac{1}{2} \frac{v_{Edy}^2}{v_{Edo}} \cot \theta \quad \text{Eq (10d)}$$

Equations 11a and 11b, on the other hand, give the magnitudes of the in-plane shear membrane forces acting on the top and bottom layers respectively. Similar to the case of the axial in-plane forces, the total in-plane shear forces over the layers is the summation of the decomposition of the direct shear force ( $n_{Edxy}$ ) plus the decomposition of the twisting moment ( $m_{Edxy}$ ) over the outer layers. If positive convention for shear is assumed, the resulting shear forces for direct shear and twisting moment will be added in the bottom layer, while the shear forces will be subtracting in the top layer. Similarly, to find the membrane axial membrane forces, the first term in Equations 11 represents the action of the total internal shear demand forces ( $n_{Edxy}$ ); the second term represents the effect of the effect of the twisting moment ( $m_{Edxy}$ ); and the third term accounts for the presence of TSHR. Again, if THSR has not been required this term will be cancelled off.

$$\eta_{Edxyb} = \eta_{Edxy} \frac{(d_z - z_b)}{d_z} + \frac{m_{Edxy}}{d_z} + \frac{1}{2} \frac{v_{Edx}^2}{v_{Edo}} \cot \theta \quad \text{Eq (11a)}$$

$$\eta_{Edxyt} = \eta_{Edxy} \frac{(d_z - z_t)}{d_z} - \frac{m_{Edxy}}{d_z} + \frac{1}{2} \frac{v_{Edx}^2}{v_{Edo}} \cot \theta \quad \text{Eq (11b)}$$

**Step 2-2: Computation of the Principal Stresses and Principal Directions.**

The stresses in the outer layers (top and bottom) are obtained by dividing the membrane forces that were computed in step 2.1 over the assumed thickness of the corresponding layer. Figure 8 shows this procedure step by step. The thickness ( $t$ ) in figure 2.7a can be either the thickness of the bottom or the top layer. Figure 2.7b shows the original state of stress after dividing the membrane forces over the corresponding thickness as explained. From this original state of stresses, the principal stresses and the corresponding principal directions can be computed, either by using the typical stresses transformation formulas of the Cauchy stress tensor, or the very familiar Mohr circle. Figure 2.7c shows the how the principal angles and stresses are found by using the Mohr circle. The most valuable parameters in this step are: the principal (or maximum) compressive stress in the concrete ( $\sigma_{pc}$ ); and its corresponding angle or direction ( $\theta_{pc}$ ). The angle  $\theta_{pc}$  goes from the principal compressive stress  $\sigma_{pc}$  to the x-axis, represented by the original state of stresses in figure 8b. These two parameters,  $\sigma_{pc}$  and  $\theta_{pc}$  will be needed to complete steps 4 and 5, respectively.

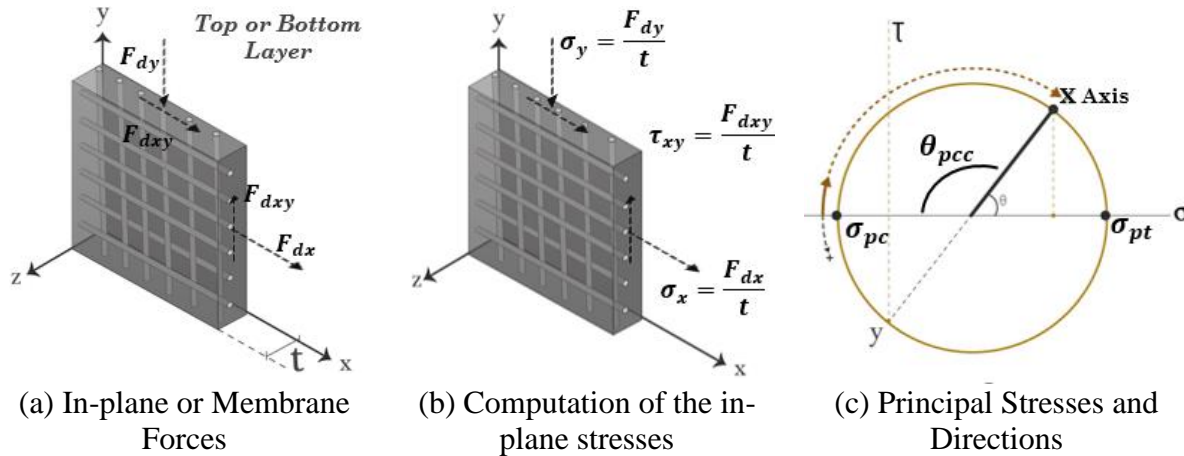


Figure 2.7. Determination of the principal stresses and principal angles.

**Step 2-3: Evaluation of the Cracking condition.**

Evaluating the cracking condition of the outer layers -as well as in the inner layers when apply- is a crucial step in the EC2 sandwich model approach. It is crucial because depending on if any of the layers is cracked or not, it will or will not need reinforcement. To verify whether the element is cracked or not, a cracking criterion, presented in equation 11, must be applied. This

cracking criterion is based on plasticity theory for concrete material, and it adopts the failure surface proposed by Ottosen (1977). The construction of this failure surface mainly depends upon the principal stresses of the material at given point and upon the four parameters  $\alpha$ ,  $\beta$ ,  $c_1$  and  $c_2$ . An explanation regarding these four parameters will be given later. The principal stresses are accommodated in terms of the stress invariants of the stress tensor  $I_1$ ,  $J_2$ , and  $J_3$ .  $I_1$  is the trace of the stress tensor, and  $J_2$  and  $J_3$  are the second and third invariants of the deviatoric part of the stress tensor, respectively. For convenience, the cracking criterion in the EC2 has been normalized against the compressive concrete media strength  $f_{cm}$ , as shown Equation 12.

$$\Phi = \alpha \frac{J_2}{f_{cm}^2} + \lambda \frac{\sqrt{J_2}}{f_{cm}^2} + \beta \frac{I_1}{f_{cm}^2} \quad \text{Eq (12)}$$

A graphic interpretation of the failure surface for applying the cracking criterion is given in Figure 2.8. If the state of principal stresses ( $\sigma_1$ ,  $\sigma_2$  and  $\sigma_3$ ) on the outer layer, represented by an aleatory point in the Westgard space, remains inside the failure surface, it means that the layer in analysis (inner or outer) is un-cracked. On the contrary, if that point resides outside of the failure surface, it means that the layer in analysis (inner or outer) is cracked. Now, for design purposes, it is enough to say that any layer of the RC panel will be considered as un-cracked if the inequality in equation 5 is satisfied ( $\Phi \leq 0$ ), and as cracked if it is not satisfied ( $\Phi > 0$ ). If the layer is un-cracked, it will be enough to verify that only the maximum compressive principal stress ( $\sigma_1$  or  $\sigma_2$ ) is less than or equal to the design compressive strength  $f_{cd}$ . If this is the case, then the design of the outer layers will be done in only two steps (step 1.1 and step 1.2 in figure 2.2) because steel reinforcement was not required. On the other hand, if the element is found to be cracked, then in-plane steel reinforcement will be required moving forward to step 1.3. As said before, the yield surface also depends upon the four parameters  $\alpha$ ,  $\beta$ ,  $c_1$  and  $c_2$ . The Eurocode gives all the formulation to find all these parameters, which can be programmed in a spreadsheet, and they will not be reproduced in this document for the sake of brevity. As an alternative for design, instead of following the long formulation procedure from the Eurocode, and/or avoiding the development of an spreadsheet if desired, Chen and Han (2007) and/or Chen (1982) provides approximate values to estimate all these parameters. The fib CEB-FIP Model code (1990) (MC-1990), in its chapter five, also provides charts to estimate the  $\alpha$ ,  $\beta$ ,  $c_1$  and the  $c_2$  parameters to apply this cracking criterion.

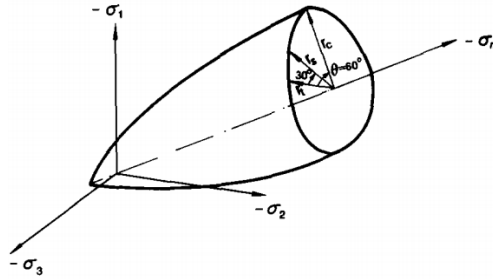


Figure 2.8. Yield Surface 3D-view, represented in the Haigh-Westergaard space. Taken from Chen (1993)

A simpler way to understand the Ottosen Cracking criteria is by considering the especial case of bi-axial stress condition in where there is no out-of-plane stress ( $\sigma_3=0$ ); and when at least one of the other principal stresses ( $\sigma_1$  or  $\sigma_2$ ) is in tension. This special case is represented in Figure 2.9 which was obtained using the experimental data of the PV panel series selected in this thesis. The continuous line represents the cracking surface of the PV series after assuming average values for the maximum compressive concrete stress ( $f'_c$ ) and the maximum tensile stress ( $f_t$ ) of 20MPa and 2MPa, respectively. The dots, on the other hand, represents the maximum principal stresses pair2 ( $\sigma_1$  and  $\sigma_2$ ) at which the PV23, then PV24 and the PV 28 panels were subjected. It was only necessary to build the tensile-compressive zone of the whole failure surface because all the stress combinations had a principal compressive stress and a principal tensile stress. As appreciated, all points are outside the failure surface, meaning that under those stress conditions, the panels are cracked, and in theory, steel reinforcement will be needed.

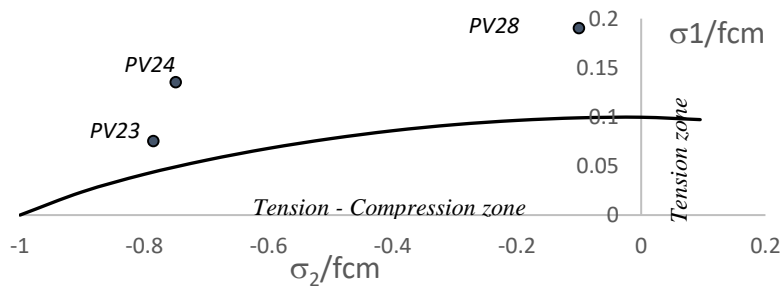


Figure 2.9. Representation of Ottosen Cracking criteria (or failure surface) for the PV series panels in the special bi-axial case

**Step 2-4: Providing Reinforcement in the Outer Layers.**

If any of the outer layers (or inner layers when applicable) are found to be cracked, then steel reinforcement needs to be provided. As mentioned earlier, the angle  $\theta_{pc}$ , found in step 2.2 is required in this step. Figure 2.9 shows how the reinforcement will be positioned inside the RC panel. It will be assumed that the direction of the reinforcement will be in parallel with the vertical and horizontal edges of the panel. A better alternative to optimize the amount of reinforcement would consist in positioning the reinforcement bars aligned with the principal directions. However, there two drawbacks when considering this option. First, it is not practical for construction purposes and it will cause delays and extra costs. The second drawback is related to the fact that in actual design there are several design combinations, which produce different state of stresses and principal directions, and therefore, it will be difficult (if not impossible) to align the reinforcement in such a way that allows to satisfy each one of those combinations.

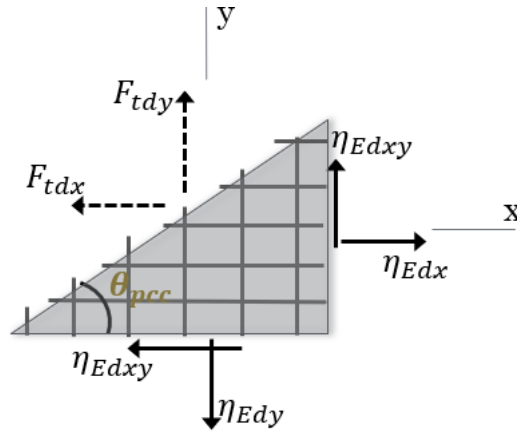


Figure 2.10. Orthonormal position of the Reinforcement Curtains in any of the faces

To estimate the required reinforcement areas for any of the outer layers, it is necessary to compute the axial forces that will be resisted by those reinforcement curtains. Equation 13a gives the magnitude of the force that will be resisted for the reinforcement running in the x-direction, while equation 13b gives the magnitude of the force for the reinforcement running in in the y-direction. As shown in the equations 13a and 13b, the magnitudes of those forces are function of the angle  $\theta_{pc}$ , which is the angle that controls the interaction between the axial and the shear membrane forces. Equation 13a and 13b indicate that the magnitude of the forces must be positive (or greater than zero). If the magnitudes of the forces are negative, meaning compressive forces,

steel reinforcement will not be required. However, even if reinforcement is not required in a particular direction, a minimum reinforcement ratio for construction proposes and/or fulfillment of service conditions need to be provided.

$$F_{tdx} = \eta_{Edx} - \eta_{Edxy} \cot(\theta_{pcc}) \geq 0 \quad \text{Eq (13a)}$$

$$F_{tdy} = \eta_{Edy} - \eta_{Edxy} \cot(\theta_{pcc}) \geq 0 \quad \text{Eq (13b)}$$

After obtaining the forces that will be resisted by the reinforcement in the x-direction and in the y-direction, the required reinforcement area per unit length can be obtained through Equations 14a and 14b, respectively. The reinforcement area per unit length is obtained by dividing the forces that the reinforcement must resist in the x-direction ( $F_{tdx}$ ), and in the y- direction, ( $F_{tdy}$ ), over the yielding stress of the reinforcement  $f_{yd} = f_y/\gamma_s$

$$A_{sx} = F_{tdx} / \gamma_s \quad \text{Eq (14a)}$$

$$A_{sy} = F_{tdy} / \gamma_s \quad \text{Eq (14b)}$$

***Step 2.5. Verification of the compressive stress capacity of the concrete.***

In this step, the compressive stress demand in the concrete over the outer layers ( $\theta_{pc}$ ) needs to be verified against the compressive concrete capacity ( $\sigma_{cd\_max}$ ). The concrete compressive stress demand ( $\theta_{pc}$ ) is found with equation 15a, while the concrete compressive capacity is found with equation 15b. Similar to the design forces that need to be resisted by the reinforcement, the concrete compressive demands also depends on the principal compressive angle  $\theta_{pcc}$ . It can be observed that for the typical case in where  $\theta_{pcc} = 45^\circ$ , the magnitude of the compressive demand will be twice the shear stress. The concrete compressive capacity, on the other hand, depends on the magnitude and direction of the principal stresses. As can be noticed, the concrete compressive capacity will be higher if the principal stresses in the outer layer are in compression, and oppositely, it will be lower if one of the principal stresses is in tension.

$$\sigma_{cd} = |\tau_{xy}| \left[ \cot(\theta_{pcc}) + \frac{1}{\cot(\theta_{pcc})} \right] \leq \sigma_{cd\_max} \quad \text{Eq (15a)}$$

$$\sigma_{cd\_max} = \begin{cases} 0.85 f_{cd} \frac{1+3.8\alpha}{(1+\alpha)^2} & \text{if } \sigma_1 \wedge \sigma_2 < 0 \\ f_{cd} \left[ 0.85 - \frac{\sigma_s}{f_{yd}} (0.85 - \nu) \right] & \text{if } \sigma_1 \vee \sigma_2 \geq 0 \end{cases} \quad \text{Eq (15b)}$$

This final sub step is also of vital importance because here it is where the iterative process between the design of the inner layer and the outer layers take place. This iterative process can be better illustrated by using Figure 2.6, and imaging variable magnitudes of lever arm distances between the top and bottom reinforcement layers in any direction. For example, if the lever arm is small it will imply that the thickness of the outer layers will be big, and therefore, the compressive stresses in the concrete in the outer layers will be low. On the contrary, if the lever arm increases, the thickness of the outer layers will decrease, and the compressive stresses over those layers will be higher. It is also worthy to note the tradeoff between the lever arm distance, the compressive stress in the outer layers, and the efficiency of the design of the panel represented by the amount of required reinforcement. For example, decreasing the lever arm distance will reduce the compressive stresses in the outer layer, but it also implies that more reinforcement area will be required. On the contrary, increasing the lever arm distance by reducing the initial assumed thickness of the outer layers will reduce the amount of required reinforcement, but at the same time, it will increase the compressive stress demand.

## 2.2 Theoretical concepts for the non-linear analysis and modeling of RC members

### 2.2.1 Uniaxial Behavior of Concrete in Compression

There are several models to represent the compressive behavior of the unconfined and/or confined concrete. Among those models are the Hognestad model (Hognestad 1951), the Kent and Park model (Kent and Park 1971), the Popovich's model (Popovics, 1973) and the Mander model (Mander et al.,1988), just to name a few. The well-known Hognestad parabola model will be used in this study. The required parameters to build the Hognestad parabolic model are: The Young (or the Elastic) modulus of the concrete ( $E_c$ ); the maximum compressive strength of the concrete  $f'_c$ ,

usually taken as 80% of the compressive strength of the cylinder at 28 days; the strain associated to that maximum compressive strength,  $\varepsilon_{co}$ , the ultimate compressive  $\varepsilon_u$  taken as 0.0038, and the compressive strength at that maximum compressive strain, taken as 85% of  $f'_c$ . All these values will be provided in a case by case basis in chapter five, which is devoted to the modelling of the panels. Figure 2.10 shows how to build a typical Hognestad compressive model for concrete.

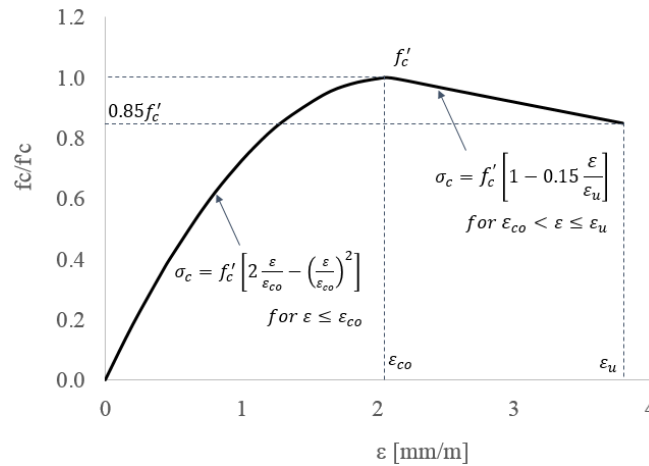


Figure 2.11. Hognestad parabola model for concrete in compression

## 2.2.2 Behavior of Concrete in Tension

The behavior of concrete in tension can be split in behavior before cracking and behavior after cracking. In most common practical situations for RC panels (or any other structural members) the concrete will be always cracked since the maximum tensile strength is very low when compared to its maximum compressive strength. Therefore, before defining the uniaxial behavior of the concrete in tension, it is necessary to have a good understanding about the behavior of the cracked concrete, and how it can be modelled. According to Chen (1982) there are three approaches than can be used for the modeling of cracked concrete: fracture-mechanics model, discrete crack model and smeared crack model. Chen (1982) also recommends that if a detailed representation of the cracking formation is desired, the fracture mechanics model and the discrete cracked models will be more appropriate for this purpose. The smeared cracked model on the other hand, will be more appropriate if the main objective is to reproduce the load deformation-deformation overall response of the RC member, without focusing in the cracking formation itself. Since one of the objectives of this thesis is to reproduce the calibrated load vs deformation curves

of the panels tests in order to estimate the capacity of the panels after introducing the reinforcement areas suggested by the PACI and the EC2 approaches, the smeared cracked model will be adopted. In addition, it is important to anticipate that both software, Shell 2000 and Abaqus, use the smeared cracked approaches in its formulation.

### ***Discrete cracked models***

The discrete crack models are more in agreement with fracture mechanics since they treat the cracks as displacement discontinuities. In the discrete crack models the cracks are forced to occur in the vicinities or boundaries of the finite elements, which biases the formation of the cracks and is perhaps the main drawback of these models. According to Menin et al (2009), the discrete crack model is more recommended when the failure of the specimen is governed by a few dominant cracks, which can also be taken as an advantage, since this failure mode do not represent the failure mode for most of the cases in reinforced concrete members. Jendele et al (2001) confirm that the discrete crack model is preferred either for the analysis unreinforced concrete or reinforced concrete members with very low reinforcement ratios.

### ***Smeared Cracked concepts***

Two important assumptions are considered in the smeared cracked models. First, the size or width of the cracks are very small compared to the size of the RC member; and second, those micro-cracks are uniformly spread through the member. Thus, the failure mode of the RC member is governed by the formation of several “small”- or spread-uniforms cracks, instead of a few macro-crack as in the case of the discrete crack models. According to the Abaqus theory manual, the smeared cracking models is suitable for most of the application in reinforced concrete. Maekawa et al (2003) also says, that the smeared cracking model has a higher range of applicability than the discrete crack model, especially when these are enhanced with the concepts of multi-directional fixed model. The smeared crack models can be also classified into three approaches in accordance with the assumed crack direction model: Rotating cracking model, fixed cracking model, and multi-directional fixed cracking model. The rotating cracking model is assumed in Shell 2000, whereas the fixed crack model is employed in Abaqus. For these reasons, only the rotating and fixed crack model will be explained in this study.

### *Rotating Smeared Crack Models*

In the rotating models, once the crack forms -after the material met a predefined cracking failure criterion- the direction of the crack is assumed to follow the direction of the principal stresses. An example of this case is a RC panel subjected to subjected to tensile and shear forces in where the cracks open first in the direction perpendicular to the maximum principal tensile strength, once the maximum tensile strength of the concrete ( $f_t$ ) is reached, and then, the direction of the crack will be change by the tensile-shear combined effect.

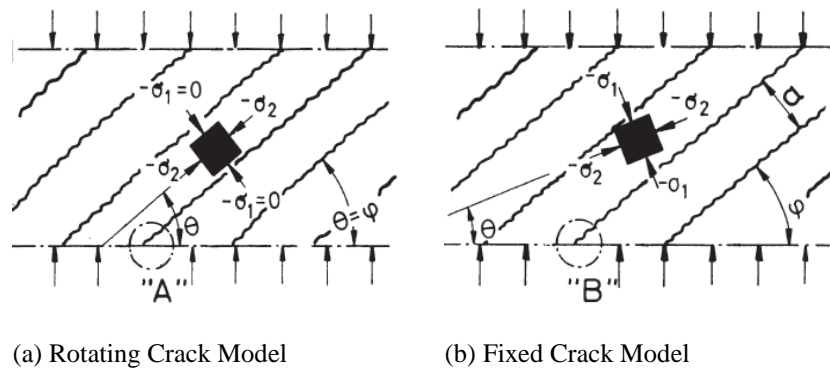


Figure 2.12. Rotating vs Fixed Crack Model. Kupfer and Bulicek (1991)

### *Fixed Smeared Crack Models*

In the fixed smeared crack models, on the other hand, as its name indicates, the direction of the crack remains fixed once they have been formed. This implies that the orientation of the cracks does not corotates with the principal axis, which raise shear stress along the cracks. Figure 2.11 gives an illustration of the rotating vs fixed approaches. Rots and Blaauwendraad (1989) pointed out that fixed smeared crack modes are more susceptible to overestimate the stiffness of RC members than the rotating smeared crack models. In order to avoid this overestimation in the stiffness, it is convenient to include a shear retention behavior (which will be explained later) into the numerical models.

### ***Tension Softening and Tension Stifening.***

Regardless the choosing between rotating or fixed smeared crack models, the behavior of the concrete in tension after cracking must be defined. According to Maekawa et al (2003) the behavior

of the cracked concrete in tension can be classified in tension stiffening for the case of reinforced concrete members; and in tension softening for the case of unreinforced concrete members. When using discrete crack models, the tensile behavior of the concrete after cracking, either tension or tension softening, can be directly simulated in the discontinuity (in the crack). However, when using smeared crack models, since there are no discontinuities, the only option to simulate the tensile behavior of the concrete after cracking is to modify the material properties. In accordance to Elenas et al (2006), the tension stiffening for the case of reinforced concrete members can be modeled by modifying either the steel reinforcement, or the concrete material properties itself. Figure 2.12 shows how to modify the steel reinforcement or the concrete to account for the tension effect in reinforced concrete members. As will be shown in the section five, only the modification of the concrete material option will be used in this study. As shown in figure 2.12 the tensile behavior of the concrete after cracking in plain concrete is more brittle than the behavior of the reinforced concrete because of the absence of steel reinforcement.

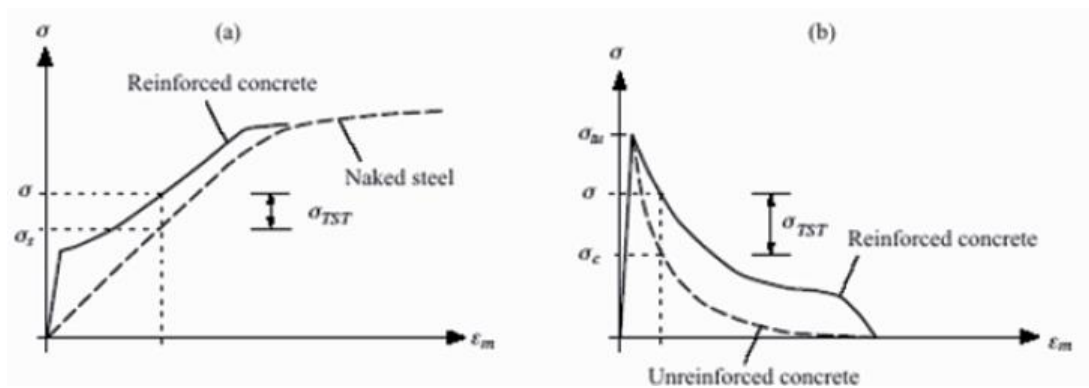


Figure 2.13. Modified Stress vs strain of material constitutive models to account for the tension stiffening effect. (Taken from Elenas et al 2006).

### *Tension Softening models*

Among the most common tension softening models for unreinforced concrete (although also used for reinforced concrete) are: the Hillerborg (1976) model, the fib CEB-FIP Model Code 1990 (MC-1990); the fib CEB-FIP Model Code 2010 (2010) (MC-2010), and the Wittman model Wittman et al (1988) which will not be used in this study. All these models are given in terms of stress vs displacement curves as shown in Figure 2.14.

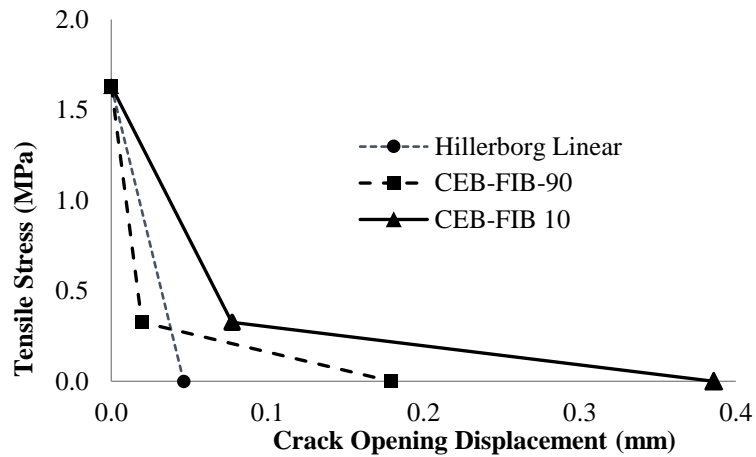


Figure 2.14. Comparison of Tension Softening curves for a 20 MPa compressive strength concrete.

Hillerborg (1976) indicated that the area under the curve (energy) that better fits with the experiment results has a simple triangular shape. Thus, the Hillerborg (1976) model is the simplest tension softening model which assumes a linear loss in tensile strength of the concrete after reaches the maximum tensile strength ( $f_t$ ). The fib-90 and the fib-10 softening models, propose a bilinear stress vs displacement curve to model the post-cracking behavior of the concrete in tension as shown in Figure 2.14. Three points are required to define or customize the tension softening effect in the concrete for these models 1. The point at maximum tensile strength ( $f_t$ ) which is reached when the concrete reached the tensile elastic strain limit  $\epsilon_t$ ; 2. The point at 20% of the maximum strength ( $0.20f_t$ ) of the fib-90 and the fib-10 model are used, and 3. The ultimate tensile strain at which the tensile stress becomes zero, depends of the Energy factor ( $G_f$ ). As an example, figure 2.13 shows the fib-90 and the fib-10 tension softening models for a concrete with a typical mean compressive strength ( $f'_c$ ) of 20 MPa.

The Energy factor ( $G_f$ ) is the most important variable to define the tension softening effect for all models.  $G_f$  represents the area under the stress vs opening cracking displacement in Figure 2.17, and it is considered as a material property. According to Uchida et al (1991), the fracture energy factor can adopt values between 0.1 to 0.15 N/mm for unreinforced concrete. In all softening models, the displacement at which a crack begins to propagate ( $w_{cr}$ ) is a very sensitive value especially in the numerical models developed in Abaqus. The  $w_{cr}$  mainly deepens upon the

tensile the energy factor and the maximum tensile strength. In the Hillerborg model which assumes a simple linear loss in strength, the displacement at which a crack begins to propagate ( $w_{cr}$ ) is calculated using equation 24.

$$w_{cr} = 2 \frac{G_f}{f_t} \quad \text{Eq (24)}$$

In the fib MC-1990 tension softening model, the Energy factor ( $G_f$ ) depends upon the maximum tensile strength, which is estimated as a function the mean compressive strength  $f_{cm}$  of the concrete, and the aggregate size. On the other hand,  $G_f$  only depends upon the tensile strength of the concrete in the fib MC-2010 model. The formulas to compute the energy factor  $G_f$ , the displacement at 20% of the tensile strength ( $w_1$ ) and the maximum or ultimate tensile strain ( $w_c$ ) for the MC-1990 tension model are given in equations 25a, 25b and 25c, respectively. fib MC-2010 model tension model, the  $\alpha_d$  and the  $\alpha_f$  factors depends are independent of the aggregate size and they adopt values of 73 and 1.0, respectively. In the fib 90 model, on the contrary they adopt different values.

$$G_f = \alpha_d * f_{cm}^{0.7} \quad \text{Eq (25a)}$$

$$w_c = \alpha_f * \frac{G_f}{f_{ctm}} \quad \text{Eq (25b)}$$

$$w_1 = 2 \frac{G_f}{f_{ctm}} - 0.15w_c \quad \text{Eq (25c)}$$

### *Tension Stiffening models*

Several models are available to account for the tension stiffening effect in the cracked concrete for reinforced concrete members. The Vecchio and Collins (1982), the Collins and Michael (1987), the Belarbi and Hsu (1994), the Bentz (2005) and the Shima et al (1987) models. In contrast to the softening models which are more commonly represented by stress vs displacement curves, the tension softening models are represented by stress vs strain curves as shown if Figure 2.14.

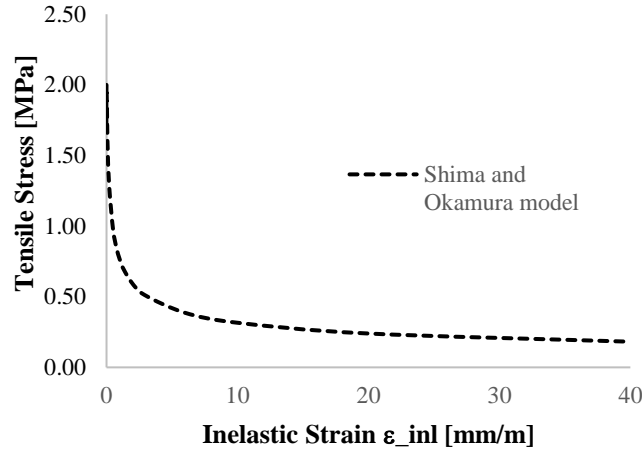


Figure 2.15. Shima et al (1987) Tension Stiffening curve for a 2.0 MPa tensile strength concrete.

The Shima et al (1987) model will be adopted in this study. According to Maekawa and Pimanmas (2003), the Shima et al (1987) model is suitable for RC members reinforcement in two direction with typical reinforcement ratios ranging from 0.1% to 2.0 %, just as the RC panels that will be analyzed in this research. An additional feature of this tension stiffening model is that according to the same Maekawa and Pimanmas (2003), it can be applied regardless the size element, crack spacing and even the orientation of the steel reinforcement. Equation 26 shows how the Shima et al (1987) model tension stiffening model can be developed as a function of the maximum tensile strength of the concrete and the type of reinforcement. The values of the parameter “c” in equation 26 are 0.4 and 0.2, for deformed bar and wire mesh, respectively.  $f_t$  is the maximum tensile strength of the concrete,  $\epsilon_t$  is the tensile strain cracking or the limit tensile elastic strain given by  $f_t/E$ , where E is the Elastic modulus of the concrete;  $\epsilon_{tu}$  is the ultimate tensile deformation usually taken as 10 times the limit elastic tensile strain ( $10\epsilon_t$ ).

$$\sigma(\epsilon) = f_t \cdot (\epsilon_{tu}/\epsilon)^c \quad \text{Eq (26)}$$

It is important to highlight that for the modeling for the majority of the RC panels in chapter 5, the maximum tensile strength ( $f_t$ ) in equation 26 was not taken as the splitting tensile cylinder test or the three-point flexural test values reported from the experiment. The maximum tensile strength ( $f_t$ ) was initially estimated by using the approximate equation from the design codes (i.e ACI 318), which is a function of the maximum compressive of the concrete ( $f_c$ ), and then calibrated, when possible, by capturing the cracking strength of the panels (i.e Cracking moment)

from their respective capacity load deformation curves. The Shell 2000 manual also suggests that  $f_t$  value must not be taken as the value reported from the split or direction tension tests, but it must be estimated using the approximate equations in design standards codes, which computes the  $f_t$  value as a function of the maximum compressive stress ( $f'_c$ ) of the concrete. According to Maekawa et al (2003), the tensile strength of the concrete in an RC member is usually less than the tensile strength measured from the cylinder test, and they recommend to calibrate the tensile strength of the cracking by matching the cracking load (i.e cracking moment or cracking shear) from the experimental capacity curve.

### *Shear retention*

When using fixed smeared concrete approaches, it is necessary to include a shear retention model in order to account for the reduction in shear transfer of the concrete along the surface of the cracks. A shear retention model accounts for the loss in shear stiffness as the cracks in the concrete opens. As said before, the no inclusion of the shear retention when using smeared fixed approaches might result in overestimation in the shear stiffness of RC members. In addition, according to Borst et al (2004), the inclusion of this shear retention factor improves the results of the fixed cracking models and reduces convergence issues during the analysis. The results are improved mainly because the shear retention factor captures at some extent the friction and the aggregate interlocking.

### **2.2.3 Modeling of Steel Reinforcement**

There are several models to simulate the behavior of conventional steel reinforcement. Steel reinforcement models can be classified in naked bar models and in embedded bar models. In the naked bar models, the strains vs strain curves representation is estimated from experiments in where a bar is tested alone in a typical tensile test. In the embedded bar, on the other hand, the test is conducted in a reinforced concrete member considering the effect of the surrounding concrete matrix. Maekawa et al (2003) said that the behavior of single isolated tested bar is different from the behavior of the same bar but embedded in the concrete matrix. Specifically, Maekawa et al (2003), affirms that a lower effective yielding stress is expected in RC members. The reduction in the yielding stress depends of the bar diameter and the spacing of the reinforcement. Moreover,

Belarbi and Hsu (1994) literally said “Yielding of a reinforced concrete panel occurs when the steel stress at the cracked section reaches the yielding strength of the bar.” The reason why a reinforcing bar in a RC cracked member might reach yielding before than in a naked bar is because of the variation of the stress level along the bar in a RC as shown in Figure 2.16. As can be seen, the stress in the bar near to the cracks are higher than the stress of the bar at midpoint between the cracks. The opposite occurs for the stresses in the concrete, in where they are minimum at the cracks, and maximum at midpoint.

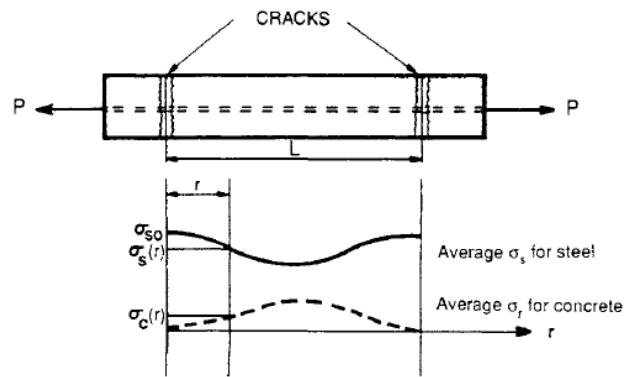


Figure 2.16. Variation of the stress along an embedded bar between two cracks. (taken from Belarbi and Hsu (1994))

### ***Models for naked bars***

Among the most common steel reinforcement “naked” bar models are: the bilinear model with no hardening, the bilinear model linear hardening and without yielding plateau, the trilinear model with hardening with yielding plateau, and the trilinear model with yielding plateau and parabolic hardening. The trilinear model with parabolic hardening might be considered the most accurate for mild or convectional reinforcement as shown in Figure 2.17. However, for most of the numerical models developed in this thesis the “naked” bar trilinear model with yielding plateau and linear hardening was enough to reproduce a good representation (or an acceptable calibrated response) of the panels. The trilinear model with linear hardening require six basic parameters: The Elastic modulus ( $E_s$ ), the yielding stress ( $f_y$ ) and its corresponding yielding strain of the bar  $\epsilon_y$ ; the strain at hardening initiation ( $\epsilon_{sh}$ ); and the stress and the strain at rupture  $f_u$  and  $\epsilon_{su}$ , respectively. All these were obtained from the experimental report of each panel. The continuous

line in Figure 2.17 shows the idealized stress vs strain curve for a naked bar using the trilinear model with hardening.

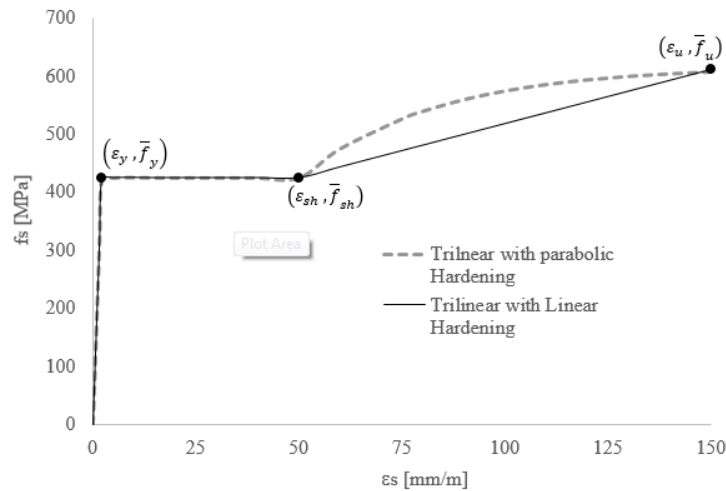


Figure 2.17. Models for “Naked” mild steel reinforcement bars

### Models for embedded bars

Some authors such as Shima et al (1987), Belarbi and Hsu (1994) and Maekawa et al (2003) developed idealized stress vs strain curves for embedded bars. The two first authors developed simplified bilinear models, while the Maekawa et al (2003) developed a trilinear model that consider the parabolic hardening in embedded bars. Maekawa et al (2003) also proposed a multilinear model in order to simplify the construction of the parabolic portion of the model. Although Maekawa et al (2003) said that the simplified bilinear give reasonable results for wall structures with relatively low tensile stress, the simplified multilinear model for embedded bars will be used in this thesis. Figure 2.17 compare the strain vs stress curves for a naked bar and an embedded bar using the simplified multilinear model proposed by Maekawa et al (2003).

As can be seen in figure 2.17, four lines comprise the simplified multilinear model for embedded bars. The first line corresponds to the initial elastic behavior the bar and is limited by the average yielding stress of the embedded bar. As said before, the most important difference between the naked and the embedded bar behaviors is the reduction of the yielding stress in the embedded bar, which is defined by the average yielding strain and stress point  $(\bar{\epsilon}_y, \bar{f}_y)$ . The average yielding stress  $(\bar{f}_y)$  is a function of the reinforcement ratio in the direction of analysis ( $\rho_x$  or  $\rho_y$ ),

the tensile strength of the concrete ( $f_{cr}$ ), and of course, the yielding strength of the naked bar ( $f_y$ ) as shown in Equation 28a. The yielding average strain ( $\bar{\epsilon}_y$ ) is found by dividing the yielding average stress over the Elastic modulus ( $E_s$ ) of the bar. The second line is limited by the point  $(\bar{\epsilon}_{sh1}, \bar{f}_{y1})$  in which the bar reaches the actual yielding strength of the “naked” bar. The third line goes from the point  $(\bar{\epsilon}_{sh1}, \bar{f}_{y1})$  to the point  $(\bar{\epsilon}_{sh2}, \bar{f}_{y2})$  which simplifies the parabolic behavior of the bar after hardening. Finally, the fourth line that goes from the point  $(\bar{\epsilon}_{sh2}, \bar{f}_{y2})$  to ultimate (or rupture) average strain and strength point  $(\bar{\epsilon}_u, \bar{f}_u)$ . This final point trends to the actual rupture strain and stress of the naked bar when the reinforcement ratio is greater than the critical reinforcement ratio ( $\rho_{cr}$ ).

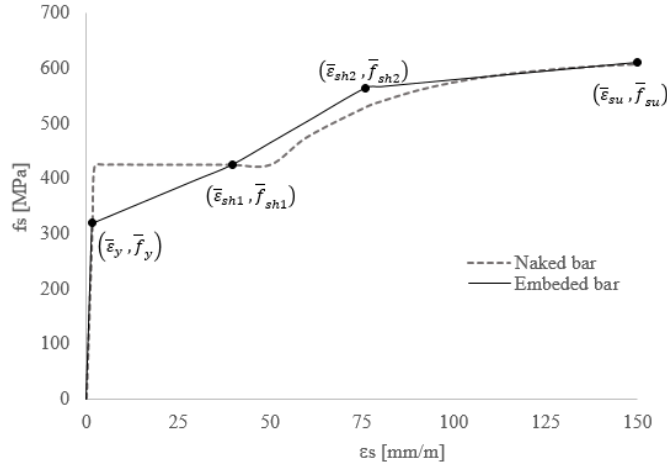


Figure 2.18. Models for “Embedded” mild steel reinforcement bars

The multilinear model proposed by Maekawa et al (2003) is built by following equations 27a through 27d.

$$f_s(\epsilon) = E_s \epsilon \text{ for } \epsilon \leq \bar{\epsilon}_y \quad \text{..Eq (27a)}$$

$$f_s(\epsilon) = \bar{f}_y + \left( \frac{\epsilon - \bar{\epsilon}_y}{\bar{\epsilon}_{sh1} - \bar{\epsilon}_y} \right) (\bar{f}_{y1} - \bar{f}_y) \text{ for } \bar{\epsilon}_y < \epsilon \leq \bar{\epsilon}_{sh1} \quad \text{..Eq (27b)}$$

$$f_s(\epsilon) = \bar{f}_{y1} + \left( \frac{\epsilon - \bar{\epsilon}_{sh1}}{\bar{\epsilon}_{sh2} - \bar{\epsilon}_{sh1}} \right) (\bar{f}_{y2} - \bar{f}_{y1}) \text{ for } \bar{\epsilon}_{sh1} < \epsilon \leq \bar{\epsilon}_{sh2} \quad \text{..Eq (27c)}$$

$$f_s(\epsilon) = \bar{f}_{y2} + \left( \frac{\epsilon - \bar{\epsilon}_{sh2}}{\bar{\epsilon}_u - \bar{\epsilon}_{sh2}} \right) (\bar{f}_u - \bar{f}_{y2}) \text{ for } \bar{\epsilon}_{sh2} < \epsilon \leq \bar{\epsilon}_u \quad \text{..Eq (27d)}$$

The formulas to estimate the yielding average stress point  $(\bar{\varepsilon}_y, \bar{f}_y)$ , are given in equation 28a and 28b. The formulas to estimate the first intermediate hardening, the second hardening point, and the rupture (or final) point are given in Equation 29, 30 and 31, respectively. However, the formulas to obtain all the additional factor in those equations will not be reproduce for space limitation, and they can be consulted in Maekawa et al (2003).

- Yielding Average strain Point

$$\bar{f}_y = f_y \left[ 1.0 - \left( \frac{\rho_{cr}}{2\rho} \right) \right] \quad \text{Eq (28a)}$$

$$\bar{\varepsilon}_y = \bar{f}_y / E_s \quad \text{Eq (28b)}$$

Where  $\rho_{cr} = \frac{f_{cr}}{f_y}$

- First Hardening point

$$\bar{\varepsilon}_{sh1} = \left( g + h \frac{\varepsilon_{sh}}{\varepsilon_y} \right) \varepsilon_y k_\rho k_{u/y} \quad \text{Eq (29a)}$$

$$\bar{f}_{y1} = \bar{f}_y + (f_y - \bar{f}_y) \phi \quad \text{Eq (29b)}$$

- Second Hardening Point

$$\bar{\varepsilon}_{sh1} = \left( \frac{\bar{\varepsilon}_{sh1} + \bar{\varepsilon}_u}{2.5} \right) \quad \text{Eq (30a)}$$

$$\bar{f}_{y2} = 1.02 \left[ \bar{f}_{y1} + \left( 1 - e^{\left( \frac{\bar{\varepsilon}_{sh1} + \bar{\varepsilon}_u}{2.5} \right)} \right) (1.01 f_u - \bar{f}_{y1}) \right] \quad \text{Eq (30b)}$$

- Rupture or ultimate stress point

$$\bar{f}_u = \left[ \frac{0.993 + 0.22 \left( \frac{f_u}{f_y} \right)^{-3}}{\left( \frac{\rho}{\rho_{cr}} \right)^2} \right] f_u \quad \text{Eq (31a)}$$

$$\bar{\varepsilon}_u = \bar{\varepsilon}_{sh1} - k * \ln \left( 1 - \frac{\bar{f}_u - \bar{f}_{y1}}{1.01 \bar{f}_u - \bar{f}_{y1}} \right) \quad \text{Eq (31b)}$$

## 2.2.4 Basic concepts of plasticity for concrete materials

According to Chen (1982) there are two basic theories to develop appropriate constitutive equations for plastic materials as concrete: the total-strain or also called deformation theory; and the flow or also called incremental theory. The Concrete Damage Plasticity (CDP) model for concrete materials in Abaqus for example, is based on the flow theory. For this reason, the basic concepts of theory of plasticity, as well as some basic concepts of continuum mechanics will be remembered first. Among those mechanics basic concepts are: the definition of the effective stress tensor, the hydrostatic stress tensor and the deviatoric stress tensor. Regarding the flow theory, which is also known as the incremental flow theory, there are three concepts that must be settled: a) the initial yielding surface shape, b) the hardening rule concept, and c) the rule of plastic flow concept. Each one of these concepts will be explained after providing some explanation about the generalities of the plasticity theory.

### *Flow theory*

In accordance to the incremental flow theory, the total strain in a point inside a stressed body can be represented by the sum of the elastic strain ( $\boldsymbol{\varepsilon}^{el}$ ) plus the plastic strain ( $\boldsymbol{\varepsilon}^{pl}$ ), as shown in Equation 32a. Now, the Effective Stress ( $\bar{\boldsymbol{\sigma}}$ ) is defined as the multiplication of the fourth order stiffness tensor ( $D_0^{el}$ ), and the subtraction of the elastic strain minus the plastic strain as show in Equation 32b.

$$\boldsymbol{\varepsilon}^{tot} = \boldsymbol{\varepsilon}^{el} + \boldsymbol{\varepsilon}^{pl} \quad \text{..Eq (32a)}$$

$$\bar{\boldsymbol{\sigma}} = D_0^{el} : (\boldsymbol{\varepsilon}^{el} - \boldsymbol{\varepsilon}^{pl}) \quad \text{..Eq (32b)}$$

The effective stress tensor can be also represented into two parts: The hydrostatic part ( $\sigma_m \mathbf{I}$ ), and the deviatoric part ( $\bar{\mathbf{S}}$ ), as shown in Equation 33a. The hydrostatic part is represented by the unit tensor ( $\mathbf{I}$ ) multiplied by an scalar quantity known as the hydrostatic pressure ( $\sigma_m$ ). The hydrostatic pressure ( $\sigma_m$ ) is nothing else that the average of the axial stress in the effective stress tensor, or is simple terms  $1/3(\sigma_1 + \sigma_2 + \sigma_3)$ . Therefore, the deviatoric part of the stress tensor ( $\bar{\mathbf{S}}$ ) can be found as the subtraction of the effective stress tensor minus the hydrostatic part ( $\sigma_m \mathbf{I}$ ) of the effective stress tensor ( $\bar{\boldsymbol{\sigma}}$ ) as shown in equation 33b.

$$\bar{\sigma} = \sigma_m \mathbf{I} + \bar{\mathbf{S}} \quad \text{..Eq (33a)}$$

$$\bar{\mathbf{S}} = \bar{\sigma} - \sigma_m \mathbf{I} \quad \text{..Eq (33b)}$$

### The Haigh-Westergaard Stress space

A geometric representation of the hydrostatic and deviatoric parts of the stress tensor are given in Figure 2.19. First, it is convenient to point out that the stress space in Figure 2.19 is defined by a set of three coordinate axis, which coincides with the three principal stresses ( $\sigma_1, \sigma_2, \sigma_3$ ) and are perpendicular to each other. This space is known as the *Haigh-Westergaard Stress space*. In other words, instead of using the conventional coordinated system defined by three arbitrary vector basis ( $x_1, x_2, x_3$ ), the Haigh-Westergaard space uses the axis of the principal stresses ( $\sigma_1, \sigma_2, \sigma_3$ ) as the coordinated axis.

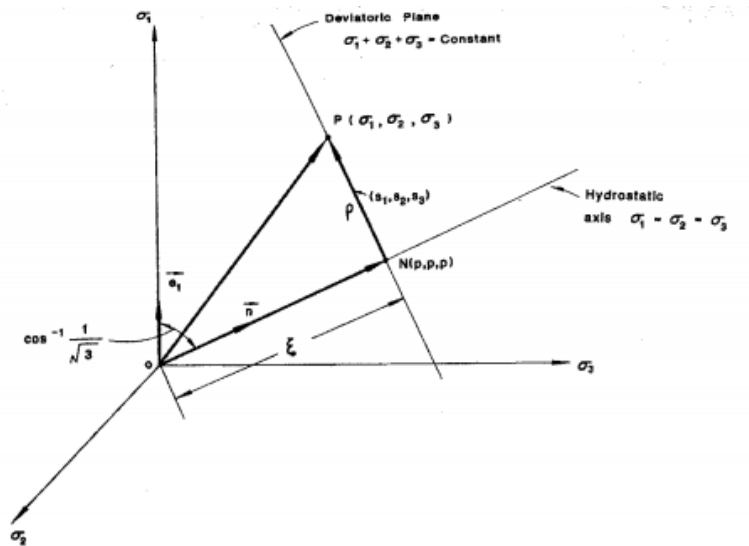


Figure 2.19. Hydrostatic and Deviatoric part of the Stress tensor. Taken from Chen and Han (2007)

An arbitrary point (P) in the Haigh-Westergaard represents the state of stress of a material point in an stressed body, as shown in Figure 2.18. If the point P, is represented by the vector OP, this vector can be represented by a *hydrostatic part* and a *deviatoric part*. The hydrostatic part (ON), is the projection of the vector (OP) along the hydrostatic axis, which is the line formed by all the points under the condition of  $\sigma_1 = \sigma_2 = \sigma_3$ . As noted, the hydrostatic axis has the same director

cosines with respect to all coordinate axis. In other words, the hydrostatic part can be defined as the dot product between the OP vector and the hydrostatic axis. On the other hand, the deviatoric part can be found as the vector subtraction of the original state of the principal state of stresses, represented by the vector (OP) minus its corresponding hydrostatic part, represented by the vector ON. A deviatoric plane, therefore, is characterized for not having any normal stress in its plane, representing thus, a state stress of pure shear. As a physical interpretation, the hydrostatic part of the tensor is associated with the axial strains and controls the change in volume of the finite element, while the deviatoric part is associated with the shear stresses and governs the distortion of the element.

**The Yield Surface Concept**

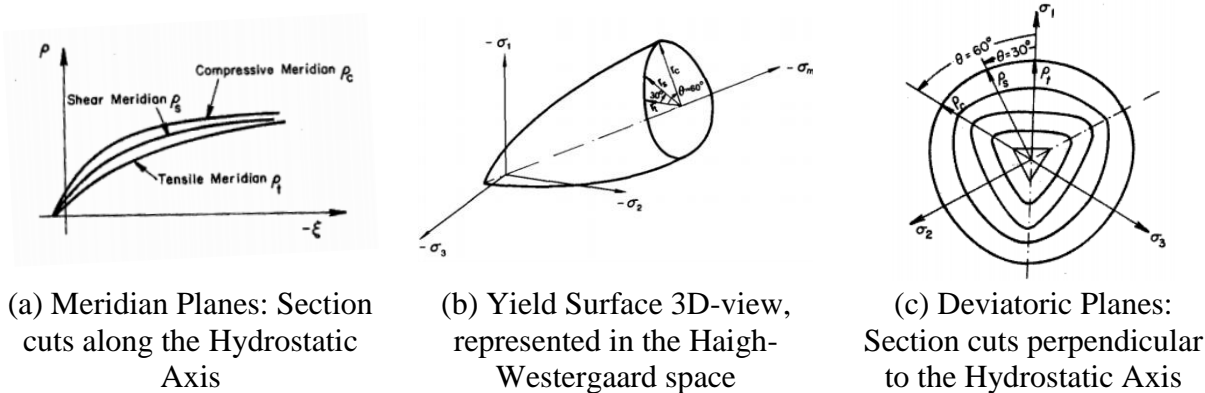


Figure 2.20. Hydrostatic and Deviatoric part of the Stress tensor. Taken from Chen and Han (2007)

A yield surface can be understood as a scalar field that is given in terms of the invariants of the Effective Stress Tensor. Since the yield surfaces are given in terms of the principal stresses, they can be better visualized and interpreted in the Haigh-Westergaard space, as shown in Figure 2.19b. For concrete materials (contrary to metallic materials) an appropriate yielding surface must be pressure dependent. It means that the yield surface change in function of the hydrostatic pressure. In Figures 2.19b and 2.19c, it is clear how the surface expands as the hydrostatic pressure increases. From a physical point of view, any element (or finite element) with a state of principal stresses located inside this yielding surface is considered to behave as elastic. On the other hand,

if the state of principal stresses is represented by point that is located outside the yield surface, it implies the material point is in the plastic range.

**The Hardening Rules (or loading Functions)**

The hardening rule defines how the yield surface changes in shape and size as the plastic deformations increase. The three typical hardening rules are: The isotropic rule, the kinematic rule and the mixed rule. Figure 2.20 gives the graphic representation of each hardening rule in a Bi-dimensional state of principal stress  $\sigma_1$  and  $\sigma_2$ .

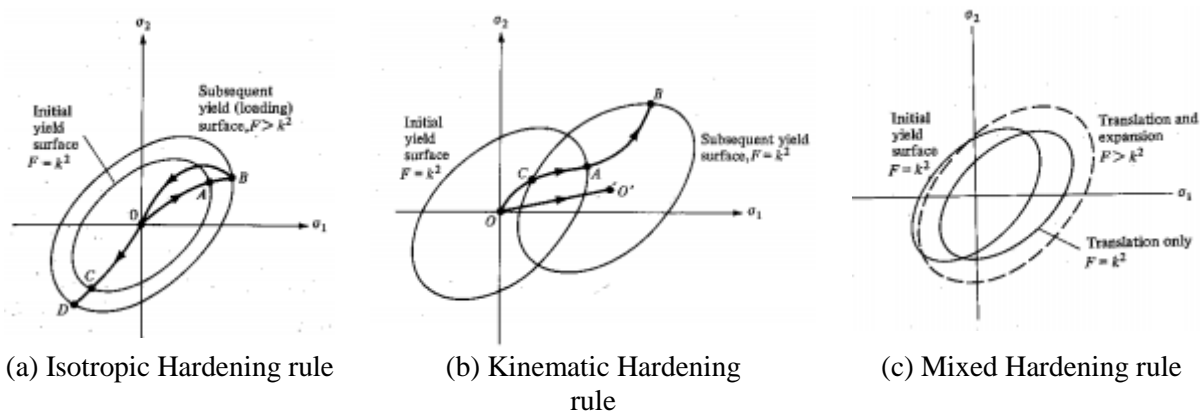
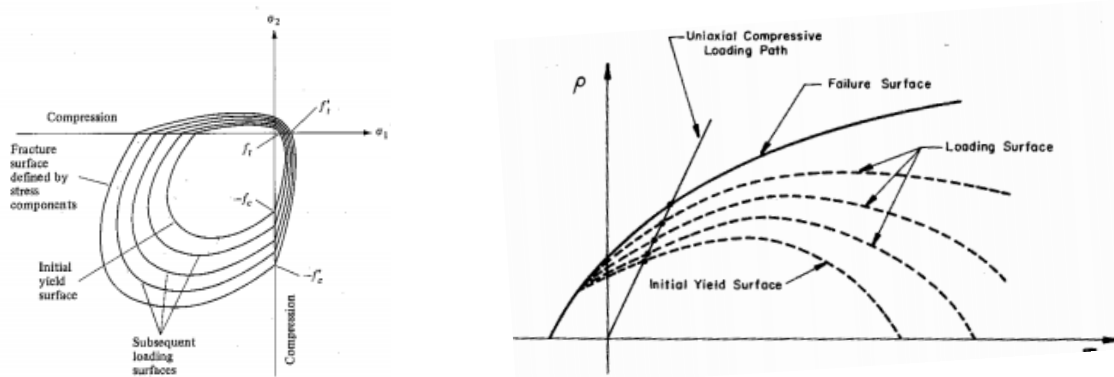


Figure 2.21. Hardening Rules Representations in bi-dimensional stress. Taken from Chen and Han (2007)

In the Isotropic hardening, in accordance with Figure 2.20a, the initial yield surface only expands but not rotates or distorts. This hardening rule is only suitable for monotonic application where the Bauschinger effect can be neglected. In the kinematic hardening, the initial yield surface keeps its original shape (do not distorts) but shift its origin to another position. In other words, the yield surface does not expand or distort but only translate. In the kinematic hardening, represented in Figure 2.20b, the Bauschinger effect can be partially captured and therefore it is suitable at some extent for cyclic loading applications. The mixed hardening combines the Isotropic and Kinematic assumptions. This means that the initial yield surface not only expands but also translates from its original position. The mixed hardening rule, represented in Figure 2.24c, is the most suitable for concrete materials.

Figure 2.20a shows typical loading functions for steel materials in bi-axial stress. In steel materials, the initial yield surface in tension are the same as the initial yield in compression if the Bauschinger effect is neglected. However, a graphic representation of work-hardening or hardening rule for concrete applications is given in Figure 2.21b. In concrete applications, the failure in tension substantially differs to the failure in compression. Figure 2.21b shows the initial yield surface, the subsequent loading surfaces (surfaces after initial yield surface), and the final failure surface. Figure 2.25a shows the yield surface and the loading surfaces in a bi-axial state of stresses, while Figure 2.25b shows the surfaces in a triaxial state of stresses but in a meridian plane.



(a) Hardening rule in a bi-axial state of stress for concrete materials

(b) Hardening rule in tri-axial state of stress for concrete materials, represented in a meridian plane.

Figure 2.22. Biaxial and Triaxial state of Hardening with non-associated flow rule for concrete applications.

In Figure 2.21a, it was assumed that the subsequent loadings as well as the final failure surface follows a similar shape to the initial yield surface. When this hardening rule is assumed, it is said that the material has an associated flow rule (the concept of flow rule will be explained later). However, according to Chen and Han (2007) this assumption is not in agreement with the most recent experimental research, in which it has been he found that the failure surface in concrete members do not necessarily follows the same path and the same shape of the initial yield surface. From figure 2.21b, on the other hand, it is clear that the initial yield surface has a close shape, whereas the subsequent failure surfaces start to open. The intermediate surfaces (or loading surfaces) stars to open change its size as the hydrostatics pressure increases. Figure 2.21b gives an example of a material with non-associated rule flow, which is more in agreement with experimentation in concrete materials.

### ***The Flow rule***

Once a material point reaches the initial yield surface, the material enters in a state of plastic flow if additional stresses or loads are induced. The plastic flow can be represented by the concept of the flow rule. In this concept, the plastic-strain-increment vector  $\dot{\boldsymbol{\epsilon}}^{pl}$  and the subsequent loading surface are related through a plastic potential function (G). The definition of a plastic potential function, similar to the definition of yield surface, is also given in terms of the invariants of the effective stress tensor. According to Lubliner et al (1989), a potential plastic flow is useful to capture the change in volume of the material (concrete in this case) when it is subjected to large inelastic or plastic deformations. Equation 34 defines the flow rule for the material when it is experiencing work-hardening, or in other words, when it is stressed beyond the initial yield surface limit.

$$\dot{\boldsymbol{\epsilon}}^{pl} = \dot{\lambda} \frac{\partial G(\bar{\boldsymbol{\sigma}})}{\partial \bar{\boldsymbol{\sigma}}} \quad \text{..Eq (34)}$$

In Equation 34,  $\dot{\boldsymbol{\epsilon}}^{pl}$  is known as the plastic strain increment vector that defines the change of the loading surfaces as the plastic strains continues.  $\dot{\lambda}$  is always positive scalar known as the hardening parameter or the plastic consistency parameter according to Lee et al (1998), and it controls the length (or magnitude) of the plastic-strain-increment vector ( $\dot{\boldsymbol{\epsilon}}^{pl}$ ). On the other hand,  $\frac{\partial G(\bar{\boldsymbol{\sigma}})}{\partial \bar{\boldsymbol{\sigma}}}$  is the gradient of the flow rule with respect to the effective stress tensor, and it defines the direction of the plastic-strain vector.

### **2.2.5 The modified Compression Field Theory**

The Modified Compression Field Theory (MCFT) is the theoretical foundation for the Shell-2000 software developed by Bentz (2000). In the MCFT, the un-cracked and the cracked concrete are treated as different materials. The cracked concrete is treated as an orthotropic material and the smeared crack rotating approach is adopted to determine the cracks orientation. The MCFT is intended for RC panels subjected to membrane (or In-plane) forces. Among the main assumptions of the MCFT is that equilibrium of forces, the compatibility of strain between the reinforcement and concrete, and the stress-strain relationship are done in term of average stress and average strain.

By average, it must be understood that both, strain and stress are measured assuming a large distance inside the panel, in such a way that several cracks are crossed, and it allows to average the strain and the stresses in the concrete and the reinforcement. As additional explanation of this concept is given in Figure 2.23. Figure 2.23a illustrates the “average” stress of a concrete plane between two cracks, while figure 2.22b shows the “averaged” stress on the surface of a crack. In the first case (stress in the middle of two cracks) the tensile stress in the concrete are higher than the average, whereas in the second case (stress on the surface), the tension stress can be considered as zero. In the second case, in which the cut is in the vicinity of the crack, the stress in the reinforcement is higher than in the first case.

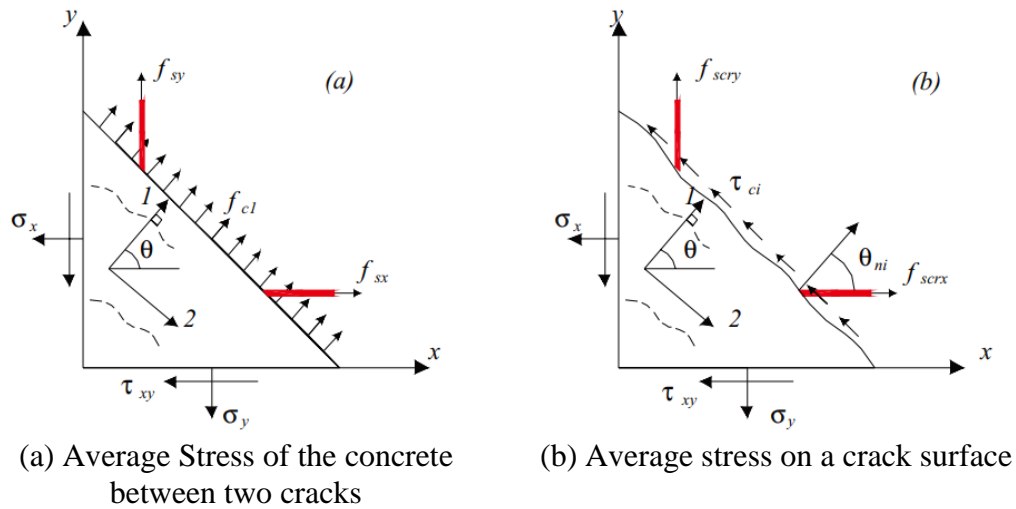


Figure 2.23. Average Stress of the concrete between two cracks and Average stress on a crack surface. Taken from Menin et al (2009)

In addition to the concepts of average stresses and strains, the MCFT is based in three basic principles: 1. deformation compatibility relationship for the average strains in the concrete and steel reinforcement; 2. equilibrium of forces between the average stress in concrete and reinforcement; and 3. constitutive relationship between cracked concrete and reinforcement represented by the tension stiffening. Other important assumptions of the MCFT theory are the followings: The reinforcement is distributed uniformly over the panel; there is perfect bonding between reinforcement and concrete ; and finally, the direction (or angles) of the principal stresses are assumed to coincide with the direction of the principal strains.

### ***Deformation Compatibility Relationship***

The MCFT assumes full compatibility of deformation (or full bond) between concrete and reinforcement. Thus, the total deformation in x-direction and y-direction is the same for the concrete and for the reinforcement as given by the equations 35a and 35b, respectively.

$$\varepsilon_x = \varepsilon_{cx} = \varepsilon_{cx} \quad \text{Eq (35a)}$$

$$\varepsilon_y = \varepsilon_{cy} = \varepsilon_{cy} \quad \text{Eq (35b)}$$

Assuming a value of shear strain ( $\gamma_{xy}$ ), and by using the well know morh's circle it is possible not only to find the principal strain in tension and compression for the concrete, but also its associated direction ( $\theta$ ). Equation (36a) gives the magnitude of the principal strain for the concrete in tension and compression, while equation (36b) defines the orientation. The principal strains, as well as the its associated directions are function of the axial strains ( $\varepsilon_x$  and  $\varepsilon_y$ ) and the shear strain ( $\gamma_{xy}$ ).

$$\varepsilon_{c1}, \varepsilon_{c2} = \frac{1}{2}(\varepsilon_x + \varepsilon_y) \pm \frac{1}{2} \left[ (\varepsilon_x - \varepsilon_y)^2 + \gamma_{xy}^2 \right]^{0.5} \quad \text{Eq (36a)}$$

$$\theta = \frac{1}{2} \tan^{-1} \left[ \frac{\gamma_{xy}}{\varepsilon_x - \varepsilon_y} \right] \quad \text{Eq (36b)}$$

### ***Equilibrium of Internal Forces***

Doing summation of infernal forces in the panel according to figure 2.24a, and again using the Mohr's circle in figure 2.24b, the relation between the average principal stresses ( $f_{c1}$  and  $f_{c2}$ ) and the average stress in the concrete ( $f_{cx}$ ) can be found. Equation 37a or 37b gives this relation. It is important to note that these equations are valid because the cracked concrete is considered as an orthotropic material in the direction of the principal stress.

$$f_{c1} = f_{cx} + \frac{\tau_{cxy}}{\tan(\theta)}, \text{ where } f_{cx} = \sigma_x - \rho_{sx} f_{sx} \quad \text{Eq (37a)}$$

$$f_{c2} = f_{cy} + \frac{\tau_{cxy}}{\cot(\theta)}, \text{ where } f_{cy} = \sigma_y - \rho_{sy} f_{sy} \quad \text{Eq (37b)}$$

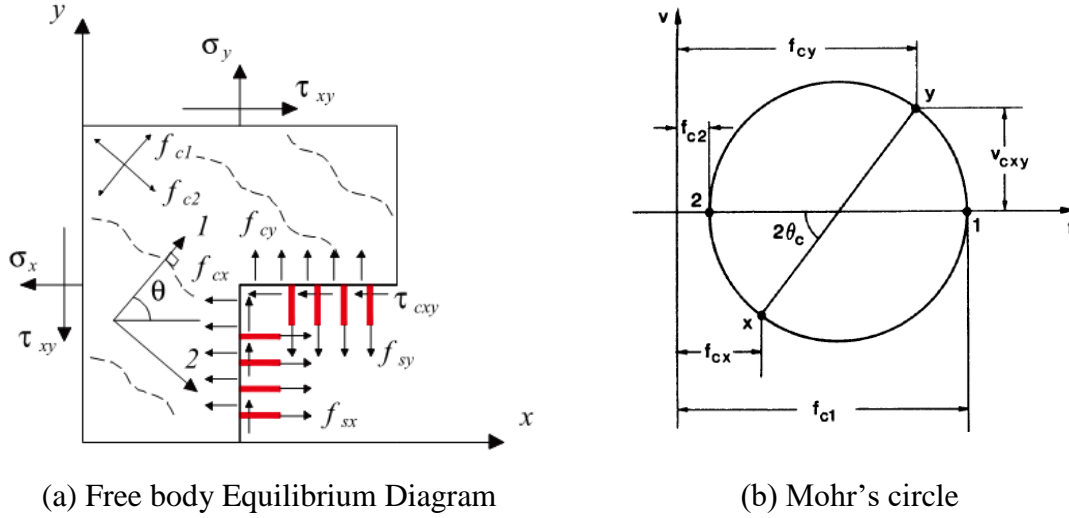


Figure 2.24. Internal Forces and principal stresses. Taken from Menin et al (2009)

### ***Constitutive Material relationship***

As explained before, the MCFT theory follows the smeared cracked theory, and the option to mimic the tension stiffening is included in the concrete. The tension stiffening model used in the MCFT is the model proposed by Vecchio and Collins (1986), given in Equation 38. Like most of the tension stiffening models, the Vecchio and Collins model have two parts: the linear elastic part which is limited by the maximum tensile strain cracking or rupture strain cracking  $\varepsilon_{cr}$  ; and the plastic part which the principal strain exceeds  $\varepsilon_{cr}$  . In equation 38,  $\varepsilon_{c1}$  is the maximum or principal tensile strain,  $E_c$  is the modulus of Elasticity of the concrete,  $f_t$  is the maximum tensile strength of the concrete.

$$f_{c1} = \begin{cases} \varepsilon_{c1} E_c & \text{if } \varepsilon_{c1} \leq \varepsilon_{cr} \\ \frac{f_t'}{1 + \sqrt{200\varepsilon_{c1}}} & \text{if } \varepsilon_{c1} > \varepsilon_{cr} \end{cases} \quad \text{Eq (38)}$$

## **2.3 Software for the Non-linear analysis and modelling of RC members**

### **2.3.1 Abaqus**

Abaqus is a multipurpose commercial software based on finite elements and developed by Dassault, 2013. It can be used to analyze and model any type of solid, such as soils, rocks, concrete, and even fluids subjected to external forces. Several researchers has used it before to model the complex non-linear behavior of different RC structural members such as beams, walls and panels

in a less proportion, as explained in the introduction of the document. Mechanics related problem can be solve by using any the two available solvers in Abaqus. The Abaqus/Implicit solver and the Abaqus/Explicit solver. Abaqus/Implicit is more suitable for static or quasi-static problems, while Abaqus/Explicit is for dynamic problems. Both solvers will be used for the modeling of the RC panels depending on the selected concrete material constitutive model. For example, for RC panels using the Concrete Damage Plasticity (CDP) and the Brittle Failure Cracking (BFC) models, the explicit solver will be used, while for RC panel using the Smeared Concrete Cracked (SMC) model, the implicit solver will be used.

The construction of the numerical models in Abaqus are more time consuming and cumbersome than in Shell-2000 (especially for novice users). This is one of the disadvantages of Abaqus regarding Shell 2000. However, Shell-2000 is more limited, not only because it is as sectional analysis software and not as finite element package, but also because the constitutive material models (either for concrete or steel reinforcement) are predefined and cannot be modified. It is worthy to mention that the selection of the concrete material model in Abaqus (CDP, BFC or SMC) requires not only of a better understanding of solid mechanics, but also a better lecture of the failure mode and the loading application forces over the panels during experimentation. The more relevant aspects for the modelling of the RC panels in Abaqus are the choosing of the finite Elements, the loading application procedure, and the material constitutive models for the concrete. Each one of these aspects will explained next.

### ***The selected finite elements in Abaqus***

Two types of models were developed in Abaqus: 2D shell models for the modeling of the SM and the PV series panels; and 3D solid models for the SP series panels. The Shell element identified as S4R, which is a 4-node doubly curved general-purpose shell with reduced integration and hourglass control was used for the 2D models. A representation of the S4R element is given in Figure 2.25a. The S4R is a Layer Composite Shell (LCS) element which allows to simulate sections with different material properties as is the case of the reinforced concrete. A very important feature and limitation of the LCS elements is that they enforce full deformation compatibility between the concrete and the reinforcement. Sener et al (2015), who used the LCS elements for the simulation of an 1:10 scaled Steel Composite (SC) nuclear power plant, also

warned about this limitation. The default amount of five integration points along the thickness of the panel as shown in Figure 2.24b, was assigned to the S4R shell element. The Abaqus manual says that this default amount is enough for most non-linear analysis. In the LCS elements, the reinforcement is modeled (or introduced) as smeared layers. The position of the different reinforcement smeared layers located inside the panels are specified taking as reference the middle plane of the panel as shown in Figure 2.24c. In addition to the location of the reinforcement, Abaqus requests the area per bar and the spacing between them.

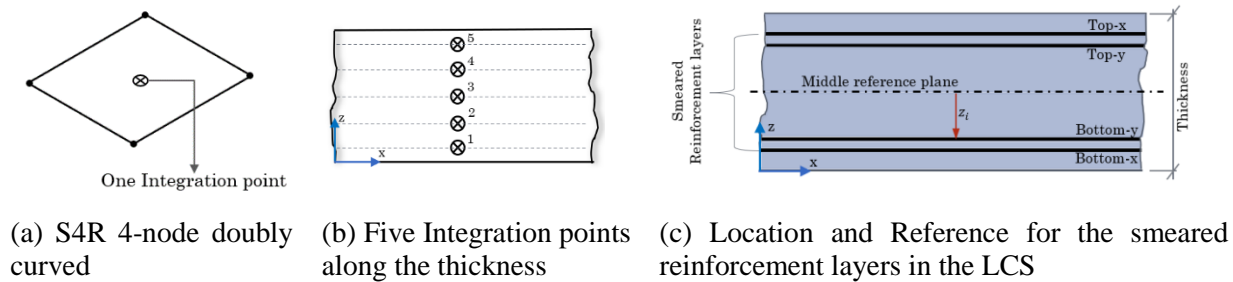


Figure 2.25. The Layer Composite Shell (LCS) SR4 finite element for the 2D Models in Abaqus.

Regarding the 3D solid models, two finite elements were used: the finite element identified as the C3D8R for the modeling of the concrete; and the finite element identified as the B31 for the modeling of the reinforcement bars. The C3D8R is defined in the Abaqus manual as a continuum 8-node linear (or first order) brick with reduced integration and hourglass control. A representation of the C3D8R is given in figure 2.26a. Perhaps the main advantage of the C3DR8 element is the reduction in analysis time since it since it only uses one integration point. However, the main disadvantage of the C3DR8, also associated with its unique integration point, is that they become susceptible to the well-known Hourglassing effect. Sun (2006) said that the Houglassing effect must be controlled because it causes to the element to become very flexible. The Hourglassing effect in all numerical models with the C3DR8 was controlled by using a refined mesh. Not only in the 3D models, but also in the 2D models, the mesh size was 50mm (2in). Finally, the B31 is defined in Abaqus as a 2-node linear beam element. This element makes part of the Timoshenko (or shear flexible) beam types, which can be subjected to very large axial strains. Another important feature of the B31 element is that its transverse shear behavior is independent to the axial stretching and bending. A representation of the B31 element is given in Figure 2.26b.

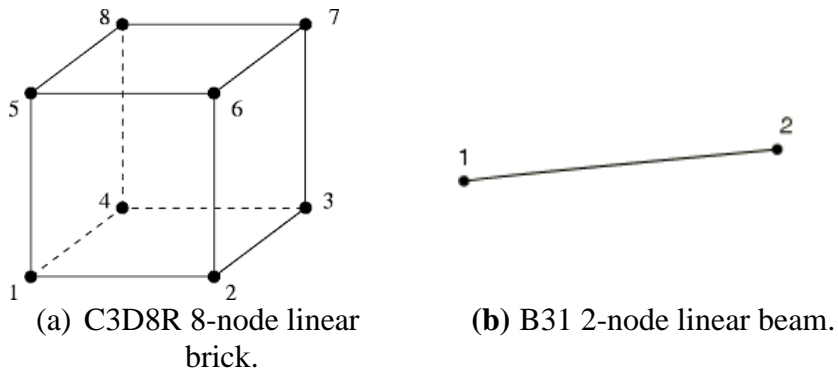


Figure 2.26. The continuum C3D8R and the B31 finite elements for the 3D models in Abaqus.

### ***The loading application Procedure in Abaqus***

Two important aspects were considered when imposing (or reproducing numerically) the loads in the Abaqus models. First is related to selection between deformation or force control procedure; and second, the definition of the load application time. Regarding the first aspect, the out-of-plate bending moment demands were load were simulated by applying deformation control by imposing rotations. The membrane forces (in-plane axial and in-plane shears) were simulated by applying force control procedure. This will be explained in more detail later in a case by case base in chapter 5. The second aspect, definition of the loading application time, define how fast (or how slow) the loads (applied either as deformation or force control) will be applied during the numerical analysis. If the loads are applied too fast, the analysis will be fast, but it will trigger dynamic effects in the response of the numerical which would reduce the accuracy if the models. It is pertinent to mention that all tests analyzed in here can be considered as quasi-static tests which lasted between 1 and 2 days to be completed. If the loads are applied too low, the chances of triggering dynamics effects will be low, but the analysis or running time will be very high, which will make the calibration process very tedious, and inefficient. For most of the 2D numerical models in Abaqus, the time analysis step was set up in 2.0 sec, while for the 3D models it was set in 0.75 sec. For efficiency, mass scaling factors of  $5e^{-6}$  and  $9e^{-6}$  were specified for the 2D and the 3D models, respectively. At the end of each analysis it was verified that the dynamic effect in the response of the models were negligible by keeping the ratio between kinetic energy and the internal deformation energy less than 2%.

### *The constitutive models for concrete materials*

There are three available constitute concrete material models in Abaqus: The Brittle failure Cracking (BFC), the Concrete Damage Plasticity (CDP), and the Smeared Cracking (SMC) models. A brief description of the theory behind each model will be given in this section. Also, an explanation regarding the most sensitive parameters foreach one of those concrete models will be provided. An important difference between the models is that the BFC does not require the definition of the uniaxial compressive behavior of the concrete, whereas the CDP and the SMC models do. The BFC does not require definition of the uniaxial compressive behavior of the concrete because it assumes this behavioral as linear elastic, being this one of its main drawbacks.

#### *The Concrete Damage Plasticity Model (CDP)*

The CDP model in Abaqus is based on theory of plasticity, and specifically on flow theory. The three most important steps in flow theory are the definition of: a) an initial yielding surface shape, b) a hardening rule, and c) a rule of plastic flow. The *yield surface* is given in terms of the vector of plastic deformation,  $\tilde{\boldsymbol{\epsilon}}^{pl} = [\tilde{\boldsymbol{\epsilon}}_c^{pl}, \tilde{\boldsymbol{\epsilon}}_c^{pl}]$ , and the Invariants of the effective stress tensor ( $\bar{\boldsymbol{\sigma}}$ ), as shown in Equation 39, where  $I_1$  is the first invariant (or trace) of the Effective stress tensor, and  $J_2$  is the second invariant of the deviatoric part of the Effective Stress tensor (S).

$$F(\bar{\boldsymbol{\sigma}}, \tilde{\boldsymbol{\epsilon}}^{pl}) = \frac{1}{1-\alpha} [\alpha I_1 + \sqrt{3} J_2 + \beta (\tilde{\boldsymbol{\epsilon}}^{pl}) \langle \bar{\boldsymbol{\sigma}}_{max} \rangle - \gamma \langle \bar{\boldsymbol{\sigma}}_{max} \rangle] - \bar{f}_c(\tilde{\boldsymbol{\epsilon}}^{pl}) = 0 \quad \text{..Eq (39)}$$

A yield surface can be understood as a scalar field that is given in terms of the invariants of the effective stress tensor. Since the yield surfaces are given in terms of the principal stresses, they can be better visualized and interpreted in the Haigh-Westergaard space, as shown in Figure 2.19. The most sensitive parameters to define yield surface in the CDP models are: the  $f_{bo}/f_{co}$  ratio, and the  $K_c$ . This ratio  $f_{bo}/f_{co}$  is related to the constant  $\alpha$  in the yield surface and affects the volume in the hydrostatic axis.  $K_c$  constant is the ratio of the second invariant of the tensile meridian to the second invariant of the compressive meridian, for a specific hydrostatic pressure. The parameter  $K_c$  controls the shape of the yield surface, and its effect is more tangible in a deviatoric plane as shown in Figure 2.20c. It will be expected that for smaller values the material will enter in the elastic regime faster than when introducing larger values.

Abaqus uses a non-associated *plastic flow* for the CDP models. This means that either the loading surface or the failure surface of the concrete have a proportioned shape to the initial yield surface, or in simpler words  $G \neq F$ . The potential plastic flow adopted by Abaqus is the Drucker & Prager model with an hyperbolic approximation is given in Equation 40. Similar to the yield surfaces, the plastic flow potential is also a function of the invariants I1 and J2, which were already explained.

$$G(\bar{\sigma}) = \sqrt{(\epsilon\sigma_{to}\tan\psi)^2 + 3J_2} - \frac{I_1}{3} \quad \text{Eq (40)}$$

The potential plastic flow used in Abaqus for the CDP models is the Drucker and Prager model (1952) with a Hyperbolic shape as shown in figure 2.25. The most sensitive parameters to define this potential are: the angle  $\beta$ , the distance  $d'$  and the eccentricity  $e$ . the angle  $\beta$  is known as the dilatancy angle, and it defines the slope in the meridian plan p-q of the plastic flow surface (G). The meridian p-q plane is the equivalent compressive meridian in the yield surface. The parameter  $d'$  is the cohesion and it is the corresponding shear strength of the material when there is no hydrostatic pressure ( $\sigma_m=0$ ). Finally, the eccentricity ( $e$ ), controls the behavior of the potential flow at positive small and hydrostatic pressure. The eccentricity is defined as the ratio between the cohesion ( $d'$ ) and the tangent of the dilatation angle ( $\beta$ ). It is also important to clarify that this potential assumes an associated plastic in the deviatoric plane, but a non-associated plastic in the meridian planes of the surface.

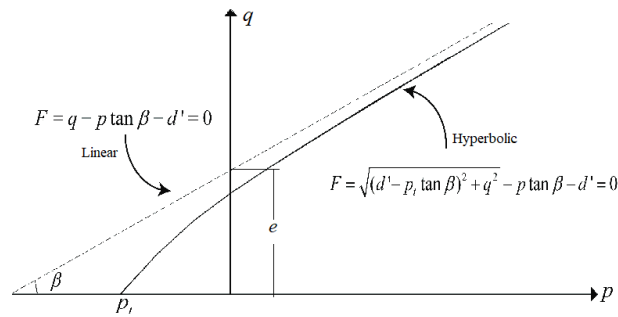


Figure 2.27. The Drucker & Prager flow rule on a Meridian plane of the yield surface.

### *The Brittle Failure Cracking Model (BFC)*

The Brittle Failure Cracking Model (BFC) for concrete materials in Abaqus is mainly intended for cases in where the behavior or failure mode of the RC members (in this case RC

Panels) is governed by tensile cracking. A brittle failure mode, with a sudden loss in strength after maximum capacity is associated with panels controlled by tensile cracking. This model assumes a linear elastic behavior for the concrete in compression, which is its most sensitive disadvantage. However, in cases where the failure of the specimen is brittle and governed by tensile cracking, this assumption is acceptable. One of advantages of this model is that it allows to remove (or delete) elements with excessive distortion (after reaching a predefined cracking criterion) which reduce convergence issues during the analysis. Another advantage of this model is that it assumes the concepts of fracture energy to relate the formation and propagation of new cracks in the concrete. The inclusion of fracture energy concepts besides facilitates the crack formation detection and is appropriate because it makes the analysis not be very sensitive to the mesh size. Finally, it must be mention that BCF is only available for the Abaqus/Explicit solver.

The BFC for concrete in Abaqus uses the smeared cracked model approach, which is combined with fracture-mechanics concepts. Abaqus employs the fixed crack model (or fixed-multidirectional) approach to account for the effect of the cracked concrete. The BFC concrete models allows to simulate the tension stiffening for reinforced concrete members, or the tension softening for un-reinforced members, although it is more intended for the latter ones. The tension softening in Abaqus can be introduced in the conventional form of stress vs strain (or cracking strain) or in terms of stress vs cracking displacement. For un-reinforced members, it is recommended to set the tension softening in terms of stress vs displacement rather that stress vs strain.

A very important aspect to take in account with the fixed crack models is that due to the potential misalignment between the principal direction and the initial fixed cracking direction, additional shear stresses rises along the crack surfaces. Rots and Blaauwendraad (1989) indicated that in smeared crack models stress-locking may rise, and the stiffness of the specimen may be overestimated. A way to alleviate this increment in shear stiffens is to introduced shear retention model, which can be explained in Figure 2.28, and is available for BFC models. The shear retention model defines at what rate the shear stiffness of the RC members degrades as the cracks opens. The shear retention model can be defined as a piecewise linear form or in a power law form, being this latter one the chosen option in this study.

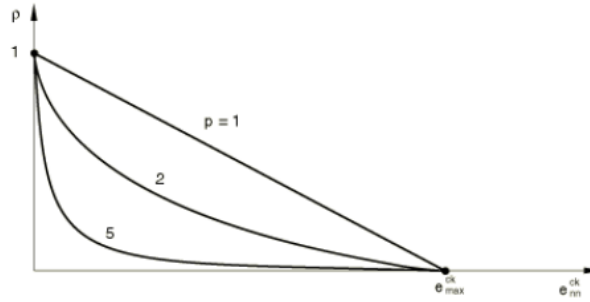


Figure 2.28. Definition of the Shear Retention according to power law in Abaqus.

The main parameters to define the shear retention model in this option are the power law factor ( $\rho$ ) and the ultimate cracking displacement/strain ( $e$ ). The power factor ( $\rho$ ) accounts for the rate of drop of the shear modulus ( $G$ ) in function of the cracking displacement/strain. The maximum displacement/strain cracking is function of the compressive strength of the concrete, the size of the aggregate, and the diameter of the reinforcement bars among others. The failure criteria is associated with the required number of cracks needed to remove a concrete element once the cracking displacement/strain (failure value) has been reached. Three failure criteria can be specified: Unidirectional, Bidirectional and Tri-directional. For the case of the RC panel no more than two cracks (or bidirectional criterion option) can be selected.

### *The Smeared Crack Mode (SMC)*

This model is called as an inelastic constitutive model for concrete in Abaqus. As its name indicates, it uses a smeared crack model to simulate the response of the cracked concrete. This model, as same as the BFC is more intended for members whose behavior and or failure mode is controlled by cracking. The SMC model might be seen as a combination of the BFC and CDP models. However, in contrast to the BFC, the smeared cracked model does not assume a linear-elastic behavior of the concrete in compression, which offers an interesting alternative when the specimen experiences high compressive stresses. The compression behavior in the SMC model is also defined by a typical uniaxial compressive curve in terms of the plastic deformations. Like the CDP model, the SMC proposes a plastic surface to simulate the nonlinear behavior of the concrete but defined by more coarse elasto-plastic model. This coarse elasto-plastic model is not as accurate as the CDP model, and it must be used with precaution being aware of its limitations.

$$f_c = \frac{1}{3}\sqrt{3}\alpha_o I_1 + \sqrt{3J_2} - \sqrt{3}\tau_c = 0 \quad \text{Eq (41)}$$

Where,

$$\alpha_o = \sqrt{3} \frac{1 - r_{bc}^\sigma}{1 - 2r_{bc}^\sigma} \text{ where } r_{bc}^\sigma = \frac{\sigma_{bc}^u}{\sigma_c^u} \approx 1.16$$

$$I_1 = \text{trace}(\bar{\sigma})$$

$$J_2 = \frac{1}{2}(\bar{s} : \bar{s})$$

$\tau_c$ : Yield Stress in state of pure shear

The main difference between the coarse elasto-plastic SMC model of and the more accurate CDP plasticity model are: 1. the yield surface is assumed linear and follows the coulomb model, as shown in Figure 2.27; 2. it assumes an associated rule flow, which is not consistent with the real behavior of the concrete, and usually over predict the capacity of the RC members; 3. The tensile yield surface, which controls the cracking behavior is also assumed to be linear and not parabolic as in the CDP model. Another important difference regarding the yielding surface of the smeared crack model is that it is given in terms of the first ( $I_1$ ) and second invariant ( $J_2$ ) of the stress tensor, as can be seen if equation 41. The parameter  $\lambda$ , and  $K_c$  that appears in the CDP model, which control the yield surface shape when the element is subjected to tri-axial compressive stress are omitted in this SMC model. Although this limitation may seem very drastic, it is important to clarify that most of the walls or panels even in industrial facilities, as in other kind of buildings are not subjected to tri-axial compressive stress, which may offer a good approximation.

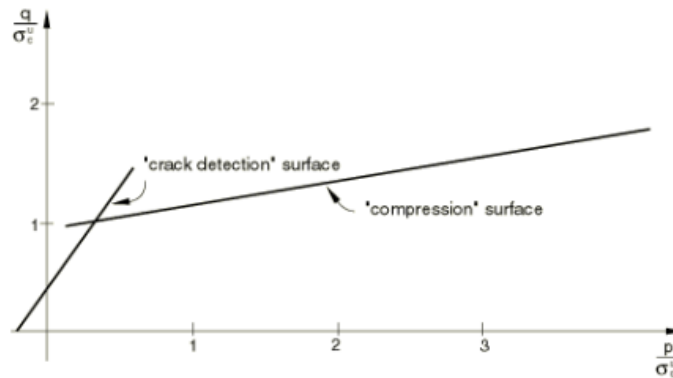


Figure 2.29. Approximate Yield surface used in the Smeared Crack Model in Abaqus

The first step to define a SMC model in Abaqus is to specify a set four ratios. These four ratios are: ratio 1, which is the ultimate biaxial compressive stress to the ultimate uniaxial compressive stress; ratio 2, which is the absolute value of the ratio of the uniaxial tensile stress at failure to the ultimate uniaxial compressive stress; ratio 3, which is the ratio of the magnitude of a principal component of plastic strain at ultimate stress in biaxial compression to the plastic strain at ultimate stress in uniaxial compression; and ratio 4, which is the ratio of the tensile principal stress at cracking, in plane stress, when the other principal stress is at the ultimate compressive value, to the tensile cracking stress under uniaxial tension. After that, the shear retention factor and tensile criteria failure must be specified. Although not mandatory, the shear retention factor in the SMC model is set up similarly to the shear retention factor in the BFC models.

The smeared cracked model will be used for those RC panels that failure in a brittle mode with high compressive stress. Although the BFC models will be used in first place for these type of panels, it will be verified if the compressive strains or stresses do not exceed the elastic compressive limit of the concrete (i.e.  $0.30f_c$  or 0.001 for stress and strain limit, respectively). If the elastic limit of the concrete in compression is exceeded, then the SMC models will be used. It is also important to mention that the Smeared cracked also allows to define a shear retention model as same as the MFC model, already explained. One of the disadvantages of the Smeared cracked models, which used implicit solvers is that is lack of numerical convergence, which produces a premature stop during the analysis.

### **2.3.2 Shell-2000**

Shell-2000 is a sectional analysis software developed by Bentz (2000). This software was intended for the analysis, design and modeling of RC shell elements subjected to in-plane and out-of-plane force simultaneously. Shell-2000 is based in the Modified Compression Field Theory (MCFT) proposed by Vecchio and Collins (1986), and it has been corroborated against experimental results with satisfactory results. For example, Bentz (2000) simulated the shear capacity of square RC panels, tested by Adebar 1984, which were subjected to out-of-plane shears; and the results experimental result of Kirschner (1986), who tested RC panels subjected to axial and bending moment. Similarly, Polack and Vecchio (1994), also reproduce analytically the experiential response of 4 large-scale RC shell elements subjected to the combined action of in-

plane shear and axial forces. Coronado et al. (2014) used this software in its analytical research, where they computed demand capacity to demand ratio (CDRs) by considering the different analyses seismic methods and design approaches.

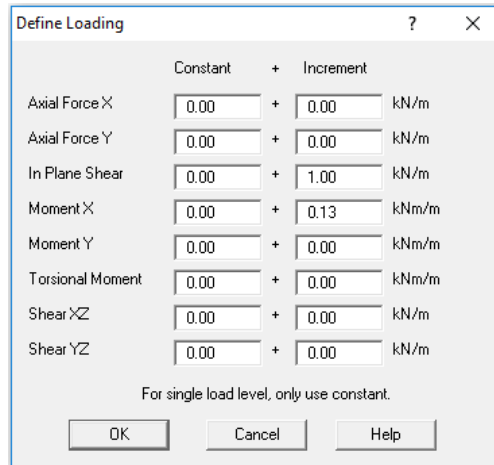


Figure 2.30. Input for the Loading combination in Shell-2000

The main advantages of Shell-2000 with respect to Abaqus is that not only the material constitutive models for concrete and reinforcement are already predefined, but also the loading application procedure. These two advantages facilitates the development of the non-linear numerical models in Shell-2000. The base curve for the concrete in compression in Shell 2000 follows the Popovic's curve model, and the tension stiffening model in Shell 2000 is the tension stiffening model proposed by Bentz (2000). Since Shell-2000 was specifically intended for the analysis of RC panels, it is very easy to apply incremental and proportional loading for more than one load, which is in agreement with the RC tested panels studied in this report. Figure 2.30 shows how to assign the loads at which the panels are being subjected in Shell-2000. First, to indicate that the loads are being applied incrementally, they must be introduced under the increment column (or vector). After that, the user input the magnitudes of the corresponding forces (i.e.  $N_x$ ,  $N_y$ ,  $M_x$ ). As an example, Figure shows the load combination of panel SE7 tested by Kirscher and Collins (1986), which was subjected to axial forces ( $N_x$  and  $N_y$ ) plus bending moment about the x-axis ( $M_x$ ). It is useful to mention that the magnitude of the load can be also introduced in relative terms instead of using the actual magnitude values. It is, instead of typing 235kN-m/m for the bending

moment ( $M_x$ ) and 1810 kN/m for the in-plane shear, it is also valid to input 0.13 and 1.00, which are the relative values that were normalized over the in-plane shear.

Finally, another important difference between Abaqus and Shell 2000 assume different smeared cracks approaches to account for the tension stiffening effect in the concrete. Abaqus assumes Smeared fixed rotating models, while Shell 2000 assumes smeared rotating crack models. In the smeared rotating models, it is not necessary to define a shear retention behavior as in the cases of fixed cracked models, since the direction of the cracks co-rotates with the principal directions and therefore no additional shear stresses rise along the crack surfaces. By using Shell 2000 will allow to indirectly evaluate which of the two smeared crack approaches (rotating or fixed) will be more accurate in capture the behavior of the panels. No additional explanation regarding the theory behind Shell 2000, nor detail about the construction of the model will be given in this document for the sake of brevity. As mentioned before, this is a very friendly software easy to catch up; and the MCFT theory, upon which this software is based on, has been available for more than four decades ago.

### 2.3.3 Membrane-2000

Membrane-2000 was also developed by Bentz (2000) and its works very similar to Shell 2000. The same background theory and modeling recommendations for Shell 2000 apply to Membrane 2000. The main difference between the Shell-2000 and Membrane-2000 is that this latter only analyzes panels subjected to in-plane or membrane forces (i.e.  $N_x$ ,  $N_y$  and  $N_{xy}$ ) as shown in Figure 2.1. The PV series panels, which subjected to membrane forces only, were modeled in this software.

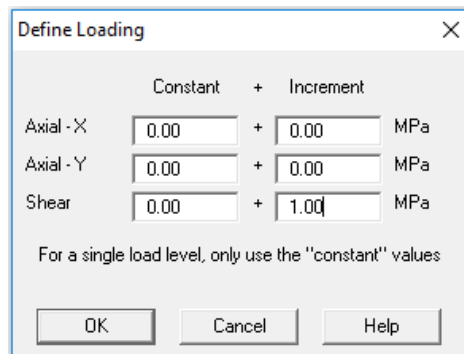


Figure 2.31. Input for the Loading combination in Shell-2000.

### 3. THE ACI-BASED DESIGN PANEL APPROACH

#### 3.1 General Description

The ACI-Panel-Based-Design Approach (PACI) design approach, as its name indicates, is entirely based in the formulation and procedures of the ACI-349 and the ACI-318.2-19 codes. Most of the design considerations of the PACI approach are specified in numeral 19.4 of the ACI-349 and in numeral 6.1 of the ACI-318.2-19 codes. These numerals provide the conceptual design requirements to compute the steel reinforcement in RC shells. The design considerations of the PACI approach can be summarized in *existing design recommendations*; and in *additional design recommendations*. The existing recommendations refer to those recommendations from the ACI 349 and the ACI 318.2-14 codes, while the additional design recommendations refer to those that were incorporated by the author. Figure 3.1 shows the convention that will be utilized to identify the internal design demands in an RC panel, and to apply the formulation of the PACI approach:  $N_x$ , and  $N_y$  are the in-plane axial forces acting in the x and y directions;  $N_{xy}$  is the in-plane shear force;  $M_x$  and  $M_y$  are the out-of-plane bending moments producing axial stresses along the x and y directions;  $M_{xy}$  is the twisting moment, and finally,  $V_{xz}$  and  $V_{yz}$  are the out-of-plane shears.

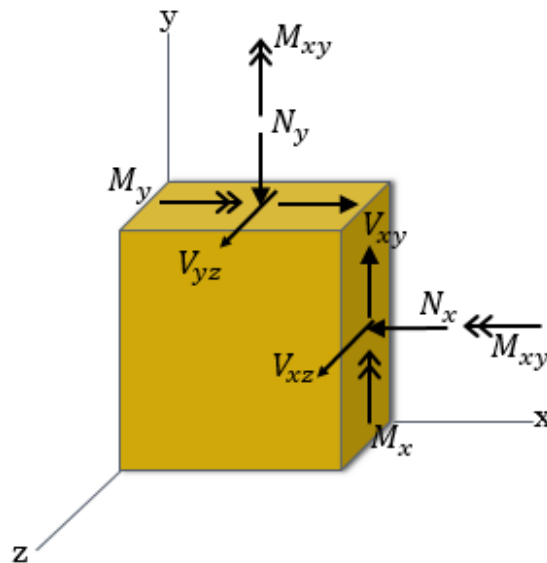


Figure 3.1. Force Convention for the application of the “PACI” Design Approach.

### 3.1.1 Existing Design Recommendations

The existing design recommendations for steel reinforcement of the PACI approach are divided in *general* existing design recommendations from chapter 19 of the ACI 349, and in *specific* existing design recommendations from the ACI 318.2-19. The general design recommendations from the ACI 349 are: a) The tensile strength of the concrete will be neglected to estimate the nominal bending capacity, the in-plane axial and the in-plane shear capacities of the panels, in accordance with the numeral 19.4.1; b) the reinforcement must be provided in at least two directions in accordance with numeral 19.4.2 (also from ACI 318.2-19) in order to account for the large number of load design combinations which also produce several principal stresses difficult to satisfy during the design; and c) the reinforcement required for flexural demands shall be computed considering the axial membrane forces, in accordance to numeral 19.4.3, which implies an axial-bending moment (P-M) interaction procedure between the in-plane axial forces ( $N_x$  and  $N_y$ ) and the out-of-plate bending moments ( $M_x$ ,  $M_y$  and  $M_{xy}$ ). A similar approach, but only applicable for SC walls is in the Design Guide 32 (DG 32) developed by Saahastaranshu and Varma (2017).

The specific existing design recommendations of the PACI approach from chapter 6 of the ACI 318.2-19 are: a) steel reinforcement should be provided to resist the tensile stress produced by the combined action of the in-plane (or membrane) forces and the out-of-plate bending moments ( $M_x$  and  $M_y$ ), and the twisting moment ( $M_{xy}$ ), in accordance to numeral 6.1.1; b) tensile reinforcement should be provided in at least two directions, according to numeral 6.1.2 for the reason previously explained; and c) reinforcement for shear must be computed following chapter 11, while reinforcement for bending must be computed following chapters 11 and 13, in accordance to numeral 6.1.4.; d) the amount of steel reinforcement must be limited in such a way that the reinforcement yield before any crushing of the concrete or buckling of the panel in order to ensure a ductile failure mode of the panel, in accordance to numeral 6.1.5; and e) equal amount of reinforcement must be provided in the outer faces in order to resist the out-of-plate bending demands, even if in one of the two outer faces requires zero or less reinforcement than the opposite face is required, in accordance with 6.1.9. This means that if for example, a reinforcement curtain that is located at the bottom face of the panels and that is running along the x-direction (bot-x) requires less reinforcement than the curtain that is located at the opposite face, top face in this case, and also running in the x-direction (top-x), then, the bot-x curtain will be constrained to have the

same amount of reinforcement required in the top-x curtain. This recommendation can be named as the *same direction opposite face* reinforcement constraint rule.

### 3.1.2 Additional Design Recommendations

There are two additional design recommendations for the application of the PACI approach. One design recommendation for the estimation of the in-plane reinforcement, and another one for the estimation of out-of-plane or Transverse Shear Reinforcement (TSHR). The first recommendation is supported by a constraint rule, similar to the opposite face rule just explained, which will be called as the *perpendicular direction same face constraint rule*. The second additional recommendation advises how to deal with the out-of-plane (or transverse) shear demands ( $V_{xz}$  and  $V_{yz}$ ). The PACI approach, in contrast to the EC2 approach, treats the out-of-plane shear demands separately, and follow the design procedure in chapter 11 of the ACI 318, which accounts for the effect of the axial forces to estimate the out-of-plane shear capacity of the panel. Additional explanations regarding the perpendicular-direction-same-face constraint rule will be provided next, while additional explanations regarding the computation of the TSHR will be given in the next numeral.

#### *The perpendicular direction same face constraint rule.*

The perpendicular direction same face constraint rule, as its name indicates, forces to use the largest amount of required reinforcement between the two component (or perpendicular) directions (x or y) in the same face (or layer) of a panel, along the direction that requires less reinforcement. In contrast to the opposite face constraint rule, which forces to impose the larger amount of required reinforcement in the opposite face but in the same (or parallel) direction, the perpendicular direction same face constraint rule forces to impose the largest amount of reinforcement in the same face, but in the perpendicular direction. This rule implies that if for example, after finding that the reinforcement ratio along the y-direction (either at the top or bottom layer) is lower than the reinforcement ratio suggested along the x-direction, then, the same reinforcement ratio in the x-direction must be provided in the y-direction, even if the approach suggested a lower reinforcement amount.

This “*perpendicular direction same face constraint rule*” was proposed for two reasons. First, to account for the effect of the potential misalignment between the direction of the reinforcement and the principal directions which is explained in numeral 6.1.7 of the ACI 318.2-19; and second, because after applying the EC2 approach, which does consider the principal stress and directions to estimate the required reinforcement, it was found that the EC2 suggested the same amount of reinforcement in both orthonormal components (or perpendicular) directions (x and y). As said in numeral 6.1.7 of the ACI 318.2-19, when there exists a deviation of more than 10 degrees between the direction of the reinforcement and the principal directions -which will be highly likely in the PACI approach because it does not account for principal stresses or directions- the design of the panel will be governed by cracking limitations at service loads. The commentary for numeral ACI 6.1.7 in the ACI 318.2-19 says that one way to limit the crack width is by increasing the amount of reinforcement, which is precisely what the perpendicular direction same face constraint rule does. At the end of this chapter, it will be shown that the procedure to compute the membrane forces that will be resisted for the reinforcement layer in the PACI approach is very similar to the procedure of the basic EC2 sandwich model approach with slightly variations.

### **3.2 Computation of the Transverse Shear Reinforcement (TSHR) if needed**

The PACI approach follows a very similar procedure to the EC2 approach to estimate the out-of-place reinforcement for the RC panels. The main difference is that instead of computing the maximum in-plane shear ( $v_{Edo}$ ) as a function of the two out-of-plane shears ( $V_{xz}$  and  $V_{yz}$ ) like the Eurocode does, the PACI treats the two out-of-plate shears separately as indicated in Figure 3.2. Transverse Shear Reinforcement (TSHR) will be only required if the out-of-plane (or transverse) shear capacity provided by the concrete alone ( $V_c$ ) is less than the out-of-plane shear demands. In other words, if any of the out-of-plane shear demands ( $V_{xz}$  or  $V_{yz}$ ) is greater than the shear capacity of the panel only provided by the concrete ( $V_c$ ), then TSHR is required. There are two important considerations when computing the out-of-plate shear capacity that is only provided by the concrete  $V_c$  in the PACI approach: 1. not all the thickness of the wall will be considered to estimate this  $V_c$ ; and 2, the beneficial effect of the compressive axial forces (if it exists) on this  $V_c$  will be disregarded. Equations 16a and 16b give the magnitude of the out-of-plane shear capacity of the panel. As can be seen in both equations, the PACI approach only considers the contribution of the concrete ( $V_{cxz}$ ).

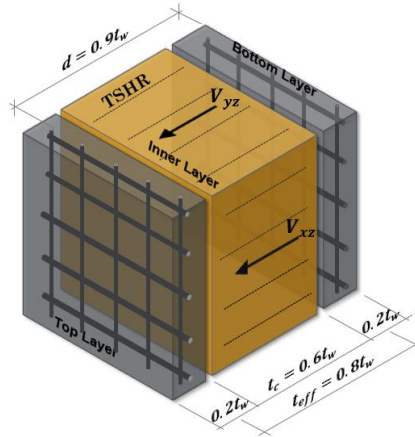


Figure 3.2. Out-of-plane shears

The PACI approach assumes that only 80% of the thickness of the panel is available to resist the out-of-plane shear demand. This 80% is assumed following the recommendations of Blaauwendraad (2010), who said that a good approximation to estimate the thickness of the outer layers when applying the sandwich model approach is 20% of the thickness of the wall ( $0.2t_w$ ). Thus, the effective thickness of the central layer of the panel, which will take most of the out-plane shear demand, can be taken as the distance between the centroids of the outer layers. Assuming that the thickness of the outer layers are  $0.2t_w$ , then the inner layers will have an effective thickness of  $0.8t_w$ , as shown in figure 3.2. This assumption was in agreement with the findings in this research. For example, when applying the EC2 approach in section 6, it was found that the average thickness for the outer layers for the SE, the SM, the ML, and the SP series panels was about 21% of their corresponding total thickness ( $0.21t_w$ ). The PV and the F series panel were not taken in consideration for this calculation because they were only subjected to membrane forces. In addition, the PV panels had a very small thickness of 70 mm.

Using an effective depth of 80% of the thickness of the wall to estimate the out-of-plane shear capacity of the wall instead of the commonly accepted 90% for beams, it goes in agreement with the fact that the PACI approach also assumes that the concrete in the outer layers is always cracked. Therefore, the thickness corresponding to the outer layers cannot be accounted for the out-of-plane shear capacity of the panel. Assuming an effective thickness of  $0.8t_w$  implies that at least the covers of the panels will not be considered in the out-of-plane shear capacity of the concrete, and thus, a significant portion of the thickness wall will be disregarded. The shear strength reduction

factor  $\phi_v$  in this case can be taken as 0.6 as recommended by the ACI-318 for seismic applications and for special structural walls in the numeral 21.2.4.1.

$$Av_{xz} = \frac{V_{xz} - \phi_v V_{cxz}}{\phi_v f_y} \quad \text{Eq (16a)}$$

$$Av_{yz} = \frac{V_{yz} - \phi_v V_{cyz}}{\phi_v f_y} \quad \text{Eq (16b)}$$

Where,

$$V_{cxz} = \begin{cases} 0.17\lambda\sqrt{f'_c}(0.6t_w) & \text{for } N_x < 0 \\ 0.17\lambda\left(1 - \frac{N_x}{14t_w}\right)\sqrt{f'_c}(0.6t_w) & \text{for } N_x > 0 \end{cases}$$

$$V_{cyz} = \begin{cases} 0.17\lambda\sqrt{f'_c}(0.6t_w) & \text{for } N_y < 0 \\ 0.17\lambda\left(1 - \frac{N_y}{14t_w}\right)\sqrt{f'_c}(0.6t_w) & \text{for } N_y > 0 \end{cases}$$

As can be seen in equations 16 and 16b,  $V_c$  is punished (decreased) if tensile axial forces are presents. However,  $V_c$  is not increased when compressive axial forces are present. In other words, the PACI approach, in contrast to the common practices in RC members, disregards the beneficial effect (or the increment) of the  $V_c$  when axial compressive forces are present. In equations 16a and 16b,  $N_x$  and  $N_y$  must be introduced as positive values if they are tensile forces, while they must be introduced as zero if they are compressive forces This is assumed, again, to add conservatism to the approach, and thus, avoiding a brittle failure. Another reason for this assumption is related to the fact that the PACI approach does not account for the principal out-of-plane shear ( $v_o$ ) and its associated direction ( $\phi_o$ ), as the EC2 does. Hence, it will not be possible to know if the normal force acting on the plane of the principal out-of-plane direction ( $\phi_o$ ), explained in section 2.1.3, is in compression or not. It will be more conservative, therefore, to disregard the beneficial effect of the axial compressive force (if it exists) on the out-of-plane shear capacity of the panels. Also, it must be recalled that the PACI approach, as well as the EC2 approach, assume that the axial forces  $N_x$  and/or  $N_y$ ) will be only resisted by the outer layers, and thus, zero (or very few) axial force will be taken by the inner layer.

It must be mentioned that some researchers, such as Blaauwendraad (2010) and the Fib CEB-FIP bulletin 45 advise to increase the panel thickness instead of providing transverse reinforcement (TSHR). They argue that placing TSHR is not practical for design purpose and it is time consuming. As explained in section 2.1 if TSHR is required/placed, it will rise additional membrane forces that needs to be taken into consideration to estimate the required in-plane reinforcement areas. The PACI approach uses a simplified expression to estimate these additional reinforcement areas based on the assumptions of the EC2 approach as will be shown at the end of the chapter in table 3.1. If a more accurate procedure to estimate these additional is desired, the consultants can follow the more accurate procedure proposed by EC2 approach or by the fib CEB-FIP Model code (1990) (MC-1990)

### 3.3 Computation of the in-plane (longitudinal and/or Transverse) Reinforcement

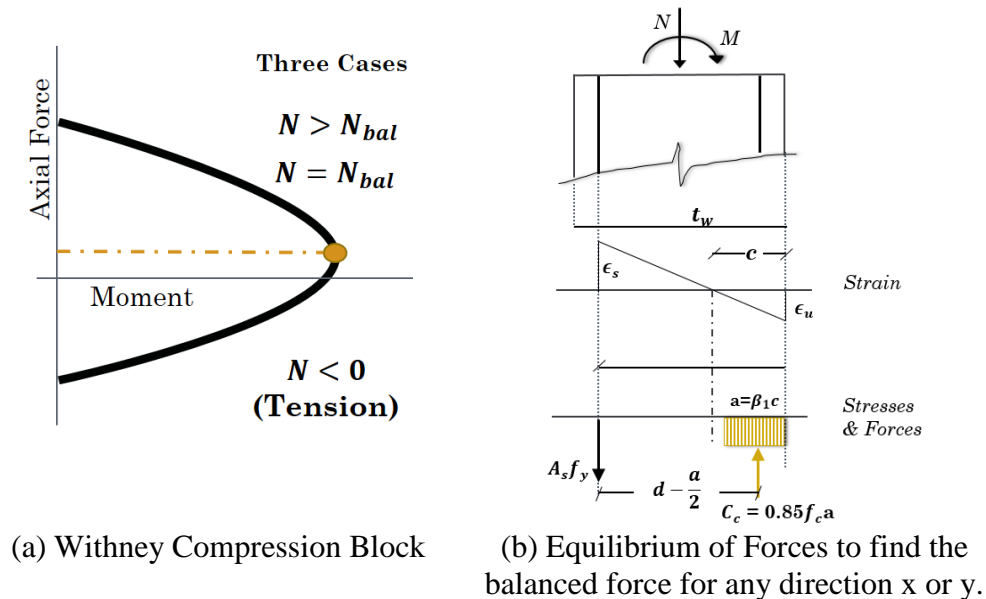


Figure 3.3. Computation of the Balanced Force for a RC panel.

One of the most important features of the PACI approach is the interaction between the axial forces and the out-of-plane bending moments. The required amount of in-plane reinforcement will depend on the magnitude of the axial forces acting in the two orthonormal directions of the panel. As shown in Figure 3.3, three cases are considered: Case 1, when the axial loads are in tension; case 2, where the axial loads are in compression, but their magnitudes are less than the balanced

force; and case 3, when the compressive axial loads are greater than the balanced force ( $N_{bal}$ ). As noted, the two last cases depend upon the magnitude of the balanced force. The computation of the balanced force follows the popular assumption of plane sections remain plane and the well-known Whitney rectangular Stress block distribution for the concrete.

Equations 17 shows how to compute the balanced force of the RC panel. It is worthwhile to mention that the third case is very unlikely to occur, since the balanced force in RC panels is considerably higher when compared against the axial demands, considering the thickness and robustness of the walls (or panels). The balanced force of RC panels either in the x or the y direction can be found with equation 1, which is based on the well-known rectangular uniform compressive stress Whitney Block for the concrete distribution, as shown in Figure 1. In Equation 1,  $\epsilon_u$  is the maximum allowed compressive strain in the concrete, usually taken as 0.003;  $f_y$  is the typical yielding stress of the reinforcement; and,  $d$  is the effective thickness of the wall as shown in figure 2.12.  $\beta_1$ , is the factor that correct the magnitude of the assumed uniform compressive stress block. This factor takes a constant value of 0.85 for  $17\text{MPa} < f_c < 28\text{MPa}$ ; For  $f_c$  values higher than 28 MPa,  $\beta_1$  decreases at a ratio of 0.05 for every 7 MPa, but it never can be lower 0.65.

$$N_{bal} \approx 0.85 f'_c a_{bal} - A_s f_y \quad \text{Eq (17)}$$

Where,

$$a_{bal} = \beta_1 c_{bal}$$

and

$$c_{bal} = \frac{\epsilon_u}{\epsilon_u + \epsilon_y} d$$

### 3.3.1 Analysis for when N is in tension

For the case when the panel is subjected to tensile forces, the PACI approach computes the required reinforcement areas of the layers as the summation of: a) the required tensile ( $A_T^{req}$ ) area due to the in-plane axial forces  $N_x$  and  $N_y$ ; b) the required area by flexion ( $A_F^{req}$ ) due to the combined flexural demands of the out-of-plane bending moments  $M_x$  and  $M_y$  and the twisting moment  $M_{xy}$ ; and c) the required reinforcement area by shear ( $A_V^{req}$ ) due to in-plane shear forces ( $N_{xy}$ ) and the twisting moment ( $M_{xy}$ ). Figure 2.13 illustrates how the axial forces that will be resisted by the reinforcement curtains (or layers) are computed in the PACI approach.

### Required reinforcement Areas due to Tensile forces ( $A_T^{req}$ )

To obtain the in-planes forces that will be resisted by the reinforcement in each layer, the PACI approach assumes that the reinforcement layers have been placed symmetrically, and that there is a unique lever arm between the layers in both direction as shown in Figure 2.13a. Figure 2.13b shows the distribution of the in-plane axial demand over each reinforcement layer along directions x and y. By doing simple statics, it is clear that if the reinforcement layer are symmetrically placed, the in-plane axial forces to be resisted by the reinforcement in each coordinated directions (x and y) will be the half of the total in-plane internal demand ( $N_x$ ).

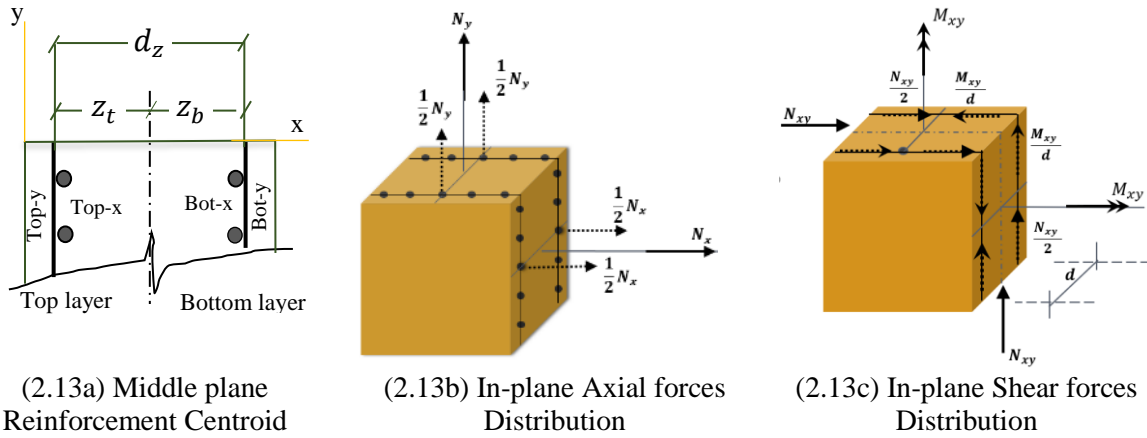


Figure 3.4. Obtention of the In-plane axial and shear forces to be resisted by the reinforcement layer.

Now, the required reinforcement areas along the x-direction ( $A_{xT}^{req}$ ), and along the y-direction ( $A_{yT}^{req}$ ), are obtained with the Equations 18a and 18b, respectively.

$$A_{xT}^{req} = \frac{1}{2} \frac{N_x}{\varphi_t f_y} \quad \text{Eq (18a)}$$

$$A_{yT}^{req} = \frac{1}{2} \frac{N_y}{\varphi_t f_y} \quad \text{Eq (18b)}$$

### Required reinforcement Area due to Flexure ( $A_F^{req}$ )

For the case when the axial loads over the panel are in tension, it is assumed that there will not be interaction between P and M, and the panel will be designed following the conventional procedure of an under-reinforced RC member. In this case, it is assumed that the reinforcement

in tension yields before the crushing of the concrete, and that the reinforcement in compression is neglected for the computation of the flexural strength of the panel. In addition, the distribution of the concrete stress in compression is assumed as uniform following the rectangular Whitney stress block approximation. Equilibrium of the internal forces in Figure 2.13b results in Equation 19a, while, equilibrium of moments about the centroid of the rebar in tension results in equation 19b.

$$0.85f'_c a_x = A_s f_y \quad \text{..Eq (19a)}$$

$$\sum M_d: A_s f_y \left( d - \frac{a_x}{2} \right) = M_x^{tot} \quad \text{..Eq (19b)}$$

The concrete stress block along the x-direction ( $a_x$ ) -necessary to compute the magnitude and the centroid of the internal compressive force developed in the concrete- is found by solving the quadratic equation 19c, resulting after combining Eq 19a and Eq 19b. Now, following a similar procedure, the compressive stress block along the y-direction ( $a_y$ ), is found through Equation 19d. The effective depth (d) in equations 19 will be taken as 90% of the total thickness of the wall ( $0.9t_w$ ). This value of  $0.9t_w$  for the effective depth is in agreement with the assumption of  $0.2t_w$  for the equivalent thickness of the outer layers explained in the numeral 3.2 of this section. The total out-of-plate bending moment demands about each coordinated axis  $M_x^{tot}$  or  $M_y^{tot}$  is taken as the summation of the out-of-plate moment about the corresponding axis plus the twisting moment ( $M_{xy}$ ), in order to satisfy the numeral 19.4.1 of the ACI-318.

$$a_x^2 - 2da_x + \frac{2|M_x^{tot}|}{0.85\phi_b f'_c} = 0 \quad \text{..Eq (19c)}$$

$$a_y^2 - 2da_y + \frac{2|M_y^{tot}|}{0.85\phi_b f'_c} = 0 \quad \text{..Eq (19d)}$$

where,  $M_x^{tot} = M_x + M_{xy}$

and  $M_y^{tot} = M_y + M_{xy}$

The required reinforcement areas due to flexion, in the x and y directions are found with Equations 19e and 19f, respectively.

$$A_{xF}^{req} = \frac{0.85f'_c a_x}{\phi_b f_y} \quad \text{..Eq (19e)}$$

$$A_{yF}^{req} = \frac{0.85f'_c a_y}{\phi_b f_y} \quad \text{..Eq (19f)}$$

***Required reinforcement area due to in-plane shear ( $A_V^{req}$ )***

The first step to estimate the reinforcement areas due to the in-plane shear is to compute the shear force that will be resisted by the reinforcement. This shear force is the result of the combined action of the total direct in-plane shear demand ( $V_{xy}$ ) and by the twisting moment ( $M_{xy}$ ). Again, by doing statics, it is clear that each reinforcement layer (or curtain) in any direction will take half on the total in-plane direct shear ( $N_{xy}$ ), plus or minus the additional shear produced by the twisting moment ( $M_{xy}$ ), as shown in Figure 2.13c. The additional in-plane shear produced by the twisting is obtained by dividing the ( $M_{xy}$ ) over the unique lever arm ( $d_z$ ). The forces due to the direct shear and the twisting moment might be adding or subtracting each other, depending on the their direction and the location of the reinforcement layer. For example, if the twisting moment acting along the y-axis is positive, as well as the in-plane shear, the force acting on the top (or front ) layer will be negative, then, they will be subtracting. On the contrary, the resulting shear forces acting on the opposite layer (bottom or Back face), will be adding each other. Now, the required reinforcement areas due to in-plane shear and twisting moment in x-direction and y-direction is given in Equation 20a and 20b, respectively. It is important to mention that in contrast to the out-of-plane shear capacity where some contribution of the concrete is considered to reduce the amount the reinforcement, the concrete contribution is totally neglected when estimating the in-plane shear reinforcement in the outer layers. The reason for this is that the PACI approach always assume that the concrete at the extremes of the panes are always cracked, and therefore, no contribution of the concrete for shear capacity must be considered. The shear strength reduction factor  $\phi_v$  in equation 20a and 20b will be taken as 0.75 as recommended in numeral 21.2.1 of the ACI-318.

$$A_{xV}^{req} = \frac{1}{2} \left( \frac{V_{ux}}{\phi_v f_y} \right) \quad \text{..Eq (20a)}$$

$$A_{yV}^{req} = \frac{1}{2} \left( \frac{V_{uy}}{\phi_v f_y} \right) \quad \text{..Eq (20b)}$$

Where,

$$V_{u(x \text{ or } y)} = \frac{N_{xy}}{2} \pm \frac{M_{xy}}{d}$$

### 3.3.2 Analysis for when N is in compression and less than or equal to $N_{bal}$

In this case, there will be no required reinforcement due to axial forces, since the panel will be subjected to compression. Therefore, only the required areas due to flexion and shear will be estimated in this special case. The contribution of the reinforcement in compression will be also disregarded to compute the capacity of the section.

#### *Required reinforcement areas due to Flexion.*

In this case, the axial vs Moment (N vs M) interaction will be considered. The internal forces equilibrium inside the RC panel for any of the directions x or y, now considering a compressive force, are given by equation 21a and 21b. It must be recalled that  $N_x$  and/or  $N_y$ , depending on the direction of the analysis, have been assumed as lower than its corresponding balanced force  $N_{bal-x}$  or  $N_{bal-y}$ .

$$0.85f'_c a = A_s f_y + N_x \quad \text{..Eq (21a)}$$

$$\sum M_d: A_s f_y \left( d - \frac{a_x}{2} \right) = M_x^{tot} \quad \text{..Eq (21b)}$$

The concrete stress block along the x-direction ( $a_x$ ), necessary to compute the magnitude and the centroid of the internal compressive force developed in the concrete, is found by solving the quadratic equation 21c, which came up after combining Eq 21a and Eq 21b. Now, following a similar procedure, the compressive stress block along the y-direction ( $a_y$ ), is found through Equation 21d. Again, the effective depth ( $d$ ) in equations 21 will be taken as 90% of the total thickness of the wall ( $0.9t_w$ ).

$$a_x^2 - 2da_x + \frac{|N_x|(2d-t_w)+2|M_x^{tot}|}{0.85\phi_b f'_c} = 0 \quad \text{..Eq (21c)}$$

$$a_y^2 - 2da_y + \frac{|N_y|(2d-t_w)+2|M_y^{tot}|}{0.85\phi_b f'_c} = 0 \quad \text{..Eq (21d)}$$

Where,

$$M_x^{tot} = M_x + M_{xy}$$

And

$$M_y^{tot} = M_y + M_{xy}$$

The required reinforcement area due to flexion, in x-direction and y-direction, are found using equations 21e and 21f, respectively.

$$A_{xF}^{req} = \frac{0.85f'_c a_x}{\phi_b f_y} \quad \text{..Eq (21e)}$$

$$A_{yF}^{req} = \frac{0.85f'_c a_y}{\phi_b f_y} \quad \text{..Eq (21f)}$$

### ***Required reinforcement areas due to in-plane Shear.***

The reinforcement areas due to in-plane shear for when the axial loads are in compression and less than the balanced force are found in the same way than when the axial loads are in tension. Therefore, the formulas in equations 20a and 20b to find the areas due to in-plane shear in the x-direction and in the y-direction, respectively will be also used for this case.

### **3.4 Analysis for when N is in compression and greater than or equal to $N_{bal}$**

Similar to the case in where the axial compressive loads are lower than the balanced forces, only the required areas due to flexion and shear will be needed in this case. Again, in order to add conservatism to the approach, the contribution of the in-plane reinforcement in compression in the capacity of the panel will be disregarded in this special case as well. The formulas to estimate the in-plane reinforcement areas required by the in-plane shear are the same than equations 20a and 20b. On the other hand, the formulas to estimate the in-plane reinforcement required by flexion when  $N > N_{bal}$  in the x-direction and in the y-direction are given by the equations 23a and 23b, respectively. It is important to highlight that while in equations 21a and 21b, it was assumed that the reinforcement in tension yielded, in equations 23a and 23b it did not.

$$A_{xF}^{req} = \frac{0.85f'_c a_x - N}{\phi_b \left(0.85 \frac{d}{a_x} - 1\right) E_s} \quad \text{Eq (23a)}$$

with,

$$a_x^2 - 2da_x + \frac{|N_x|(2d - t_w) + 2|M_x^{tot}|}{0.85\phi_b f'_c} = 0$$

and

$$A_{yF}^{req} = \frac{0.85f'_c a_y - N}{\phi_b \left(0.85 \frac{d}{a_y} - 1\right) E_s} \quad \text{Eq (23b)}$$

Where,

$$a_y^2 - 2da_y + \frac{|N_y|(2d - t_w) + 2|M_y^{tot}|}{0.85\phi_b f'_c} = 0$$

### 3.5 Analysis for when N is in compression and greater than or equal to N<sub>bal</sub>

Table 3.1 summarizes the set of equations to obtain the required reinforcement areas, for any of the three cases analyzed in here: a) when N<sub>x</sub> and/or N<sub>y</sub> are tensile forces; b) when N<sub>x</sub> and/or N<sub>y</sub> are compressive forces but their magnitudes are equal to or less than the balance forces (N<sub>bal</sub>); and c) when N<sub>x</sub> and/or N<sub>y</sub> are compressive forces but their magnitudes are greater than the balance forces (N<sub>bal</sub>). As shown in table 3.1, when the axial forces acting on the panel are in compression in the direction of analysis, there is no need to provide reinforcement due to the axial forces.

Table 3.1. Summary of Equations to obtain the required reinforcement areas in the PACI approach

Required areas	Case 1: N is in tension	Case 2. (N in compression but $N < N_{bal}$ )	Case 3. (N in compression but $N > N_{bal}$ )
$A_T^{req}$	$A_{xT}^{req} = \frac{1}{2} \frac{N_x}{\phi_t f_y}$	No Apply	No Apply
$A_F^{req}$	$A_{xF}^{req} = \frac{0.85 f_c' a_x}{\phi_b f_y}$ <p>After solving,</p> $a_x^2 - 2da_x + \frac{2 M_x^{tot} }{0.85\phi_b f_c'} = 0$	$A_{xF}^{req} = \frac{0.85 f_c' a_x}{\phi_b f_y}$ <p>After solving,</p> $a_x^2 - 2da_x + \frac{ N_x (2d - t_w) + 2 M_x^{tot} }{0.85\phi_b f_c'} = 0$	$A_{xF}^{req} = \frac{0.85 f_c' a_x - N}{\phi_b \left(0.85 \frac{d}{a_x} - 1\right) E_s}$ <p>After solving,</p> $a_x^2 - 2da_x + \frac{ N_x (2d - t_w) + 2 M_x^{tot} }{0.85\phi_b f_c'} = 0$
$A_V^{req}$	$A_{xV}^{req} = \frac{1}{2} \frac{N_{xy}}{\phi_v f_y}$	$A_{xV}^{req} = \frac{1}{2} \frac{N_{xy}}{\phi_v f_y}$	$A_{xV}^{req} = \frac{1}{2} \frac{N_{xy}}{\phi_v f_y}$
$A_{Vxz}^{req}$	$A_{Vsh}^{req} = 1.25 \frac{V_{xz}^2}{V_o f_{yh}}$	$A_{sh}^{Vxz} = 1.25 \frac{V_{xz}^2}{V_o f_{yh}}$	$A_{sh}^{Vxz} = 1.25 \frac{V_{xz}^2}{V_o f_{yh}}$
Total Required Area	$A_{Tot}^{req} = A_{xT}^{req} + A_{xF}^{req} + A_{xV}^{req} + A_{Vxz}^{req}$	$A_{Tot}^{req} = A_{xF}^{req} + A_{xV}^{req} + A_{Vxz}^{req}$	$A_{Tot}^{req} = A_{xF}^{req} + A_{xV}^{req} + A_{Vxz}^{req}$

### 3.6 Conceptual comparison between the EC2 and the PACI design Approaches

Equations 23a, 23b and 23c compare how the EC2, the MC-1990 and the PACI approaches, respectively, estimate the magnitude of the force that will be resisted by a reinforcement curtain that is first, located at the bottom face of the panel; and second, running along the y-direction. Comparing these three equations helps to understand some of the basic concepts of the PACI approach. If the reinforcement layers haven been symmetrically placed inside the panel —as it is assumed in the PACI approach— the first terms in all equations will be always half of the corresponding total axial ( $1/2 N_y$ ). The second term, corresponding to the areas required for flexion, will be quite different because the PACI approach, contrary to the EC2 and the MC-1990 approaches, uses the P-M interaction to estimate this reinforcement area, as previously explained. The third and fourth terms, in both equations, will become equal if: a) the  $\cot \theta_{pcc}$ , in equation 23a, is assumed to be 1.0, neglecting thus, any interaction between the in-plane axial force and the in-plane shear forces; and b) the reinforcement is placed symmetrically, meaning that half of the total in-plane shear demand ( $1/2 N_{xy}$ ) will be taken by this curtain reinforcement; and c) the value of  $k$ , in equation 23b is assumed as 1.0, as recommended by the MC-1990. Finally, the fifth term, corresponding the area required to resist the additional membrane forces when TSHR is required, can be estimated conservatively by assuming that the  $\cot(\theta)$  is always equal to 2.5, which is the upper limit value indicated by the EC2 approach. It is worthy to recall that if TSHR is not required, this fifth term will be canceled out in both equations. The 1.25 appears after dividing the upper limit of 2.5 by 2, which comes from static, since each outer curtain will take half of the additional membrane force that rise because of to the presence of THSR. This fifth term will be canceled out in all three equations, 23a, 23b and 23c, if TSHR is not placed or required. It is worthwhile to mention that all strength reduction factors in equation 23c must be taken as 1.0 to allow the comparison between all equations.

$$F_{bry} = A_{syb} f_y = N_y \frac{(d_z - z_b)}{d_z} + \frac{M_y}{d_z} + \left[ N_{xy} \frac{(d_z - z_b)}{d_z} + \frac{M_{xy}}{d_z} \right] \cot(\theta_{pcc}) + \frac{1}{2} \frac{V_{yz}^2}{V_o} \cot \theta \quad \text{..Eq (23a)}$$

$$F_{bry} = A_{syb} f_y = \frac{1}{2} N_y + \frac{M_y}{d_z} + k \left[ N_{xy} \frac{(d_z - z_b)}{d_z} + \frac{M_{xy}}{d_z} \right] + \frac{V_y^2}{2v_o \tan \theta} \quad \text{..Eq (23b)}$$

$$F_{bry} = A_{syb} f_y = \frac{1}{2} \frac{N_y}{\phi_t} + \frac{0.85 f'_c a_y}{\phi_b} + \left[ \frac{1}{2} \frac{N_y}{\phi_v} + \frac{M_{xy}}{d_z} \right] + 1.25 \frac{V_y^2}{V_o} \quad \text{..Eq (23c)}$$

After considering all the assumptions and simplifications involved in the PACI approach, and after comparing it against the EC2 sandwich model, it might be said that this approach is as a mix of a basic sandwich model approach combined with the very familiar design concepts of balanced force and Whitney stress concrete block for RC members loaded in flexural-compression given in the ACI 349 and ACI 318 design codes.

## 4. METHODOLOGY

The methodology of this thesis can be described in three phases: *The development phase; the validation phase; and the implementation phase.* Two activities comprise the *development phase.* The first one is the development of the simplified PACI design approach, and the second one is the explanation and exploration of the EC2 design approach. The main products associated to this development phase are: a) the creation of a spreadsheet in Mathcad to estimate the reinforcement areas suggested by the PACI and the EC2 design approaches; and b) the development of a flowchart design to facilitate the application of the EC2 design approach.

In the *validation phase,* the results of the PACI approach will be validated by using experimental data. Two types of results will be validated in this phase: a) the areas of reinforcement (or reinforcement ratios) suggested by the PACI approach; and b) the estimated numerical capacities of the panels considering those reinforcement suggested areas. Three activities can be identified in this validation phase: a) the selection of the experimental data; b) the estimation of the reinforcement areas suggested by the two approaches and their comparison against the experimental quantities; and c) the estimation of the numerical capacities of the panels after introducing those reinforcement areas suggested by the PACI approach into calibrated numerical models and their comparison against the experimental reported capacities. The product associated to this last activity is the development of calibrated numerical models in Shell-2000, Membrane-2000 and Abaqus. The results of the PACI approach will be also compared against the results of the more accurate EC2 mechanics-based design approach in this validation phase.

In the *implementation phase,* the applicability of the PACI approach (as well as for the EC2 approach) for industrial facilities will be evaluated by using analytical data. In this thesis, analytical data refers to the analytical set of demands extracted from the analysis of an actual industrial facility (for example, AP1000(R), US-APWR(R), etc.). Contrary to the experimental data, in which the set of demands consists of no more than two or three demands, the set of demands in the analytical data consists of the complete set of eight internal design demands estimated from finite element analysis (FEM). Two activities describe this last phase: selection of the analytical data and estimation of the Capacity-to-Demand ratios (CDRs) of the panels. These

CDRs will be useful to verify the safety of both design approaches. Figure 4.1 illustrates the methodology of this thesis, highlighting all the products associated in each phase.

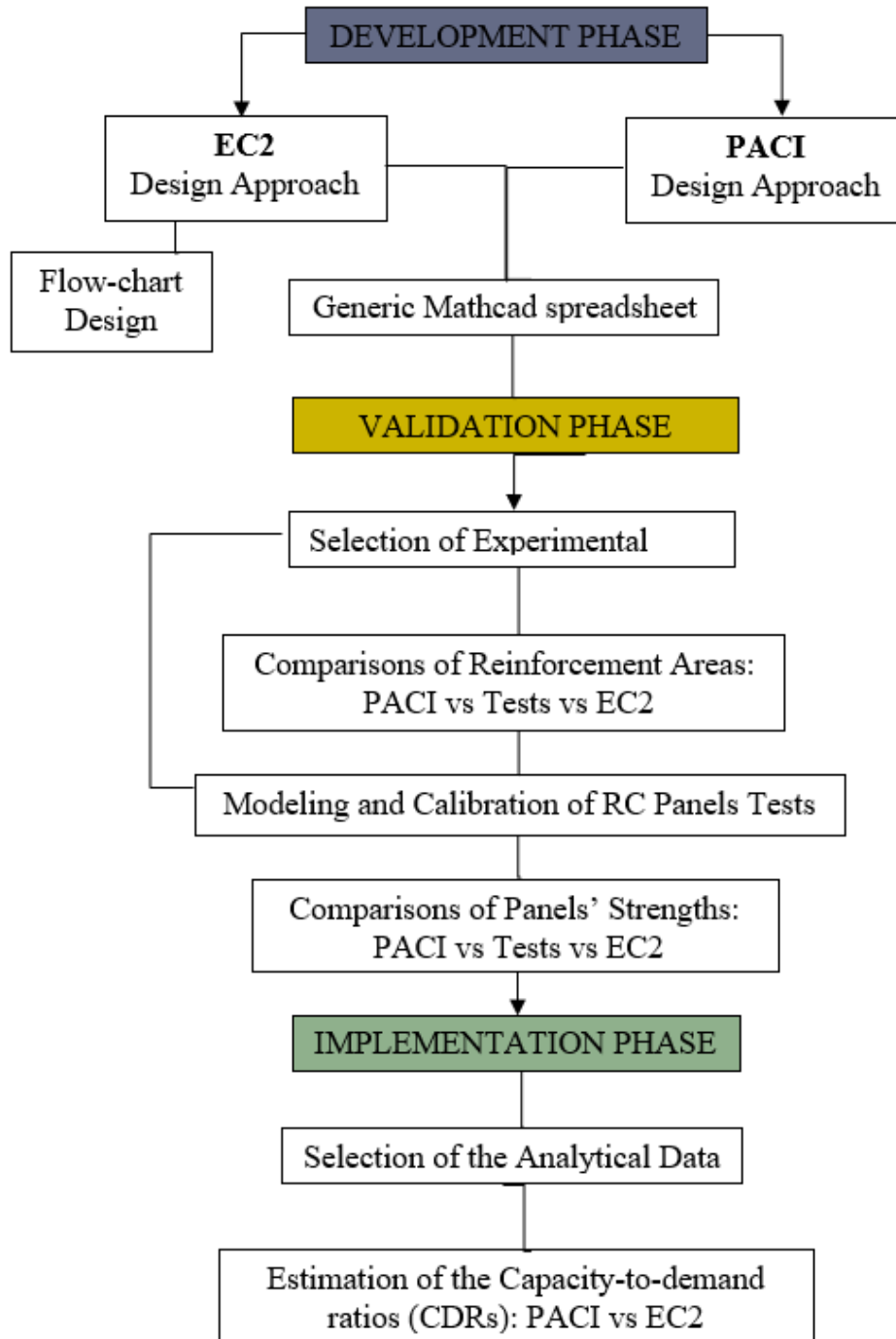


Figure 4.1. Flowchart methodology.

## **4.1 Development Phase**

Two activities comprise the development phase: a) the exploration and explanation of the EC2 design approach, and b) the development of the ACI-panel-based-Design (PACI) approach.

### **4.1.1 Development of the PACI design approach**

The theory, concepts and procedure of the PACI design approach will be developed in this phase. The main feature of this approach is that it will be entirely based in the concepts and formulation of the ACI-318.2-19 and the ACI-349 codes. The PACI approach will consider most of the design requirements and rules for the estimation of the steel reinforcement in RC shells, which are specified in chapter 6 and in chapter 19 of the ACI-318.2-19 and the ACI-349 codes. An important feature of the PACI approach is that it will consider the axial load vs bending moment (P-M) interaction to estimate the in-plane reinforcement, as specified in chapter 10 of the ACI-318-19. For this end, the PACI approach uses the well-known concepts of balanced force and Whitney stress block for concrete members. Three cases, depending on the magnitudes of the axial loads acting on the panels will be considered: 1. When the axial loads are in tension; 2. When the axial loads are in compression but their magnitudes are less than or equal to the balanced force; and 3. When the axial loads are in compression, but their magnitude are greater than balanced force. The PACI approach will also consider the interaction between the axial forces and the shear capacity of the panels following the formulations of the chapter 11 in the ACI-318.

### **4.1.2 Explanation and exploration of the Eurocode (EC2) design approach**

As mentioned in the introduction of this document, the EC2 sandwich model has not been widely explored in industrial applications. One of the reasons for this is perhaps because some concepts and procedures of the EC2 approach might be overwhelming and difficult to apply at some extent. For example, the simultaneous verification of the out-of-plane shear capacity of the inner layer of the panel, and the required amount of in-plane reinforcement, and the compressive stress verification of the outer layers, can be a little tricky to follow because it implies a trial and error process. Similarly, applying the cracking criteria of the EC2 approach, which is based on principal stress and plasticity concepts, and by which it is determined if the panel requires reinforcement in any of its layers, deserves additional explanation. Therefore, this activity will

focus in the explanation of all the theory, procedure, and assumptions of the EC2 design approach. The main product of this activity is the development of a flow chart design, which will facilitate the applicability of the EC2 design approach.

#### **4.1.3 Development of a spreadsheet for the estimation of the steel reinforcement.**

A generic spreadsheet in Mathcad will be created in this activity. The details of the calculations for the estimation of steel reinforcement areas will be given in this spreadsheet. The EC2 and PACI design approaches will share the same input data in this generic spreadsheet. The common input data in this spreadsheet are the thickness of the panel, the material specification for the concrete and steel reinforcement, the cover and lever arm distances of the reinforcement curtains (or layers) and the loading application pattern (i.e.  $N_x$ ,  $M_x$ ,  $V_{xy}$ , etc). The spreadsheet will compare the reinforcement areas suggested by the approaches in terms of reinforcement ratio or expressed in area per unit length (i.e.  $\text{cm}^2/\text{m}$ ) as expressed in the experiments. This spreadsheet is the main product in this activity.

#### **4.2 Validation Phase**

In this phase, the results of the PACI approach will be validated by using experimental data. Specifically, two types of results will be validated: a) the areas of reinforcement (or reinforcement ratios) suggested by the PACI approach; and b) the estimated numerical capacities of the panels considering those reinforcement suggested areas. Three activities can be identified in this validation phase: a) the selection of the experimental data; b) the estimation of the reinforcement areas suggested by the two approaches and their comparison against the experimental quantities; c) the estimation of the numerical capacities of the panels after introducing those reinforcement areas suggested by the PACI approaches into calibrated numerical models and their comparison against the experimental reported capacities. The main product associated with this last activity is the development of calibrated numerical models in Shell-2000, Membrane-2000 and Abaqus. Likewise, the results of the PACI approach will be also compared against the results of the more accurate EC2 mechanics-based design approach. Since the EC2 design approach has a more rigorous design procedure than the PACI approach, more conservative results for this latter will be expected.

#### 4.2.1 Selected RC panel tests.

Twenty one RC panel tests were selected to validate the results of the PACI approach: four of the SE panels series subjected to in-plane shear and/or bending Moment, tested by Kirscher (1986) and Kirscher and Collins (1986); four of the PV panel series subjected to in-plane tensile forces and in-plane shear forces tested by Vecchio (1981) and Vecchio and Collins (1982); three of the SM panels series subjected to axial Loads and/or bending moment tested Polack and Veccio (1994); three of the F panels series subjected to axial tension and compression forces tested by Belarbi and Hsu (1995); four of the SP series tested by Adebar (1989) and Adebar and Collins (1994) subjected to in-plane shear and out-of-plane shear forces and moments; three of the ML panel series tested by Marti et al (1987), which was subjected to twisting moment only. Figure 4.2 illustrates the loading application pattern of the selected experimental data.

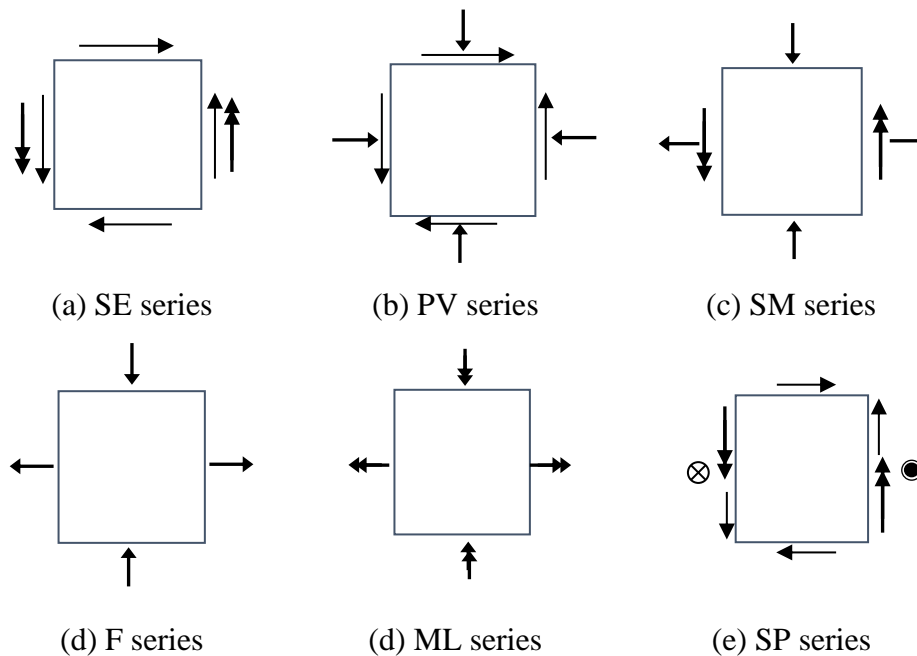


Figure 4.2. Loading Pattern for the Experimental data.

#### 4.2.2 Estimation of the reinforcement areas suggested by the PACI and the EC2 approaches.

The procedure to estimate the required reinforcement areas suggested by the two design approaches was as follows. First, it was assumed that the reinforcement areas provided during the tests of the panels are unknown. Second, the set of capacities reported from the experiments (i.e

$N_{xy}$ ,  $M_x$ ,  $M_{xy}$ , etc) were taken as the design “demands”. Subsequently, with those design “demands”, and keeping the original dimensions of the tested RC panels, the required areas of reinforcement were computed following both, the PACI and the EC2 design approaches. The reinforcement areas required by PACI and the EC2 the approaches will be called in this document the PACI and the EC2 suggested areas. Finally, these suggested reinforcement areas will be compared against the reinforcement areas provided during the tests.

Since all experiments reported the provided reinforcement area per layer inside the panel, it is necessary to define a convention to identify each reinforcement layer. Four layers were identified in all panels. Two layers of reinforcement running parallel to direction x, one located in the top (Top-x), another one located at the (Bottom-x). Similarly, two layers running parallel to the y axis, one at the top and the other one in the bottom of the panel, Top-y and Bottom-y, respectively. Figure 2.6, which was repeated here in Figure 4.2 helps to visualize the layers identification in this thesis. Comparing the suggested reinforcement areas against the experimental reinforcement areas might be considered as an indirect way of validation. For instance, if the PACI (or the EC2) approach suggest areas equal to or higher than the areas provided during the experiment it can be inferred that the approach is safe. The contrary will be inferred if the any of the approaches suggested lees amount of reinforcement. However, as will be shown later, non-linear analysis will be conducted in order to estimate the nominal capacities of the panels after introducing those suggested reinforcement areas.

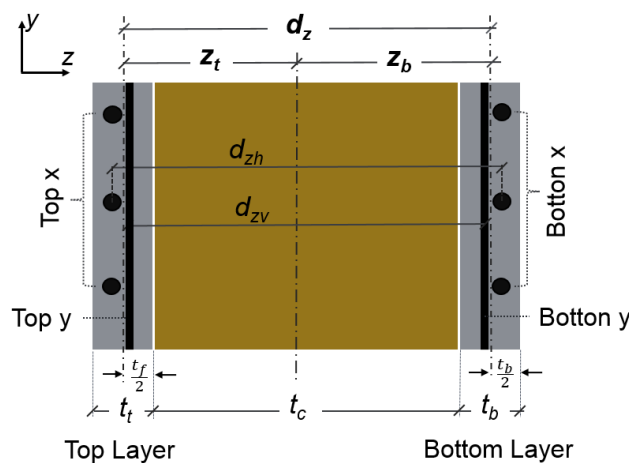


Figure 4.3. Identification of the Reinforcement Curtains (or layers).

### **4.2.3 Estimation of the Numerical capacities of the Panels**

#### ***Calibration of the numerical models for the experimental data***

The response of the 21 RC panels tests selected in this research will be numerically reproduced and calibrated in this activity. The numerical models must be able to reproduce the non-linear response of the RC panel during the experimentation in terms of force vs deformation capacity curves. The numerical models will be developed in Shell 2000, Membrane 2000, and/or Abaqus. It will be tried first to develop the numerical models in Shell-2000 or Membrane-2000 since they are much easier to develop than in Abaqus. If any of these two software do not reproduce the response of the panels with an acceptable level, then the numerical models for those specific panels will be developed in Abaqus. These calibrated models will be needed to estimate the numerical capacities of the panes after introducing the reinforcement areas suggested by any of two design approaches (PACI or EC2).

#### ***Estimation of the numerical capacities of the panels***

The procedure to estimate the numerical nominal capacities of the panels will be the following. First, the PACI and the EC2 suggested reinforcement areas will be introduced into the calibrated numerical models developed in Abaqus and/or Shell 2000. From those numerical models, the numerical capacity curves (or load vs deformation curves) will be obtained. Finally, the numerical set of nominal capacities (i.e.  $N_x$ ,  $N_{xy}$  or  $M_x$ ) for each panel, and for each corresponding set of “demands”, will be extracted from those numerical capacity curves. The PACI approach will be considered as safe if the numerical capacities are equal to or greater than experimental capacities of the panels. Comparing the estimated numerical nominal capacities of the panels against the experimental capacities is perhaps a more direct way of validation. As will be shown later in chapter 6, there were several cases in which the EC2 approach suggested less reinforcement areas than the reinforcement areas provided during the experiments. Despite this, the estimated numerical capacities reached by the panels in the numerical models were close to the experimental reported capacities, demonstrating thus, the accuracy and efficiency of the EC2 approach.

### **4.3 Implementation Phase**

In this phase, the applicability of the PACI approach for industrial facilities will be evaluated by using analytical data. Analytical data is referred to here as the analytical set of demands extracted from the analysis of an actual industrial facility (for example, AP1000(R), US-APWR(R), etc.). Contrary to the experimental data, in which the set of demands consists of two and no more than three demands, the analytical data consists in the whole eight internal design demands typical in shells. The applicability EC2 approach, which has not been widely explored in industrial applications, will be also evaluated in this phase. Two activities are identified in this phase: selection of the analytical data; and estimation of the Capacity-to-demand ratios (CDRs).

#### **4.3.1 Selection of the Analytical data**

Two set of analytical demands were selected in this section. One set of demands (8 demands in total as typical for shell elements) was extracted for the load combination 4 of a critical located shell element of the RP-1000 Steel Composite (SC) reservoir tank. The other set of demands was extracted for the same critical located shell element under load combination 6. Load combination 4 is characterized by low tension axial forces and relatively low out-of-plane shears whereas, load combination 6 is characterized by high compressive load and high out-of-plate shears. These design demand values are in the public domain and they can be found in the Design Demands Documents (DCD) report authored by Westinghouse (2011).

#### **4.3.2 Estimation of the Capacity-to-Demand ratios for the analytical data**

The estimation of the Capacity-to-Demand ratios (CDRs) by which the safety of the PACI (as well as the EC2) approach was verified will be conducted in this activity. The way to compute these CDRs ratios is as follows. First, the set of demands for each analytical case were used to estimate the required reinforcement following both the EC2 and the PACI design approaches. Second, non-linear numerical models in Shell 2000, which considered those reinforcement areas calculated in the first step, will be developed to reproduce the numerical capacity curves of the panels. Third, the safety of the design approach was verified by extracting the set of nominal capacities from the numerical capacity curves in step 2, and comparing them against the corresponding analytical set of demands. The design will be considered as satisfactory if the

individual nominal capacities from the numerical models are greater than or equal to the individual analytical demands; or in other words, when the CDRs are greater than or equal to 1.0.

## **5. MODELING AND CALIBRATION OF THE EXPERIMENTAL DATA**

As mentioned in the methodology of this document, twenty one (21) panel tests were selected to validate the results of the EC2 and the PACI design approaches. The selected panels series analyzed in here were: four (4) panels of the SE series subjected to in-plane shear and/or Bending Moment, tested by Kirscher (1986) and Kirscher and Collins (1986); three (3) panels of the PV series subjected to in-plane tensile forces and in-plane shear forces tested by Vecchio (1981) and Vecchio and Collins (1982); four (4) panels of the SM series subjected to axial loads and/or bending moment tested Polack and Vecchio (1994); three (3) panels of the F series subjected to axial tension and compression forces tested by Belarbi and Hsu (1995); three (3) panels of the ML series tested by Marti et al (1987), which was subjected to twisting moment only; and four (4) panels of the SP series subjected to in-plane shear and out-of-plane shear forces and its associated out-of-plate bending moment tested by Adebar (1989) and Adebar and Collins (1994). Three software were used for the modeling and calibration of the panels: Shell-2000, Membrane-2000 and Abaqus. The SM and the SP panel series were simulated in Abaqus, while the PV panel series were simulated in membrane 2000. The rests of the panels were simulated in Shell-2000. The main objective in this section is the calibration of the experimental response of all selected panels. The numerical models developed in this section were able to reproduce the experimental capacity curves of the panels within an acceptable accuracy. These calibrated numerical models will be used to validate both design approaches later on in Chapter 6 . A brief description, as well as all the modeling details for each test will be provided in this chapter. Finally, a comparison between the experimental curve and the calibrated numerical curves will be also given for each selected panel.

### **5.1 Modeling and Calibration of the SE series panels**

#### **5.1.1 Description of the SE series panels tests**

The SE panel series were tested by Kirschner (1986). These panels were subjected to a combination of in-plane shear and out-of-plane bending moment as indicated figure 5.1. Four of the SE series panels were selected in this research: the SE1, the SE3, the SE4 and the SE7 panels. The SE1 panel was only subjected to in-plane shear as shown in Figure 5.1a, which reached a

maximum in-plane shear capacity of 1930 kN/m. The SE3 was only subjected to uniaxial bending moment about the x-axis as indicate in Figure 5.1b, reaching a maximum flexural moment capacity of 520 kN\*m/m. Finally, the SE4 and SE7 which panel which were subjected to in-plane shear and bending moment at  $M_x:V_{xy}$  proportions of 1:0.13 and 1:0.5, respectively. The SE4 panel reached the maximums of in-plane shear ( $V_{xy}$ ) and out-of-plate moment ( $M_x$ ) of 960 kN/m and 480 kN-m/m. The SE7 panel, on the other hand, reached the maximums of in-plane shear ( $N_{xy}$ ) and out-of-plate moment ( $M_x$ ) of 1810 kN/m and 230 kN-m/m. The panels were rectangular with a length of 1500 mm, and with a thickness of 316 mm. The reinforcement of the panels consisted in two reinforcement layers of designation bar 20M each 72mm (20M@72mm) running along the x-direction, and two reinforcement layers of designation bar 10M each 72mm (10M@72mm) running along the y-direction. An scheme of the reinforcement provided during the tests of the panels in any of the faces (top or bottom) is shown in figure 5.1.

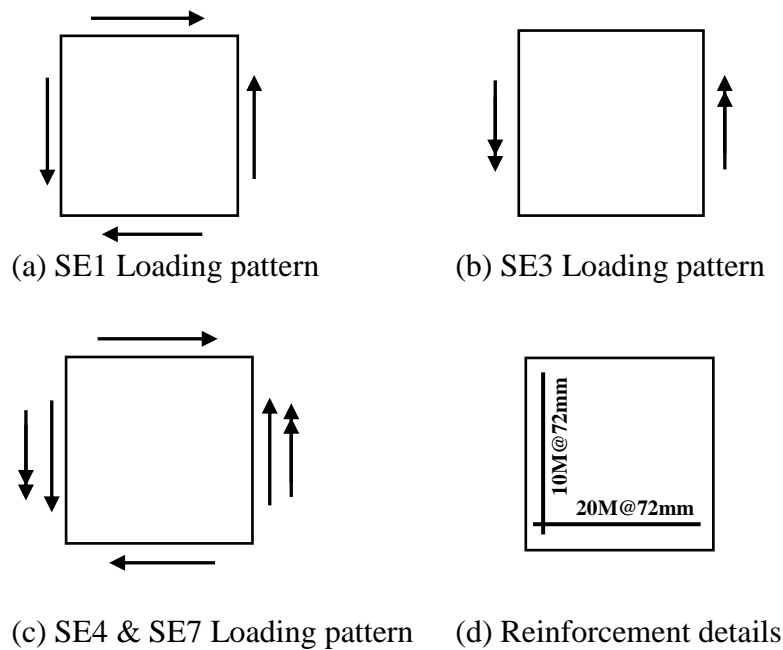


Figure 5.1. Loading Application Pattern and Reinforcement details for the SE series panels.

### 5.1.2 Modeling details of the SE series panel Tests

The modeling of the SE series panels was conducted in Shell-2000. Although it was tried to better capture the experimental response of the panels using Abaqus as well, it was not possible. It seems that for the SE series panels, the smeared cracked rotating approach of Shell-2000 offers

a better solution than the smeared cracked fixed approach assume in Abaqus. All the input for the modeling of the SE series panels are summarized in figure 5.2. The screenshot in Figure 5.2 was automatically displayed by Shell-2000 once the models have been completed. Figure 5.2 shows the constitutive material models for the concrete and steel reinforcement in the left-interior portion; the loading combination in relative terms just above the materials models; and the reinforcement configuration of the reinforcement curtains inside the panel. All numerical model developed in Shell 2000, including these SE series had two common aspects. First, the base curve for the concrete in compression was defined by selecting the Popoviciis/Thorenfeldt/Collins option; and second, the compression softening was defined by selecting the Vecchio and Collins 1986 option.

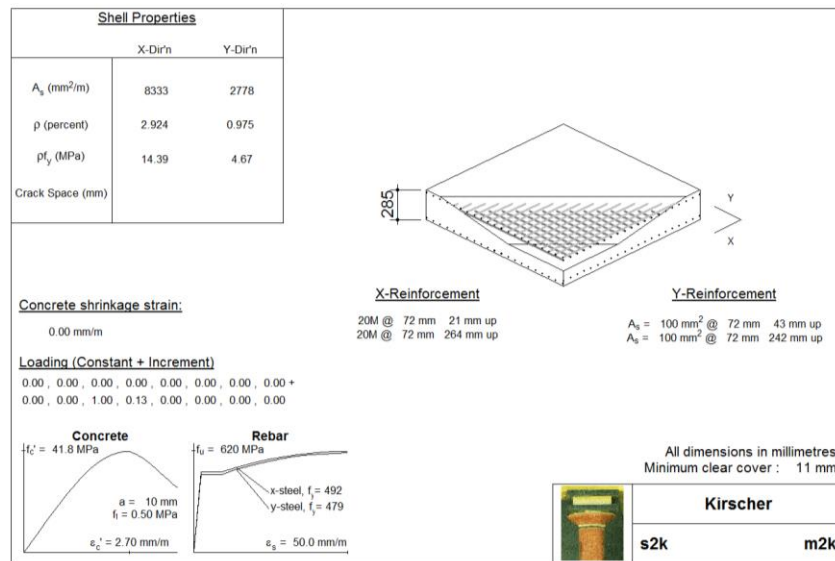


Figure 5.2. Modeling details for the SE7 panel

Table 5.1 in below summarizes all the specific values to define the behavior of the concrete in tension and in compression, as well as the behavior of the steel reinforcement bars running in both directions x and y.

Table 5.1. Material constitutive data for modeling of the SE series panels

Concrete	SE1	SE3	SE4	SE7
Cylinder strength (MPa)	42.5	46.1	42.2	41.8
Tension strength (Mpa)	2.0	2.0	3.9	1.0
Peak strain (mm/m)	2.5	2.7	2.5	2.7
Aggregate size (mm)	10	10	10	10

Table 5.1 continued

Tension stiffening factor		1.0	1.0	1.0	0.8
<b>Reinforcement Properties</b>					
#3 bars in x-direction	Elastic Modulus (MPa)	190000	200000	200000	200000
	Yield strength (MPa)	425	492	492	492
	Strain at hardening (mm/m)	9.0	9.0	9.0	9.0
	Rupture strain (mm/m)	50	50	50	50
	Ultimate strength (MPa)	620	620	620	620
#2 bars in y-direction	Elastic Modulus (MPa)	200000	200000	200000	200000
	Yield strength (MPa)	479	479	479	479
	Strain at hardening (mm/m)	9.0	9.0	9.0	9.0
	Rupture strain (mm/m)	50	50	50	50
	Ultimate strength (MPa)	611	611	611	611

### 5.1.3 Calibrated or Adjusted Responses for the SE series panels

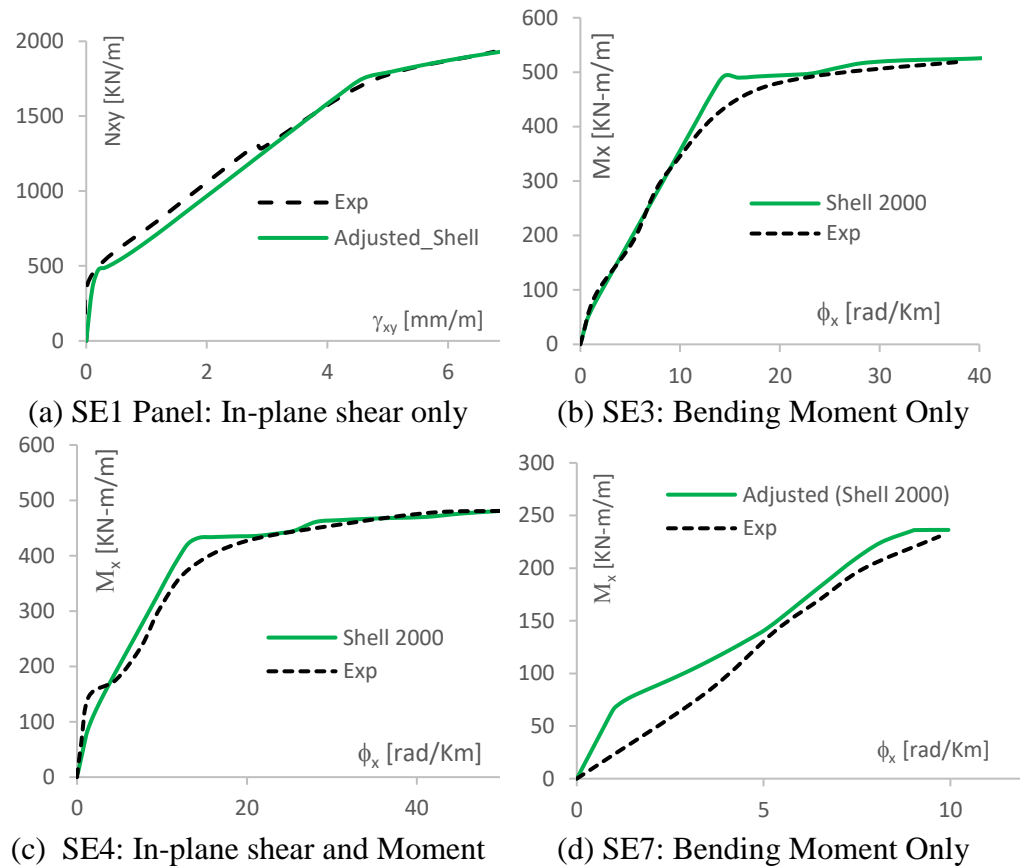


Figure 5.3. Comparison Between experimental and numerical load vs deformation curves for the SE series panels.

Figure 5.3 shows the calibrated numerical capacity curves for the SE series panels. Figure 4.3a correspond to the in-plane shear force vs shear distortion for panels SE1, which was only subjected to in-plane shear. Figure 4.3b corresponds to the moment vs curvature capacity curve for panels SE3 which was subjected to bending moment only. Figure 4.3c and 4.3d correspond to the capacity curves for panels SE4 and SE7 which were subjected to the combined action of in-plane shear plus bending moments. The numerical models captured very well the experimental response for the SE1 and the SE3 panels. Specifically, these models were able to capture the cracking capacities, the post cracking stiffness and the ultimate in-plane shear capacity of the panels. For panels SE4 and SE7, subjected to simultaneous in-plane shear force and out-of-plane bending moment action, the numerical model lost some accuracy especially for the cracking capacity and for the post-cracking stiffness. However, the ultimate capacities for these two panels were well captured by the models.

## **5.2 Modeling and Calibration of the SM series panels.**

### **5.2.1 Description of the SM series panels tests**

The SM panel series were tested by Polak and Vecchio (1994). These panels were subjected to a combination of in-plane axial forces and out-of-plane bending moments as indicated figure 5.4. Three of the SM series panels were selected in this research: The SM1, the SM2 and the SM3 panels. The SM1 panel was only subjected to out-of-plane bending moment about the y-direction, producing axial stresses in the x-direction, as shown in Figure 4.4a. This panel reached a maximum out-of-plane bending moment capacity of 477 kN-m/m. The SM2 on the other hand, was subjected to the combined action of compressive axial forces and uniaxial bending about the y-axis as indicated in Figure 4.4b. This panel reached a maximum compressive axial force in the x-direction of 1206 kN/m, a maximum of compressive axial force of 1684 kN/m in the y-direction, and a maximum of out-of-plane bending moment about the y-axis of 421 kN\*m/m. Finally, the SM3 was subjected to biaxial out-of-plane bending moment. This panel reached the maximums of 488 kN\*m/m for the moment about the y-axis, which produces axial stresses in the x-direction ( $M_x$ ); and a maximum 151 kN/m for the bending moment about the y-direction, which produces axial stresses in the y-direction ( $M_y$ ). The panels were rectangular with a length of 1500 mm, and a thickness of 316mm. All panels had a reinforcement ration of 1.25% for the bottom and top layers

in the x-direction, and a reinforcement ratio of 0.42% for the bottom and top layers running in the y-direction. Details of the reinforcement configuration are presented in Figure 5.4d. The reinforcement along the x-direction of the panel consisted in two reinforcement curtains of designation bar 20M each 75 mm (20M@75mm), while the reinforcement along the y-direction consisted in designation bar 10M each 75mm (10M@75mm).

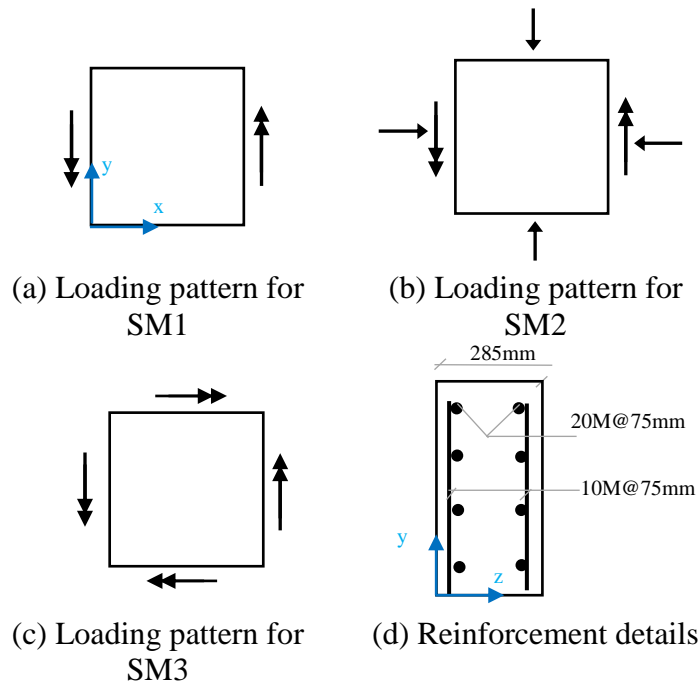
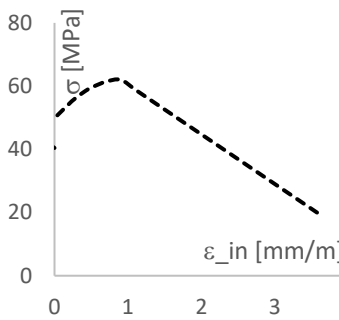


Figure 5.4. Loading Application Pattern and Reinforcement details for the SM series Panels.

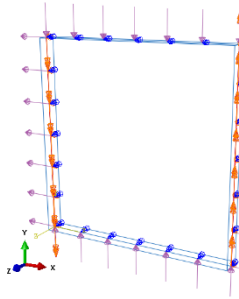
### 5.2.2 Modeling details for the SM series panels

The SM series numerical models were developed in Abaqus. The SM1 and the SM2 panels were modeled using the CDP concrete model, while the SM3 was modeled using the BFC concrete model. Although the first option was to develop these models in Shell-2000, it was not possible to reproduce a consistent numerical response for panels SM2 and SM3 in this software. Specifically, the models in Shell-2000 did not exhibit any non-linear response, and after several iterations, the analysis stepped as soon as the panels reached yielding. Figure 5.5 shows the modeling procedure as well as the main input information to reproduce the calibrated numerical for the SM2 panel in Abaqus. The curve to simulate the uniaxial behavior of the concrete in compression, shown in Figure 5.5a, was defined using the hognestad parabola model, which was built by using the data in table 5.2. The behavior of the concrete in tension in figure 4.5b, was defined by using the Shima

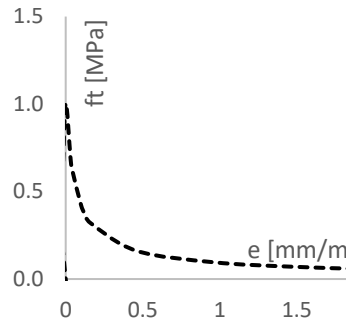
tension stiffening model (Shima et al 1987), following equation 26, where  $c$  was taken 0.2 because the reinforcement consisted in conventional deformed bars. The values to define the tension softening model are consigned in table 5.2. Finally, the uniaxial behavior of the steel reinforcement in both directions are shown in figure 5.5c.



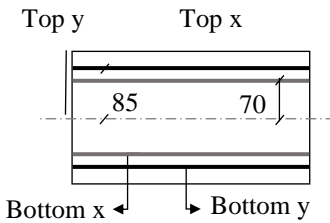
5.5a. Concrete in compression



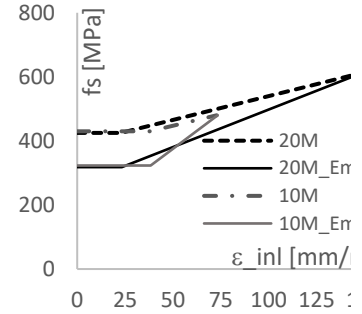
5.5d. Loading application and Boundary conditions



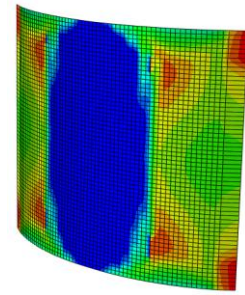
5.5b. Concrete in Tension



5.5e. Area and location of the reinforcement layers inside the LCS finite element



5.5c. Steel Reinforcement



5.5f. Deformed shape and mesh size of 25x25mm

Figure 5.5. Modeling details for the SM2 panel.

The calibration of the numerical capacity curves for the SM2 and SM3 panels against their respective experimental curves were one of the more challenging among all numerical models reproduced in this thesis. For the case of the SM2 panel, which was subjected to a combination of axial load and bending moment, it was found after several trials, that after introducing the reinforcement properties as exactly reported from the experiment (i.e., yielding stress and strain), it was not possible to match the experimental response of the panels with an acceptable accuracy. To calibrate the numerical curves for those two panels, it was necessary to modify the material properties of the steel reinforcement as recommended by Maekawa et al (2003). Maekawa et al

(2003) suggests that the yielding stress of a reinforcement bar embedded in concrete is lower than the yielding strength exhibited by the same bar but in an isolated test. Figure 5.5c shows the reduction in yielding stress for the bars running in both directions of the panels. As observed, the yielding stress of the bars running in the x-direction drops from 425 Pa to 318 MPa, whereas the yielding strength of the bars in the y-reduction drop from 430 MPa to 323 MPa. The ultimate strength of the bars on the other hand, was introduced as reported. Table 5.2 summarizes the material constitutive details to reproduce the calibrated numerical curve for the SM1 and the SM2 panel.

Table 5.2. Material constitutive data for modeling of the SM1 and SM2 panels

<b>Concrete</b>		SM1	SM2
Modulus of Elasticity (MPa)		18000	23000
Poisson ratio		0.18	0.18
<b>Concrete in Compression</b>			
Strength at elastic limit $f_{ce}$ (MPa)		33.60	37.63
Strain at elastic limit $\epsilon_{ce}$ (mm/m)		0.93	0.94
Maximum Compressive strength $f_{co}$ (MPa)		47	62
Strain at max compressive stress $\epsilon_{co}$ (mm/m)		2.0	2.6
Ultimate Compressive strength $f_{cu}$ (MPa)		40	43.38
Ultimate compressive strain $\epsilon_{cu}$ (mm/m)		3.4	4
<b>Concrete in Tension</b>			
Tension strength (MPa)		2.0	2.0
Strength at elastic limit (mm/m)		0.11	0.087
Ultimate strain (mm/m)		4.0	4.0
<b>CDP model specialized parameters</b>			
Dilation angle (f)		10	10
Eccentricity (e)		0.1	0.1
fcb / fc ratio		1.16	1.16
Second invariant Kc		0.67	0.67
<b>Reinforcement Properties</b>			
#3 bars in x-direction	Elastic Modulus (MPa)	190000	200000
	Yield strength (MPa)	425	318*
	Strain at hardening (mm/m)	9.0	9.0
	Rupture strain (mm/m)	50	50
	Ultimate strength (MPa)	611	611
#2 bars in y-direction	Elastic Modulus (MPa)	200000	200000
	Yield strength (MPa)	479	323*
	Strain at hardening (mm/m)	9.0	9.0
	Rupture strain (mm/m)	50	50
	Ultimate strength (MPa)	611	480

\* Reduced yielding stress values.

Figure 5.5d shows the boundary conditions and the applied forces for the simulation of the SM series panels. The out-of-plane bending moment demand about the y-axis was applied as deformation control by imposing rotation at the vertical edges of the panel. The axial loads, on the other hand, were applied as force control using approximate values. The magnitude of this non-reported axial forces were approximately estimated by multiplying the maximum bending moment reported from the experiment (421 kN\*m/m) by four (4) as indicated in the proportional loading. Thus, the axial forces in tension and compression along the x-axis and the y-axis respectively, were estimated in 1684 KN/m for panel SM2. The vertical edges of the panel were restricted to translate in the out-of-plane direction (z-axis), and the x-y plane was restricted to rotate about the z-axis as well. Inducing the out-of-plane bending moment as deformation control, allowed to directly compare the bending moment capacity reported from the experiment, against the bending capacities estimated through the numerical models after introducing the areas of reinforcement suggested for each design approach.

Figure 5.5e shows the details for the introduction of the reinforcement inside the LCS element. As explained in section 2, the areas of reinforcement of a single bar, the spacing between the bars, and the location of each curtain layer must be specified in the LCS elements. Figure 5.5e shows that all bars were #5 layers and spaced at the same distance of 75mm (#5@75mm) in all layers. Figure 5.5e also shows the location of the reinforcement curtains the cross section, taken as reference the middle plane of the panels. For the calibration of the experimental curve, these distances were taken exactly as reported during the experiment. Finally, Figure 5.5f shows the deformed shape of the SM2 panel as well as the size mesh of 25mm x 25mm. All panels were simulated following the same procedure in Abaqus, but considering the specific reported concrete material properties, and the magnitude and direction of the axial forces.

The SM3 panel on the other hand, which was subjected to biaxial bending moments, particularly resulted being very sensitive to the ratio between the applied rotation about the y-axis and the rotation about x-axis ( $\theta_y/\theta_x$ ). It is worthy to clarify that the higher amount of reinforcement in panel SM3 (as well as for all the SM panels) was placed running along the x-direction, as indicated in figures 5.5c and 5.5d. The lower amount of reinforcement, on the other hand, was placed running along the y-direction. Thus, the capacity moment curve ( $M_x-\phi_x$ ) in figure 5.6c was reproduced by imposing certain rotation about the vertical y-axis of the panels, whereas the

capacity moment curve ( $M_y-\phi_y$ ), in figure 5.6d, was reproduced by imposing a different rotation about the vertical y-axis of the panels. The sensitive rotation ratio issue can be explained in the following way. When imposing a high ( $\theta_y/\theta_x$ ) rotation ratio, the experimental capacity moment curve ( $M_x-\phi_x$ ) was well captured by the numerical model. However, under the same rotation ratio ( $\theta_y/\theta_x$ ), the experimental capacity moment curve ( $M_y-\phi_y$ ) exhibited a sudden drop in strength after yielding, which do not correspond to the reality of the test. The opposite occurred when imposing a low rotation ratio. In this case, the experimental capacity curve ( $M_y-\phi_y$ ) was well captured by the numerical model, but the numerical capacity curve ( $M_x-\phi_x$ ) lost accuracy, by also showing a sudden lost on strength after yielding.

Table 5.3. Material constitutive data for modeling of the SM3 panel using BFC model in Abaqus

<b>Concrete</b>		SM3-Mx and My
Modulus of Elasticity (MPa)		26600
Poisson ratio		0.18
<i>Concrete in Tension FIP 90</i>		
Aggregate size (mm)		10
Tension strength (MPa)		1.4
Strain at elastic limit (mm/m)		0.053
Ultimate tensile strain (mm/m)		3.8
Brittle Shear Behavior: Power Law		
Strain at total loss of tensile strength $\epsilon^{ck}$ (mm/m)		3.8
Shear retention facto $\rho$		1.0
Brittle failure		
Failure criteria		Bidirectional
Direct cracking failure displacement (mm/m)		0.0951
<b>Reinforcement Properties</b>		
20M bars in the x-direction	Elastic Modulus (MPa)	200000
	Yield strength (MPa)	400.7*
	Rupture strain	148
	Ultimate strength (MPa)	611
10M bars in the y-direction	Elastic Modulus (MPa)	200000
	Yield strength (MPa)	370.2*
	Rupture strain (mm/m)	148
	Ultimate strength (MPa)	480

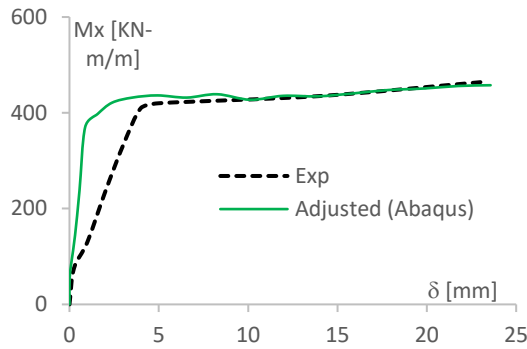
\* Reduced yielding stress values.

There were two solutions to overcome this rotation ratio sensitivity issue. First, the development of two separately numerical models: One model to reproduce the experimental moment capacity curve ( $M_x-\phi_x$ ), associated with the strongest bending capacity of the panel; and another model to reproduce the experimental moment capacity curve ( $M_y-\phi_y$ ), associated with the

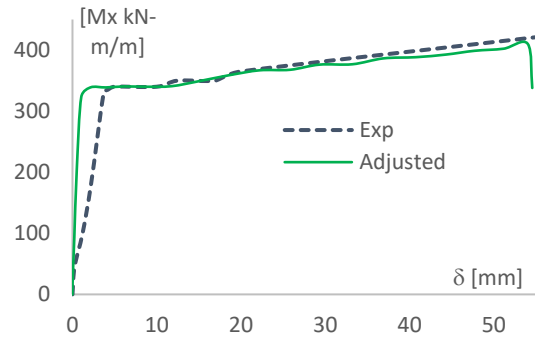
weakest bending capacity of the panel. The two models for the SM3 panel were the same except for the only difference in the applied rotation ratio. The applied rotations  $\theta_y$  and  $\theta_x$  to reproduce the  $M_x-\phi_x$  curve were 0.67 rad and 0.14 rad, respectively; while applied rotations  $\theta_y$  and  $\theta_x$  to reproduce the  $M_y-\phi_y$  curve were 0.14 rad and 0.52 rad. The second solution was to use the BFC concrete model instead of the CDP concrete model. The models with BFC were not only less sensitive to the rotation ratio, but also and produced more stable curves. Table 5.3 summarizes all the values to define the concrete and the steel reinforcement properties for the BFC concrete model in in Abaqus.

### **5.2.3 Adjusted Responses for the SM series panels**

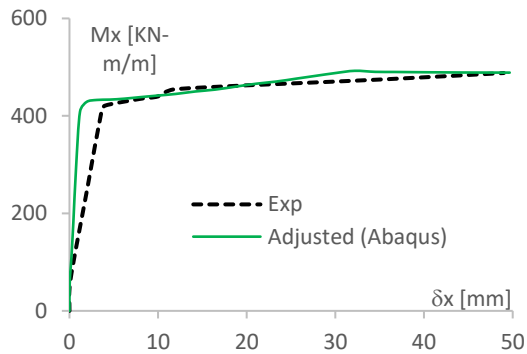
Figure 5.6 compares the calibrated numerical curve and the reported experimental capacity curve for the SM series. Figure 5.6a corresponds to the moment vs displacement curve of the panel SM1 which was subjected to out-of-plate bending only. Figure 5.6b corresponds to panel SM2, which was subjected to axial compressive and axial tension loads in y and x directions, plus out-of-plate bending moment about the y-axis, which produces normal stress along the x-direction. Figures 4.6c and 4.6d correspond to panel SM3 subjected to biaxial moment.



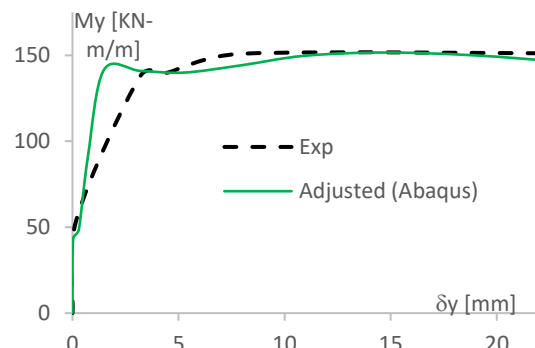
(a) SM1 Panel: Bending Moment about the x-axis only ( $M_x$ )



(b) SM2: Bending Moment about the x-axis ( $M_x$ ) and Compressive axial forces ( $N_x$  and  $N_y$ )



(c) SM3: Bi-axial Bending Moments  $M_x$  and  $M_y$



(d) SM3: Bi-axial Bending Moments  $M_x$  and  $M_y$

Figure 5.6. Comparison Between experimental and numerical load vs deformation curves for the SM series panels.

A common feature in all numerical curves in Figure 5.6 is the lack of accuracy in capturing the stiffness of the panels after cracking. The reason for this is related to the fact that the Layer Composite Shell (LCS) elements in Abaqus assume perfect bonding between the concrete and the steel reinforcement, by which the reduction in stiffness provoked by the slippage between the two materials is not captured. However, the cracking moment, the yielding moment, and the ultimate flexural capacities were properly captured by the numerical models.

### 5.3 Analysis and results for the PV series panels.

#### 5.3.1 Description of the PV series panels tests

The PV series panels were subjected to the combined action of in-plane shear and axial forces as shown in figure 5.7. Panels PV23, PV24 and PV25 were subjected in-plane shear plus compressive axial forces, while panel PV28 was subjected to in-plane shear plus tensile axial forces. The load proportions ( $N_{xy} : N_x : N_y$ ), at which panels PV23, PV25 and PV27 were subjected were 1:-0.38:-0.38, 1:-0.69:-.69, and 1:0.8:0.8, respectively. The load proportion ( $N_{xy} : N_x : N_y$ ), at which PV28 panel was subjected was 1:+0.28:+0.28. The dimension of the panels, as well as the reinforcement details are shown in Figure 5.7. The panels were rectangular with a length of 890 mm and a thickness of 70 mm. The reinforcement in all panels consisted in designation bar No 2 each 50 mm (#2@50mm) in both layers (top and bottom) and in both directions, as shown in figure 5.7c.

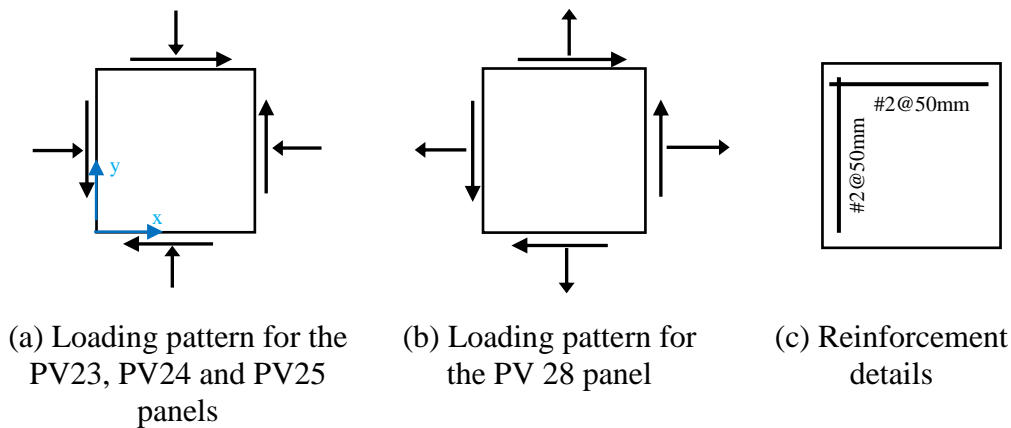


Figure 5.7. Loading Application Pattern and Reinforcement details for the PV series panel.

#### 5.3.2 Modeling details and calibration of the PV series panels

Two software were employed to model the response of the PV series models, Abaqus and Membrane-2000. Although the first option was to develop these models in Shell 2000, it was not possible to reproduce a consistent curve in this software. Specifically, the models in Shell-2000 did not exhibit any non-linear response. After several iterations applying proportional loading, the analysis for all PV series panels stopped as soon they reached yielding or even before. Since Shell-2000 did not produce satisfactory numerical response, it was decided to develop numerical models

in Abaqus. The model in Abaqus produced very satisfactory results but a very high price in time. It was particularly difficult to calibrate the numerical response of these PV series using the SMC concrete models. Then, (unfortunately or fortunately depending on the point of view) the author realized that because the PV panels were only subjected to membrane forces, the Membrane-2000 software can be used for the analysis. The results of Membrane-2000 were satisfactory, and they were obtained very easily compared to Abaqus. It is worthy to mention that the numerical models in Abaqus were developed long before the creation of the numerical models in membrane 2000. However, since the work was already done, it was decided to show both results because it is useful to compare the results between the software. As explained earlier, Abaqus assumes the smeared fixed crack approach, while Membrane-2000 (same as Shell 2000) assumes the rotating smeared crack approach. Details for the modeling of the PV panels in Membrane-2000 and in Abaqus will be given next.

### ***Modelling Details in Abaqus.***

The Smeared Cracked Model (SMC) for concrete materials was used to develop the numerical models in Abaqus. Figure 5.8 explains the modeling procedure in Abaqus for the PV28 panel in Abaqus. The curve to simulate the uniaxial behavior of the concrete in compression, shown in Figure 5.8a, was defined using the hognestad parabola model, which was built using the data in table 5.4. The behavior of the concrete in tension in figure 5.8b, was defined by using the FIB 90 model, and the specific values are given in table 5.4. Finally, the uniaxial behavior of steel reinforcement in both directions are shown in figure 5.8c. Like for the cases of the SM2 and the SM3 panels, the yielding stress of the reinforcement for the PV28 panel were slightly modified (reduced) following the recommendation of Maekawa et al (2003).

Figure 5.8d shows the Boundary Conditions (BCs) and the applied forces for the simulation of the panels. There was no need to specify any BCs in the model because the models reached equilibrium itself just by applying the in-plane shear forces. The load application for these PV series panels, different to the SM2 panel, in which the loads were applied as combination of deformation and force control, was entirely applied as force control. This means that both, the in-plane shear force, and the axial forces, were applied as force control, since there is no possible to apply in-plane shear deformation (or distortion) to the LCS elements in Abaqus. The disadvantage

of applying force control to impose the deformations is that the numerical strength (or capacity) of the panels cannot be directly estimated as same as when deformation control is applied. In these cases, the calibration of the models were conducted by imposing the maximum reported force combination ( $N_x$  and  $N_{xy}$ ) in each panel, and trying to match the corresponding maximum in-plane shear deformation  $\gamma_{xy}$ .

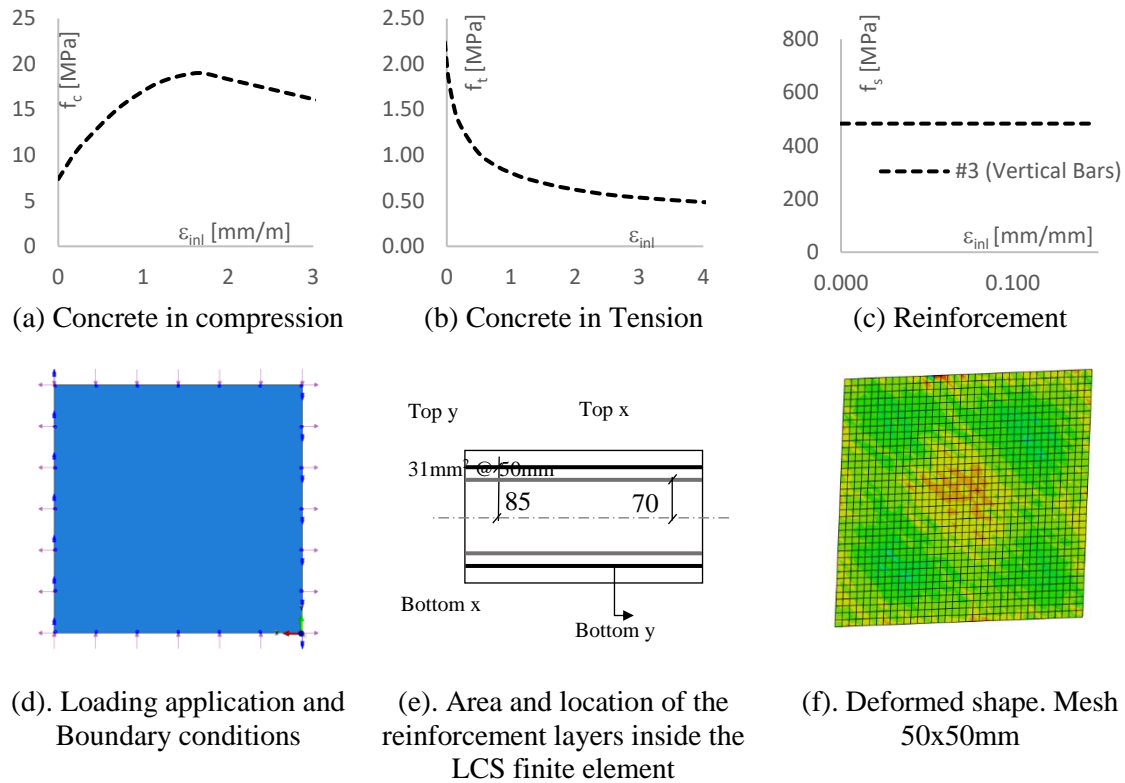


Figure 5.8. Modeling details for the PV28 panel.

Figure 5.8e shows the details for the modeling of the reinforcement inside the LCS element. As can be seen in Figure 5.8e, the reinforcement was equal in all directions and in both faces, which consisted in designation bar #2 each 50 mm (#2@50mm). The distances from the centroid of the LCS element (central axis line of the cross section of the panel) to the centroid of each curtain layer are also given in Figure 5.8e. For the calibration of the experimental curve, these distances were taken exact as reported during the experiments. Finally, Figure 5.8d shows the 50x50 mm size mesh of the elements and the deformed shape in the final stage for the PV28 panels specifically. All panels were simulated following the same procedure in Abaqus but considering

the specific reported concrete material properties, and the magnitude and direction of the axial forces.

**Modelling Details in Membrane 2000.**

Figure 5.9 shows the main input for the modelling of the PV28 panel in Membrane 2000. As observed in the loading combination, the applied loading ratio between in-plane axial forces and in-plane shear forces were 0.28:1.0. The clear cover of the reinforcement layer running in the x-direction was set in 6 mm as specified in the experiment. As explained in the background, the models in Membrane 2000 were a lot easier than in Abaqus. The advantage of having developed the numerical models in Membrane 2000, is that it allowed to directly compare the capacity of the panels in terms of forces and not in terms of deformation as was the case when using Abaqus.

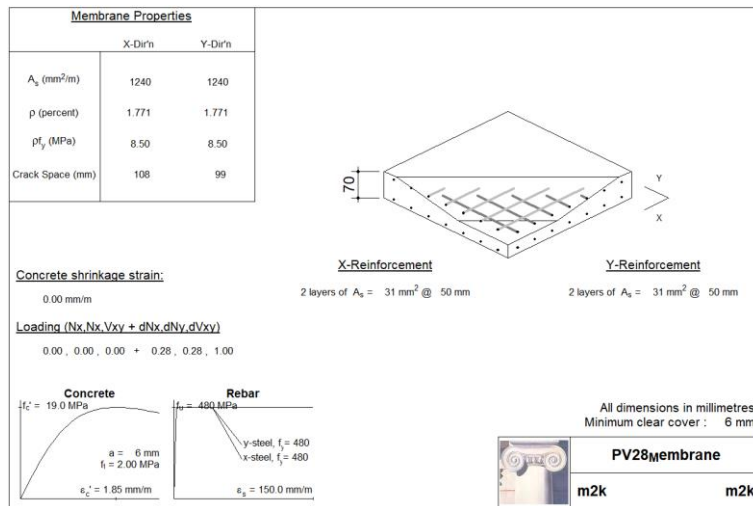


Figure 5.9. Main Modeling Inputs in Membrane 2000 for the PV28 Panel

Table 5.4 summarizes the material properties values utilized to develop the numerical models in both software. As can be noted, the main differences are in the lower values of yielding stress for the steel reinforcement. One possible explanation for this is that since Abaqus follows the fixed smeared cracked approach, which might overestimate the higher stiffness in comparison to the rotating smeared cracked approach assumed in membrane 2000. One way to compensate the higher overestimation of the stiffness in the Abaqus models is to reduce the young modulus of the steel reinforcement.

Table 5.4. Material constitutive data for modeling of the PV series panels using the SMC model in Abaqus

<b>Concrete</b>		PV23		PV24		PV25		PV28	
		Abaqus	Memb	Abaqus	Memb	Abaqus	Memb	Abaqus	Memb
Modulus of Elasticity (MPa)		20000	19424	23000	19277	23000	18979	20000	21461
Poisson ratio		0.16	-	0.18	-	0.18	-	0.18	-
<i>Concrete in Compression</i>									
Strength at elastic limit $f_{ce}$ (MPa)		7.39	7.35	9.0	8.06	7.22	8.06	7.89	7.85
Strain at elastic limit $\epsilon_{ce}$ (mm/m)		0.44		0.38	0.44	0.38	0.39	0.44	0.39
Maximum Compressive strength $f_{co}$ (MPa)		25	25	20	20	19.25	19.2	19.0	19
Strain at max compressive stress $\epsilon_{co}$ (mm/m)		2.0	2.3	1.9	2.1	1.8	2.1	2.0	1.85
Ultimate Compressive strength $f_{cu}$ (MPa)		15.93	21.5	21.48	18.5	15.4	17.83	15.93	17.83
Ultimate compressive strain $\epsilon_{cu}$ (mm/m)		3.4	3.45	3.4	3.15	3.4	3.15	3.4	2.7
<i>Tension stiffening</i>									
Ratio 2		0.14	-	0.116	-	0.15	-	0.113	-
Maximum tensile strength (MPa)		2.66	-	2.0	-	2.89	2.0	2.15	-
Ultimate strain (mm/m)		4.5	-	4.0	-	2.84	-	6	-
Shear retention									
pho_close		1	-	1	-	1	-	1	-
Eps_Max (mm/m)		4.5	-	0.1	-	2.84	-	6	-
<b>Reinforcement Properties</b>									
#2 bars in the x and y directi ons	Elastic Modulus (MPa)	175000	200000	185000	200000	167000	200000	185000	195000
	Yield strength	420	518	492	492	466	466	N.A.	480
	Strain at hardening (mm/m)	60	50	50	50	N.A.	50	150	50
	Rupture strain (mm/m)	127.6	130	130	130	50	100	50	150
	Ultimate strength (MPa)	460	518	492	492	466	466	480	480

### 5.3.3 Calibrated or adjusted Responses for the PV series Panels

The comparison between the experimental and the numerical capacity curves for the PV series panels are shown in Figure 5.10. The capacity curves of the PV series were originally reported in terms of shear stress vs shear strain (or distortion). However, to be consistent with all panels analyzed in here, the shear stress was converted to in-plane shear force per unit length by multiplying by the thickness of the panels. Three curves are observed in figure 5.10: The black and discontinuous line represent the experimental curve; the green and dotted line is the adjusted (or calibrated) curve from Abaqus; and the green and continuous line represents the adjusted curve generated in Membrane-2000.

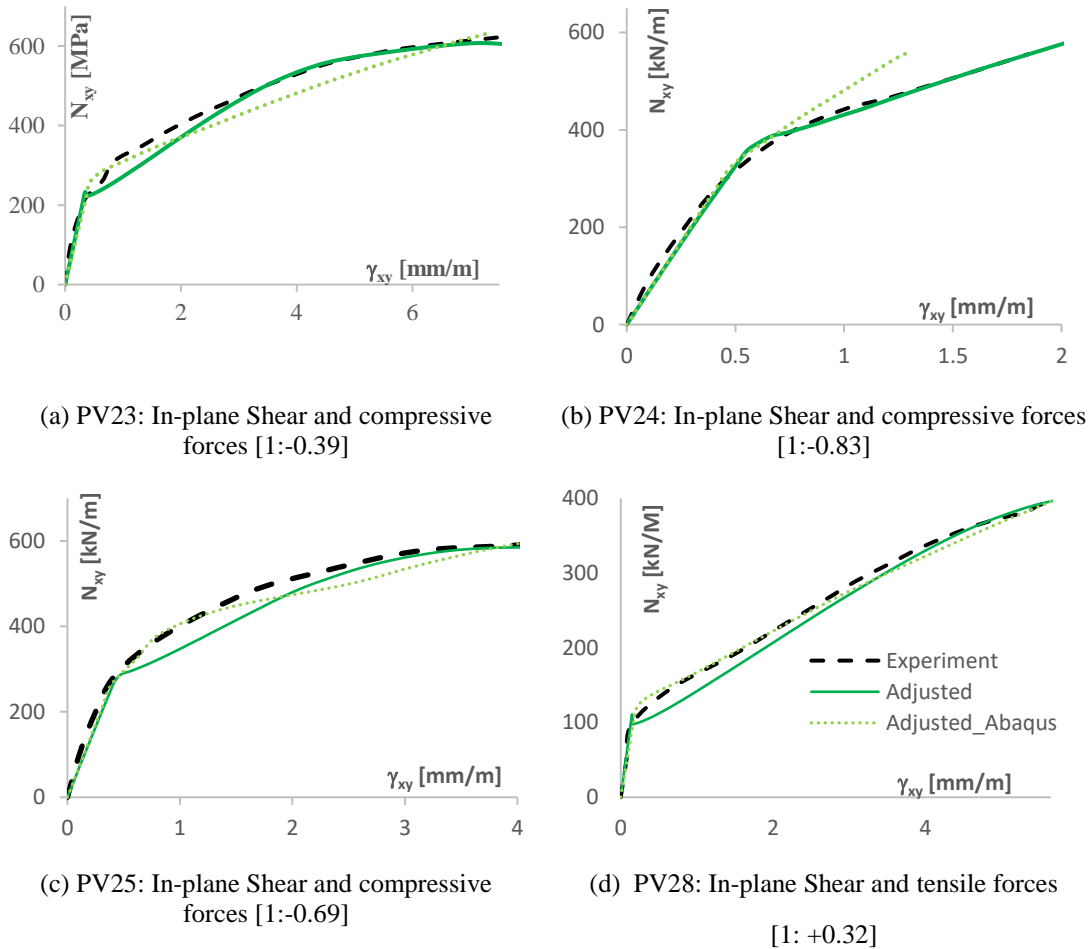


Figure 5.10. Comparison between experimental and numerical load vs deformation curves for the PV series panels.

Both, the numerical curves from Abaqus, and the numerical curve from Membrane-2000 show an acceptable agreement with the experimental curves. Both numerical curves were able to capture very well the cracking and the ultimate in-plane shear capacities reported from the experiments. The numerical curve from Abaqus for panel PV24, however, does not show a good agreement with the experimental curve after cracking. It is important to highlight that the results of the EC2 and the PACI approach were validated only by using the numerical curves from Membrane 2000. There were three reason for this selection: First, as just explained, the curve in Abaqus for panels PV24 was not consistent with the experiment. Second, the shell 2000 curves show a better agreement at ultimate capacities with the experimental curves; and third, because the Membrane-2000 curves give the maximum capacities of panels directly in terms of strength and not in terms of deformation as was the case for the curves in Abaqus.

#### **5.3.4 Modeling and Calibration of the F series panels Description of the F series panels tests**

The F series panels were tested by Belarbi and Hsu (1995). These panels were subjected to axial forces only. In-plane axial tensile forces along the x-direction, and in-plane compressive axial forces along the y-direction. The panels were loaded with different ratios of compression over tensile forces ( $N_y/N_x$ ) in the following manner. The  $N_y/N_x$  loading ratios values for the F2, the F3 and the F4 panels were 2, 3, and 4 respectively. Panel F2 reached a maximum compressive stress of 11.85 MPa, which correspond to a maximum compression load of 2110 kN/m. Panel 23 reported a maximum compressive stress of 18.75 MPa, corresponding to a maximum compressive load of 3374 kN/m. Finally, panels F4 reached a maximum compressive stress of 20.85 MPa, which correspond to a maximum compression load of 3753 kN/m. The dimension of the panels, as well as the reinforcement details are shown in Figure 5.10. The reinforcement ratio in the x-direction was 1.27 %, while the reinforcement direction along the y-direction was on only 0.54%.

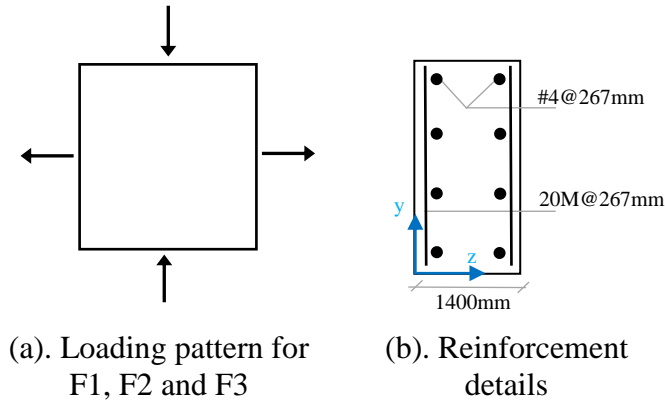


Figure 5.11. Loading Application Pattern and Reinforcement details for the PV series panel.

### 5.3.5 Modeling details and calibration of the F series panels tests.

The modeling of the F series panels was conducted in Shell 2000. Although it was tried to better capture the experimental response of the panels using Abaqus as well, the Shell 2000 models offered the same level of accuracy and at a much less time and effort. Figure 5.11 shows the details for the modeling of the F2 panel. The material properties for the concrete and steel reinforcement are shown in the left-interior portion of the figure; the loading combination in relative terms are given just above the materials models; and the reinforcement configuration of the reinforcement curtains inside the panel are shown almost in the center of the figure. Panel F4 and F5 were pretty much the same but changing the material properties shown table 5.5, and of course, their respective  $N_y/N_x$  loading ratio. Table 5.4 summarizes all the specific values to define the behavior of the concrete in compression and in tension, as well as the behavior of the steel reinforcement bars running in both directions x and y. For these panels there was no need to modify the yielding stress of the reinforcement bars reported in the experiments.

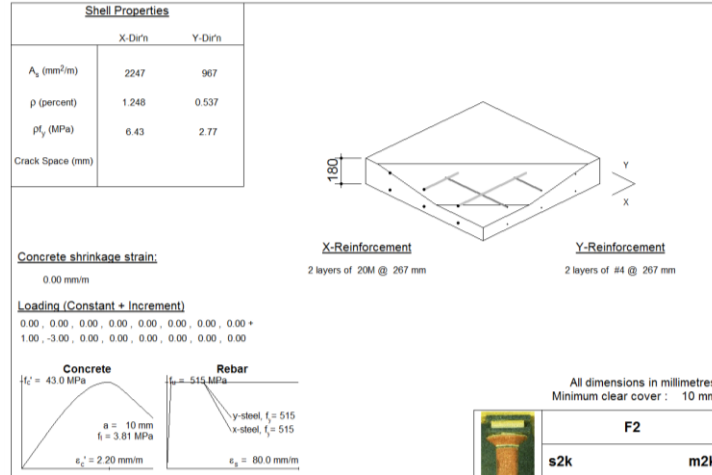


Figure 5.12. Example of general input data for the modeling of the F-series panels.

Table 5.5. Material constitutive data for modeling of the F series panels in Shell 2000

Concrete		F2	F3	F4
Cylinder strength (MPa)		40.0	43.0	42.2
Tension strength (MPa)		2.0	3.81	3.9
Peak strain (mm/m)		2.6	2.2	2.5
Aggregate size (mm)		10	10	10
Tension stiffening factor		1.0	1.0	1.0
Reinforcement Properties				
20M bars in x-direction	Elastic Modulus (MPa)	200000	180000	190000
	Yield strength (MPa)	490	515	490
	Strain at hardening (mm/m)	20	20	9.0
	Rupture strain	80	80	50
	Ultimate strength (MPa)	530	490	530
#4 bars in y-direction	Elastic Modulus	200000	180000	190000
	Yield strength (MPa)	490	515	530
	Strain at hardening (mm/m)	20	20	20
	Rupture strain (mm/m)	80	80	80
	Ultimate strength (MPa)	530	530	530

### 5.3.6 Adjusted or Calibrated numerical curves for the F-series panels

The agreement between the calibrated numerical curves and the experimental capacity curves was acceptable. The numerical models in Shell 2000 capture very well the experimental response of panels F3 and F4, and with less accuracy the response of panel F2. The error of the maximum reported compressive stress capacity in the y-direction of the panels, and the maximum estimated numerical capacities were 5%, 1%, and 5%, for panels F2, F3, and F4, respectively.

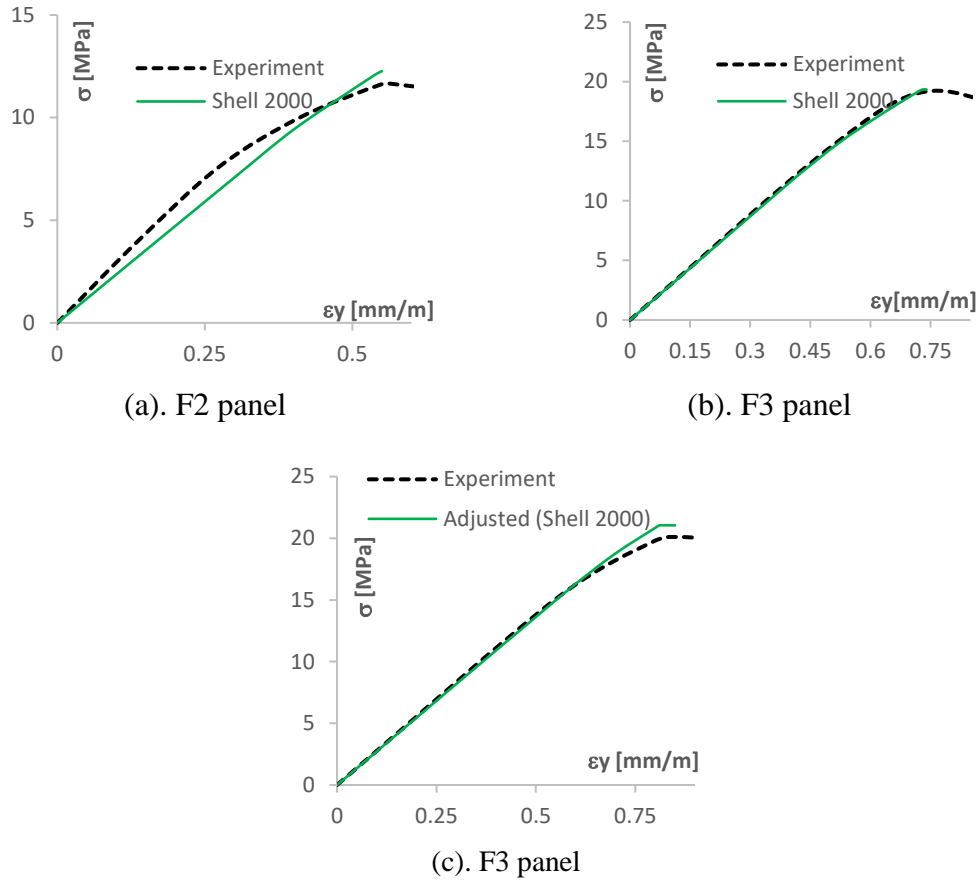


Figure 5.13. Comparison between experimental and numerical load vs deformation curves for the PV series panels

## 5.4 Modeling and calibration of the ML series panels.

### 5.4.1 Description of the tests

The ML panel series were tested by Marti et al (1987). Details about the F series panels tests are given in Figure 5.14. These panels were subjected to twisting moment only as indicated in figure 5.13a. Three panels, the ML1, the ML2 and the ML9 were selected in this research. These reached the maximum twisting moment capacities of 45 kN\*m/m, 69 kN\*m/m, and 101 kN\*m/m, respectively. The panels were rectangular and had a length of 1700 mm, and a thickness of 200mm. Each reinforcement layer for the ML1, the ML2 and the ML9 panels consisted in 10M@200mm, 10M@100mm, and 15M@100mm, which also represents reinforcement ratios of 0.25%, 0.5%, and 1%, respectively.

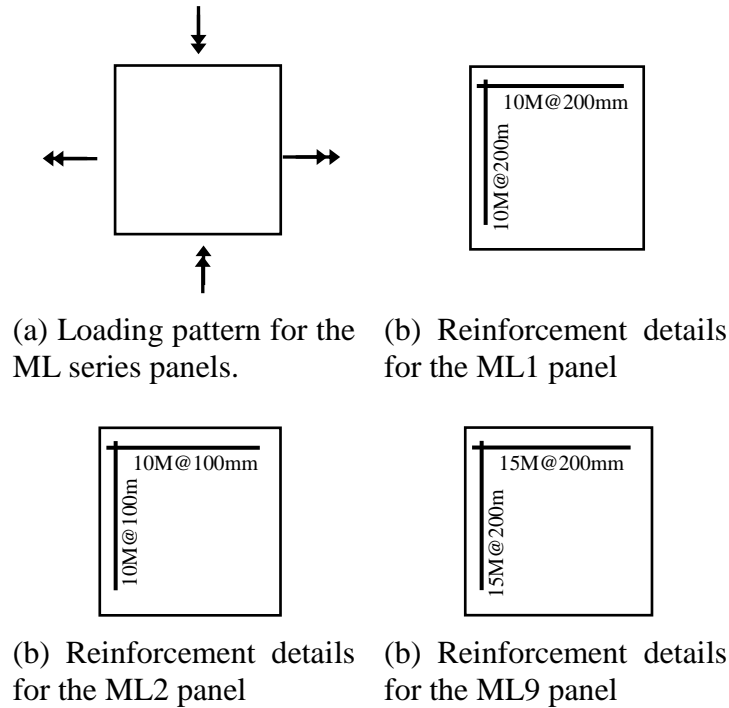


Figure 5.14. Loading application pattern and reinforcement detail for the F series panels.

#### 5.4.2 Modeling details for the ML series panel.

The modeling of the ML series panels was conducted in Shell 2000. Although it was also tried to reproduce the experimental response of the panels using Abaqus as well, it was no possible to apply consistently the twisting moment in the LCS elements. The details for the modeling of the ML2 panel, which are automatically displayed by shell 2000 once the model was completed, are summarized in figure 5.15. The material models for the concrete and steel reinforcement are shown in the left-interior portion of figure 5.15; the loading combination in relative terms are given just above the materials models; and the reinforcement configuration of the reinforcement curtains (r layers) inside the panel, are almost in the center of the figure. The details for the modeling of ML1 and the ML9 models were pretty much the same, but changing some material properties and of course, the reinforcement configurations explained in figure 5.14. The material properties for each ML panel are given in table 5.6.

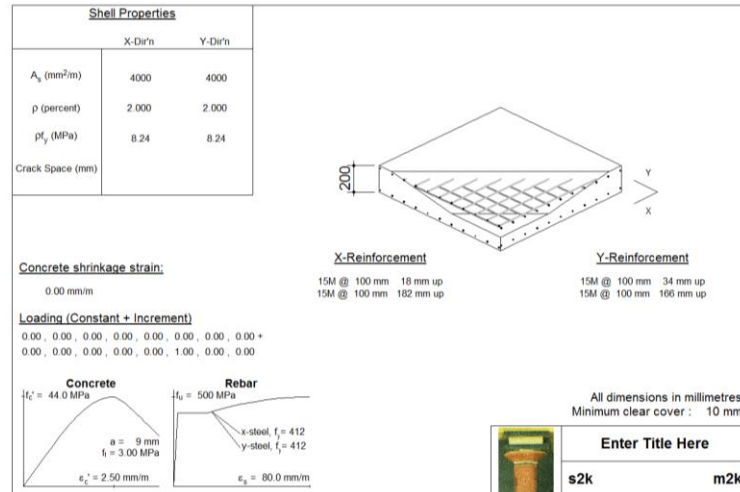


Figure 5.15. General input data for the modeling of the ML2 panel.

Table 5.6. Material constitutive data for modeling of the ML series in Shell 2000

Concrete		ML1	ML2	ML9
Cylinder strength (MPa)		46.7	36.2	44.4
Tension strength (MPa)		2.4	2.6	3.1
Peak strain (mm/m)		2.7	2.7	2.7
Aggregate size (mm)		10	10	10
Tension stiffening factor		0.8	0.8	0.8
Reinforcement Properties				
20M bars in x-direction	Elastic Modulus (MPa)	160000*	160000*	170000*
	Yield strength	551	551	412
	Strain at hardening (mm/m)	20	20	20
	Rupture strain (mm/m)	80	80	80
	Ultimate strength (MPa)	551	551	412

\* Not reported value.

### 5.4.3 Calibrated or Adjusted Responses for the ML series panels

With the numerical models in Shell 2000, it was possible to capture very well the cracking and the ultimate twisting capacities of the ML panels as appreciated in Figure 5.15. Even the post-cracking behavior of panels (excepting for the ML1 panel) was well captured by the numerical models. However, in order to obtain this good agreement between the numerical and the experimental curves, a relatively low young modulus for the steel reinforcement was introduced as shown in table 5.6. It must be noted that the Marti et al (1987) did not reported the young's

modulus of the reinforcement, and they also said that the all bars did not exhibit a clear yielding plateau.

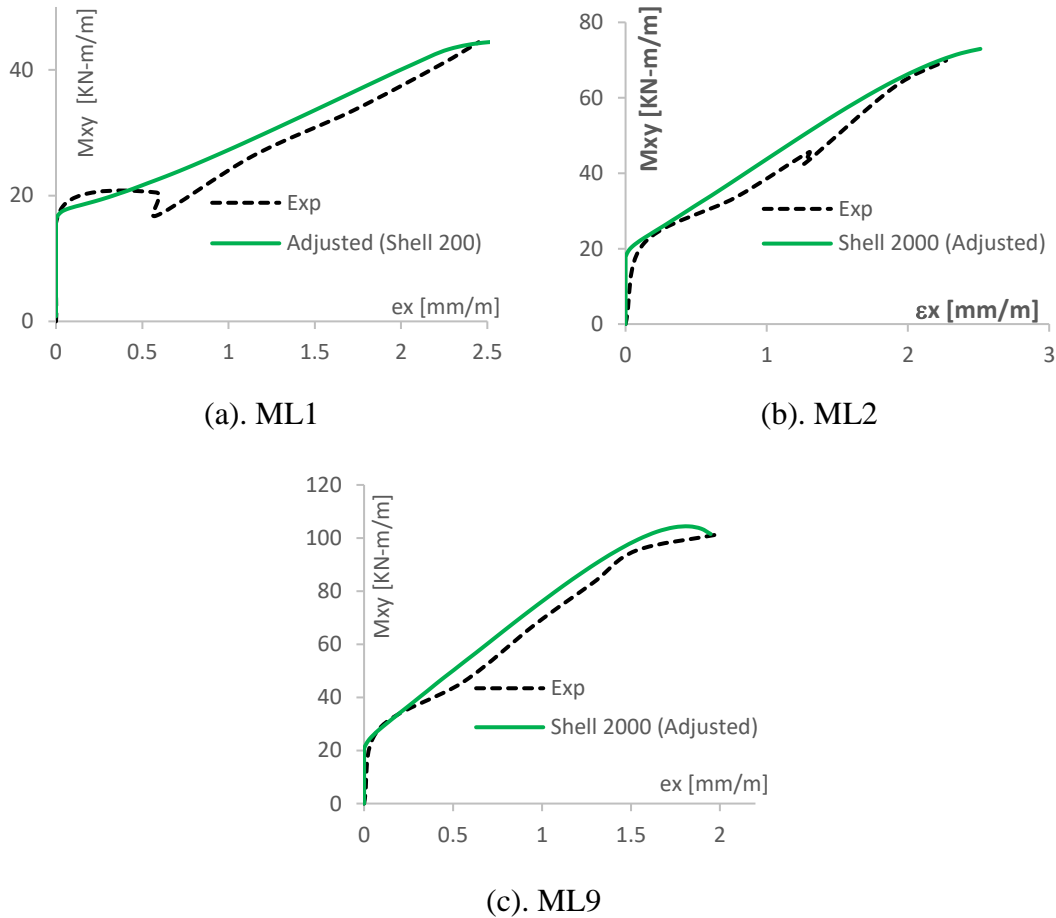


Figure 5.16. Comparison Between experimental and numerical load vs deformation curves for the ML series panels.

## 5.5 Modeling and Calibration of the SP series panels.

### 5.5.1 Description of the SP series panel Tests

The SP panel series were tested by Adebar and Collins (1994). These panels were subjected to a combination of out-of-plane shear, out-of-plate bending moments and in-plane as indicated figure 5.17. Four of the nine SP panels were selected in this research: SP2, SP3, SP7 and SP9. The SP2 and the SP9 panels were subjected to a combination of out-of-plane bending moment and out-of-plane shear as shown in Figure 5.17a, while the SP7 and SP9 panels were not only subjected to out-of-plane shears and its associated out-of-plate bending moments, but also to in-plane shear,

as shown in Figure 5.17b. The panels were also rectangular with a length of 1600mm and a thickness of 310 mm. In contrast to other panels analyzed in this thesis, the in-plane reinforcement of these SP series panels was not uniformly distributed. As shown in figure 5.17, the reinforcement was arranged by lumping three 20M bars each 250mm (3 20M@250mm), which is equivalent to  $37.5 \text{ cm}^2/\text{m}$ . At the same time, the three lumped 20M bars were spaced each at 54 mm from each other. The in-plane reinforcement was equal in all directions and in both faces. These panels also contained a relative low amount of out-of-plane (or transverse) reinforcement of  $8\text{cm}^2/\text{m}^2$  (8%) provided with T-headed 8 mm diameter bars.

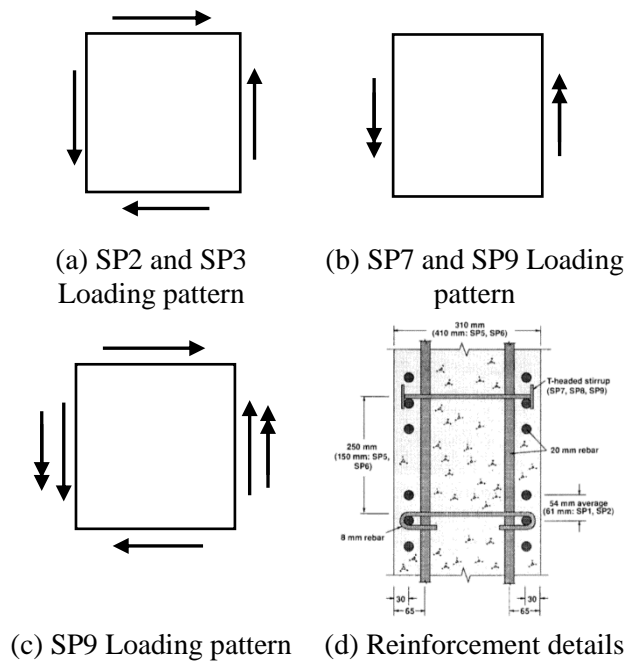


Figure 5.17. Loading application pattern and reinforcement details for the SE series panels.

### 5.5.2 Modeling details of the SP series panel Tests

The modeling of the SP series panels was conducted in Abaqus. Although it was tried to develop models in Shell-2000 as well, it was not possible to reproduce consistent numerical responses in this software. It was decided then to develop more accurate 3D solid models (instead of the simplified 2D models as done previously with the other panels) with the aim of capturing the behavior of the out-of-plate reinforcement, which has an important influence in the responses of the panels. It is convenient to recall that with the 2D Layer Composite Shell (2D-LCS) models in Abaqus it is not possible to model the out-of-plane or transverse shear reinforcement. Figure 5.8

explains the modeling procedure in Abaqus for the SP7 panel. The concrete damage plasticity model was chosen to simulate the non-linear behavior of the concrete. The curve to simulate the uniaxial behavior of the concrete in compression, shown in Figure 5.8a, was defined using the hognestad parabola model, which was built with the data in table 5.7. The behavior of the concrete in tension in figure 5.8b, was defined by using the Shima et al (1987) model, and the specific values are given in table 5.7. Finally, the uniaxial behavior of steel reinforcement in both directions are shown in figure 5.8c. In these cases, it was no necessary to modify (reduce) the yielding stress of the in-plane reinforcement a did for the SM series panels.

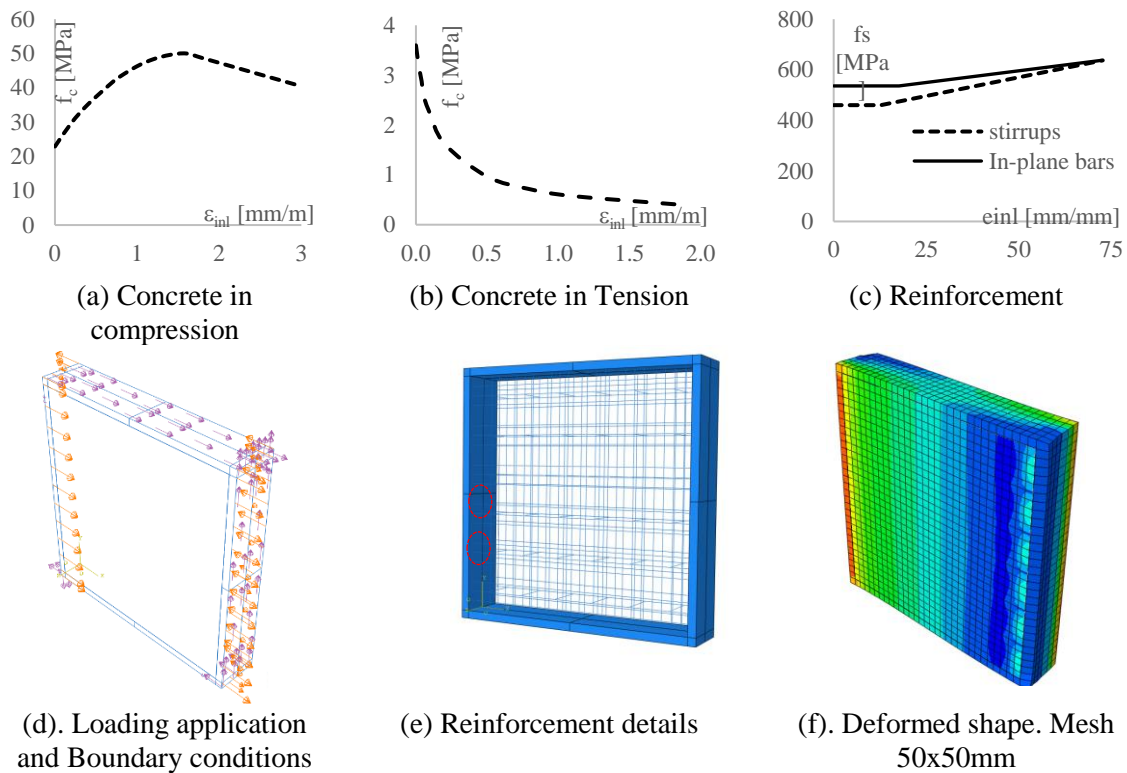


Figure 5.18. Modeling details for the SP7 panel.

Table 5.7. Material constitutive data for modeling of the SE series panels

<b>Concrete</b>	SP2 & SP3	SP7 & SP9
Modulus of Elasticity (MPa)	34666	34666
Poisson ratio	0.2	0.2
Concrete in Compression		
Strength at elastic limit $f_{ce}$ (MPa)	22.89	22.89
Strain at elastic limit $\epsilon_{ce}$ (mm/m)	0.66	0.66
Maximum Compressive strength $f_{co}$ (MPa)	50	50
Strain at max compressive stress $\epsilon_{co}$ (mm/m)	2.26	2.26

Table 5.7 continued

Ultimate Compressive strength $f_{cu}$ (MPa)		25.63	25.63
Ultimate compressive strain $e_{cu}$ (mm/m)		4.0	4.0
Concrete in Tension			
Tension strength (MPa)		3.6	3.6
Strength at elastic limit (mm/m)		0.10	0.10
Ultimate strain (mm/m)		1.37	1.37
<b>CDP model specialized parameters</b>			
Dilation angle (f)		15	15
Eccentricity (e)		0.1	0.1
fcb / fc ratio		1.16	1.16
Second invariant Kc		0.67	0.67
<b>Reinforcement Properties</b>			
20M bars in the x and y directions	Elastic Modulus (MPa)	200000	200000
	Yield strength (MPa)	480	536
	Strain at hardening (mm/m)	15	20
	Rupture strain (mm/m)	75	75
	Ultimate strength (MPa)	660	637
Stirrups in the transverse direction	Elastic Modulus (MPa)	200000	200000
	Yield strength (MPa)	460	460
	Strain at hardening (mm/m)	28	28
	Rupture strain (mm/m)	75	75
	Ultimate strength (MPa)	570	570

Figure 5.8d shows the Boundary Conditions (BCs) and the applied forces to the model. The only BC for this panel were restriction in translation along the z-axis at the vertical edges. As said before, the applied loads for this panel were the out-of-plate shear forces ( $V_{xz}$ ) and its associated bending moments ( $M_x$ ), plus in-plane shear force ( $N_{xy}$ ). The out-of-plane shear capacity of the panels was estimated after applying rotations about the y-axis at the vertical edges of the panels, and then reading and adding the out-of-plane shear reactions at the same edges. Then, the total out-plate shear reaction was divided by the length of the panels (1.6m) to obtain the out-of-plane shear capacity per linear unit. as cab be seen in figure 5.18. In other words, the out-of-plate shear capacity was obtained by internal equilibrium of the model after applying moments as rotations at the edges of the panels. The rotations at the vertical edges were applied as boundary conditions using an analytical field formula than induced linear variable deformations along the x-axis. The variable deformation was given as a function of the distance z ( $0.005z$ ) along the thickness of the panel. Thus, the maximum imposed axial deformations, at the top and bottom faces of the panel, were +0.75mm and -0.75mm, while the deformation at the center of the panels was zero. Finally, the in-plane shear force was applied as force control, and it was introduced by applying an ununiform shear stress of 1.23 MPa as shown in Figure 5.18. This shear stress

magnitude corresponds to the maximum out-of-plane shear force per linear meter reported during the test.

Figure 5.8e shows the details for the modeling of the reinforcement inside the panel. Both, the in-plane, and the out-of-plane reinforcement were simulated using the 2-node “beam” B31 finite element. Full deformation compatibility between concrete and steel reinforcement was assumed by applying the typical embedded region constraint, where the concrete was declared as the host region, and the reinforcement the embedded region. While the yielding strength of the reinforcement for panels SP2 and SP3 was reported in 480 MPa, the yielding strength for panels SP7 and SP9 was reported in 536MPa. Finally, Figure 5.8d shows the 50x50 mm size mesh of the elements and the deformed shape in the final stage for the SP7 panel specifically. It is clear how the deformed shape follows like a “S” shape, creating one positive curvature in one end and a negative curvature in the other end of the panel. The selected finite element for the concrete was the C3D8R 8-node linear brick with reduced integration and hourglass control. All SP panels were simulated following the same procedure in Abaqus but considering the specific reported concrete material properties, and the magnitudes of the in-plane shear forces. Panels SP2, SP3 and SP9 were modeled same as panels SP2, but changing the loading pattern explained in figure 5.17. The concrete material properties for all panels were the same assuming average tensile and compressive strengths of 3.6MPa and 50MPa for the concrete, respectively.

### **5.5.3 Calibrated or adjusted responses for the SP series panels**

Figure 5.19 shows the comparison between the experimental and the numerical curves for the SP series panels. The experimental principal transverse shear stress vs transverse shear strain curve ( $v_o$  vs  $\gamma_{xz}$ ) for the SP7 panel was given by Adebar and Collins (1994), while the SP2 and the SP9 experimental curves are found in Adebar (1989). The transverse shear strains, as specified by Adebar and Collins (1994), were measured in unbounded stirrups. The experimental curves were originally given in terms of transverse stress. However, in order to be consistent with the all the experimental curves in this thesis, they were converted to out-plate forces by multiplying by the thickness of the panels. For unknown reasons, the maximums out-of-plate shear capacities of the panels were not reached in any on the experimental curves in Figure 5.19. Judging by the values, it seems that those maximum values in the curves match with the yielding capacities of the panels

rather than the ultimate (or maximum) capacities reported by Adebar and Collins (1994). However, these maximum values, which can be found in tables 6.12 in chapter 6, were included in Figure 5.19

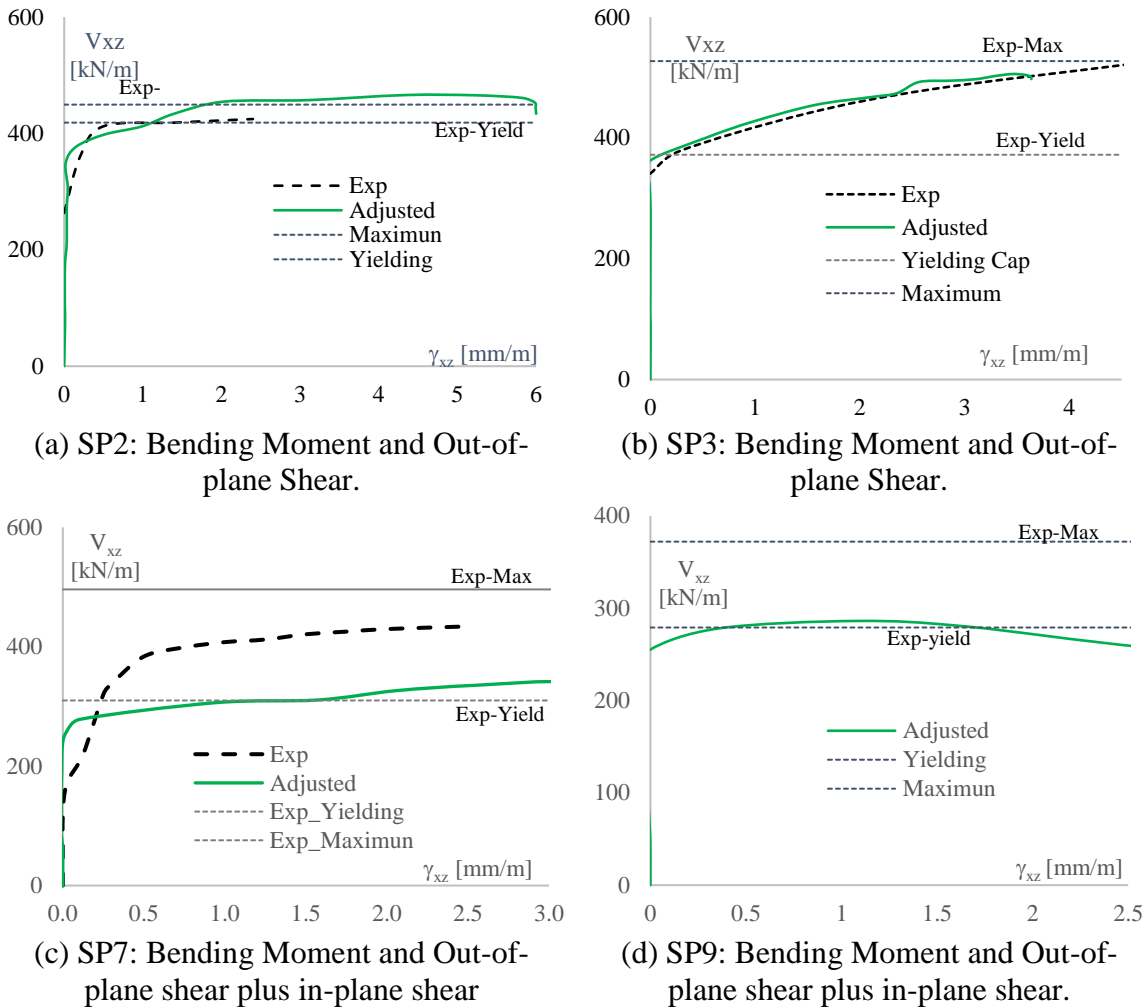


Figure 5.19. Comparison Between experimental and numerical load vs deformation curves for the SP series panels.

As appreciated in Figure 5.19, the numerical curves of panels SP2, SP3 and SP7 are in a good agreement with their corresponding experimental curves. The experimental curve for panel for panel SP9 was not found neither in the research of Adebar (1989) nor in the work of Adebar and Collins (1994). The numerical model for panels SP2 was able to capture the cracking, the yielding, and the ultimate capacities with reasonable accuracy. The SP2 model overestimated the capacity of the panel in only 2% as shown in figure 5.19a. The numerical models for panels SP3 and SP7 were able to capture the cracking and the yielding capacities of the panels with acceptable

accuracy, but not the maximum capacities. In these cases, the SP3 and the SP7 numerical models underestimated the transverse shear capacities reported from the experiments in about 19% and 32%, respectively. The maximum transverse shear capacity for panel SP9 was reported in 372 kN/m, while the maximum capacity from the numerical models was estimated in 286 kN/m, which means the numerical model underestimated the shear capacity in about 23%. Although at first sight it may seem obvious that the numerical models are not reliable because the percentages of underestimation are very high, it is actually the opposite. Adebar and Collins (1994) said that the ultimate capacity for panels SP3, SP7 and SP9 might have been unintentionally increased or overestimated because of the installation of yokes during the tests. They explicitly said “*it appears that that artificial restraint did exist in specimens SP3, SP7 and SP9 after significant transverse expansion occurred*”. In other words, the models can be considered as reliable because they confirmed that the ultimate capacities of these three panels might have been overestimated during the experiments.

## 6. VALIDATION OF THE APPROACHES BY USING EXPERIMENTAL DATA

The results of the PACI and the EC2 approaches, will be validated in this chapter. As explained in the methodology, the two types of results to validate are: a) the areas of reinforcement (or reinforcement ratios) suggested by both design approaches; and b) the estimated numerical capacities of the panels after introducing those reinforcement areas suggested by the PACI and the EC2 design approaches. Both results (reinforcement suggested areas and estimated numerical capacities) will be compared against the areas provided during the experiment, and against the ultimate capacities reported from the tests. Comparing the suggested reinforcement areas against the areas provided during the experiments can be considered as an indirect way of validation. If the approaches suggest at least the same reinforcement areas than those provided during the experiments, it can be inferred that these results are safe. Nevertheless, it will be shown through this chapter, that there were several cases in which either, one of the two approaches, or both, suggested less reinforcement than the reinforcement provided during the experiments. However, it will be demonstrated that despite the reduction in reinforcement suggested by the approaches, the panels reached similar numerical capacities than the ultimate capacities reported from the experiments. Comparing the estimated numerical capacities against the capacities reported from the tests will be considered as a direct way of validation. If the estimated numerical capacities of the panels are greater than or equal to the capacities reported from the tests, the results will be considered as satisfactory.

### 6.1 Validation of results using Experimental data

#### 6.1.1 Validation of results using the SE series panels

##### *Estimation of the suggested reinforcement areas*

Table 6.1 shows the comparison between the areas of reinforcement suggested by the PACI approach and the areas suggested by the EC2 approach for the SE series panels. Table 6.1 also shows the differences between the reinforcement areas provided during the experiment and the reinforcement areas suggested by the two design approaches. For the SE1 panel, which was subjected to in-plane shear only, both design approaches suggested a total area of 78.4 cm<sup>2</sup>/m,

which represents a 71% of the total reinforcement area provided during the experiment. Something similar occurred for panel SE3 which was subjected to bending moment only. In this case, the total reinforcement areas suggested by the EC2 and the PACI approaches were 106.4 cm<sup>2</sup>/m and 104.4 cm<sup>2</sup>/m, which represent 96% and 94% of the reinforcement provided during the test. Because both approaches suggested less reinforcement than the reinforcement provided during the test, it may seem that both approaches produced non-conservative results for the SE1 and the SE3 panels. However, it will be shown later through non-linear analysis, that despite the reduction in reinforcement suggested by the approaches, the panels not only reach but also exceed the capacity experimental capacity.

More differences between the reinforcement areas suggested by the approaches were observed for panels SE4 and SE7. These two panels were subjected to a combined action of in-plane shear and bending moment. For panel SE4, for example, the PACI approach suggested a total reinforcement area of 106.6 cm<sup>2</sup>/m, while the EC2 approach suggested a total of 126 cm<sup>2</sup>/m, which represents 96% and 113% of the reinforcement provided during the experiments. Similarly, for the SE7 panel, the PACI approach suggested higher amount of reinforcement than the EC2 approach. While the EC2 approach suggested a total area of 87.2 cm<sup>2</sup>/m, the PACI approach suggested 116 cm<sup>2</sup>/m, quantities that represent 79% and 105% of the reinforcement provided during the experiments.

Table 6.1. Comparison between the suggested reinforcement areas by the PACI and EC2 design approach, and against the reinforcement area provided in the experiment

SE Series	Proportional Loading	Reinforcement per Layer in [cm <sup>2</sup> /m]						As Ratios
		Layers	Top X	Top Y	Bot X	Bot Y	As Tot	
SE	M <sub>x</sub> : N <sub>xy</sub>	Tests	41.8	13.9	41.8	13.9	111	
SE1	0 : 1	<b>EC2</b>	19.6	19.6	19.6	19.6	78.4	<b>0.71</b>
		<b>PACI</b>	19.6	19.6	19.6	19.6	78.4	<b>0.71</b>
SE3	1 : 0	<b>EC2</b>	47.5	47.5	5.7*	5.7*	106.4	<b>0.96</b>
		<b>PACI</b>	46.5	46.5	5.7*	5.7*	104.4	<b>0.94</b>
SE4	1: 0.5	<b>EC2</b>	47.6	47.6	5.7*	5.7*	106.6	<b>0.96</b>
		<b>PACI</b>	53	53	10	10	126	<b>1.13</b>
SE7	1 : 0.13	<b>EC2</b>	32.6	32.6	11	11	87.2	<b>0.79</b>
		<b>PACI</b>	39	39	19	19	116	<b>1.05</b>

\*Minimum reinforcement ratio specified as 0.2% the thickness of the panel (0.002t<sub>w</sub>)

### Analysis and comparison between the experimental and the numerical capacity curves

The comparison between the numerical curves and the experimental curves for the SE series panels are shown in Figure 6.1. Four curves can be observed for each selected panel in Figure 6.1. The darker discontinuous line, identified with the name *Exp*, represents the curve that was reproduced from the experiments. The green and continuous line, identified with the name of *Num\_ρ<sub>test</sub>*, represents the calibrated numerical curve developed in any of three non-linear analysis software used in this thesis (Shell 2000, Membrane 2000 and Abaqus). The blue line, identified as *Num\_ρ<sub>EC2</sub>*, represents the numerical capacity curve of the panels after specifying the reinforcement areas and the lever arm distances suggested by the EC2 approach into the calibrated numerical models. Finally, the red and dotted line, identified with the name of *Num\_ρ<sub>PACI</sub>*, represents the numerical capacity curve of the panels after introducing the reinforcement areas suggested by the PACI approach. This same line convention will be used for the identification of the capacity curves for the rest of the panels analyzed in this thesis.

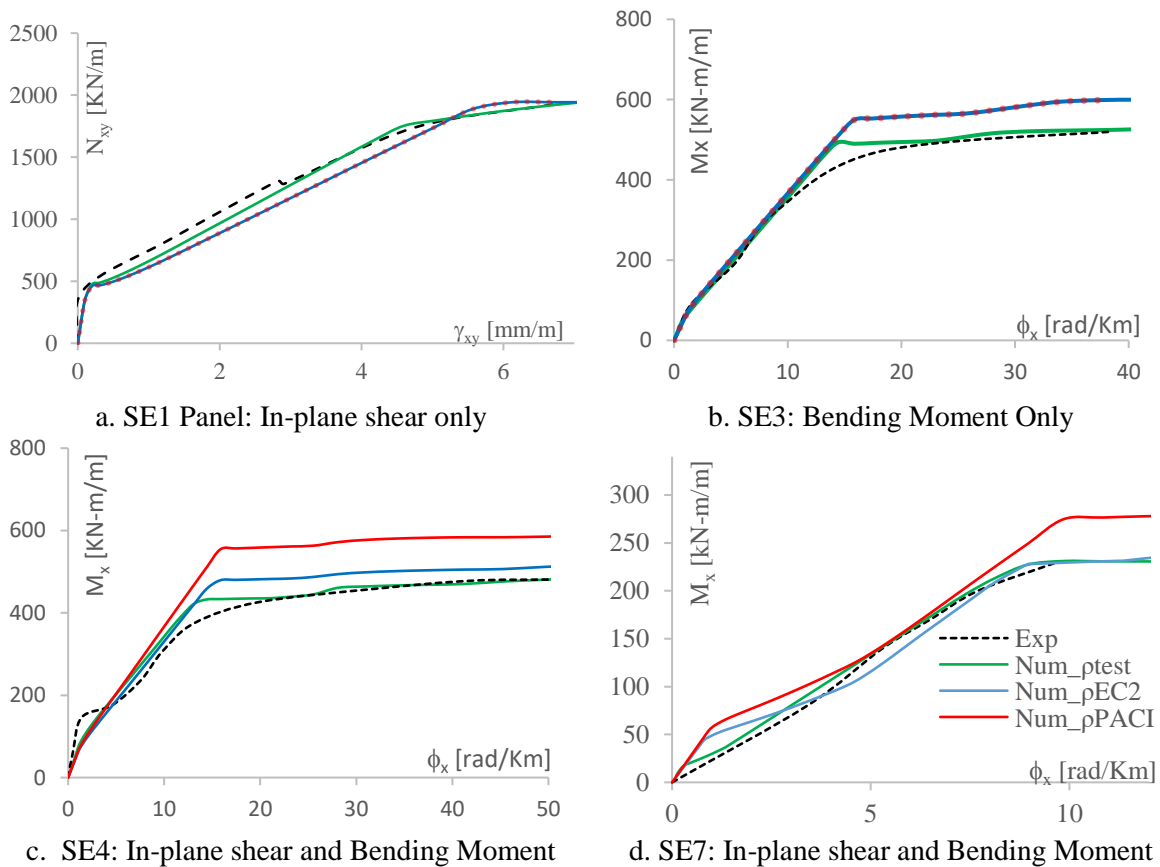


Figure 6.1. Comparison between experimental and numerical load vs deformation curves for the SE series panels.

For obvious reasons, the calibrated or adjusted numerical curve was developed first considering the same reinforcement ratio and cover distances from the tests. Then, the EC2 and the PACI design numerical curves were computed later after changing the reinforcement areas provided during the experiment, for the reinforcement area suggested by the EC2 and the PACI, design approaches, respectively. The cover distances were also changed because as explained in chapters 2 and 3, both design approaches assume a unique lever arm distance between the reinforcement layers.

The EC2 and the PACI numerical curves follow the same path in panels SE1 and SE3 as shown in figures 6.1a and 6.1b, respectively. The curves follow the same path because both design approaches suggested equal and similar amount of reinforcement for these two panels. For example, size designation bar 10M each 50 mm (10M@50mm) were used to satisfy the  $19.6 \text{ cm}^2/\text{m}$  reinforcement areas suggested by both approaches for the SE1 panel. In the same way, since the reinforcement areas suggested by the EC2 and the PACI approaches were very similar ( $106.4 \text{ cm}^2/\text{m}^2$  and  $104.4 \text{ cm}^2/\text{m}^2$ , respectively) for panel SE3, both were satisfied by providing the same amount and same reinforcement configuration. Specifically, the numerical EC2 and PACI curves for panel SM3 was obtained after introducing 20M@60mm in the x-direction, and #3@125mm in the y-direction, with a clear cover distance of 20mm.

For panels SE4 and SE7, on the other hand, there was an evident difference between the PACI and the EC2 design curves. Because the PACI approach suggested more reinforcement areas than the EC2 approach, the PACI design curve developed higher post-cracking stiffness and ultimate capacities than both, the EC2 design curve and the experimental curves. For these two panels, especially for panel SE7, it can be observed that the EC2 design capacity curves follow very closely the same path of the experimental curve. The areas of reinforcement suggested by the EC2 approach for the SE4 panel were satisfied by using the same reinforcement configuration provided for panel SE3: 20M@60mm in the x-direction, and #3@125mm in the y-direction. On the other hand, the areas suggested by the approach were satisfied using 20M@55mm in the x-direction, and #3@125mm. The areas of reinforcement suggested by the EC2 approach for the SE7 panel were satisfied by using 20M@90mm in the x-direction, and 10M@90mm in the y-direction. On the other hand, the areas of reinforcement suggested by the PACI approach for the SE7 panel were satisfied by using 20M@75mm in the x-direction, and 10M@55mm in the y-

direction .The clear cover distances for the bars running along the x and y directions were 20 mm and 35mm, respectively.

It is interesting to note how despite the reduction in reinforcement suggested by the EC2 approach for panels SE1 and SE7, the corresponding EC2 design curves reached the same experimental capacity of the panels. Another interesting feature to note from figure 6.1d, corresponding to panel SE7, is that the experimental curve did not show evidence of yielding in the reinforcement, whereas both numerical curves the EC2 and the PACI did. This goes in agreement with the experiment, since Kirscher and Collins (1986) argued that there was no evidence of reinforcement yielding during the test. The anticipated yielding of the reinforcement of the EC2 curve has perfect sense, since the EC2 suggested 21% less of the reinforcement provided during the experiment.

#### ***Comparison between the experimental and the numerical capacities.***

Table 6.2 compares the reported experimental capacities against the numerical capacities of the panels after introducing the areas of reinforcement suggested by the PACI and the EC2 design approaches. Depending on the panel, one or two experimental capacities were reported. The number of experimental reported capacities is equal to the number of loads applied in a specific test. For example, panels SE1 and SE3, which were subjected in-plane shear ( $N_{xy}$ ) and out-of-plate bending moment ( $M_x$ ), respectively, reported only one experimental capacity. For panels SE4 and SE7, on the other hand, both reported two experimental capacities: in-plane shear and out-of-plane bending capacities. The numerical capacities for each panel were extracted from the numerical capacity curves in Figure 6.1.

As observed in table 6.2, all numerical over experimental capacity ratios ( $C_{EC2}/C_{exp}$  and  $C_{PACI}/C_{exp}$ ) are greater than 1, which means that both design approaches are safe. However, the capacity ratios obtained by the EC2 ( $C_{EC2}/C_{exp}$ ) design approach were all lower than the capacity ratios obtained from the PACI approach ( $C_{PACI}/C_{exp}$ ). This was expected given the simplified methodology of the PACI approach. In average, the increment in the capacities for the SE series panel, after introducing the reinforcement areas suggested by the PACI approach were about 21% compared against the experimental capacities. From table 6.2, it is clear how the reinforcement suggested in the EC2 approach results in similar numerical capacities -and even

slightly higher capacities- than the experiment, in spite the suggested reduction in reinforcement. The average increment in capacities of the panels after introducing the reinforcement areas suggested by the EC2 approach was 6%. This fact confirms than the EC2 approach is not only safe but is also very efficient at least for RC panels with this load combination.

Table 6.2. Comparison between the estimated numerical capacities, and the reported experimental capacities for the SE series panels

SE Series	External Applied demands	Experimental Capacities ( $C_{exp}$ )	EC2 Numerical Capacities ( $C_{EC2}$ )	$\frac{C_{EC2}}{C_{exp}}$	PACI Numerical Capacities ( $C_{PACI}$ )	$\frac{C_{EC2}}{C_{exp}}$
SE1	$N_{xy}$ [kN/m]	1930	1943	1.01	2160	1.11
SE3	$M_{xy}$ [KN-m/m]	520	600	1.15	600	1.15
SE4	$M_x$ [kN]	480	521	1.08	586	1.22
	$N_{xy}$ [KN-m/m]	960	1041	1.08	1172	1.22
SE7	$M_x$ [kN]	230	235	1.02	300	1.30
	$N_{xy}$ [KN/m]	1810	1811	1.00	2310	1.28

It must be considered, however, that the capacity of the panels might had be increased because of the increment in the lever arm distances that were used to estimate the reinforcement areas suggested by the approaches. To clarify this point, the lever arm distances, and the clear cover distances reported in the experiments, are not the same than those specified in the numerical models. As explained before, since both approaches assume a unique (or average) lever arm distance to estimate the required reinforcement areas, neither the values of these lever arm distances nor the clear cover distances specified in the numerical models, will be equal to the values utilized in the experiments. For example, the lever arm distances between the bars running along the x-direction, and along the y-direction, for panel SE3, were 243mm and 199mm, respectively; while the same lever arm distances specified in the numerical model were 235mm and 215mm. As can be noted, the lever arm distances in the numerical models are greater than the lever arm distances utilized during the experiment, which might have increased the bending capacity in panel SE3.

## 6.1.2 Validation of results using the SM series panels

### *Estimation of the suggested reinforcement areas*

Table 6.3 shows the differences between the reinforcement areas provided during the experiments and the reinforcement areas suggested by the PACI and the EC2 design approaches for the SM series panels. Both design approaches suggested similar amount of reinforcement areas. For instance, the PACI and the EC2 approach suggested 96.2 cm<sup>2</sup>/m and 98.4 cm<sup>2</sup>/m, which represents 91% and 93% of the reinforcement provided in the experiments, for the SM1 panel. For the SM2 panel, the PACI and the EC2 approach suggested 95.4 cm<sup>2</sup>/m and 91.2cm<sup>2</sup>/m, which represents 90% and 86% of the reinforcement provided in the experiments, respectively. For the SM3 panel, the EC2 and the PACI approach suggested 115 cm<sup>2</sup>/m and 112 cm<sup>2</sup>/m, which represents 108% and 106% of the reinforcement provided in the experiments, respectively. Both approaches suggested less reinforcement areas than the areas provided during the experiments for panels SM1 and SM2. It will be shown later that despite both approaches suggested less reinforcement areas than the areas provided during the tests for panels SM1 and SM2, the panels were able to reach the capacities reported in their respective tests. Finally, for panel SM3, both approaches suggested higher reinforcement areas than the areas provided during the experiment.

Table 6.3. Comparison between the suggested reinforcement areas by the PACI and EC2 design approach, and against the reinforcement area provided in the experiment

SM series	Proportional Loading $M_x : M_y : N_y : N_x$	Reinforcement per Layer in [cm <sup>2</sup> /m]						As Ratios
		Layers	Top X	Top Y	Bot X	Bot Y	As Tot	
SM1	1 : 0 : 0 : 0	Test	39.5	39.5	6.32	6.32	106	
		EC2	41.8	41.8	6.32	6.32	96.2	0.91
SM2	1:0:0.375:0.375	PACI	42.9	42.9	6.32	6.32	98.4	0.93
		EC2	41.4	41.4	6.32	6.32	95.4	0.90
SM3	1 : 1 : -0 : -0	PACI	39.3	39.3	6.32	6.32	91.2	0.86
		EC2	43.8	43.8	13.50	13.50	115	1.08
		PACI	43.3	43.3	12.75	12.75	112	1.06

### *Analysis and comparison between the experimental and the numerical capacity curves*

Two aspects can be highlighted when comparing the experimental curves, and the numerical curves in figure 6.2 First, there is an excellent agreement between the experimental curves and the adjusted numerical curves for all the SM series panels. Second, the differences

between the PACI and the EC2 numerical capacity curves are negligible. The PACI and the EC2 numerical curves follows pretty much the same paths because both design approaches suggested very similar amounts of reinforcement for all the SM series panels according to table 6.3. For example, the reinforcement area of  $41.8 \text{ cm}^2/\text{m}$  and  $42.9 \text{ cm}^2/\text{m}$  suggested by the EC2 and the PACI approaches respectively, for panel SM1 (see table 6.3), were satisfied by providing the following reinforcement layer (or curtain) configuration: designation bar 20M spaced each 70mm (20M@70mm) along the x and y directions at the top face of the panel; and designation bar 10M spaced each 70 mm (10M@70mm) at the bottom face of the panel.

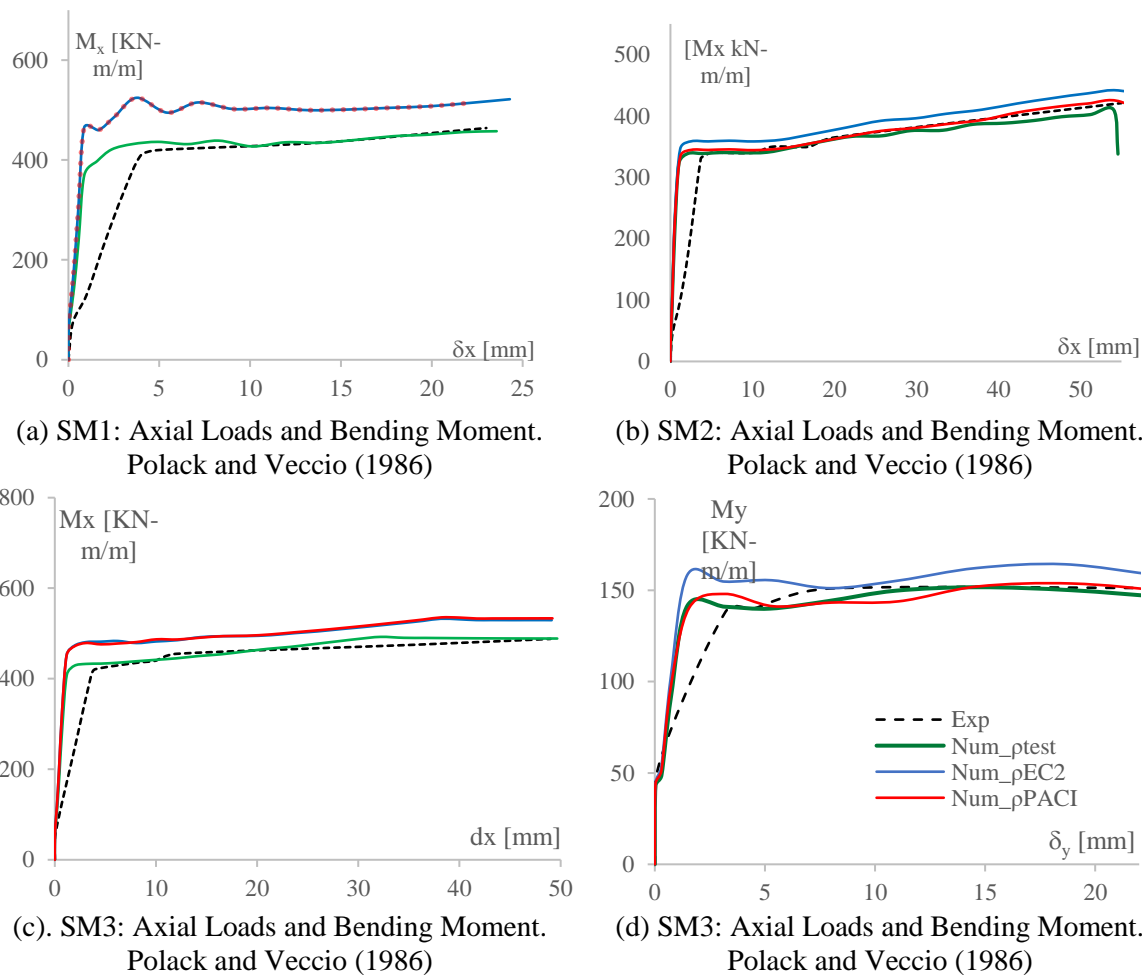


Figure 6.2. Comparison Between experimental and numerical load vs deformation curves for the SM series panels.

The reinforcement area of  $41.4 \text{ cm}^2/\text{m}$  suggested by the EC2 approach in table 6.3 for panel SM2 was satisfied by providing the following layers reinforcement configuration: 20M@72mm

in the x and y directions at the top face of the panel; and 10M@160mm in the bottom face of the panel, also in both directions. On the other hand, the reinforcement area of 39.3 cm<sup>2</sup>/m suggested by the PACI approach for panel SM2 was satisfied by providing the following configuration: 20M@75mm in the x and y directions at the top face of the panel; and 10M@160mm at the bottom face of the panel, also in both directions. Finally, the reinforcement areas of 43.8cm<sup>2</sup>/m and 43.3cm<sup>2</sup>/m suggested by the EC2 and the PACI approach, were satisfied by providing: 20M@75mm in the x and y directions at the top face of the panel; and 10M@75mm at the bottom face of the panel, also in both directions.

***Comparison between the experimental and the numerical capacities.***

Table 6.4 compares the capacities reported from the experiments, against the EC2 and the PACI numerical capacities of the SM series panels. As explained before, these numerical capacities were estimated by introducing the respective reinforcement areas suggested by each approach into the calibrated numerical models developed in section 5. The values of the estimated numerical capacities were extracted from the corresponding numerical curves in Figure 6.2. Table 6.4 also shows the numerical over experimental ( $C_{EC2}/C_{exp}$  and  $C_{PACI}/C_{exp}$ ) capacity ratios of the panels. As observed, all numerical over experimental ratios were greater than 1, by which it can be inferred that both approaches provided safe results.

Table 6.4. Experimental reported capacities vs estimated numerical capacities

SM Series	External demands Applied	Experimental Capacities ( $C_{exp}$ )	EC2 Numerical Capacities ( $C_{EC2}$ )	$\frac{C_{EC2}}{C_{exp}}$	PACI Numerical Capacities ( $C_{PACI}$ )	$\frac{C_{EC2}}{C_{exp}}$
SM1	Mx [KN-m/m]	477	483	1.04	483	1.04
SM2	Nx [KN/m]	1684*	1700	1.00	1700	1.00
	Ny [KN/m]	1684*	1460	0.87	1460	0.87
	Mx [KN-m/m]	421	441	1.05	423	1.00
SM3	Mx [KN/m]	488	533	1.09	535	1.10
	My [KN-m/m]	151	158	1.05	154	1.02

\*. Supposed values not reported from experiment.

The EC2 numerical capacities for panels SM2 and SM3 were slightly higher than the PACI numerical capacities because the EC2 approach suggested slightly higher amount of reinforcement

as shown in table 6.3. However, none of the numerical over experimental capacity ratios ( $C_{EC2}/C_{exp}$  and  $C_{PACI}/C_{exp}$ ) when using the PACI approach was less than one 1.0, which confirms the safety of the approach despite its simplicity. The tensile ( $N_x$ ) and compressive ( $N_y$ ) axial capacities of the SM2 panel cannot be compared because they were not explicit reported from the experiments. These values were estimated by multiplying the experimental moment capacity of the panel (421 kN-m/m) by four, according to the proportional loading pattern.

### **6.1.3 Validation of results using the PV series panels**

#### ***Estimation of the suggested reinforcement areas***

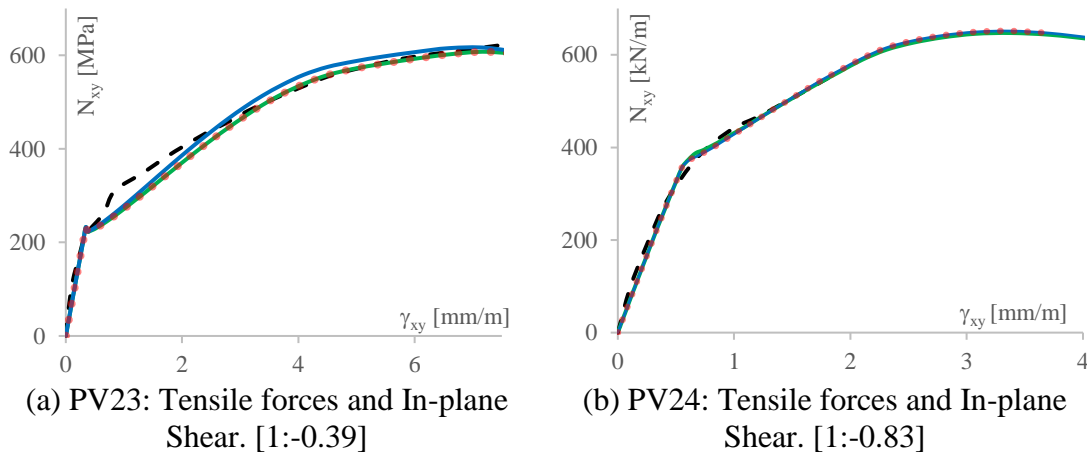
Table 6.5 compares the reinforcement areas suggested by the PACI and the EC2 approaches, against the reinforcement areas provided during the experiments for the PV series panels. The more significant differences between the areas suggested by the PACI and the EC2 approaches were found in panel PV23. While the EC2 approach suggested 29.2 cm<sup>2</sup>/m, which represents 17% more of the reinforcement provided during the experiment, the PACI approach suggested 24 cm<sup>2</sup>/m, which meant a reduction in reinforcement of roughly 4%. This was one of the cases in which the PACI approach suggested less reinforcement than both, the reinforcement suggested by the EC2 approach and the reinforcement provided during the experiment. For panel PV24, the EC2 and the PACI approach suggested reinforcement areas of 22.4 cm<sup>2</sup>/m and 22.6 cm<sup>2</sup>/m respectively, which represents about 90% of the reinforcement total area provided in the experiment. For the PV25 panel, the EC2 approach suggested less reinforcement than the PACI approach. While the EC2 suggested 90% of the reinforcement areas provided during the experiment, the PACI approach suggested 2% of additional reinforcement compared against the experiment. Finally, both approaches suggested 22.4 cm<sup>2</sup>/m of reinforcement for the PV28 panel, which also represents 90% of the reinforcement provided during the test.

Table 6.5. Comparison between the suggested reinforcement areas by the PACI and EC2 design approach, and against the reinforcement area provided in the experiment

PV series	Proportional Loading	Reinforcement per Layer in [cm <sup>2</sup> /m]						As Tot	As Ratios
		Layers	Top X	Top Y	Bot X	Bot Y			
	N <sub>xy</sub> : N <sub>y</sub> : N <sub>x</sub>	Test	6.25	6.25	6.25	6.25	25		
PV23	1 : -0.39 : -0.39	EC2	7.3	7.3	7.3	7.3	29.2	1.17	
		PACI	6.0	6.0	6.0	6.0	24	0.96	
PV24	1: -0.83 : -0.83	EC2	5.6	5.6	5.6	5.6	22.4	0.90	
		PACI	5.65	5.65	5.65	5.65	22.6	0.90	
PV25	1 : -0.69 : -0.69	EC2	5.6	5.6	5.6	5.6	22.4	0.90	
		PACI	6.4	6.4	6.4	6.4	25.6	1.02	
PV28	1: 0.32 : 0.32	EC2	5.6	5.6	5.6	5.6	22.4	0.90	
		PACI	5.6	5.6	5.6	5.6	22.4	0.90	

***Analysis and Comparison between the experimental and numerical capacity curves.***

The capacity curves of the PV series were originally reported in terms of shear stress vs shear strain (or distortion). However, in order to be consistent with the rests of the other panels studied in here, the shear stress was converted into in-plane shear force per unit length by multiplying by the thickness of the panels. The transformed  $N_{xy}$  vs  $\gamma_{xy}$  capacity curves for the PV series are shown inf Figure 6.3. Although there were calibrated curves from Abaqus and Membrane-2000, only the latter ones are shown in Figure 6.3. The reason for this is because as explained in chapter 5, the Membrane-2000 software gives the capacity of the panels in terms of strength directly, which is more in agreement with the conventional design procedure.



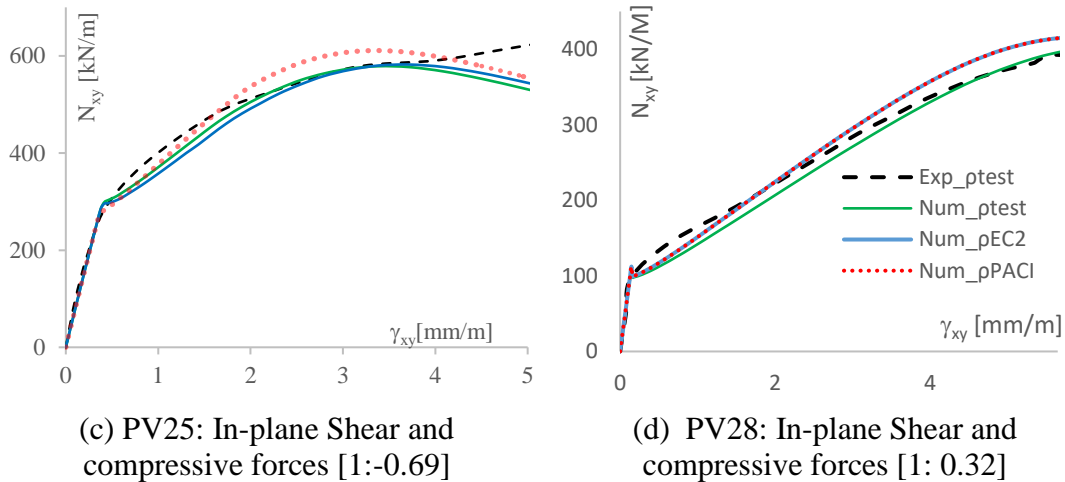


Figure 6.3. Comparison between experimental and numerical load vs deformation curves for the PV series panels.

An acceptable agreement between the adjusted numerical curves and the experimental curves for all PV series panels can be appreciated in Figure 6.3. The maximum capacities were very well captured by the numerical models in Shell-2000. However, the models did not capture very accurately the behavior of the panels after cracking for panels PV23 and PV25. In panel PV23, the PACI numerical curve follows the same path than the adjusted curve because it suggested a similar amount of reinforcement than the provided during the experiment. Specifically, the 6.0 cm<sup>2</sup>/m suggested by the PACI approach for this panel in each layer was satisfied by providing designation bar #2 each 50 mm (#2@50mm). The reinforcement area suggested by the EC2 approach for panel PV23 was satisfied by providing #2@45mm in each layer. Similarly, the PACI and the EC2 numerical curves for panels PV24 and PV28 follow the same path because both approaches suggested similar reinforcement areas. The reinforcement areas suggested by the two approaches for the PV24 and the PV28 panels in each reinforcement layer were satisfied using #2@55mm. Finally, the areas suggested by the EC2 and the PACI approach for panel PV25 in each layer were satisfied by providing #2@55 mm and #2@50mm, respectively.

***Comparison between the experimental and numerical capacities.***

Table 6.6 shows the comparison between the experimental capacities reported during the tests, against the estimated numerical capacities for the PV series panels. The numerical capacities

of panels PV24 and PV28 were higher than the corresponding capacities reported in the experiments, while the numerical capacities for the PV23 and PV25 were lower. However, panel PV25 reached 94% and 96% of the capacity reported during the experiments after introducing the reinforcement areas suggested by the EC2 and the PACI approach, respectively. In the same way the PV23 panel reached 99% and 98% of the experimental capacity of the panel after introducing the areas suggested by the EC2 and the PACI approaches. The obvious reason why panels PV23 and PV25 came up with little lower capacities is that both approaches suggested less amount of reinforcement as explained in table 6.5.

Another reason why the capacities for the panels PV23 and PV25 did not reach the capacities reported in the experiment after introducing the reinforcement areas suggested by the approaches, is related to the fact that all PV panels were built with a higher compressive concrete strength ( $f'_c$ ) around its perimeter. In the case of the PV23 panel for example, the core concrete had a compressive strength of 20.5 MPa, while the strength for the concrete around the perimeter was specified in 35 MPa. This means that the  $f'_c$  in the perimeter was almost 1.5 higher than the concrete in the core of the panel. The capacities in table 6.6 were estimated using the  $f'_c$  in the center of the panels. Just by changing these values of  $f'_c$  into the numerical model, the strength of the PV23 panel increases to 653 kN/m and 667 kN/m when following the EC2 and the PACI approaches, respectively. These alternative numerical capacities would had represented Num/Exp capacity ratios of 1.05 and 1.07 for the PACI and the EC2 approaches, respectively, meaning than both approaches were safe. However, it has to kept in mind that the Num/Exp capacities ratios for the PV23 and the PV5 panels were very close to 1.0 for both approaches, which can be easily by incorporating strength reduction factor as usually done in actual design.

Table 6.6. Experimental reported capacities vs estimated numerical capacities for the PV series.

PV series	External Applied demands	Experimental Capacities ( $C_{exp}$ )	EC2 Numerical Capacities ( $C_{EC2}$ )	$\frac{C_{EC2}}{C_{exp}}$	PACI Numerical Capacities ( $C_{PACI}$ )	$\frac{C_{EC2}}{C_{exp}}$
PV23	$N_{xy}$ [kN/m]	621	616	0.99	607	0.98
PV24	$N_{xy}$ [kN/m]	556	658	1.18	658	1.18
PV25	$N_{xy}$ [kN/m]	639	602	0.94	616	0.96
PV28	$N_{xy}$ [kN/m]	393	413	1.05	413	1.05

#### 6.1.4 Validation of results using the F series panels

##### *Estimation of the suggested reinforcement areas*

Table 6.7 shows the differences between the reinforcement areas provided during the experiment and the reinforcement areas suggested by the two design approaches for the F series panels. These panels reported the highest differences between the reinforcement areas provided during the experiment and the reinforcement areas suggested by the design approaches. As can be observed in table 6.7, both design approaches suggested more reinforcement areas than the experimentally provided. Specifically, the approaches suggested 31%, 40% and 17% more of the reinforcement provided during the tests for panels F2, F3 and F3, respectively. In average, however, the approaches suggested 29% more than the reinforcement utilized in each test, which is still reasonable pay to price, especially for the PACI approach given its simplicity. It is not clear why under this simple loading combination, not even the EC2 approach suggested reinforcement areas closer to those provided during the experiments. One possible explanation, might be related high spacing of the reinforcement bars which was measured in 267 mm. It must be mentioned that the spacing of reinforcement in the rest of series panels did not exceed 100 mm in either of the two orthogonal directions of the panels. Another explanation is that the area of reinforcement in the y-direction for each face is twice the times the area that appears in table 6.7. This means that instead of using  $4.8\text{cm}^2/\text{m}$ , the actual value would be  $9.6\text{ cm}^2/\text{m}$ . In fact, this is not very clear according to the experimental research of Belarbi and Hsu (2005). Assuming that the reinforcement area in the y-direction be  $9.6\text{cm}^2/\text{m}$  (and not  $4.8\text{cm}^2/\text{m}$ ) the total reinforcement area provided during the test will be  $41.7\text{cm}^2/\text{m}$ , which will be more in agreement with the reinforcement areas suggested by the approaches.

Table 6.7. Comparison between the suggested reinforcement areas by the PACI and EC2 design approach against the reinforcement area provided in the experiment.

F series	Proportional Loading Nx : Ny	Reinforcement per Layer in [cm <sup>2</sup> /m]						As Ratios
		Layers	Top X	Top Y	Bot X	Bot Y	As Tot	
		Test	11.25	4.8	11.25	4.80	32.1	
F2	0.5 : -1	EC2	10.5	10.5	10.5	10.5	42.0	1.31
		PACI	10.5	10.5	10.5	10.5	42.0	1.31
F3	0.5 : -1.5	EC2	11.2	11.2	11.2	11.2	44.8	1.40
		PACI	11.2	11.2	11.2	11.2	44.8	1.40
F4	0.5 : -2	EC2	9.4	9.4	9.4	9.4	37.6	1.17
		PACI	9.4	9.4	9.4	9.4	37.6	1.17

### *Comparison between experimental and numerical capacity curves*

The experimental capacity curves of the F-series were originally reported in terms of axial stress vs axial strain. To be consistent with the rest of the rest of the capacity curves analyzed in here, the axial stress was transformed to axial force by multiplying by the thickness of the panel (180mm). Thus, the capacity curve for the F-series are presented in figure 6.4 in terms of axial compressive force vs longitudinal (or axial) strain. The agreement between the curves of the calibrated models and the experimental capacity curves was acceptable. As appreciated in Figure 6.4, the PACI and the EC2 design capacity curves are the same because both approaches suggested the same amount of reinforcement for these panels. Also, there was not much difference between all numerical curves and the experimental curve despite the considerable difference between the reinforcement areas suggested by the approaches and the areas provided during the experiments. A possible explanation for this is that all panels were loaded to high compressive forces which provoked the brittle failure mode of concrete crushing, and also restricted the effect of the reinforcement in the behavior of the panels. In fact, the F3 and the F4 panels were subjected to axial compressive forces that exceed 1.35 and 1.55 times their corresponding in balanced forces in the y-direction of the panels, respectively.

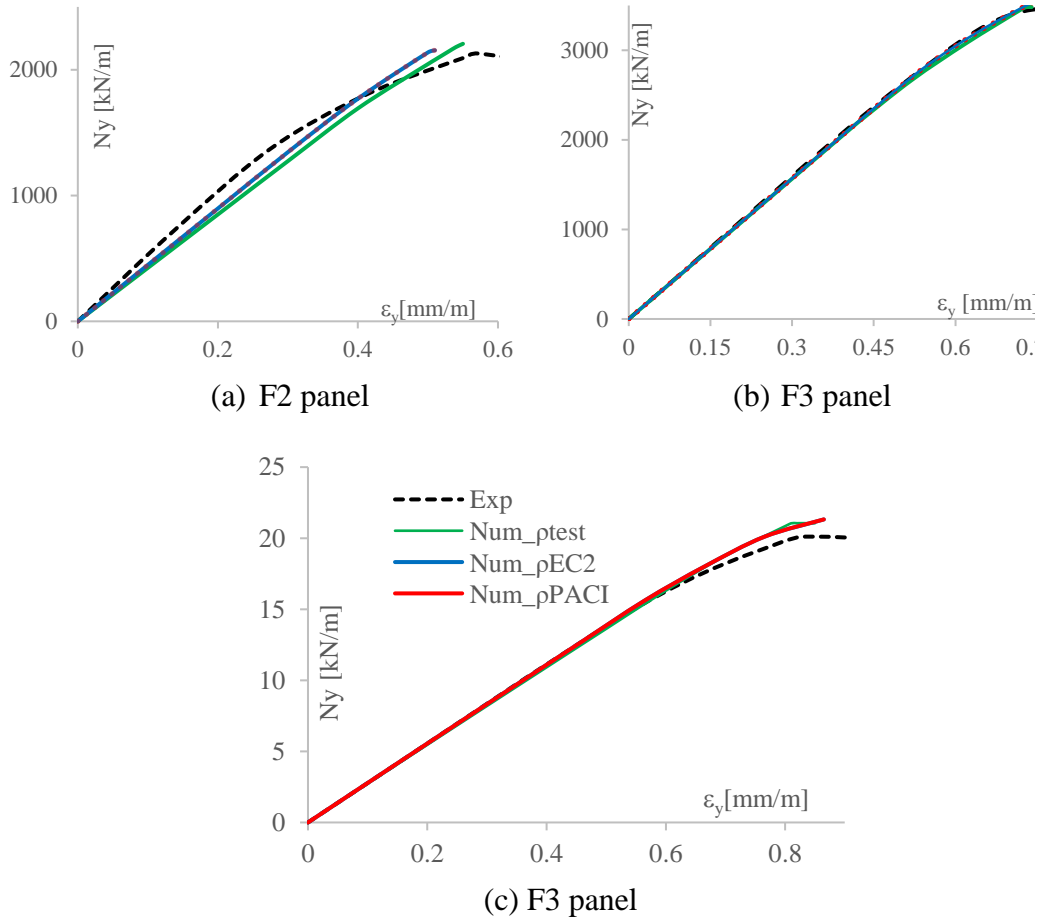


Figure 6.4. Comparison between experimental and numerical load vs deformation curves for the F series panels.

***Analysis and comparison between the numerical and experimental capacities***

Table 6.8 compares the estimated numerical capacities of the panels against the ultimate capacities reported from the experiment. Again, the EC2 and the PACI numerical capacities were obtained after introducing the reinforcement areas suggested by the corresponding approaches into the calibrated numerical model developed in Shell-2000. Two things can be noted when analyzing the Numerical capacities ( $C_{EC2}$  and/or  $C_{EC2}$ ) over Experimental capacity ( $C_{exp}$ ) ratios. First, The ratios are the same because both approaches suggested the same amount of reinforcement for each panel; and second, all capacity ratios ( $C_{EC2}/C_{exp}$  and  $C_{PACI}/C_{exp}$ ) are greater than 1, by which it can be inferred that both design approaches are safe.

Table 6.8. Experimental reported capacities vs estimated numerical capacities for the F series.

F series	External Applied demands	Experimental Capacities ( $C_{exp}$ )	EC2 Numerical Capacities ( $C_{EC2}$ )	$\frac{C_{EC2}}{C_{exp}}$	PACI Numerical Capacities ( $C_{PACI}$ )	$\frac{C_{EC2}}{C_{exp}}$
F2	Ny [KN/m]	-2140	-2155	1.01	-2155	1.01
	Nx [KN/m]	-1070	1077	1.01	1077	1.01
F3	Ny [KN/m]	-3452	-3505	1.01	-3505	1.01
	Nx [KN/m]	1086	1168	1.08	1168	1.08
F4	Ny [KN/m]	-3713	-3838	1.03	-3838	1.03
	Nx [KN/m]	928	959	1.03	959	1.03

### 6.1.5 Validation of results using the ML series panels

#### *Estimation of the suggested reinforcement areas*

Both, the PACI and the EC2 approaches suggested very similar reinforcement areas to those provided during the experiment for the ML panels as shown in table 6.9. The main difference was found in the ML1 panel in which the EC2 approach suggested 6% more of the reinforcement used in the experiment, while the PACI approach suggested the same amount of reinforcement provided during the experiment. The two approaches suggested less reinforcement areas than those provided during the experiment for panels ML2 and ML9. For the ML2 panel and the ML9 panels, both design approaches suggested 85% and 82% of the total reinforcement area provided in the experiments. Blaauwendraad (2010) also estimated areas of reinforcement for the ML9 panel considering the MC90 basic sandwich model, the advanced Lourenco and Figueras (1993) model, and a non-linear analysis procedure, which were 16.4 cm<sup>2</sup>/m, 19.4 cm<sup>2</sup>/m, respectively. The same Blaauwendraad (2010) concluded that for high twisting moment demands, the results of the EC2 approach are not reliable because it suggested less amount of reinforcement, when compared against the experiment, and against a more accurate non-linear analysis. It must be noted that the estimated reinforcement areas reported by Blaauwendraad (2010) for panel ML9, 16.4 cm<sup>2</sup>, and the values suggested in this thesis following the EC2 sandwich model approach are the same. However, it will be shown later that although both approaches suggested less reinforcement than the reinforcement provided during the experiments for these two panels, they reached similar twisting moment capacities than those reported from their respective tests.

Table 6.9. Comparison between the suggested reinforcement areas by the PACI and EC2 design approach, and against the reinforcement area provided in the experiment.

ML Series	Proportional Loading	Reinforcement per Layer in [cm <sup>2</sup> /m]						As Ratios
		Layers	Top X	Top Y	Bot X	Bot Y	As Tot	
ML1	Mxy	Test	5.0	5.0	5.0	5.0	20.0	
	1	EC2	5.0	5.0	5.0	5.0	20.0	1.06
		PACI	5.0	5.0	5.0	5.0	20.0	1.00
ML2	Mxy	Test	10	10	10	10	40.0	
	1	EC2	8.5	8.5	8.5	8.5	34.0	0.85
		PACI	8.5	8.5	8.5	8.5	34.0	0.85
ML9	Mxy	Test	20	20	20	20	80.0	
	1	EC2	16.4	16.4	16.4	16.4	65.6	0.82
		PACI	16.4	16.4	16.4	16.4	65.6	0.82

### *Analysis and comparison between the numerical and experimental capacity curves*

As mentioned in chapter 5, the numerical models in Shell-2000 captured very well the experimental curves of the panels. As for other panels, the PACI and the EC2 design capacities curves follows the same path for these ML series panels. Again, the reason for this is that both approaches suggested the same reinforcement areas. The main difference between the numerical adjusted and the numerical PACI and EC2 capacities curves are in the post-cracking stiffness of the panels. The PACI and the EC2 design curves of panels ML2 and ML9 show a reduction in the post-cracking stiffness of the panels, which is attributable to of the reduction in reinforcement areas (compared to the areas provided during the experiments) suggested by the approaches according to table 6.9. There was no reduction in the stiffness of panel ML1 because both approaches suggested the same of reinforcement provided during the experiment. The reinforcement areas suggested by the approaches in table 6.9 for panel ML1 were satisfied by providing designation bar 10M each 200mm (10M@200mm) in all four reinforcement layers. The reinforcement areas suggested by each design approaches the for panel ML2 and ML9 in all four layers were satisfied by providing 10M@125mm and #5@125, respectively.

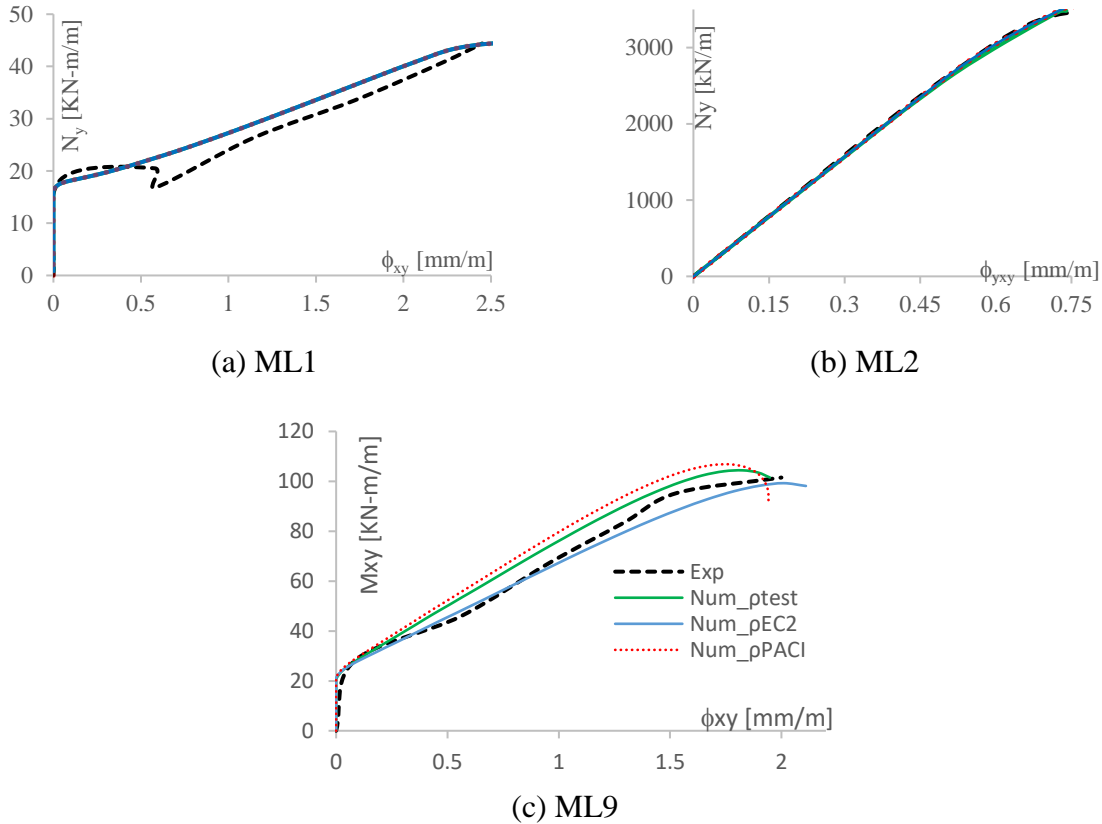


Figure 6.5. Comparison Between experimental and numerical load vs deformation curves for the ML series panels.

### ***Comparison between the experimental and numerical capacities***

Table 6.10 summarizes and compares the experimental reported capacities against the numerical capacities of the panels obtained after introducing the reinforcement areas suggested by the EC2 and the PACI design approaches. Since both approaches suggested the same amount of reinforcement for all ML series panels, there was no differences between the estimated numerical capacities. While the ML1 reached the maximum twisting moment capacity reported from the experiment, the ML2 and the ML9 panels did not. The obvious reason for this is that both design approaches suggested less reinforcement areas than the areas provided during the test for the ML2 and the ML9 panels, as explained in table 6.9. However, the ML2 and the ML9 reached 96% and 97% of the capacities reported from the experiments. Although it may seem that the approaches were not safe for the ML2 and the ML9 panels with high twisting moments, it must be highlighted that the reinforcement suggested areas for these two panels were estimated without considering

any type strength reduction factor as is usually done in actual design applications. In other words, the safety or conservatism of the two approaches might be increased by considering strength reduction factors.

Table 6.10. Experimental reported capacities vs estimated numerical capacities.

ML Series	External Applied demands	Experimental Capacities ( $C_{exp}$ )	EC2 Numerical Capacities ( $C_{EC2}$ )	$\frac{C_{EC2}}{C_{exp}}$	PACI Numerical Capacities ( $C_{PACI}$ )	$\frac{C_{EC2}}{C_{exp}}$
ML1	$M_{xy}$ [KN-m/m]	44.5	44.5	1.00	44.5	1.00
ML2	$M_{xy}$ [KN-m/m]	69.5	66.8	0.96	66.8	0.96
ML9	$M_{xy}$ [KN-m/m]	101.5	98.3	0.97	98.3	0.97

### 6.1.6 Validation of results using the SP series panels

#### *Estimation of the suggested reinforcement areas*

Table 6.11 shows the differences between the reinforcement areas provided during the experiment, and the reinforcement areas suggested by the two design approaches for the SP series panels. Four of the SP panels were selected in this research: Panels SP2, SP3, SP7 and SP9. While panels SP2 and SP3 were only subjected to out-of-plate forces (it means, transverse shear and its associated bending moments), panels SP7 and SP9 were subjected to out-plate forces plus in-plane shear. It is worthy to point out that these panels were the only ones in which it was possible to evaluate the accuracy of the two approaches when estimating in-plane and out-of-plane reinforcement.

Both approaches suggested similar reinforcement areas than the areas provided during the tests for panels SP2 and SP3. However, there are important differences between the areas of reinforcement suggested by the approaches, against the areas of reinforcement provided during the tests for panels SP7 and SP9. Specifically, for panels SP7, while the EC2 approach suggested only 9% more reinforcement than that provided in the experiment, the PACI approach suggested 32% more. Similarly, while the EC2 approach suggested only 16% of additional reinforcement compared against the experiment, the PACI approach suggested 36% more reinforcement for panel SP9. The average increments in in-plane reinforcement suggested by the EC2 and the PACI

approach, compared to the reinforcement provided during the tests for the SP series panels, were 8% and 18%, respectively. Again, the 18% of additional reinforcement suggested by the PACI approach seems reasonable given the simplicity of the approach.

The explanation why the PACI approach suggested more reinforcement for panels SP7 and SP9 is related to the fact these two panels were subjected to high in-plane shears. Here it is important to highlight the difference about how both approaches deal with the in-plane shear demands. While the EC2 approach considers an interaction between the in-plane axial forces and the in-plane shear forces when estimating the forces that will be resisted by the reinforcement, as shown in equations 13a and d13b, the PACI approach does not. Thus, the PACI approach simply absorbs all the in-plane shear demand as it is, disregarding any possible reduction in the forces that will be resisted by the reinforcement in the outer layers.

Table 6.11. Comparison between the suggested reinforcement areas by the PACI and EC2 design approach, and against the reinforcement area provided in the experiment

SP series	Proportional Loading $N_{xy} : M_x : V_{xz}$	Reinforcement per Layer in [cm <sup>2</sup> /m]							Ash Transverse cm <sup>2</sup> /m <sup>2</sup>
		Layers	Top X	Top Y	Bot X	Bot Y	As Tot	As Ratios	
SP2	0.0 : 0.8 : 1.0	Test	31.7	31.7	31.7	31.7	127		8.0
		EC2	32.2	32.2	32.2	32.2	129	1.02	15.0
		PACI	31.4	31.4	31.4	31.4	126	1.00	12.0
SP3	0.0 : 0.8 : 1.0	Test	36.0	36.0	36.0	36.0	144		8.0
		EC2	37.7	37.7	37.7	37.7	151	1.05	17.7
		PACI	37.1	37.1	37.1	37.1	148	1.03	20.0
SP7	4.0 : 0.8 : 1.0	Test	37.5	37.5	37.5	37.5	150		8.0
		EC2	41.0	41.0	41.0	41.0	164	1.09	17.3
		PACI	49.6	49.6	49.6	49.6	198	1.32	16.3
SP9	8.0 : 0.8 : 1.0	Test	37.5	37.5	37.5	37.5	150		8.0
		EC2	43.5	43.5	43.5	43.5	174	1.16	14.1
		PACI	51.0	51.0	51.0	51.0	204	1.36	6.45

Contrary to the in-plane reinforcement, both design approaches suggested considerably more Transverse Shear Reinforcement (TSHR) than what was provided during the tests for the 3 out of the 4 SP panels series. For example, for panel SP2, the EC2 and the PACI approaches suggested 1.87 and 1.5 times the reinforcement provided in the test. For panel SP3, the EC2 and the PACI approaches suggested 2.2 and 2.5 times the TSHR provided in the tests. For panels SP7, the EC2 and the PACI approaches suggested 2.2 and 2.0 times the TSHR provided during their

respective tests. Similarly, for panel SP9, the EC2 suggested 1.76 times the TSHR provided in tests. One explanation why both approaches suggested considerably more TSHR than what was provided during the tests is related to the fact, as explained in chapter 5, that the ultimate out-of-plane shear capacity of panels SP3, SP7, and SP9 was likely overestimated during the experiments. On the other hand, it must be highlighted how the EC2 approach suggested more TSHR than both, the reinforcement provided in the tests, and the reinforcement suggested by the PACI approach. The reason for this is that the EC2 approach, contrary to the PACI approach, does not consider any contribution of the concrete when estimating the TSHR as explained in chapter 2.

It is interesting to note how for panel SP2, which was the only panel whose ultimate out-of-plane shear capacity was not overestimated according to Adebar and Collins (1994), the PACI approach did not overestimated the required TSHR as much as the EC2 approach did. Panel SP9 was the only for which the PACI approach suggested less TSHR than that provided during the test. Specifically, the PACI approach suggested 80% of the total TSHR from the test, and there are two possible explanations for this reduction. First, it seems that this panel did not fail in out-of-plane shear, according to the damage description at final stage given by Adebar (1989). Adebar (1989), reported that the concrete in the outer layers of the panel was totally crushed and there was no evidence of rupture in the stirrups (transverse reinforcement). The high in-plane shear at which panel SP9 was subjected, might have triggered the crushing in the concrete before any out-of-plane shear failure. The second explanation is that the magnitude of the ultimate experimental out-of-plane shear capacity of this SP9 panel, reported in 372kN/m, was the lowest among the others. The fact that panel SP9 did not fail in out-of-plane shear infers that less TSHR might have been utilized during the test, as suggested by the PACI approach. Moreover, it will be demonstrated in the next section that in spite of the reduction in TSHR suggested by the PACI approach, the SP9 panel was able to reach the maximum out-of-plane shear capacity reported during the test.

### ***Analysis and comparison between the experimental and the numerical capacity curves***

The numerical capacity curves for the SP series panels are shown in figure 6.6. Each panel in figure 6.6 has four lines, excepting for panels SP9 which only has only three. The darker discontinuous line, identified with name *Exp* represents the curve that was reproduced from the experiments. The green and continuous line, identified with name *Num\_ρ<sub>test</sub>*, was obtained

modelling the panels using the actual reinforcement areas and covers specified in the experiments. Finally, the blue and red lines, called with the names  $Num\_ρ_{EC2}$  and  $Num\_ρ_{PACI}$ , were obtained after introducing the reinforcement areas suggested by the EC2 and the PACI approaches, respectively; These capacity curves, as explained in chapter 5, were initially given in terms of principal transverse shear stress vs transverse strain ( $v_o$  vs  $γ_{xz}$ ). However, to be consistent with the convention utilized in this thesis, the transverse shear stress was transformed into transverse shear force ( $V_o$ ) by multiplying by the thickness of the panel.

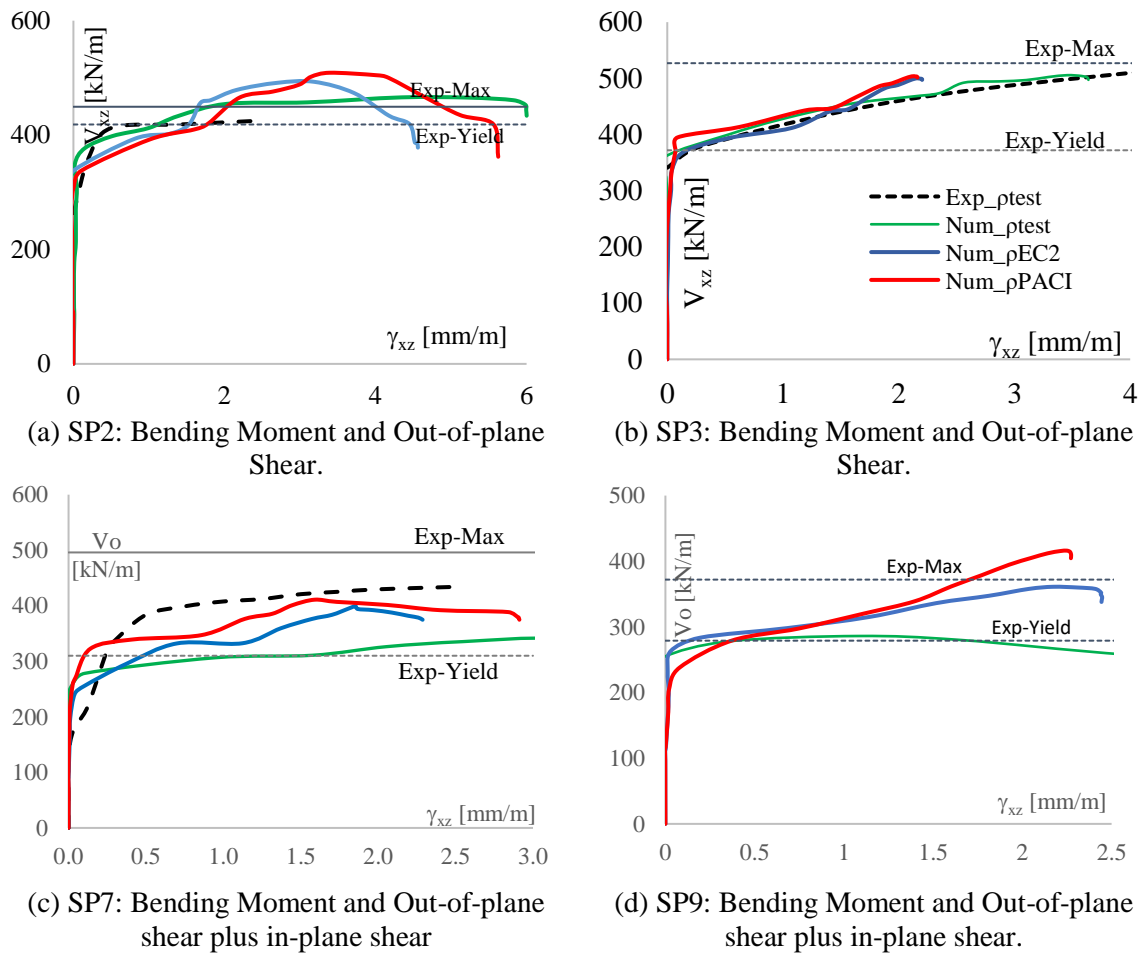


Figure 6.6. Comparison Between experimental and numerical load vs deformation curves for the SP series panels.

Before continuing analyzing the behavior of the panels after introducing the areas of reinforcement suggested by the approaches, it is convenient to recall that none of the experimental

capacity curves (black discontinuous curves) points out the maximum out-of-plate shear capacities. For this reason, and to provide additional explanations, the yielding and the maximum capacities of the panels have been included for all panels in figure 6.6 as dotted lines. It can be observed that the PACI numerical curves reached slightly higher capacities than the capacities reached by the EC2 numerical curves for all SP panels. This was expected, because in all cases, the PACI approach suggested more in-plane and more out-of-plane shear reinforcement than the EC2 approach. It calls the attention how in spite the PACI approach suggested more reinforcement than the EC2 approach for panels SP2 and SP9, they did not develop a substantial higher out-plate shear capacity. Again, it confirms that although the PACI approach produces conservative results, it is not as efficient as the EC2 approach.

***Comparison between the experimental and the numerical capacities.***

Table 6.12 compares the experimental capacities ( $C_{exp}$ ) against the EC2 and the PACI numerical capacities,  $C_{EC2}$  and  $C_{PACI}$ , respectively. The EC2 and PACI numerical capacities of the panels were extracted from the corresponding numerical capacities curves in Figure 6.6. Since panels SP2 and SP3 were subjected to out-of-plate bending moments and out-of-plane shear, table 6.12 only shows two capacities: bending moment capacity ( $M_{xz}$ ) and Out-of-plate shear capacity ( $V_{xz}$ ). Panels SP7 and SP9, on the other hand, in addition to bending moment and the out-of-plane shear capacities, also show the in-plane shear capacities ( $N_{xy}$ ). However, only the out-of-plate shear capacities will be commented in here because these were the only capacities reported during the tests. The out-of-plate bending moment, and the in-plane shear capacities in table 6.12 were estimated following the proportional loading values (specified in the first column of table 6.12) for each panel. As shown in table 6.12, all numerical over experimental capacities ratios  $C_{PACI}/C_{exp}$  for all panels SP2 and SP9 are greater than 1.0. This confirms that the PACI approach produced safe results because it suggested enough reinforcement areas to reach the “design” demands of both panels. On the contrary, ratios for panels SP3 and SP9, it may seem that the PACI approach did not produce safe results because their corresponding  $C_{PACI}/C_{exp}$  ratios were lower than 1.0. The same may be said about the EC2 approach for panels SP3, SP7 and SP9, whose  $C_{EC2}/C_{exp}$  ratios were also lower than 1.0. However, it must be recalled that, according to Adebar and Collins (1994), the out-of-plane shear capacity of these three panels was likely overestimated during

experimentation, as explained in chapter 5. Thus, it is difficult to judge as unsafe the results of any of the approaches for these three panels. Although the differences between the numerical over experimental capacities ratios ( $C_{PACI}/C_{exp}$ ) in table 6.12 are negligible, it can be noted the PACI approach produced more conservative results than the EC2 approach in all SP panels. Specifically, for panel SP2, the  $C_{PACI}/C_{exp}$  and the  $C_{PACI}/C_{exp}$  ratios after introducing the areas suggested by the PACI and the EC2 approaches were 1.13 and 1.10. Similarly, for panel SP3, the  $C_{PACI}/C_{exp}$  and the  $C_{PACI}/C_{exp}$  ratios after introducing the areas suggested by the PACI and the EC2 approaches were 0.96 and 0.95. Following the same trend, the  $C_{PACI}/C_{exp}$  and the  $C_{PACI}/C_{exp}$  ratios for panel SP7 after introducing the areas suggested by the PACI and the EC2 approaches were 0.83 and 0.80. Finally, for panel SP9, the  $C_{PACI}/C_{exp}$  and the  $C_{PACI}/C_{exp}$  ratios were 1.12 and 0.97, respectively.

Table 6.12. Experimental reported capacities vs estimated numerical capacities

SP Series	External Applied "Demands"	Experimental Capacities ( $C_{exp}$ )	EC2 Numerical Capacities ( $C_{EC2}$ )	$\frac{C_{EC2}}{C_{exp}}$	PACI Numerical Capacities ( $C_{PACI}$ )	$\frac{C_{PACI}}{C_{exp}}$
SP2	$M_o$ [KN-m/m]	360	394	1.10	407	1.13
	$V_o$ [KN/m]	450	493	1.10	509	1.13
SP3	$M_o$ [KN-m/m]	422	400	0.95	402	0.95
	$V_o$ [KN/m]	527	500	0.95	504	0.96
SP7	$N_{xy}$ [KN/m]	1984	1600	0.80	1644	0.83
	$M_o$ [KN-m/m]	397	320	0.80	329	0.83
	$V_o$ [KN/m]	496	399	0.80	411	0.83
SP9	$N_{xy}$ [KN/m]	2976	2888	0.97	3328	1.12
	$M_o$ [KN-m/m]	298	289	0.97	333	1.12
	$V_o$ [KN/m]	372	361	0.97	416	1.12

### 6.1.7 Summary of results for the experimental data.

#### *Comparison between the suggested and experimental reinforcement areas*

Table 6.13 compares the reinforcement areas provided during the experiments ( $A_{s,exp}$ ), against the reinforcement areas suggested by the EC2 approach ( $A_{s,EC2}$ ) for all 21 panels. In 12 out of the 21 panels analyzed in here, the  $A_{s,EC2}/A_{s,exp}$  reinforcement ratios were lower than 1.0. This means that the EC2 approach suggested less reinforcement than the reinforcement provided during the test. In 9 panels the EC2 approach suggested more than the reinforcement provided during the experiments, which were panels PV23, SM3, F2, F3, F4, and SP2, SP3, SP7

and SP9. However, it must be again emphasized that the experimental results of panels SP3, SP7 and SP9 are not reliable, and therefore, they might not be considered in this account. Also, even after considering the ambiguous results of the F series panels, the average of additional reinforcement suggested by the EC2 approach compared to the reinforcement provided during tests, for these panels was about 22%. The fact that the EC2 approach suggested less reinforcement areas than the areas provided during the test in 12 (and perhaps in 15, counting panels SP2, SP7 and SP9) out of the 21 panels analyze in here, shows the accuracy and efficiency of this approach.

Table 6.13. Experimental vs suggested reinforcement areas by the EC2 approach.

Series	Proportional	Reinforcement per Layer in [cm <sup>2</sup> /m]						$\frac{A_{s,EC2}}{A_{s,Exp}}$
		Layers	Top X	Top Y	Bot X	Bot Y	As Tot	
SE	$M_x : N_{xy}$	Tests	41.8	13.9	41.8	13.9	111	
SE1	0 : 1	EC2	19.6	19.6	19.6	19.6	78.4	0.71
SE3	1 : 0	EC2	47.5	47.5	5.7*	5.7*	106.4	0.96
SE4	1 : 0.5	EC2	47.6	47.6	5.7*	5.7*	106.6	0.96
SE7	1 : 0.13	EC2	32.6	32.6	11	11	87.2	0.79
PV	$N_{xy} : N_x : N_y$	Test	6.25	6.25	6.25	6.25	25	
PV23	1 : -0.39 : -0.39	EC2	7.3	7.3	7.3	7.3	29.2	1.17
PV24	1 : -0.83 : -0.83	EC2	5.6	5.6	5.6	5.6	22.4	0.9
PV25	1 : -0.69 : -0.69	EC2	5.6	5.6	5.6	5.6	22.4	0.9
PV28	1 : 0.32 : 0.32	EC2	5.6	5.6	5.6	5.6	22.4	0.9
SM	$M_x : M_y : N_y : N_x$	Test	39.5	39.5	13.3	13.3	106	
SM1	1 : 0 : 0 : 0	EC2	41.8	41.8	6.32*	6.32*	96.2	0.91
SM2	1:0: -0.37: -0.37	EC2	41.4	41.4	6.32*	6.32*	95.4	0.9
SM3	1 : 1 : -0 : -0	EC2	43.8	43.8	13.5	13.5	115	1.08
F	$N_x : N_y$	Test	11.25	4.8	11.25	4.8	32.1	
F2	0.5 : -1	EC2	10.5	10.5	10.5	10.5	42	1.31
F3	0.33 : -1	EC2	11.2	11.2	11.2	11.2	44.8	1.4
F4	0.25 : -1	EC2	9.4	9.4	9.4	9.4	37.6	1.17
ML	$M_{xy}$	Test	5	5	5	5	20	
ML1	1	EC2	5	5	5	5	20	1.00
ML2	$M_{xy}$	Test	10	10	10	10	40	
	1	EC2	8.5	8.5	8.5	8.5	34	0.85
ML9	$M_{xy}$	Test	20	20	20	20	80	
	1	EC2	16.4	16.4	16.4	16.4	65.6	0.82
SP	$N_{xy} : M_x : V_{xz}$	Test	31.7	31.7	31.7	31.7	127	
SP2	0.0 : 0.8 : 1.0	EC2	32.2	32.2	32.2	32.2	129	1.02
SP3	0.0 : 0.8 : 1.0	Test	36.0	36.0	36.0	36.0	144	
		EC2	37.7	37.7	37.7	37.7	151	1.05
SP7	4.0 : 0.8 : 1.0	Test	37.5	37.5	37.5	37.5	150	
		EC2	41.0	41.0	41.0	41.0	164	1.09
SP9	8.0 : 0.8 : 1.0	Test	37.5	37.5	37.5	37.5	150	
		EC2	43.5	43.5	43.5	43.5	174	1.16

\*Minimum reinforcement ratio, estimated as 0.2% of the thickness of the panels ( $0.002t_w$ )

Table 6.14. Comparison between experimental vs estimated reinforcement areas suggested by the PACI design approach.

Series	Proportional Loading	Reinforcement per Layer in [cm <sup>2</sup> /m]						$\frac{A_{s\_PACI}}{A_{s\_Exp}}$
		Layers	Top X	Top Y	Bot X	Bot Y	As Tot	
SE	$M_x : N_{xy}$	Tests	41.8	13.9	41.8	13.9	111	
SE1	0 : 1	PACI	19.6	19.6	19.6	19.6	78.4	0.71
SE3	1 : 0	PACI	46.5	46.5	5.7*	5.7*	104.4	0.94
SE4	1: 0.5	PACI	53	53	10	10	126	1.13
SE7	1: 0.13	PACI	39	39	19	19	116	1.05
PV	$N_{xy} : N_x : N_y$	Test	6.25	6.25	6.25	6.25	25	
PV23	1 : -0.39 : -0.39	PACI	6	6	6	6	24	0.96
PV24	1: -0.83 : -0.83	PACI	5.65	5.65	5.65	5.65	22.6	0.9
PV25	1 : -0.69 : -69	PACI	6.4	6.4	6.4	6.4	25.6	1.02
PV28	1: 0.32 : 0.32	PACI	5.6	5.6	5.6	5.6	22.4	0.9
SM	$M_x : M_y : N_y : N_x$	Test	39.5	39.5	13.3	13.3	106	
SM1	1 : 0 : 0 : 0	PACI	42.9	42.9	6.32*	6.32*	98.4	0.93
SM2	1:0: -0.37: -0.37	PACI	39.3	39.3	6.32*	6.32*	91.2	0.86
SM3	1 : 1 : -0 : -0	PACI	43.3	43.3	12.75	12.75	112	1.06
F	$N_x : N_y$	Test	11.25	4.8	11.25	4.8	32.1	
F2	0.5 : -1	PACI	10.5	10.5	10.5	10.5	42	1.31
F3	0.33 : -1	PACI	11.2	11.2	11.2	11.2	44.8	1.4
F4	0.25 : -1	PACI	9.4	9.4	9.4	9.4	37.6	1.17
ML	$M_{xy}$	Test	5	5	5	5	20	
ML1	1	PACI	5	5	5	5	20	1
ML2	$M_{xy}$	Test	10	10	10	10	40	
	1	PACI	8.5	8.5	8.5	8.5	34	0.85
ML9	$M_{xy}$	Test	20	20	20	20	80	
	1	PACI	16.4	16.4	16.4	16.4	65.6	0.82
SP	$N_{xy} : M_x : V_{xz}$	Test	31.7	31.7	31.7	31.7	127	
SP2	0.0 : 0.8 : 1.0	PACI	31.4	31.4	31.4	31.4	126	1.00
SP3	0.0 : 0.8 : 1.0	Test	36.0	36.0	36.0	36.0	144	
		PACI	37.1	37.1	37.1	37.1	148	1.03
SP7	4.0 : 0.8 : 1.0	Test	37.5	37.5	37.5	37.5	150	
		PACI	49.6	49.6	49.6	49.6	198	1.32
SP9	8.0 : 0.8 : 1.0	Test	37.5	37.5	37.5	37.5	150	
		PACI	51.0	51.0	51.0	51.0	204	1.36

\*Minimum reinforcement ratio, estimated as 0.2% of the thickness of the panels ( $0.002t_w$ )

Table 6.14 summarizes and compares the reinforcement areas provided during the experiments ( $A_{s\_exp}$ ), against the reinforcement areas suggested by the PACI approach ( $A_{s\_PACI}$ ). There were 11 out of the 21 panels analyzed in here for which the PACI approach suggested equal to or less reinforcement areas than the areas provided during the tests. These were panels SE1, SE3, PV23, PV24, PV28, SM1, SM2, ML1, ML2, ML9, SP2. On the contrary, there were 10 out of the 21 panels, which were panels SE4, SE7, PV25, SM3, F2, F3, F4, SP2, and SP9 for which

the PACI approach suggested more reinforcement than what was provided during the tests. On average, The PACI approach 17% of additional reinforcement areas for these 10 tests.

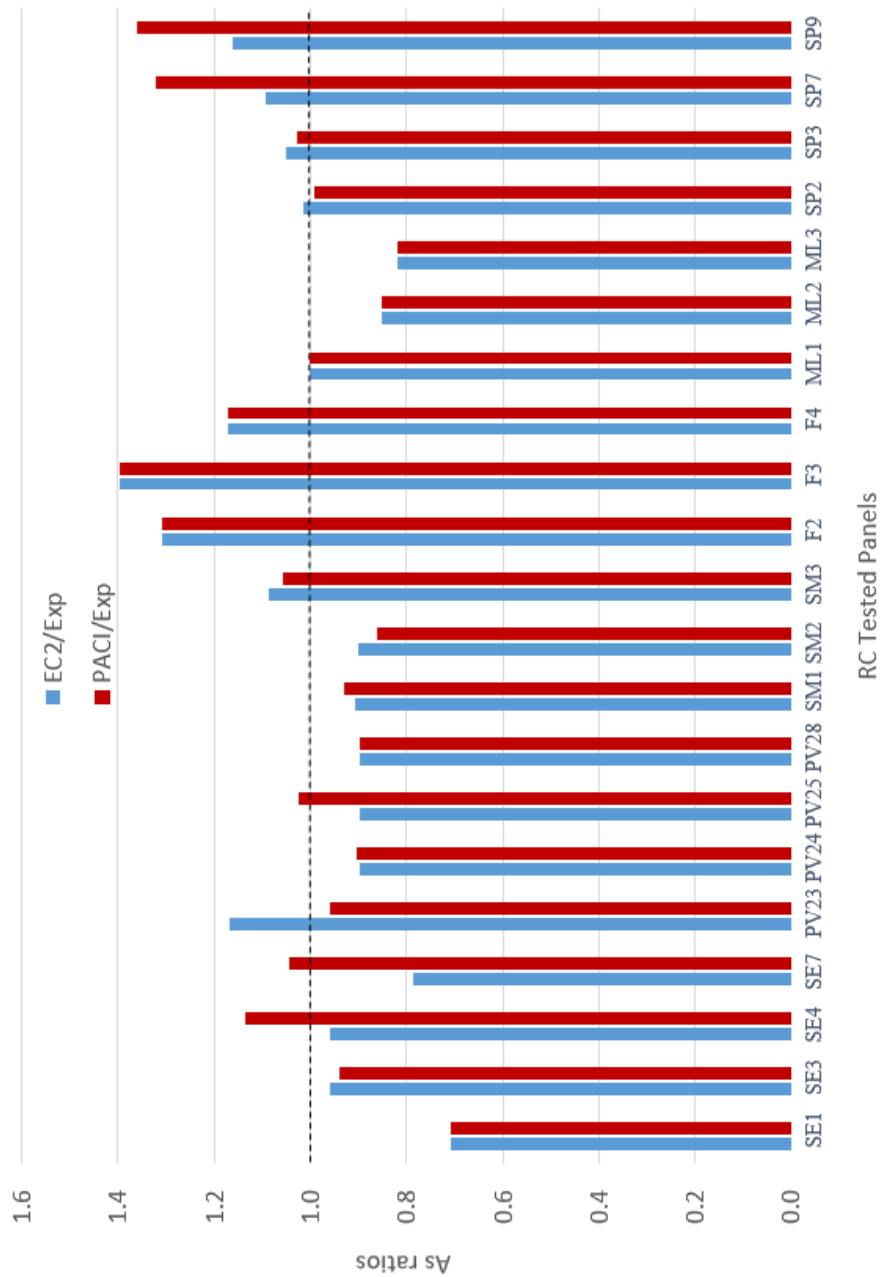


Figure 6.7. Comparison between the experimental provided in-plane reinforcement areas against the in-plane reinforcement areas suggested by the PACI and the EC2 approaches.

Finally, Figure 6.7 compares the total reinforcement areas suggested by the PACI approach against the total reinforcement areas suggested by the EC2, and the areas provided during the

experiment. In figure 6.15, the EC2 and the PACI suggested reinforcement areas were normalized against the experimental areas. From figure 6.15, it can be seen how both approaches suggested similar amount of reinforcement for almost all panels. The higher discrepancies between the areas suggested by the approaches occurred in panels SE4, SE7, PV23, PV25, SP7 and SP9. For all these 6 panels, it is clear how the PACI approach suggested more reinforcement than the EC2 approach. In addition, the PACI approach did not only suggested more reinforcement areas than the EC2 approach, but also more than the reinforcement areas provided during their respective tests for these panels. It is important to highlight that one common feature of these 6 panels, is that they were all subjected to in-plane shear demands. The fact that for these panels subjected to in-plane shear demands the PACI approach always produced more conservative results (or more specifically, suggested more reinforcement areas) is expected because the PACI approach deals with the in-plane shear demands a more conservative way than the EC2 approach.

#### ***Comparison between numerical and experimental capacities of the panels***

Table 6.15 summarizes and compares the experimental capacities ( $C_{exp}$ ) against the estimated numerical capacities of the panels after using non-linear analysis. It is important to recall that for the design of the panels the maximum reported capacities were taken as the “design demands”, and thus, the numerical over experimental capacities ratios ( $C_{EC2}/C_{exp}$  and  $C_{PACI}/C_{exp}$ ) in table 6.14 were computed as the ratio between the estimated numerical capacities to the experimental capacities or design demands. As can be seen in table 6.14, the Capacity-to-Demand Ratios (CDRs) for most of the panels are greater than or equal to 1.0, which means that the panels reached either the same or larger capacities than the capacities reported from the experiments after considering the reinforcement areas suggested by both design approaches. For all these panels, it can be inferred therefore, that both approaches produced safe results.

It is also important to note in 4 of the 5 panels (which were panels PV23, PV24 and ML21 and ML9) the areas suggested by the PACI approach resulted in nominal capacities slightly lower than the capacities reported in the experiments. One common feature of these 5 panels is that all of them were only subjected to one single external demand, which is very unlikely (or far from reality) in real design situations. On the other hand, in those experimental cases subjected to two or three external demands, which are closer to real design situations, the PACI approach produced

conservative results. For example, for the SP series, which were subjected to in-plane shear forces, out-of-plate shear forces and bending moments, the PACI approach always suggested more reinforcement areas than both, the areas suggested by the EC2 approach, and the areas provided during the tests. Another example were the SE series which were also subjected to in-plane shear and out-of-plate bending demands. Again, in these experimental cases the PACI approach suggested more reinforcement areas than both, the areas suggested by the EC2 approach, and the areas provided in the tests. A simple explanation why the PACI approach produce more conservative results is that in the PACI approach -in contrast to the EC2 approach- the in-plane reinforcement is designed to absorb all the in-plane shear demand, without considering any interaction with the axial demand forces (or stresses). Thus, any possible reduction in the in-plane shear that will be resisted by the in-plane reinforcement in the outer layers is neglected.

Figure 6.8 shows the comparison between the CDRs obtained after using the EC2 and the PACI approach. As can be seen in Figure 6.8 it is easier to identify which panels (after introducing either the PACI or the EC2 approach) did not reach the same magnitudes of the capacities reported during the experiments; or in other words, panels that reported numerical over experimental capacity ratios ( $C_{PACI}/C_{exp}$  or the  $C_{EC2}/C_{exp}$ ) lower than 1.0. Although there were a few cases such as panels SM2, PV23, PV25, ML2, ML9, SP3, SP7 and SP9 in which either the  $C_{PACI}/C_{exp}$  or the  $C_{EC2}/C_{exp}$  ratios were lower than 1.0, it might not be inferred right away that any of the approaches did not produce safe results. In a case by case scenario it must be recalled that: a) the axial compressive capacity force of the SM2 panel was not reported in the experiment, and it was approximately estimated by multiplying the bending capacity of the panel by four, according to the proportional loading pattern. This means that the value for the axial experimental capacity in the SM2 panel might had been lower than the value consigned in table 6.14; b) the PV series panels were built and tested with higher concrete compressive strip of about 100 mm of thickness along its perimeter, which was not considered neither when computing the required reinforcement areas, nor when developing the models developed in shell 2000; and, c) not only the PACI approach, but also the EC2 approach produced non-conservative results for the ML2 and the ML9 panels, which were subjected to high twisting moment demands. Blaauwendraad (2010), also cautioned about the limitation of the EC2 approach for this type of loading. Finally, the out-of-plane shear capacities reported for panels SP7 and SP9 were probably overestimated during experimentation. In addition, it must be considered that all the reinforcement areas suggested by any of the two

approaches were estimated without considering any kind of strength reduction factors ( $\phi_b$ ,  $\phi_v$ ,  $\phi_t$ , etc). By including strength reduction factors, which is mandatory in real design applications, the reinforcement areas suggested by the approaches should have been higher, and therefore, the numerical capacities will increase as well.

Table 6.15. Comparison between experimental and numerical capacities

Series	Panel	External Applied "Design Demands"	Experimental Capacities ( $C_{exp}$ )	EC2 Numerical Capacities ( $C_{EC2}$ )	$\frac{C_{EC2}}{C_{exp}}$	PACI Numerical Capacities ( $C_{PACI}$ )	$\frac{C_{PACI}}{C_{exp}}$
SE Series	SE1	$N_{xy}$ [kN/m]	1930	1943	1.01	2160	1.11
	SE3	$N_{xy}$ [kN-m/m]	520	600	1.15	600	1.15
	SE4	$M_x$ [kN]	480	521	1.08	586	1.22
		$N_{xy}$ [kN-m/m]	960	1041	1.08	1172	1.22
	SE7	$M_x$ [kN]	230	235	1.02	300	1.30
		$N_{xy}$ [kN/m]	1810	1811	1.00	2310	1.28
SM Series	SM1	$M_x$ [kN-m/m]	477	483	1.04	483	1.04
	SM2	$N_x$ [kN /m]	1684*	1700	1.00	1700	1.00
		$N_y$ [kN /m]	1684*	1460	0.87	1460	0.87
		$M_x$ [kN -m/m]	421	441	1.05	423	1.00
	SM3	$M_x$ [kN /m]	488	533	1.09	535	1.10
		$M_y$ [kN -m/m]	151	158	1.05	154	1.02
PV series	PV23	$N_{xy}$ [kN/m]	621	616	0.99	607	0.98
	PV24	$N_{xy}$ [kN/m]	556	658	1.18	658	1.18
	PV25	$N_{xy}$ [kN/m]	639	602	0.94	616	0.96
	PV28	$N_{xy}$ [kN/m]	393	413	1.05	413	1.05
F Series	F2	$N_y$ [kN /m]	-2140	-2155	1.01	-2155	1.01
		$N_x$ [kN /m]	-1070	1077	1.01	1077	1.01
	F3	$N_y$ [kN /m]	-3452	-3505	1.01	-3505	1.01
		$N_x$ [kN /m]	1086	1168	1.08	1168	1.08
	F4	$N_y$ [kN /m]	-3713	-3838	1.03	-3838	1.03
		$N_x$ [kN /m]	928	959	1.03	959	1.03
ML Series	ML1	$M_{xy}$ [kN -m/m]	44.5	44.5	1.00	44.5	1.00
	ML2	$M_{xy}$ [kN -m/m]	69.5	66.8	0.96	66.8	0.96
	ML9	$M_{xy}$ [kN -m/m]	101.5	98.3	0.97	98.3	0.97
SP Series	SP2	$M_x$ [kN-m/m]	360	394	1.10	407	1.13
		$V_x$ [kN/m]	450	493	1.10	509	1.13
	SP3	$M_x$ [kN-m/m]	422	400	0.95	402	0.95
		$V_x$ [kN/m]	527	500	0.95	504	0.96
	SP7	$N_{xy}$ [kN/m]	1984	1600	0.80	1644	0.83
		$M_x$ [kN-m/m]	397	320	0.80	329	0.83
		$V_x$ [kN/m]	496	399	0.80	411	0.83
	SP9	$N_{xy}$ [kN/m]	2976	2888	0.97	3328	1.12
		$M_x$ [kN-m/m]	298	289	0.97	333	1.12
		$V_x$ [kN/m]	372	361	0.97	416	1.12

\*Estimated (not reported) values.

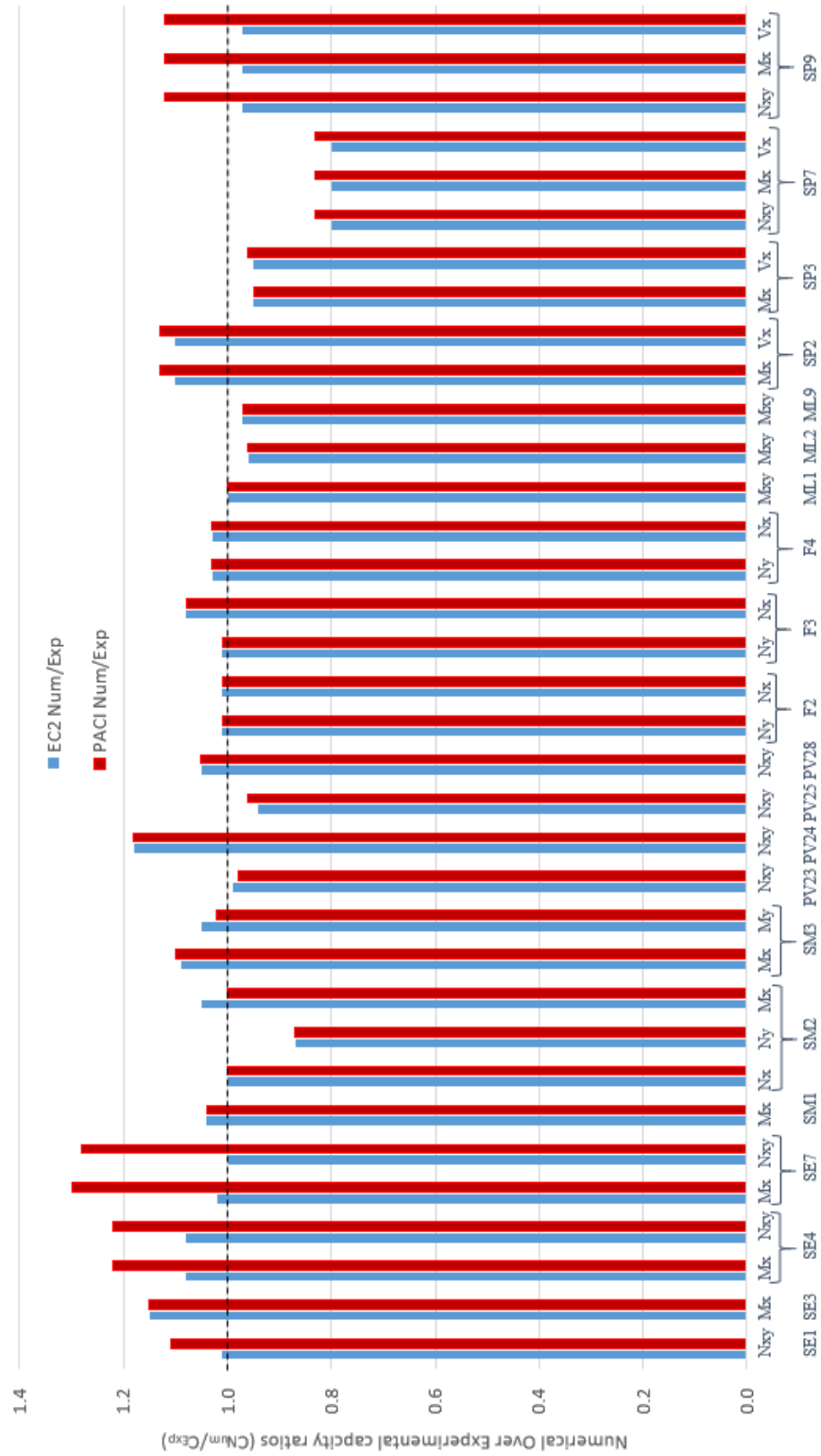


Figure 6.8. Comparison between the EC2 and the PACI Capacity-to-Demand Ratios for all the panels.

## **7. IMPLEMENTATION OF THE DESIGN APPROACHES USING ANALYTICAL DATA.**

This chapter focus in the implementation of the PACI and the EC2 approaches in industrial facilities. Analytical data will be used to evaluate the applicability of both design approaches. Analytical data refers in here as the analytical set of demands extracted from the analysis of an actual industrial facility (for example, AP1000(R), US-APWR(R), etc.). Contrary to the experimental data, in which the set of demands consists in no more than two or three demands, the set of demands in the analytical data consists in the complete set of eight internal design demands resulting from a 2D (or 3D) finite element analysis (FEM) shell model. Two analytical cases, each of those associated to a different load combination were selected. The analytical case 1 corresponds to the design combination 4 of the analysis, which is characterized by low axial forces and low out-of-plane shear forces. High axial compressive forces and high out-of-plane shear forces, on the other hand, characterize the analytical case 2, which comes from the design combination 6 in the DCD document. Since when using analytical data there is no experimental data to compare with, the results of the design approaches will be considered as satisfactory if the estimated numerical capacities are greater than or equal to the analytical design demands. Two activities describe this implementation phase: description of the analytical data; and estimation of the Capacity-to-Demand ratios (CDRs) of the panels. These CDRs will be useful to verify the safety of both design approaches. Like some of the experimental data, the numerical design capacities for the analytical data will be extracted from numerical models developed in Shell 2000.

### **7.1 Description of the analytical data.**

Figure 7.1 shows the set of demands for the two analytical cases. These analytical cases corresponds to the estimated design demands of a critical shell element of a Steel Composite (SC) AP-1000 compact nuclear power plant model. The element is located at a critical location in where the stresses are high. The magnitudes of those design demand can be found in the DCD document published by Westinghouse (2011). The analytical case 1 corresponds to the design combination 4 of the analysis, which is characterized by low axial forces and low out-of-plane shear forces.

High axial compressive forces and high out-of-plane shear forces, on the other hand, characterize the analytical case 2, which comes from the design combination 6 in the DCD document.

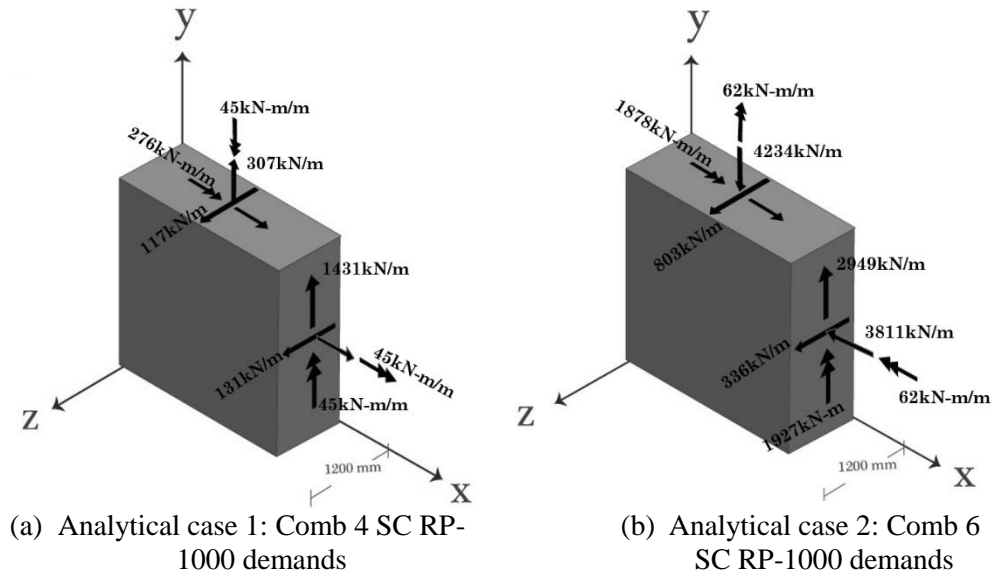


Figure 7.1. Analytical cases

## 7.2 Estimation of the required reinforcement areas.

Table 6.13 shows the reinforcement areas suggested by the PACI ( $A_{s\_PACI}$ ) and the EC2 ( $A_{s\_EC2}$ ) design approaches for both analytical cases. Columns 3 through 6 indicate the required partial reinforcement areas per layer, while column six indicates the total required reinforcement by the approaches. The total required reinforcement areas are the summation of the partial required reinforcement areas per layer. As can be noted in table 6.13, the total reinforcement areas required by the PACI approach ( $A_{s\_PACI}$ ) were always higher than the corresponding required areas by the EC2 ( $A_{s\_EC2}$ ) design approach. The ratio of the total required reinforcement areas between the PACI and the EC2 approaches ( $A_{s\_PACI}/A_{s\_EC2}$ ) for analytical case 1 was 1.16. This means that the PACI approach required 16% of additional in-plane reinforcement than the EC2 for the analytical case 1 (comb 4).

For analytical case 2, on the other hand, there were considerable differences between the reinforcement areas suggested by both approaches. First, the EC2 approach suggested the minimum amount of reinforcement in each layer which is estimated as 0.2% times the thickness of the wall ( $0.002t_w$ ). Second, the EC2 approach suggested a total reinforcement area of 96.0

cm<sup>2</sup>/m, while the PACI approach suggested 118 cm<sup>2</sup>/m. This means that the PACI approach suggested 28% more in-plane reinforcement than the EC2 approach. On average, the PACI approach suggested 22% more additional in-plane reinforcement than the EC approach for both analytical cases. Again, this amount of additional reinforcement suggested by the PACI approach in comparison to the EC2 approach seems reasonable, especially after considering all simplifications of the approach. None of the approaches suggested out-of-plane shear reinforcement because the wall was considerably thick (1200 mm), and thus, the out-of-plane shear capacity that is only provided by the concrete was enough to resist the out-of-plane shear demands. However, the minimum amounts of shear reinforcement of 0.11% and 0.09% suggested by the Eurocode and by the ACI 318 codes, respectively, was considered for the design of the analytical cases.

Table 7.1. Required reinforcement areas suggested for both Analytical cases.

Analytical Cases	In-plane Reinforcement per Layer in [cm <sup>2</sup> /m]						$\frac{A_{s\_PACI}}{A_{s\_Exp}}$	TSHR cm <sup>2</sup> /m <sup>2</sup>
	Approach	Top X	Top Y	Bot X	Bot Y	A <sub>s</sub> Tot		
Case 1 (Comb 4 DCD)	EC2	24.0	24.0	26.0	26.0	100	1.16	11.0
	PACI	29.0	29.0	29.0	29.0	116		9.0
Case 2 (Comb 6 DCD)	EC2	24.0	24.0	24.0	24.0	96.0	1.28	11.0
	PACI	30.8	30.8	30.8	30.8	123		9.0

### 7.3 Modeling and non-linear analysis of the Analytical cases.

Both analytical cases were modelled in Shell-2000. Figure 7.2 shows most of the required input data to reproduce the numerical models for the analytical cases 1. In this analytical case 1, the design compressive strength for the concrete and its maximum tensile strength, were taken as 28 MPa and 3.0 MPa, respectively. The yielding and the ultimate strength of the reinforcement were taken as 420 MPa and 600 MPa, respectively. Similarly, for the analytical case 2, the design compressive strength for the concrete and its maximum tensile strength, were taken as 40 MPa and 3.0MPa, respectively. The yielding and the ultimate strength of the reinforcement were taken as 500MPa and 625MPa. The tension stiffening factor, and the aggregate size for both analytical cases were assumed as 1.0, and 19 mm, respectively. Because of space limitation, only the details for the development of the numerical models to estimate the numerical capacities of the panels after introducing the areas of reinforcement suggested by the PACI approach for the analytical

cases 1 and 2, are shown in figures 7.2 and 7.3 respectively. While the in-plane reinforcement areas required by the PACI approach for the analytical case 1 were satisfied by introducing bars No7 each 160mm (#7@160mm), the required areas for the analytical case 2 were satisfied by introducing bars No7 each 120mm (#7@120mm). The out-of-plane shear reinforcement, on the other hand, for both design approaches and for both analytical cases was satisfied by providing bars No 3 each 250 mm (#3@250 mm).

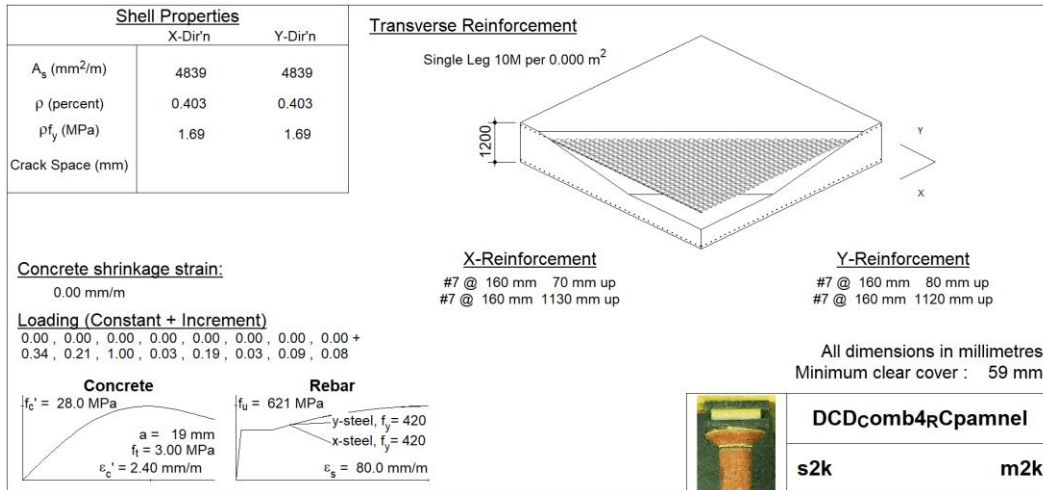


Figure 7.2. Modeling details for analytical case 1. Reinforcement suggested by the PACI approach.

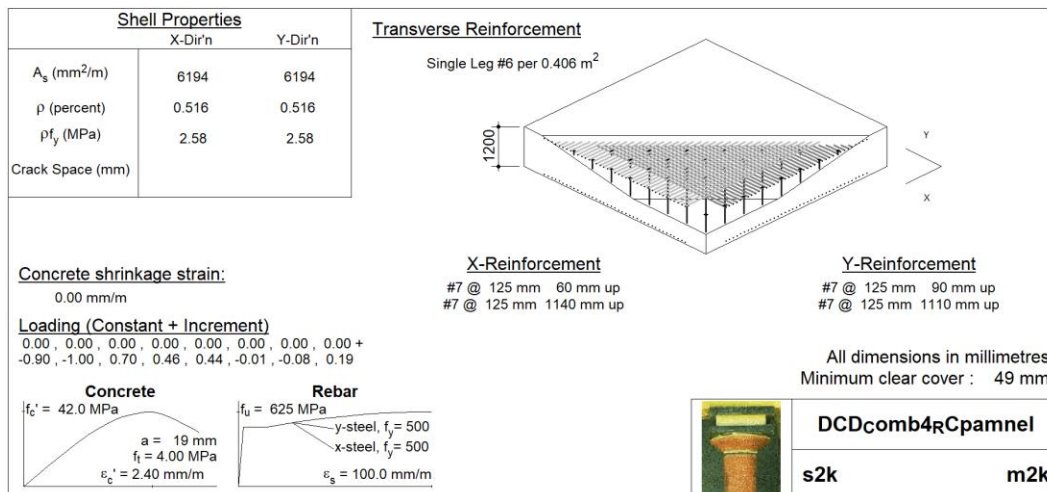


Figure 7.3. Modeling details for analytical case 2. Reinforcement suggested by the PACI approach.

## 7.4 Estimation of the numerical capacities of the panels

### 7.4.1 Numerical Capacity curves for the analytical cases

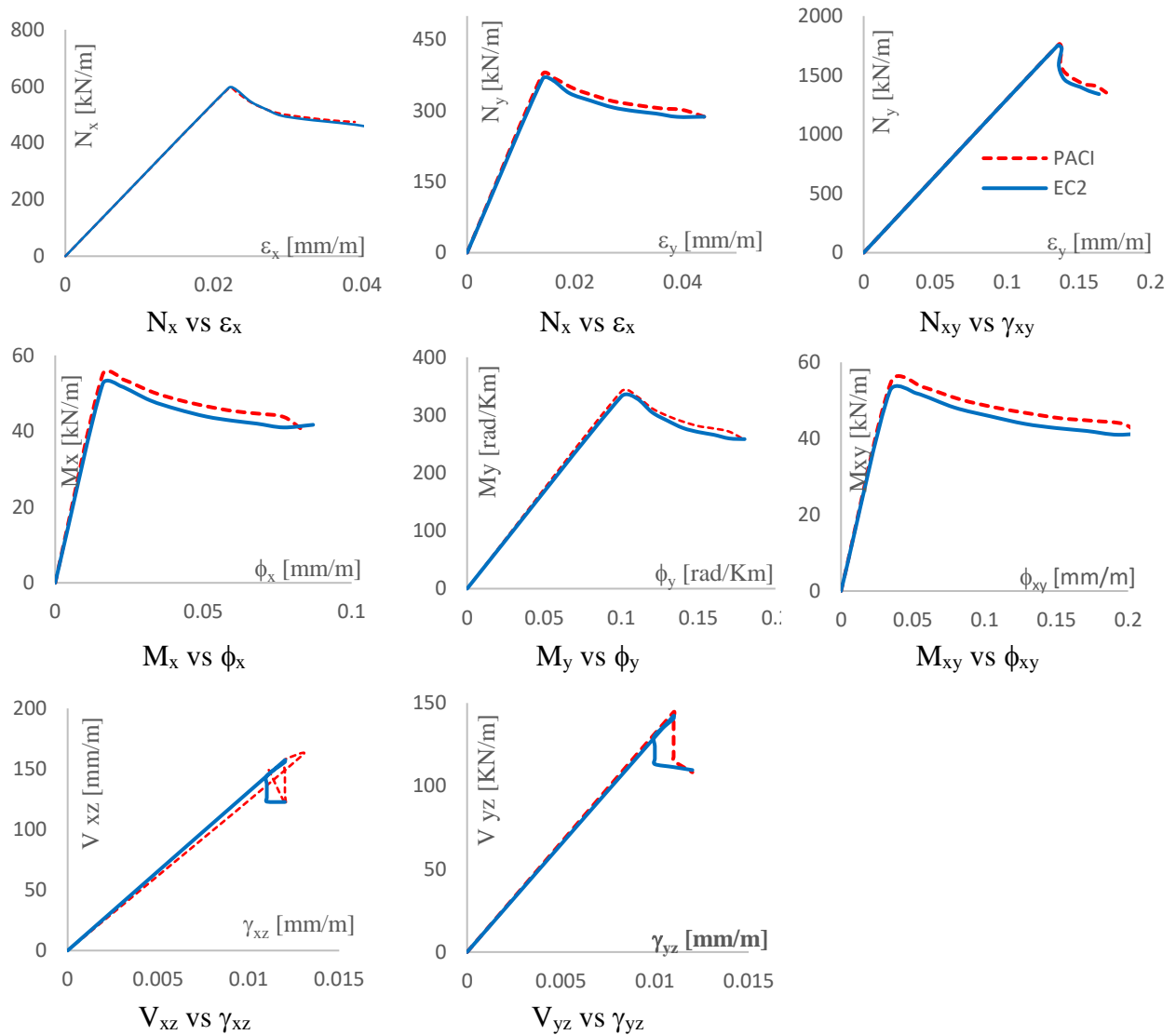


Figure 7.4. PACI and EC2 Numerical Capacity curves for analytical case 1

Figures 7.4 and 7.5 shows the capacity curves for analytical cases 1 and 2, respectively. Each figure shows eight capacity curves, one curve for each internal demand (i.e.  $N_x$ ,  $M_x$ ,  $N_{xy}$ , etc). The blue and continuous lines in figure 7.5 represents the numerical capacity curves after introducing the reinforcement suggested by the EC2 approach; whereas the red and discontinuous line represent the numerical capacity curves after introducing the reinforcement suggested by the PACI approach. As observed in figure 7.4. the differences between the EC2 and the PACI the

numerical curves for the analytical case 1 are negligible because both approaches suggested very similar amount of reinforcement. However, it can be noted how the PACI curve reaches slightly higher capacities than the EC2 curves. On the contrary, there are more differences between the PACI and the EC2 capacities curves in figure 7.5. For example, it is clear how after introducing the reinforcement areas suggested by the PACI approach, the panels do not only reach higher capacities, but also develop higher post-cracking stiffness than the curves after introducing the reinforcement areas suggested by the EC2 approach. These higher capacities and stiffnesses, of course, are consequence of the higher reinforcement areas suggested by the PACI approach.

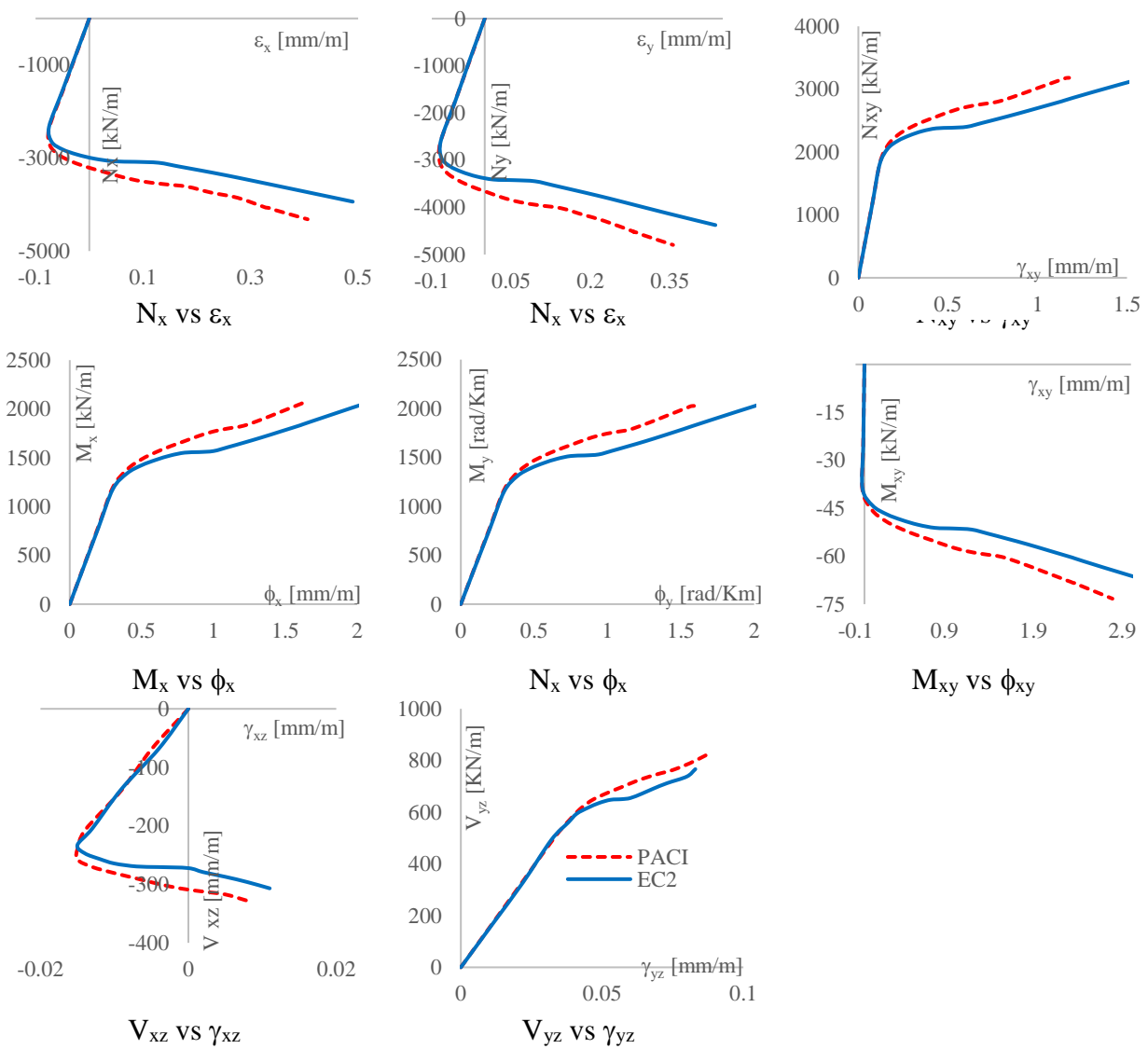


Figure 7.5. PACI and EC2 Numerical Capacity curves for analytical case 2

#### 7.4.2 Comparison between the PACI and the EC2 numerical capacities

Table 7.2 and 7.3 summarize the set of numerical capacities for the analytical case 1 and for the analytical case 2, respectively. The numerical set of capacities of the analytical cases were extracted from the numerical capacity curves in Figures 7.4 and 7.5. Table 7.2 and 7.3 also give the capacity-to-demand ratios (CDRs) for each internal demand and for each design approach. As observed, the CDR reported for both approaches are all greater than 1.0 for the two analytical cases. The average CDRs for the analytical case 1, after applying the PACI and the EC2 approaches were 1.23 and 1.20, respectively. On the other hand, the average CDR for analytical case 2, after introducing the reinforcement areas suggested by the PACI and EC2 approaches were 1.13 and 1.03, respectively.

Table 7.2. Capacity-to Demand-Ratios (CDRs) for the analytical case 1.

Demands ( $R_u$ )		Capacities ( $Rn_{PACI}$ )	$\frac{Rn_{PACI}}{R_u}$	Capacities ( $Rn_{EC2}$ )	CDRs
Nx [kN/m]	482	595	1.23	579	1.20
Ny [kN/m]	307	379	1.23	367	1.21
Nxy [kN/m]	1431	1768	1.24	1741	1.22
Mx[kN-m/m]	44.5	55.0	1.24	54.1	1.21
My [kN-m/m]	276	341	1.24	332	1.22
Mxy [kN-m/m]	44.5	55.0	1.24	54.1	1.21
Vxz [kN/m]	131	162	1.24	159	1.21
Vyz [kN/m]	117	144	1.23	142	1.21

Table 7.3. Capacity-to Demand-Ratios (CDRs) for the analytical case 2.

Demands ( $R_u$ )		Capacities $Rn_{PACI}$	$\frac{Rn_{PACI}}{R_u}$	Capacities $Rn_{EC2}$	CDRs
Nx [kN/m]	-3811	-4398	1.13	-3713	1.03
Ny [kN/m]	-4234	-4886	1.13	-4375	1.03
Nxy [kN/m]	2949	3405	1.13	3050	1.03
Mx[kN-m/m]	1927	2182	1.13	1991	1.03
My [kN-m/m]	1878	2129	1.13	1943	1.03
Mxy [kN-m/m]	-62	-71.9	1.13	65.6	1.03
Vxz [kN/m]	-336	-379	1.13	346	1.03
Vyz [kN/m]	803	911	1.13	831	1.03

The higher CDRs after using the PACI approach was expected since this approach follows a more conservative procedure. As found in the experimental cases in chapter 6, when the panels are subjected to high in-plane shear demands, particularly in analytical case 2, the results of the PACI approach tends to be more conservative than the EC2 approach. Since both design approaches produced CDRs higher than 1.0 in both analytical cases, it can be said that both approaches are safe for industrial applications. However, it must be said that the PACI approach is not as accurate and efficient as the EC2 approach. In spite that the PACI approach suggested 16% and 23% more in-plane reinforcement than that suggested by the EC2 approach for analytical case 1 and 2, respectively, the panels did not reached much higher capacities than the capacities reached by the panels after introducing the areas suggested by the EC2 approach. Nevertheless, these additional percentages of reinforcement areas suggested by the PACI approach, when compared against the EC2 approach seems a reasonable fair price to pay given all the simplification of the former.

## 8. CONCLUSIONS

The conclusions of this research work can be summarized into three parts. These include conclusions regarding the: (1) Eurocode “Sandwich” Model design approach (EC2); (2) proposed ACI-Panel-Based-Design-Approach (PACI), and (3) modeling and calibration of the RC panels.

With respect to the Eurocode (EC2) approach, known as the “sandwich” model, which is based on plasticity principles and mechanics, the following conclusions can be drawn:

- The reinforcement areas calculated using the EC2 approach compare reasonably with the reinforcement areas provided in the RC panels tested by other researchers, which were analyzed in chapter 6. There were eleven of the twenty-one (11/21) cases in which the EC2 design approach suggested less reinforcement than the reinforcement provided during their respective experiments. In these cases, the reduction in the reinforcement suggested by the EC2 approach with respect to the reinforcement provided during the experiments was on average 19%. The reason why the EC2 suggested less reinforcement than provided during the experiments for panels SE1, SE4, SE7, SM1 and SM2, is that all these panels had more reinforcement than the reinforcement they needed. All these panels were symmetrically reinforced having equal amount of reinforcement in their top and bottom layers (or faces). However, they were only subjected to out-of-plate bending moment about one direction, which produced axial tensile stresses in one of their faces and compression stresses in their opposite faces. Thus, the reinforcement that was in the faces where the bending moment produced compression stresses, might have been omitted (or reduced given the case). Another reason that explains why the EC2 suggested less reinforcement than the reinforcement provided during tests for the SE series panels is that, as also mentioned by Blaauwendraad (2010), not all the reinforcement yielded. This means not all the reinforcement provided during the test might have been required.
- There were few cases in which the EC2 “sandwich” model approach suggested more reinforcement than the reinforcement provided during the experiments. These cases were panels PV23, SM3, F2, F3, F4 and SP2. In these cases, the increment in

reinforcement suggested by the EC2 approach, with respect to the reinforcement provided during the experiments, was on average 22%. It must be noted, however, that the F series were the panels for which both design approaches (the EC2 and the PACI) reported the highest suggested over experimental reinforcement ratios. It was explained in chapter 6 that one of the reasons why both approaches resulted in such as high suggested over experimental reinforcement areas was that it is not clear what was the actual reinforcement areas provided during the tests. Leaving out the F series, the average on increment in reinforcement areas suggested by the EC2 approach in comparison against the reinforcement areas provided in the tests, for panels PV23, SM3 and SP2 would be 15%. Not only by the fact that the EC2 approach suggested, on average, roughly  $\mp 20\%$  of the areas of reinforcement what were provided during the experiments for all 21 panels analyze in here, but also by the fact that these suggested reinforcement areas did not drastically change the behavior of the panels — which was confirmed by estimating the numerical capacities of the panels after introducing those suggested reinforcement areas into calibrated numerical models— *it can be concluded that the EC2 approach produced reliable results.*

- ***The EC2 sandwich model demonstrated to be not only safe and reliable, but also to be a potential tool for optimization of reinforcement in RC panels.*** Even in those experimental cases in which the EC2 design approach suggested less (or much less) reinforcement than the reinforcement provided during the experiments, the non-linear models showed that the panels reached, at least, the capacities reported during the experiments. This was confirmed after analyzing the ratios between numerical capacities obtained following the EC2 approach ( $C_{EC2}$ ) and the capacities reported for the experiments ( $C_{exp}$ ). The ( $C_{EC2}$ ) numerical capacities of the panels were estimated after introducing the reinforcement areas suggested by the EC2 approach ( $A_{S\_EC2}$ ) into previously calibrated numerical models. The  $A_{S\_EC2}$  were estimated assuming the experimental reported capacities as the design “demands”, and then applying the EC2 sandwich models approach. The average numerical over experimental capacities ratios ( $C_{EC2}/C_{exp}$ ) for those cases in which the EC2 suggested less reinforcement than what was provided during the experiments was about 1.09. These cases were panels SE1,

SE3, SE4, SE7, PV24, PV25, PV28, SM1, SM2, ML2, ML9 SP3, SP7 and SP9. Similarly, in those cases in which the EC2 suggested more reinforcement than what was provided during the experiments, the estimated numerical capacities, as expected, were never less than the capacities reported from the experiments. The average numerical over experimental capacities ( $C_{EC2}/C_{exp}$ ) ratios for these cases was about 1.05.

- There were also experimental cases in which the EC2 suggested reinforcement areas that resulted in numerical over experimental capacities ratios ( $C_{EC2}/C_{exp}$ ) lower than 1.0. These cases were panels PV23, PV25, ML2 and ML9, with  $C_{EC2}/C_{exp}$  values of 0.98, 0.96, 0.96 and 0.97, respectively. However, there are some aspects that need to be considered before concluding that the EC2 did not produce safe results for these panels. In the case of the PV series, as was explained in chapter 6, these panels were built with a higher strength concrete strips of 100 mm thick around their perimeter, which might have been increased the actual capacity of the panels. The ML series, on the other hand, which were subjected to moderate to high twisting moments, might be considered as those few cases that put in evidence the limitations of the EC2 approach. This was also advised by Blaauwendraad (2010) who also applied the EC2 approach to estimate the reinforcement area for the ML1 and the ML9 panels. However, in real applications, it is very unlikely to find panels only subjected to a single demand, and in this specific case, with only twisting moment demand. In addition, it must be considered too that these CDRs were very close to 1.0; and that the computation of the required reinforcement areas when following the EC2 design approach, did not include any type of strength reduction factors (i.e  $\phi_t$ ,  $\phi_b$ ,  $\phi_v$ , etc). In other words, the underestimation in the amount of reinforcement suggested by the EC2 approach for these ML panel series can be easily corrected by just including some reduction strength design factors as usually done in practice.
- ***The EC2 sandwich model also proved to be safe and efficient for the design of RC panels in industrial facilities.*** The safety and efficiency of the EC2 approach were also tested using analytical data. Analytical data refers in here as the analytical set of

demands extracted from the analysis of an actual industrial facility (for example, AP1000(R), US-APWR(R), etc.). There were two analytical cases each of those associated with a different load combination according to the Design Control Document (DCD) published by Westinghouse (2011). Analytical case 1, associated with load combination 4, according to the DCD document, was characterized by having axial tension forces and relatively low out-of-plane shears, while analytical case 2, associated with load combination 6, was characterized by having high axial compressive forces and high out-of-plane shears. After applying the EC2 approach to estimate the amount of required reinforcement, it was found through non-linear analysis that the set of capacities of the panel were always greater than the set of demands for both analytical cases. This was confirmed by analyzing the Capacity-to-Demand Ratios (CDRs) for these two analytical cases. The CDRs for the analytical case 1, and for the analytical case 2 were 1.20 and 1.03, respectively. The reason why the CDRs were greater in the analytical case 1 than in the analytical 2 is related to the high out-plane shears and the high compressive forces that characterize analytical case 2.

With respect to the exploration of the proposed PACI design approach, which was mainly intended for daily use in consulting firms, the following conclusions can be drawn:

- The areas of reinforcement suggested by the PACI approach were also in agreement with the areas provided for the experimental cases. There were cases in which the PACI approach suggested more reinforcement, and other cases in which it suggested less reinforcement than what was provided during the tests. For example, the PACI approach suggested on average 15% of additional reinforcement than that provided during the experiments for 10 out of the 21 (10/21) panels analyzed in this thesis. Similar to the EC2 approach, there were also cases in which the PACI approach suggested less reinforcement than that provided during the experiments such as in panels SE1, SE3, PV23, PV24, PV28, SM1, SM2, ML2, ML9, SP3 and SP7. On average, the reduction in reinforcement suggested by the PACI approach for these panels was 11%.

- Like the EC2 “sandwich” model approach, ***the PACI approach also demonstrated to be safe and reliable for the design of RC panels***. This was confirmed after analyzing the ratios between numerical capacities obtained following the PACI approach ( $C_{PACI}$ ) and the capacities reported for the experiments ( $C_{exp}$ ). The  $C_{PACI}$  and  $C_{EC2}$  are the numerical capacities of the panels after introducing the areas of reinforcement suggested by the PACI and the EC2 approaches,  $C_{PACI}$  and  $C_{EC2}$ , respectively. There were 9 out of 21 (9/21) panels that reported, on average,  $C_{PACI}/C_{EC2}$  ratios of 1.13. This means that the after introducing the reinforcement by the PACI approach into the calibrated numerical models, the panels reached higher numerical capacities after introducing the reinforcement areas suggested by the EC2 approach. There were also 7 out of 21 (7/21) panels with  $C_{PACI}/C_{EC2}$  ratios equal to 1.0, which means that they reached the same nominal capacities after introducing either the reinforcement areas suggested by the PACI or by the EC2 approaches
  
- On the contrary, there were 7 out of 21 panels that reached lower numerical capacities when introducing the reinforcement areas suggested by the PACI and the EC2 approaches into the calibrated numerical models. These were panels SM2, PV23, PV25, ML2, ML9, SP3 and SP7, whose  $C_{PACI}/C_{EC2}$  ratios were 0.87, 0.98, 0.96, 0.96, 0.97, 0.96 and 0.83, respectively. However, it might not be inferred right away that any of the approaches did not produce safe results. In a case by case scenario it must be recalled that:

  - the axial compressive capacity force of the SM2 panel was not reported in the experiment, and it was approximately estimated by multiplying the bending capacity of the panel by four, according to the proportional loading pattern. This means that the value for the axial experimental capacity in the SM2 panel might had been lower than the value consigned in table 6.14.
  - the PV series panels were built and tested with higher concrete compressive strip of about 100 mm of thickness along its perimeter, which was not considered neither when computing the required reinforcement areas, nor when developing the models developed in shell 2000.

- not only the PACI approach, but also the EC2 approach produced non-conservative results for the ML2 and the ML9 panels, which were subjected to high twisting moment demands. Blaauwendraad (2010), also cautioned about the limitation of the EC2 approach for this type of loading.
  - the out-of-plane shear capacities reported for panels SP7 and SP9 were probably overestimated during experimentation. In addition, it must be considered that all the reinforcement areas suggested by any of the two approaches were estimated without considering any kind of strength reduction factors ( $\phi_b$ ,  $\phi_v$ ,  $\phi_t$ , etc). By including strength reduction factors, which is mandatory in real design applications, the reinforcement areas suggested by the approaches should have been higher, and therefore, the numerical capacities will increase as well.
- Based on the results from the 21 experimental cases analyzed in chapter 6, ***it can be concluded that the PACI approach is more conservative than the EC2 approach***, which is supported by the following two facts:
    - First, it must be highlighted that in 15 out of the 21 panels the PACI approach suggested more than or equal reinforcement than that reinforcement suggested by EC2 approach. On average, the PACI approach suggested 7% additional in-plane reinforcement than the reinforcement provided during the tests. This additional average 7% of additional reinforcement suggested by the PACI approach seems (reasonable) given the simplicity of the former.
    - Second, in 15 out of 21 cases, the panels developed higher numerical capacities when introducing the reinforcement areas into the calibrated numerical models, than when introducing the reinforcement areas suggested by the EC2 approach. On average, the numerical capacities for these 15 panels were 10% greater when introducing the reinforcement areas suggested by the PACI approach (into the calibrated numerical models) than when introducing the reinforcement areas suggested by the EC2 approach.

- However, it must be mentioned that the PACI approach is not as accurate and efficient as the EC2 design approach. This was expected because the EC2 approach uses a more precise design theory based on cracking criteria and principal stresses which are not considered in the PACI approach.
- The tendency of the PACI approach to produce more conservative results than the EC2 approach was maintained when it was used to estimate the reinforcement areas in the two analytical cases in chapter 7. These two cases were represented by two sets of eight internal design demands extracted from the seismic analysis of AP1000® structure. These two sets of demands can be found in the Design Control Document (DCD) authored by Westinghouse (2011). The analytical case 1 was represented by the load combination 4, while the analytical case 2 was represented by the load combination 6. Comb 4 was characterized by having low out-of-plane shear demands with low axial tensile forces, while comb 6 was characterized by having high out-of-plane shear demands and high axial compressive forces. The PACI approach suggested 16% and 28% more in-plane reinforcement than the EC2 approach, for the analytical case 1 and for the analytical case 2, respectively. Again, these percentages of additional reinforcement suggested by the PACI approach regarding the EC2 approach seems reasonable given the simplifications of the former. Similarly, both design approaches, in theory, did not suggest out-of-plane shear reinforcement in any of the two analytical cases. The reason for this is that the wall in the analytical cases was very thick (1200mm), by which the out-of-plane shear capacity that is only provided by the concrete ( $V_c$ ) in both was enough to resist the out-of-plane shear demands. However, a minimum amount of transverse reinforcement, as usual done in actual design applications, was considered.
- One of the reasons why the PACI approach produces more conservative results than the EC2 approach is related to the way in which each approach deals with the in-plane axial forces and the in-plane shear forces. While the EC2 approach considers an interaction between the in-plane axial forces and the in-plane shear forces when estimating the forces that will be resisted by the reinforcement, as shown in equations 13a and d13b, the PACI approach does not. Thus, the PACI approach simply absorbs all the in-plane shear demand

as it is, disregarding any possible reduction in the forces that will be resisted by the reinforcement in the outer layers. This goes in agreement with the fact that in the PACI approach the outer layers are considered always cracked, and therefore, their contribution for the in-plane and/or the out-plane shear capacity must be neglected.

- The PACI design approach can be considered a mix of a basic sandwich model approach combined with the very basic and familiar RC design concepts (such as the balanced force, and the Whitney stress concrete block concepts) given in the ACI codes. In general, the PACI approach produced more conservative results than the EC2 approach. However, the PACI approach is simpler to implement at an industrial level since it follows the very familiar concepts for design of RC members suggested by the ACI 349 and ACI 318.2-19.

With respect to the modeling and non-linear analysis of the RC panels analyzed in this research, the following conclusions can be addressed.

- The methodology for the modeling and calibration of the of the RC panels tests in chapter 6 was the following. The Shell-2000 and the Membrane-2000 were first used to simulate the experimental response of the panels. This two software were used first because they allow the development of non-linear numerical models much faster and easier than in Abaqus. If the numerical capacity curves (i.e  $M_x$  vs  $\phi_x$ ,  $N_x$  vs  $\epsilon_x$  etc., depending on the load at which the panels were subjected) reproduced in Shell-2000 were not accurate enough with the experimental capacity curves, then 2D numerical models in Abaqus were developed. Finally, if not even the 2D numerical models in Abaqus were enough to capture the experimental response of the panels, then 3D numerical models in Abaqus were developed.
- The panels for which the Shell-2000 software was enough to reproduce accurate numerical responses were the SE, the F, and the ML series panels. Panels for which it was possible to capture or reproduce with good accuracy their experimental response with Membrane-2000 were the PV series. Panels for which it was necessary to develop 2D numerical models in Abaqus were the SM and the PV series. This means that the PV series was

simulated using both Abaqus and Membrane-2000. The reason for this is that the 2D numerical models in Abaqus for the PV series were developed before realizing that Membrane-2000 was able to reproduce accurate numerical responses too. It was decided then to show the comparison between the numerical response obtained from Abaqus and from Membrane-2000 for these PV series. Finally, panels for which it was necessary to develop 3D numerical models in Abaqus were only the SP series panels.

- The main feature of the 2D Abaqus models was that the reinforcement and concrete were simulated using a Layer Composite Shell (LCS) finite element identified as S4R. The S4R is a 4-node doubly curved general-purpose shell with reduced integration and hourglass control. On the other hand, the main feature of the 3D models is that the concrete was simulated using the solid continuum 8-node linear (or first order) brick with reduced integration and hourglass control C3D8R, while the reinforcement was the B31 2-node linear beam finite element. In the LCS elements, full compatibility deformation is by default forced between the concrete and the steel reinforcement, whereas in the 3D models the full deformation compatibility is enforced by assigning the well-known “embedded” region constraint.
- It was not possible to reproduce a consistent response for those SE panels subjected to in-bending moment and in-plane shear in Abaqus. Judging by the accuracy of the numerical curves reproduced in Shell-2000 for these SE panels, it might be concluded that the Modified Field Compression Theory (MCFT) and the smeared rotating cracked model to simulate the response of cracked concrete, assumed in this software, are appropriate to simulate the response of the SE series panels. On the other hand, for panels SM2 and SM3 which were subjected to axial forces plus bending moment ( $N_x$ ,  $N_y$  and  $M_x$ ); and biaxial flexural moments ( $M_x$  and  $M_y$ ), respectively, Shell -2000 was not able to produce any response beyond the elastic regime. For this reason, 2D numerical models were developed for the SM series panels. It is fair to mention that the response of the SM1 panel, which was only subjected to uniaxial bending moment ( $M_x$ ) was well captured either in Shell-2000 or in Abaqus. However, the numerical curve developed in Shell-2000 for this panel was omitted for the sake of brevity.

- ***One of the most important aspects during the modeling of the SM series in the 2D models in Abaqus, is that it was necessary to modify the steel material properties.*** More specifically, the yielding stress that was reported in the experiments for the steel reinforcement had to be reduced following the Maekawa et al (2003) recommendations. This was the only way to capture with an acceptable accuracy the yielding of the SM series panels. It is important to recall the Maekawa et al (2003) recommended to reduce the yielding stress of the reinforcement for modeling purposes, because they found that the response of an “embedded” bar in concrete differs to the response of a “non-embedded” bar. The Concrete Damage Plasticity (CDP) and the Brittle Failure Cracking (BFC) concrete models were used to develop the SM2 and the SM3 numerical models in Abaqus. The properties of the steel reinforcement were also slightly modified for the SE series. Like for the SM panels series, the properties of the steel reinforcement were also slightly modified of the SE panels. Again, the behavior of the SE panels series was also governed by yielding of the reinforcement in tension. Contrary to other panels whose behavior was not controlled by yielding of reinforcement, such as the PV series, the SP series, and the ML series, there was no need to modify the properties of the steel reinforcement by reducing its yielding stress. ***Therefore, it can be concluded that for the modeling of panels with a failure mode different from the yielding of the reinforcement in tension, it might be not necessary to modify the properties of the steel reinforcement, and more specifically, reduce its yielding stress.***
- The 2D numerical models with LCS did not reproduce an accurate numerical response for the SP series panels. One of the reasons that explains this lack of accuracy is that the SR4 finite element is not recommended when transverse deformations are important, as probably was the case for the SP panels. For this reason, it was necessary to develop 3D numerical models instead of the computationally cheaper LCS-2D models for these panels. Another option, which was not explored in here, would have been to use the thick-only shell S8R, instead of the general shell purpose SR4. In the S8R shell elements, in contrast to the SR4 elements, the transverse shear deformations are not neglected during the analysis. It must be recalled that the SP series was subjected to large transverse shears which might have been induced large transverse shear deformation to the panels. However,

since the S8R is more computationally expensive, because they are second-order elements, it was decided to developed 3D models with the very efficient C3D8R solid elements.

## 9. LIMITATIONS

Although both design approaches, the PACI and the EC2 approaches, were validated using experimental and analytical data as demonstrated in chapters 6 and 7, respectively, it is prudent to define the limitations for their applicability. There are two limitations for the application of both approaches.

The first limitation is set by considering the ranges of reinforcement ratios and concrete compressive strength utilized in chapter 6. As explained in chapters 5 and 6, twenty-one panel tests were analyzed in this research. These 21 tests were used to validate the results of both design approaches. Thus, it is important to specify the ranges (minimum and maximum values) of the combined reinforcement ratios ( $\rho_o$ ) as well as the maximum compressive concrete strength ( $f_c$ ) of those tests. The combined reinforcement ratio ( $\rho_o$ ) was taken as the summation of the reinforcement ratios running along one of the coordinated directions (i.e. in the x-direction) plus the reinforcement ratio running along the perpendicular direction (i.e. in the y-direction). Also, this combined reinforcement ratio refers to the amount of reinforcement in only one of the two faces of the panels, top or bottom. Specifically, the minimum combined reinforcement ratio ( $\rho_o$ ) per face (or layer), represented by the SM series panels was 0.4%, while the maximum combined reinforcement ratio per layer, represented by the SP panels was 2.4%. Thus, the minimum and maximum reinforcement combined ratio for which the results of both design approaches can be applied are 0.4% and 2.4%, respectively. In addition, most of the specimens, excepting the F series, had a minimum out-of-plane reinforcement ratio of 0.08% (or 8.0cm<sup>2</sup>/m<sup>2</sup>). Similarly, the range of applicability regarding the ultimate compressive strength of the concrete oscillates between the minimum of 20.0 MPa set by the PV series, and 60.0 MPa set by the SM series. Beyond these limits, it is not possible to say if either of the design approaches will produce reliable results, and the approaches must be used with caution, which is the responsibility of the designer.

The second limitation is related to the estimation of the design demands, which are not in the scope of this thesis. None of the design approaches advise how to estimate the design demands for their respective application. In other words, neither the EC2 or the PACI design approaches provide guidelines to conduct the structural analysis (which must include gravitational, seismic, transient loads among others) with the aim of estimating the design demands. The estimation of

the design demands is responsibility of the consultant, which must follow the current recommendations for the modeling and analysis of walled-type structures such as those in industrial facilities. Recommendations for the analysis and modeling of safety related walled-type nuclear facilities can be found in the ASCE 4. A specific application of these recommendations is presented in AP1000 Design Control Document (AP-1000 DCD) published by Westinghouse. This DCD shows an example of how practicing engineers use the recommendations to calculate design demands. Similar DCD examples can be found in the literature illustrating how practicing engineers generally implement ASCE 4 recommendations for calculating design demands.

The ASCE 4, in chapter 3, for example provides guidelines for the selection of the finite element and the mesh size for the development of the numerical models for the analysis. In chapter 4, it provides a very detailed description about the available analysis methods suitable for nuclear facilities such as the Linear Response-Spectrum Analysis (LRSA), the Linear Response-History Analysis (LRHA), and the Non-Linear Static Analysis (NLSA, also known as "pushover") among others. In the same chapter 4, the ASCE 4 describes not only the type of loads for which the facilities must be designed, but also advises how to combine those loads to obtain the design demands. The well-known 100-40-40 rule, which is explained in chapter 4 as well, indicates how to estimate the seismic demands over the walls, considering that the design earthquakes are represented by a set of three orthonormal accelerations components as commonly accepted. Finally, chapter 5 of the ASCE 4 gives recommendations to include, if needed, soil-structure interaction in the analysis.

AP1000 DCD also includes generic recommendations for conduct analysis of walled-type structures. The AP1000 DCD, which was the source from where the analytical design demands were extracted to implement both design approaches in chapter 7 of this thesis, also provides very detailed guidelines about what type loads were included in the analysis, and how they were combined for design purposes. Among the most relevant analysis guidelines provided by the DCD are: the selection of the appropriate finite element, the definition of the appropriate stiffness in terms of gross or transformed areas, and the definition of damping ratios. Other more specific analysis guidelines about how to estimate the hydrodynamic and thermal design demands can be also found in the AP1000 DCD.

There is also an important limitation regarding the estimation of the design demands, which can be also classified as a topic of future research. This limitation is related to the definition of the approximate section cut length, over the which the design demands are averaged in the numerical models developed with shell elements. This is an important limitation because, as pointed out by Coronado et al 2000, when using the Element-by-Element design Technique (ELE) -which is the most consistent and accurate method when dealing with shell elements- the ACI 349 does not give advice about what should be an appropriate section cut-length to account for the spread of plasticity in the in-plane direction of the wall panel. Considering figure 1.1, which shows the stress variation of the structure in analysis, it is clear that the stress is not constant over the walls. In some parts, the stresses are higher than in others, and furthermore, the magnitude of these stresses can change rapidly along any direction. Therefore, if the designer considers to follow the Element-by-Element level Technique (ELE), which consists in design portions (or sections) of the wall, the immediate question that rises is, what should be the length of the section cut?

The definition of an appropriate section cut length is, in fact, an important topic among both researchers and consultants nowadays. There is plenty of room for research in this regard. As a suggestion -but subjected to further investigation- this section cut length might be initially taken as one time the thickness of the panel ( $1.0t_w$ ) when the gradient of the out-of-plane moments, in this case the out-of-plane shears is higher than 60% of the estimated shear strength, and as two times the thickness of the wall ( $2.0 t_w$ ) when this gradient of the bending moments is lower than 60% of the estimated shear strength. Moreover, contrary to what is done in the practice today, the author of this thesis believes that instead of cutting segments of the wall in one single direction, the section (or portion) of the wall to be designed, when following the ELE technique, must be cut in two orthogonal directions. Thus, a rectangular wall-panel, defined by the length of the section cut length ( $1.0 t_w$  or  $2.0 t_w$ ) will be formed. This wall-panel, or simply called panel in this thesis, will allow to account for the variation of the stresses in the two perpendicular directions of analysis. Again, the estimation of the design demands (8 in total as commonly accepted) for shell is exclusively responsibility of the consultant, and both the PACI and the EC2 design approaches, are only limited to suggest amount the in-plane and out-of-plane reinforcement ratios, after those design demands have been specified.

## 10. FUTURE RESEARCH

It is desirable to test Reinforced Concrete (RC) specimen panels designed accordingly to both approaches analyzed in here: the PACI and the EC2 approaches. The panels will be subjected to proportional loading considering two or more types of loads, as explained in chapter 6. These tests will help to corroborate the safety of both design approaches. Taking advantage of the equipment capacity and experience of the personnel in the Bowen Lab, it is attainable to build a universal testing machine for the testing of these RC panels (or shells). There are other universities such the University Houston (TX) and the University of Toronto (Canada), which have gained important knowledge and experience in this regard. Purdue University might use all this experience and knowledge to build its own universal testing machine. In addition, it might be said that there are still relative few experiments of RC panels subjected to proportional loading, which means that there is still room for experimentation.

From a design point of view, it will be necessary to investigate if the PACI and the EC2 sandwich model approach are also suitable for safety-related facilities such as nuclear power plants. It must be highlighted that, in this thesis, the PACI and the EC2 design approaches produced satisfactory results only for ultimate limit states, and not for service limit states such as cracking or deflections control. The cracking limit state in safety-related facilities, which controls the releasing of environmental toxins into the environment, is usually more difficult to satisfy than the ultimate state.

Finally, from a modeling perspective, it will be worthwhile to develop 2D and/or 3D numerical models in Abaqus for those panels in which it was only necessary to develop numerical models in Shell-2000. This will allow one to measure the accuracy of the Shell-2000 software regarding the more accurate finite element models in Abaqus. As mentioned before, Shell-2000 is a very friendly software that can be easily implemented at the industrial level. Similarly, it was found that either the 2D or the 3D numerical models in Abaqus failed in capturing the experimental responses of the panels after cracking, because these models did not include any slippage model between steel reinforcement and concrete. Therefore, it will be valuable to include a slip model between the concrete and reinforcement, instead of simply assuming fully bonded compatibility deformation between them.

## REFERENCES

- Abbas, R. M., & Awazli, A. G. (2017). Behavior of Reinforced Concrete Columns Subjected to Axial Load and Cyclic Lateral Load. *Journal of Engineering*, 23(2), 21–40.
- ACI Committee 318. (2019). *Building Code Requirements for structural concrete: (ACI 318-19); and commentary (ACI 318R-19)*. Farmington Hills, MI: American Concrete Institute.
- ACI Committee 318.2. (2019). *Building code Requirements for concrete thin shells (ACI 318.2-19); and Commentary (ACI 318.2R-19)*. Farmington Hills, MI: American Concrete Institute.
- ACI Committee 349. (2013). *Code requirements for nuclear Safety-related concrete structures (ACI 349-13); and Commentary (ACI 349-13)*. Farmington Hills, MI: American Concrete Institute.
- Adebar, P., & Collins, M. P. (1994). Shear Design of Concrete Offshore Structures. *Structural Journal*, 91(3), 324–335.
- Adebar, P. E. (1989). *Shear design of concrete offshore structures*. University of Toronto Dept. of Civil Engineering.
- Ahmed, A. (2014). Modeling of a reinforced concrete beam subjected to impact vibration using ABAQUS. *Journal of Civil and Structural Engineering*, 4, 227–236. <https://doi.org/10.6088/ijcser.201304010023>
- Aschheim, M., Hernández-Montes, E., & Gil-Martín, L. M. (2008). Design of Optimally Reinforced RC Beam, Column, and Wall Sections. *Journal of Structural Engineering*, 134(2), 231–239.
- Basu, P. K., Labbé, P. B., & Naus, D. J. (2013). Nuclear power plant concrete structures. *Transactions, SMiRT-22*. IASMiRT, San Fransisco, CA.
- Belarbi, A., & Hsu, T. T. C. (1994). Constitutive Laws of Concrete in Tension and Reinforcing Bars Stiffened By Concrete. *Structural Journal*, 91(4), 465–474.
- Belarbi, A., & Hsu, T. T. C. (1995). Constitutive Laws of Softened Concrete in Biaxial Tension Compression. *Structural Journal*, 92(5), 562–573.

Bentz, E. C. (2000). “*Sectional Analysis of Reinforced Concrete Members*”. University of Toronto, Department of Civil Engineering.

Bentz, E. C. (2005). Explaining the Riddle of Tension Stiffening Models for Shear Panel Experiments. *Journal of Structural Engineering*, 131(9), 1422–1425.

Bhardwaj, S., & Varma, A. (2017). *Design Guide 32: Design of Modular Steel-Plate Composite Walls for Safety-Related Nuclear Facilities* (First). American Institute of Steel Construction (AISC).

Blaauwendraad, J. (2010). *Plates and FEM* (Vol. 171). Springer Netherlands.

Borst, R. de, Remmers, J. J. C., Needleman, A., & Abellan, M.-A. (2004). Discrete vs smeared crack models for concrete fracture: Bridging the gap. *International Journal for Numerical and Analytical Methods in Geomechanics*, 28(7-8), 583–607.

British Standards Institution. (2004). *Eurocode 2: Design of concrete structures*. British Standards Institution.

Charalambidi, B. G., Rousakis, T. C., & Karabinis, A. I. (n.d.). *Finite element modeling of reinforced concrete columns seismically strengthened through jpaacrkteiatilnFgRP jacketing*. 11.

Chen, W. F. (1993). Concrete plasticity: Macro- and microapproaches. *International Journal of Mechanical Sciences*, 35(12), 1097–1109. [https://doi.org/10.1016/0020-7403\(93\)90058-3](https://doi.org/10.1016/0020-7403(93)90058-3)

Chen, W. F., & Han, D. J. (2007). *Plasticity for structural engineers*. Fort Lauderdale, FL: J. Ross Publishing.

Collins, M. P. (Michael P., Kirschner, U., & Engineering, U. of T. D. of C. (1986). *Investigating the Behaviour of Reinforced Concrete Shell Elements*. University of Toronto, Department of Civil Engineering.

Collins, M. P., & Mitchell, D. (1987). *Prestressed concrete basics* (1st ed). Canadian Prestressed Concrete Institute.

Comit E Euro-international Du B Eton. (1993). *CEB-FIP (1990): Fib Model Code for Concrete Structures*. T. Telford.

- Comit E Euro-international Du B Eton. (2010). *CEB-FIP (2010) Fib Model Code for Concrete Structures*. fib Fédération internationale du béton.
- Coronado C., Malushte S.R., Munshi J., & Verma N. (2009). A Rational Seismic Design Approach for Reinforced Concrete Walls for Nuclear Power Plants. *SMiRT 20*. 20th International Conference on Structural Mechanics in Reactor Technology (SMiRT 20), Espoo, Finland.
- Dassault Systemes Simulia Corp., A. (2013). *Abaqus User's Manual*.
- Demir, A., Öztürk, H., & Dok, G. (2016). 3D Numerical Modeling of RC Deep Beam Behavior by Nonlinear Finite Element Analysis. *Disaster Science and Engineering*, 2, 13–18.
- Design Guide 32: Design of Modular Steel-Plate Composite Walls for Safety-Related Nuclear Facilities / Request PDF*. (n.d.). ResearchGate. Retrieved July 2, 2020.
- Earij, A., Alfano, G., Cashell, K., & Zhou, X. (2017). Nonlinear three-dimensional finite-element modelling of reinforced-concrete beams: Computational challenges and experimental validation. *Engineering Failure Analysis*, 82, 92–115.
- Elenas, A., Vasiliadis, L., Pouliou, E., & Emmanouilidou, N. (2006). Influence of tension stiffening effect on design and behaviour of reinforced concrete structures. *Measuring, Monitoring and Modeling Concrete Properties*, 215–220.
- Emtiaz, M. (2017). Numerical Analysis of a Reinforced Concrete Slab-Column Connection Subjected to Lateral & Vertical Loading. *Hong Kong*, 6.
- Farrar, C. R., Reed, J. W., & Salmon, M. W. (1993). Failure Modes of Low-Rise Shear Walls. *Journal of Energy Engineering*, 119(2), 119–138.
- Gebreyohannes, A. S., Clifton, G. C., & Butterworth, J. W. (2012). Finite element modeling of non-ductile RC walls. *15 WCEE*. 15th World Conference on Earthquake Engineering 2012, Lisboa, Portugal.
- Gupta, A. K. (1986). Combined Membrane and Flexural Reinforcement in Plates and Shells. *Journal of Structural Engineering*, 112(3), 550–557.
- Hamada, M., & Kuno, M. (Eds.). (2017). *Earthquake Engineering for Nuclear Facilities*. Springer Singapore.

- Hillerborg, A., Modéer, M., & Petersson, P.-E. (1976). Analysis of crack formation and crack growth in concrete by means of fracture mechanics and finite elements. *Cement and Concrete Research*, 6(6), 773–781.
- Hognestad, E. (n.d.). A study of Combined Bending and Axial Load in Reinforced Concrete Members, University of Illinois Eng. *Exper. Station Bull. Ser.*, 399.
- IAEA. (2011). *Non-linear response to a type of seismic input motion*. International Atomic Energy Agency.
- Jendele, L., Cervenka, J., Saouma, V., & Pukl, R. (2001). *On the choice between discrete or smeared approach in practical structural FE analyses of concrete structures*.
- Kent, D. C., & Park, R. (1971). FLEXURAL MEMBERS WITH CONFINED CONCRETE. *Journal of the Structural Division*.
- Kezmane, A., Boukais, S., & Hamizi, M. (2016). Numerical simulation of squat reinforced concrete wall strengthened by FRP composite material. *Frontiers of Structural and Civil Engineering*, 10(4), 445–455.
- Khani, J., Bozorg, M., & Zahrai, S. M. (2018). Investigating Seismic Behavior of Reinforced Concrete Columns with SFRP Using Finite Element Method. *American Journal of Engineering and Applied Sciences*.
- Kirschner, U. (1986). *Investigating the Behaviour of Reinforced Concrete Shell Elements*. Thesis (Ph.D.)--University of Toronto.
- Kupfer, H., & Bulicek, H. (1991). Comparison of Fixed and Rotating Crack Models in Shear Design of Slender Concrete Beams. *Progress in Structural Engineering*, 129–138.
- Labbé, P., Pegon, P., Molina, J., Gallois, C., & Chauvel, D. (2016). The SAFE Experimental Research on the Frequency Dependence of Shear Wall Seismic Design Margins. *Journal of Earthquake Engineering*, 20(1), 101–128.
- Lee, J., & Fenves, G. L. (1998). Plastic-Damage Model for Cyclic Loading of Concrete Structures. *Journal of Engineering Mechanics*, 124(8), 892–900.

- Li, J., Wang, Y., Lu, Z., & Xia, B. (2018). Shaking table test and numerical simulation of a superimposed reinforced concrete shear wall structure. *The Structural Design of Tall and Special Buildings*, 27(2), e1412.
- Lourenço, P. B., & Figueiras, J. A. (1993). Automatic Design of Reinforcement in concrete plates and shells. *Engineering Computations*.
- Lourenço Paulo B., & Figueiras Joaquim A. (1995). Solution for the Design of Reinforced Concrete Plates and Shells. *Journal of Structural Engineering*, 121(5), 815–823.
- Lublinder, J., Oliver, J., Oller, S., & Oñate, E. (1989). A plastic-damage model for concrete. *Int. J. Solids and Structures*.
- Maekawa, K., Pimanmas, A., & Okamura, H. (2003). *Nonlinear Mechanics of Reinforced Concrete*. Spon Press.
- Maekawa, K., Vecchio, F., Bayrak, O., Bentz, E., Blaauwendraad, J., Cervenka, J., Cervenka, V., Ishida, T., Jirasek, M., Kaufmann, W., Kollegger, J., Kuchma, D., Lee, H. J., Mancini, G., Monti, G., Ozbolt, J., Preisinger, C., Spacone, E., & Tjhin, T. (2008). *Practitioners' Guide to Finite Element Modelling of Reinforced Concrete Structures: State-of-art Report* (fib. The International Federation for Structural Concrete & S. Foster, Eds.). fib. The International Federation for Structural Concrete.
- Mander, J. B., Priestley, M. J. N., & Park, R. (1988). Theoretical Stress-Strain Model for Confined Concrete. *Journal of Structural Engineering*, 114(8), 1804–1826.
- Mansour, M., & Hsu, T. T. C. (2005). Behavior of Reinforced Concrete Elements under Cyclic Shear. II: Theoretical Model. *Journal of Structural Engineering*, 131(1), 54–65.
- Marti, P. (1991). Dimensioning and detailing. *IABSE Colloquim Report*, 62, 441–443.
- Marti, P., Leesti, P., & Khalifa, W. U. (1987). Torsion Tests on Reinforced Concrete Slab Elements. *Journal of Structural Engineering*, 113(5), 994–1010.
- Menin, R. C. G., Trautwein, L. M., & Bittencourt, T. N. (2009a). Modelos de fissuração distribuída em vigas de concreto armado pelo método dos elementos finitos. *Revista IBRACON de Estruturas e Materiais*, 2(2), 166–200.

- Menin, R. C. G., Trautwein, L. M., & Bittencourt, T. N. (2009b). Smearred crack models for reinforced concrete beams by finite element method. *Revista IBRACON de Estruturas e Materiais*, 2(2), 166–200.
- Ohmori, N., Takahashi, T., Haruji, T., Inoue, N., Kurihara, K., & Watanabe, S. (1989). Experimental Studies on Nonlinear Behaviours of Reinforced Concrete Panels Subjected to Cyclic In-plane Shear. *Journal of Structural and Construction Engineering (Transactions of AIJ)*, 403, 105–118.
- Ottosen, N. S. (1977). A Failure Criterion for Concrete. *American Society of Civil Engineers. Engineering Mechanics Division. Journal*, 103(4), 527–535.
- Polak, M. A., & Vecchio, F. J. (1994). Reinforced Concrete Shell Elements Subjected to Bending and Membrane Loads. *Structural Journal*, 91(3), 261–268.
- Popovics, S. (1973). A numerical approach to the complete stress-strain curve of concrete. *Cement and Concrete Research*, 3(5), 583–599.
- Rahimian, A. (2019). Biaxial Principal Stress Interaction Diagram for Reinforced Concrete Membrane Elements. *Structural Journal*, 116(3), 119–133.
- Rašeta, A., Čurčin, A. S., Džolev, I., Šešlija, M., & Nadaški, D. (n.d.). *Nonlinear static analysis of RC wall using ABAQUS program*. 9.
- Reitenbach, G., & Hylko, J. (2015). Seismic Hazard Resiliency at US Nuclear Power Plants. *Power*, 159(4), 86–93.
- Ren, W., Sneed, L. H., Yang, Y., & He, R. (2015). Numerical Simulation of Prestressed Precast Concrete Bridge Deck Panels Using Damage Plasticity Model. *International Journal of Concrete Structures and Materials*, 9(1), 45–54.
- Rots, J. G., & Blaauwendraad, J. (1989). Crack Models for Concrete, Discrete or Smearred? Fixed, Multi-Directional or Rotating? *HERON*, 34 (1), 1989.
- Salem, H., & Maekawa, K. (1999). Spatially averaged tensile mechanics for cracked concrete and reinforcement under highly inelastic range. *Doboku Gakkai Ronbunshu*, 1999(613), 277–293. [https://doi.org/10.2208/jscej.1999.613\\_277](https://doi.org/10.2208/jscej.1999.613_277)

- Sener, K. C., Varma, A. H., Booth, P. N., & Fujimoto, R. (2015). Seismic behavior of a containment internal structure consisting of composite SC walls. *Nuclear Engineering and Design*, 295, 804–816. <https://doi.org/10.1016/j.nucengdes.2015.07.038>
- Sengupta, P., & Li, B. (2016). Seismic Fragility Assessment of Lightly Reinforced Concrete Structural Walls. *Journal of Earthquake Engineering*. <https://www.tandfonline.com/doi/abs/10.1080/13632469.2015.1104755>
- Sima, H., Chou, L., & Okamura, H. (1987). Micro and macro models for bond behavior in reinforced concrete. *Journal of the Faculty of Engineering, The University of Tokyo (B)*, 39(2).
- Sun, E. (2006). *Shear Locking and Hourglassing in MSC Nastran, ABAQUS, and ANSYS*.
- Uchida, Y., Rokugo, K., & Koyanagi, W. (1991). Determination of tension softening diagrams of concrete by means of bending tests. *Doboku Gakkai Ronbunshu*, 1991(426), 203–212.
- Varma, A. H., Malushte, S. R., Sener, K. C., & Lai, Z. (2014). Steel-plate composite (SC) walls for safety related nuclear facilities: Design for in-plane forces and out-of-plane moments. *Nuclear Engineering and Design*, 269, 240–249.
- Vecchio, F. (1982). *The response of reinforced concrete to in-plane shear and normal stresses*. Department of Civil Engineering, University of Toronto.
- Vecchio, F. J., & Collins, M. P. (1986). The modified compression-field theory for reinforced concrete elements subjected to shear. *ACI J.*, 83(2), 219–231.
- Westinghouse. (2011). *AP1000 Design Control Document*. Westinghouse Electric Company. <https://www.nrc.gov/docs/ML1117/ML11171A303.pdf>
- Wittmann, F. H., Rokugo, K., Brühwiler, E., Mihashi, H., & Simonin, P. (1988). Fracture energy and strain softening of concrete as determined by means of compact tension specimens. *Materials and Structures*, 21(1), 21–32.
- Xu, S.-Y., & Zhang, J. (2008, October 1). Hysteretic models for reinforced concrete columns considering axial-shear-flexural interaction. *14th World Conference on Earthquake Engineering*. 14 WCEE, Beijing, China.

Yazdani, H., Khatibinia, M., Gharehbaghi, S., & Hatami, K. (2017). Probabilistic Performance-Based Optimum Seismic Design of RC Structures Considering Soil–Structure Interaction Effects. *ASCE-ASME Journal of Risk and Uncertainty in Engineering Systems, Part A: Civil Engineering*, 3(2), G4016004.

Zeng, X. (2017). Finite Element Analysis of Square RC Columns Confined by Different Configurations of Transverse Reinforcement. *The Open Civil Engineering Journal*, 11(1).

# APPENDIX A. SPREADSHEET IN MATHCAD

## A.1 Eurocode Sandwich model approach (EC2) EXAMPLE

### Design Demands

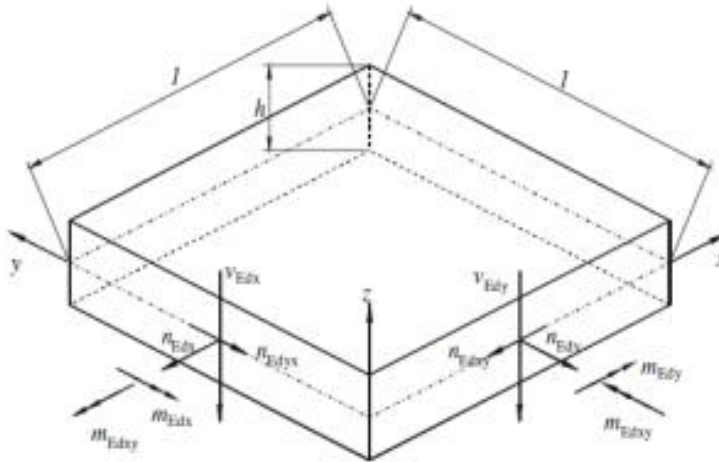


Figure 1. In-plane and Out-of-plane Internal Forces

In-plane axial force along the x-direction	$n_{Edx} := -3811 \frac{kN}{m}$
In-plane axial along the y-direction	$n_{Edy} := -4234 \frac{kN}{m}$
In-plane shear force along the y-direction	$v_{Edxy} := 2949 \frac{kN}{m}$
Out-of-plate bending moment acting about the y-axis, producing axial stresses along the x-direction	$m_{Edx} := 1927 kN \cdot \frac{m}{m}$
Out-of-plate bending moment acting about the x-axis, producing axial stresses along the y-direction	$m_{Edy} := 1878 kN \cdot \frac{m}{m}$
Out-of-plate twisting moment	$m_{Edxy} := -62 \frac{kN \cdot m}{m}$
Out-of-plate transverse shear acting perpendicular to the x-axis and along the z-direction	$v_{Edx} := -336 \frac{kN}{m}$
Out-of-plate transverse shear acting perpendicular to the x-axis and along the z-direction	$v_{Edy} := 803 \frac{kN}{m}$

## Material Properties

### Concrete

Characteristic Compressive Cylinder Strength at 28 days

$$f_{ck} = 40 \text{ MPa}$$

Partial Factor for Concrete (Recommended)

$$\gamma_c = 1.0$$

Design Value of Concrete Compressive Strength

$$f_{cd} = \alpha_{cc} \cdot \frac{f_{ck}}{\gamma_c} = 42 \cdot \text{MPa}$$

Mean Compressive Strength at 28 days

$$f_{cm} = f_{ck} + 8 \text{ MPa} = 50 \cdot \text{MPa}$$

Mean Tensile Concrete Strength

$$f_{ctm} = 0.3 \text{ MPa} \cdot \left( \frac{f_{ck}}{\text{MPa}} \right)^{0.667} = 3.6 \cdot \text{MPa}$$

Design Value of Tensile Strength

$$f_{ctd} = \alpha_{ct} \cdot \frac{0.7 \cdot f_{ctm}}{\gamma_c} = 2.5 \cdot \text{MPa}$$

### Reinforcement

Design Yielding Stress

$$f_y = 500 \text{ MPa}$$

Partial Factor for Concrete (Recommended)

$$\gamma_s = 1.0$$

Yielding Stress

$$f_{yd} = \frac{f_y}{\gamma_s} = 500 \cdot \text{MPa}$$

### Step 3. Definition of the Sandwich Model -Layers thicknesses-

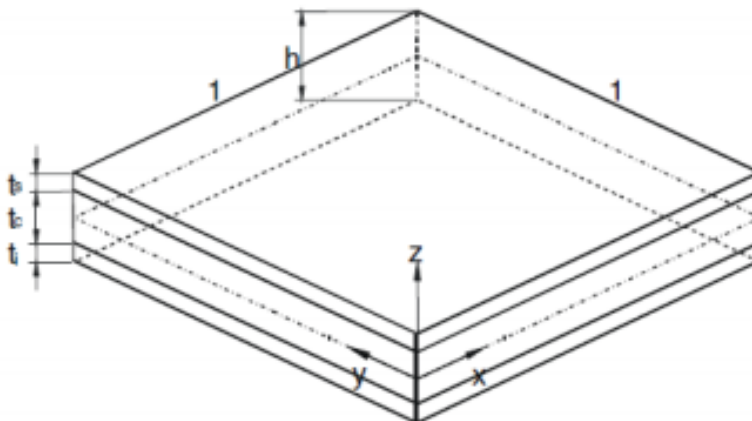


Figure 2. Thickness Layers Distribution

Thickness of the panel	$t_w \approx 1200\text{mm}$
Thickness of the top Layer	$t_s \approx 0.125 \cdot t_w = 150\text{mm}$
Thickness of the bottom Layer	$t_i \approx 0.125 \cdot t_w = 150\text{mm}$
Thickness of the Inner Layer	$t_c \approx t_w - t_s - t_i = 900\text{mm}$
Centroid to the top reinforcement curtain	$z_s \approx 0.5(t_w - t_s) = 525\text{mm}$
Centroid to the bottom reinforcement curtain	$z_i \approx 0.5(t_w - t_i) = 525\text{mm}$
Lever Arm Distance	$d_z \approx z_s + z_i = 1050\text{mm}$
Effective Depth	$d_{sz} \approx d_z + \frac{t_i}{2} = 1125\text{mm}$
Cover along x-dir	$\text{cover} \approx t_w - d_{sz} = 75\text{mm}$
Cover along y-dir	$\text{cover}_y \approx t_w - d_z - \frac{t_s}{2} = 75\text{mm}$

### DESIGN / VERIFICATION OF THE INNER LAYER

Direction of the principal out-of-plane shear  $\varphi_\sigma \approx \begin{cases} \text{atan}\left(\frac{v_{Edy}}{v_{Edx}}\right) & \text{if } v_{Edx} \neq 0 \\ 90\text{deg} & \text{otherwise} \end{cases} = -67.3\text{deg}$

Magnitude of the Out-of-Plane Shear in the Principal Out-of-plane Direction

$$v_{Edo} \approx \sqrt{v_{Edx}^2 + v_{Edy}^2} = 870 \cdot \frac{\text{kN}}{\text{m}}$$

### Out-of-plane shear capacity only provided by the Concrete

Initial Factors

Concrete Safety Factor	$C_{Rdc} \approx 0.18$
	$\gamma_c = 1$
	$k_f \approx 0.0$
Effective depth	$d_1 \approx t_s + t_c + 0.5 \cdot t_i = 1125\text{mm}$
	$d_2 \approx t_i + t_c + 0.5 \cdot t_s = 1125\text{mm}$
	$d_v \approx \min(d_1, d_2) = 1125\text{mm}$

**Assumed Reinforcement: Assume minimum reinforcement ratio**

Assume minimum reinforcement ratio  $\rho_{min} \approx 0.2\%$

Rebar Ration along the x Direction  $\rho_{xi} \approx 2 \cdot \rho_{min} = 0.4\%$

Rebar Ration along the y Direction  $\rho_{yi} \approx 2 \cdot \rho_{min} = 0.4\%$

$$A_{sx\_min} \approx \rho_{min} \cdot t_w = 24 \cdot \frac{cm^2}{m}$$

$$A_{sy\_min} \approx \rho_{min} \cdot t_w = 24 \cdot \frac{cm^2}{m}$$

Effective reinforcement Ratio  $\rho_{li} \approx \rho_{xi} \cdot (\cos(\varphi_o))^2 + \rho_{yi} \cdot (\sin(\varphi_o))^2 = 0.4\%$

$$k_v \approx \begin{cases} \left(1 + \sqrt{\frac{200mm}{d_v}}\right) & \text{if } 1 + \sqrt{\frac{200mm}{d_v}} \leq 2 \\ 2.0 & \text{otherwise} \end{cases} = 1.42$$

Minimum Concrete Shear Capacity  $V_{min} \approx 0.035 MPa \cdot k_v \cdot \sqrt{\frac{f_{ck}}{MPa}} \cdot d_z = 394 \cdot \frac{kN}{m}$

**Magnitude of the Axial Load in the Principal Out-of-plane Direction**

$$N_{Ed} \approx \frac{\eta_{Edx} + \eta_{Edy}}{2} + \frac{\eta_{Edx} - \eta_{Edy}}{2} \cdot \cos(2 \cdot \varphi_o) = -4171 \cdot \frac{kN}{m}$$

**Concrete Shear Capacity, accounting for axial force if in Compression**

$$\sigma_{cp\_max} \approx 0.2 \cdot f_{cd} = 8 \cdot MPa$$

$$\sigma_{cp} \approx \begin{cases} \frac{|N_{Ed}|}{t_c} & \text{if } \frac{|N_{Ed}|}{t_c} \leq \sigma_{cp\_max} \\ \sigma_{cp\_max} & \text{otherwise} \end{cases} = 4.63 \cdot MPa$$

$$V_{Rdc} \approx \begin{cases} \left[ \left( \frac{C_{Rdc}}{\gamma_c} \cdot k_v \cdot \sqrt{100 \cdot \rho_{li} \cdot \frac{f_{ck}}{MPa}} \cdot MPa + k_l \sigma_{cp} \right) \cdot d_z \right] & \text{if } N_{Ed} \leq 0 \\ \left( \frac{C_{Rdc}}{\gamma_c} \cdot k_v \cdot \sqrt{100 \cdot \rho_{li} \cdot \frac{f_{ck}}{MPa}} \cdot MPa - k_l \sigma_{cp} \right) \cdot d_z & \text{otherwise} \end{cases} = 1407 \cdot \frac{kN}{m}$$

### Out-of-plane shear capacity only when TRSH is placed

Yielding stress of the TRSH  $f_{ywd} := f_y = 500 \cdot \text{MPa}$

1.0 for non-prestressed structures  $\beta_{cw} := 1.0$

Recall concrete compressive strength  $f_{ck} := 40 \text{MPa}$

$$v_f := 0.6 \cdot \left( 1 - \frac{f_{ck}}{250 \text{MPa}} \right) = 0.499$$

$$\theta_i := 0.5 \cdot \text{asin} \left( 2 \cdot \frac{\sqrt{E_d o}}{\alpha_{cw} \cdot l_w \cdot v_f \cdot f_{cd}} \right) = 2 \cdot \text{deg}$$

$$\theta := \begin{cases} 45 \text{deg} & \text{if } \theta_i > 45 \text{deg} \\ 21.8 \text{deg} & \text{if } \theta_i < 21.8 \text{deg} \\ \theta_i & \text{otherwise} \end{cases} = \cdot \text{deg}$$

$$V_{Rd\_max} := \frac{\alpha_{cw} \cdot l_w \cdot v_f \cdot f_{cd}}{\cot(\theta) + \tan(\theta)} = 8341.6 \cdot \frac{\text{kN}}{\text{m}}$$

Diameter of one TSHR bar  $d_{tsh} := \frac{6}{8} \text{in}$

Unit Steel Area provided by the Rebar  $A_{sw} := \pi \cdot \frac{d_{tsh}^2}{4} = 285 \cdot \text{mm}^2$

Maximum Required Spacing  $s_t := \sqrt{\frac{d_z \cdot \cot(\theta) \cdot A_{sw} \cdot f_{ywd}}{\sqrt{E_d o}}} = 327.8 \cdot \text{mm}$

Adjusted Spacing for THRS  $S_{TH} := \text{Floor}(s_t, 25 \text{mm}) = 325 \cdot \text{mm}$

$$V_{Rds} := \frac{A_{sw} \cdot f_{ywd} \cdot \cot(\theta)}{S_{TH}} = 877.2 \cdot \frac{\text{kN}}{\text{m}}$$

Shear Capacity with THRS  $V_{Rdc\_THRS} := \min(V_{Rd\_max}, V_{Rds}) = 877.2 \cdot \frac{\text{kN}}{\text{m}}$

Required Transverse Reinforcement Ratio

$$\rho_z := \begin{cases} \frac{(\sqrt{E_d o} - 0.0V_{Rdc}) \cdot \tan(\theta)}{d_z \cdot f_{yd}} & \text{if } \sqrt{E_d o} > V_{Rdc} \\ 0 & \text{otherwise} \end{cases} = 0 \frac{\text{cm}^2}{\text{m}^2}$$

## Membranes Forces & Stresses due to the Presence of Transverse Shear Reinforcement [THSR]

Axial Force acting on x-dir  $\eta_{Edxs} \approx \eta_{Edx} \cdot \frac{(d_z - z_s)}{d_z} + \frac{m_{Edx}}{d_z} + \frac{1}{2} \cdot \eta_{Edxc} = -70 \cdot \frac{kN}{m}$

Axial Force acting on y-dir  $\eta_{Edys} \approx \eta_{Edy} \cdot \frac{(d_z - z_s)}{d_z} - \frac{m_{Edy}}{d_z} + \frac{1}{2} \cdot \eta_{Edyc} = -3906 \cdot \frac{kN}{m}$

Shear Force  $\eta_{Edxys} \approx \eta_{Edxy} \cdot \frac{(d_z - z_s)}{d_z} - \frac{m_{Edxy}}{d_z} + \frac{1}{2} \cdot \eta_{Edxyc} = 1533.5 \cdot \frac{kN}{m}$

### Computing the principal stresses and directions in the top outer layer

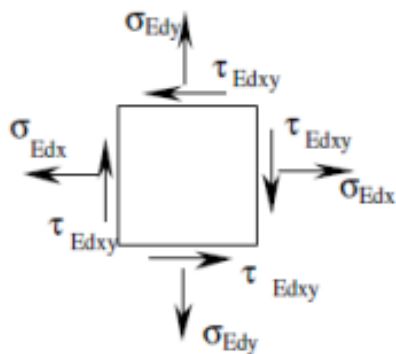
Total membrane forces acting in the top Layer

Axial Force acting on x-dir  $\eta_{Edxs} \approx \eta_{Edx} \cdot \frac{(d_z - z_s)}{d_z} + \frac{m_{Edx}}{d_z} + \frac{1}{2} \cdot \eta_{Edxc} = -70 \cdot \frac{kN}{m}$

Axial Force acting on y-dir  $\eta_{Edys} \approx \eta_{Edy} \cdot \frac{(d_z - z_s)}{d_z} - \frac{m_{Edy}}{d_z} + \frac{1}{2} \cdot \eta_{Edyc} = -3906 \cdot \frac{kN}{m}$

Shear Force  $\eta_{Edxys} \approx \eta_{Edxy} \cdot \frac{(d_z - z_s)}{d_z} - \frac{m_{Edxy}}{d_z} + \frac{1}{2} \cdot \eta_{Edxyc} = 1533.5 \cdot \frac{kN}{m}$

Stresses in the Top Layer



$$\sigma_{y\_sup} \approx \frac{\eta_{Edys}}{t_s} = -26 \cdot MPa$$

$$\tau_{xy\_sup} \approx \frac{\eta_{Edxys}}{t_s} = 10.2 \cdot MPa$$

$$\sigma_{x\_sup} \approx \frac{\eta_{Edxs}}{t_s} = -0.5 \cdot MPa$$

$$c_{c\_sup} \approx \frac{\sigma_{x\_sup} + \sigma_{y\_sup}}{2} = -13.3 \cdot MPa$$

### Principal Stresses

$$\text{Max Shear Stress (radius)} \quad r_{sup} := \sqrt{\left(\frac{\sigma_{x\_sup} - \sigma_{y\_sup}}{2}\right)^2 + \tau_{xy\_sup}^2} = 13.5 \cdot \text{MPa}$$

$$\text{Max principal stress 1} \quad \sigma_{1t} := c_{c\_sup} + r_{sup} = 3.1 \cdot \text{MPa}$$

$$\text{Max principal stress 2} \quad \sigma_{2t} := c_{c\_sup} - r_{sup} = -23.8 \cdot \text{MPa}$$

$$\alpha_{mt} := \begin{cases} \text{atan}\left(\frac{|\tau_{xy\_sup}|}{|\sigma_{x\_sup} - c_{c\_sup}|}\right) & \text{if } \sigma_{x\_sup} \neq c_{c\_sup} \\ 90\text{deg} & \text{otherwise} \end{cases} = 37.2 \cdot \text{deg}$$

$$\theta_{pcct} := \begin{cases} -(90\text{deg} - 0.5 \cdot \alpha_{mt}) & \text{if } \sigma_{x\_sup} > c_{c\_sup} \wedge \tau_{xy\_sup} > 0 \\ -0.5 \cdot \alpha_{mt} & \text{if } \sigma_{x\_sup} < c_{c\_sup} \wedge \tau_{xy\_sup} > 0 \\ 90\text{deg} - 0.5 \cdot \alpha_{mt} & \text{if } \sigma_{x\_sup} > c_{c\_sup} \wedge \tau_{xy\_sup} < 0 \\ 0.5 \cdot \alpha_{mt} & \text{if } \sigma_{x\_sup} < c_{c\_sup} \wedge \tau_{xy\_sup} < 0 \\ -\text{atan}\left(\frac{\tau_{xy\_sup}}{|\tau_{xy\_sup}|}\right) & \text{if } \sigma_{x\_sup} = c_{c\_sup} \end{cases} = -71.4 \cdot \text{deg}$$

### Applying the cracking criteria for the top outer layer

Angle from the principal Compressive Stress to the X- axis

$$\sigma_{mt} := \frac{(\sigma_{1t} + \sigma_{2t} + \sigma_{3t})}{3} = -6.9 \cdot \text{MPa}$$

$$I_{1t} := \sigma_{1t} + \sigma_{2t} + \sigma_{3t} = -20.7 \cdot \text{MPa}$$

$$J_{2sup} := \frac{1}{6} \cdot [(\sigma_{1t} - \sigma_{2t})^2 + (\sigma_{2t} - \sigma_{3t})^2 + (\sigma_{3t} - \sigma_{1t})^2] = 217.7 \cdot \text{MPa}^2$$

$$J_{3sup} := (\sigma_{1t} - \sigma_{mt}) \cdot (\sigma_{2t} - \sigma_{mt}) \cdot (\sigma_{3t} - \sigma_{mt}) = -1.17 \times 10^3 \cdot \text{MPa}^3$$

$$k_{sup} := \frac{f_{cm}}{f_{cm}} = 0.073$$

$$\alpha_{sup} := \frac{1}{9 \cdot k_{sup}^{1.4}} = 4.371$$

$$c_{1sup} := \frac{1}{0.7 \cdot k_{sup}^{0.9}} = 15.14$$

$$c_{2sup} := 1 - 6.8 \cdot (k_{sup} - 0.07)^2 = 1$$

$$\beta_{sup} := \frac{1}{3.7 \cdot k_{sup}^{1.1}} = 4.84$$

$$\cos 3\theta := \frac{3 \cdot \sqrt{3}}{2} \cdot \frac{J_{3sup}}{J_{2sup}^{1.5}} = -0.949$$

$$\lambda_{sup} := \begin{cases} c_{1sup} \cdot \cos\left(\frac{1}{3} \arccos(c_{2sup} \cdot \cos 3\theta)\right) & \text{if } \cos 3\theta \geq 0 \\ c_{1sup} \cdot \cos\left(\frac{\pi}{3} - \frac{1}{3} \arccos(-c_{2sup} \cdot \cos 3\theta)\right) & \text{otherwise} \end{cases} = 8.9$$

Ottosen Criteria  $\phi_{sup} := \alpha_{sup} \cdot \frac{J_{2sup}}{f_{cm}} + \lambda_{sup} \cdot \frac{\sqrt{J_{2sup}}}{f_{cm}} + \beta_{sup} \cdot \frac{I_{1t}}{f_{cm}} - 1 = 0.01$

$$Crack\_Condition\_sup := \begin{cases} \text{"Uncracked"} & \text{if } \phi_{sup} \leq 0 \\ \text{"Cracked"} & \text{if } \phi_{sup} > 0 \end{cases} = \text{"Cracked"}$$

### Computing the required steel reinforcement area in the top outer layer

Tensile forces to be resisted by the reinforcement curtains

Recalling the Angle from the principal Compressive Stress to the x- axis  $\theta_{pcct} = -71.4 \cdot \text{deg}$

Tensile force to be resisted by the reinforcement curtain along the x-direction

$$F_{rsx} := \begin{cases} \eta_{Edxs} - \eta_{Edxys} \cdot \cot(\theta_{pcct}) & \text{if } \eta_{Edxs} - \eta_{Edxys} \cdot \cot(\theta_{pcct}) \geq 0 \\ 0 & \text{otherwise} \end{cases} = 471.2 \cdot \frac{kN}{m}$$

Tensile force to be resisted by the reinforcement curtain along the y-direction

$$F_{rsy} := \begin{cases} \eta_{Edys} - \eta_{Edxys} \cdot \tan(\theta_{pcct}) & \text{if } \eta_{Edys} - \eta_{Edxys} \cdot \tan(\theta_{pcct}) \geq 0 \\ 0 & \text{otherwise} \end{cases} = 471 \cdot \frac{kN}{m}$$

### Computing the required steel reinforcement area in the top outer layer

Recalling the Angle from the principal Compressive Stress to the X- axis  $\theta_{pccb} = -14.4\text{-deg}$

Tensile force to be resisted by the reinforcement curtain along the x-direction

$$F_{rbx} := \begin{cases} \eta E d x_i - \eta E d x y_i \cdot \cot(\theta_{pccb}) & \text{if } \eta E d x_i - \eta E d x y_i \cdot \cot(\theta_{pccb}) \geq 0 \\ 0 & \text{otherwise} \end{cases} = 696 \cdot \frac{kN}{m}$$

Tensile force to be resisted by the reinforcement curtain along the y-direction

$$F_{rby} := \begin{cases} \eta E d y_i - \eta E d x y_i \cdot \tan(\theta_{pccb}) & \text{if } \eta E d y_i - \eta E d x y_i \cdot \tan(\theta_{pccb}) \geq 0 \\ 0 & \text{otherwise} \end{cases} = 696 \cdot \frac{kN}{m}$$

### Summarizing the required reinforcement areas

$$A_{reqEC2} := \begin{bmatrix} \max \left[ \frac{F_{rsx}}{f_{yd}}, A_{s\_minEC2} \right] \\ \max \left[ \frac{F_{rsy}}{f_{yd}}, A_{s\_minEC2} \right] \\ \max \left[ \frac{F_{rbx}}{f_{yd}}, A_{s\_minEC2} \right] \\ \max \left[ \frac{F_{rby}}{f_{yd}}, A_{s\_minEC2} \right] \end{bmatrix} = \begin{pmatrix} 24 \\ 24 \\ 24 \\ 24 \end{pmatrix} \cdot \frac{cm^2}{m}$$

	<i>Top</i>		<i>Bottom</i>	
<i>Layers</i>	<i>x</i>	<i>y</i>	<i>x</i>	<i>y</i>
$A_{reqEC2}^T$	24	24	24	24

$$= \begin{pmatrix} 24 & 24 & 24 & 24 \end{pmatrix} \frac{cm^2}{m}$$

## Verification of the compressive stress capacity of the concrete in the top Layer

### Compressive Stress Demand in the Concrete

$$\sigma_{cdu\_sup} := \tau_{xy\_sup} \cdot \left( \cot(\theta_{pcct}) + \frac{1}{\cot(\theta_{pcct})} \right) = -27 \cdot \text{MPa}$$

$$\sigma_{cdu\_045t} := |\tau_{xy\_sup}| \cdot \left( \cot(\theta_{45t}) + \frac{1}{\cot(\theta_{45t})} \right) = -16.3 \cdot \text{MPa}$$

### Compressive Stress Capacity on the Concrete

$$\sigma_s := \max\left(\frac{F_{rsx}}{t_s}, \frac{F_{rsy}}{t_s}\right) = 3.1 \cdot \text{MPa}$$

$$v := 0.6 \cdot \left(1 - \frac{f_{ck}}{250 \text{MPa}}\right) = 0.5$$

$$\alpha_{top} := \begin{cases} \frac{\max(\sigma_{1t}, \sigma_{2t})}{\max(\sigma_{1t}, \sigma_{2t})} & \text{if } \sigma_{1t} < 0 \wedge \sigma_{2t} < 0 \wedge \frac{\max(\sigma_{1t}, \sigma_{2t})}{\max(\sigma_{1t}, \sigma_{2t})} \leq 1 \\ 0 & \text{otherwise} \end{cases} = 0$$

$$\sigma_{cd\_maxTop} := \begin{cases} 0.85 \cdot f_{cd} \cdot \left[ \frac{1 + 3.8 \alpha_{top}}{(1 + \alpha_{top})^2} \right] & \text{if } (\sigma_{1t} < 0 \wedge \sigma_{2t} < 0) \\ f_{cd} \cdot \left[ 0.85 - \frac{\sigma_s}{f_{yd}} \cdot (0.85 - v) \right] & \text{if } (\sigma_{1t} > 0 \vee \sigma_{2t} > 0) \wedge \left( \frac{F_{rsx}}{t_s} < f_{yd} \vee \frac{F_{rsy}}{t_s} < f_{yd} \right) \end{cases}$$

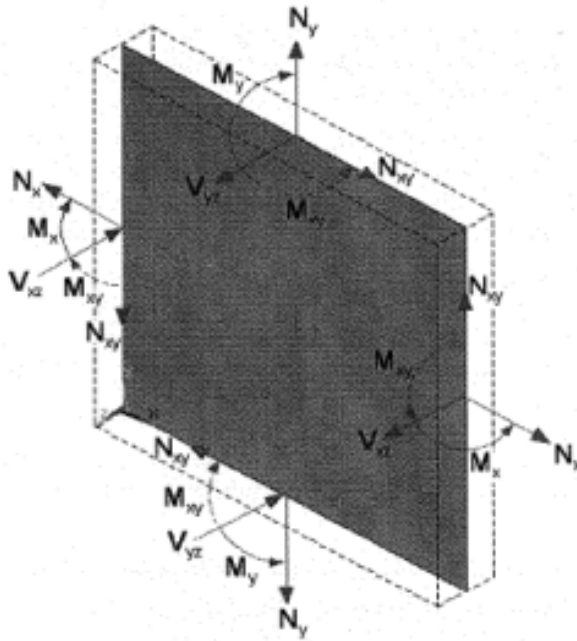
Compressive Capacity  $\sigma_{cd\_maxTop} = 35.6 \cdot \text{MPa}$

Compressive Demand  $|\sigma_{cdu\_sup}| = 27 \cdot \text{MPa}$

CDP Ratio  $\frac{\sigma_{cd\_maxTop}}{|\sigma_{cdu\_sup}|} = 1.32$

$$\text{Check\_Concrete\_Stress} := \begin{cases} \text{"Ok\_scu < fc"} & \text{if } |\sigma_{cdu\_sup}| \leq \sigma_{cd\_maxTop} \\ \text{"NG-Modify Layers"} & \text{otherwise} \end{cases} = \text{"Ok\_scu < fc"}$$

## A.2 ACI-Panel-Based-Design-Approach (PACI) EXAMPLE



Total Flexural Moment creating Stresses on X

Total Flexural Moment creating Stresses on Y

Recalling the Effective Depth

Recalling the Cover

### Reduction Factors According to the ACI

Tensile Reduction Factor	$\phi_t \approx 1.0$
Density Concrete Factor	$\lambda_w \approx 1.0$
Bending Reduction Factor	$\phi_b \approx 1.0$
Shear Reduction Factor	$\phi_v \approx 1.0$
Out-of-plane Shear Reduction Factor	$\phi_{vt} \approx 0.6$

$$N_x \approx \eta E d x = -3811 \cdot \frac{kN}{m}$$

$$N_y \approx \eta E d y = -4234 \cdot \frac{kN}{m}$$

$$N_{xy} \approx \eta E d x y = 2949 \cdot \frac{kN}{m}$$

$$V_{xz} \approx v E d x = -336 \cdot \frac{kN}{m}$$

$$V_{yz} \approx v E d y = 803 \cdot \frac{kN}{m}$$

$$M_x \approx m E d x = 1927 \cdot \frac{kN \cdot m}{m}$$

$$M_y \approx m E d y = 1878 \cdot \frac{kN \cdot m}{m}$$

$$M_{xy} \approx m E d x y = -62 \cdot \frac{kN \cdot m}{m}$$

$$M_{cx} \approx M_x + M_{xy} = 1865 \cdot \frac{kN \cdot m}{m}$$

$$M_{cy} \approx M_y + M_{xy} = 1816 \cdot \frac{kN \cdot m}{m}$$

$$d \approx 0.9 \cdot t_w = 1.08 \cdot m$$

$$d_{sw} \approx 0.8 \cdot t_w$$

$$cover = 75 \cdot mm$$

$$f_c \approx f_{cd} = 42 \cdot MPa$$

## Design / Verification of the out-of-Plane Shear Capacity

Maximum contribution of the concrete  $V_{ct\_lim} = 0.83 \cdot \lambda \cdot \sqrt{\frac{f_{cd}}{MPa}} \cdot MPa \cdot (0.6 \cdot t_w) = 3873 \cdot \frac{kN}{m}$

Recalling Out-of-Plane Shear acting over the Face x  $V_{xz} = -336 \cdot \frac{kN}{m}$

Contribution of the Concrete in Shear

$$V_{cxz} = \begin{cases} 0.17 \cdot \lambda \cdot \sqrt{\frac{f_{cd}}{MPa}} \cdot MPa \cdot (0.6 \cdot t_w) & \text{if } N_x \leq 0 \\ 0 & \text{if } N_x > 0 \end{cases} = 793 \cdot \frac{kN}{m}$$

$$\phi_{vf} \cdot V_{cxz} = 475.9 \cdot \frac{kN}{m}$$

$$A_{vxz} = \begin{cases} \frac{|V_{cxz}| - \phi_{vf} \frac{V_{cxz}}{2}}{\phi_{vf} f_y} & \text{if } |V_{xz}| \geq \phi_{vf} V_{cxz} \\ 0 & \text{otherwise} \end{cases} = 0 \cdot \frac{cm^2}{m}$$

$$THSR_{xz} = \begin{cases} \text{"No THSR Required"} & \text{if } A_{vxz} \leq 0 \\ \text{"Inc tw or THSR is Required"} & \text{otherwise} \end{cases} = \text{"No THSR Required"}$$

Recalling Out-of-Plane Shear acting over the Face y  $V_{yz} = 803 \cdot \frac{kN}{m}$

Contribution of the Concrete in Shear  $V_{cyz} = \begin{cases} 0.17 \cdot \lambda \cdot \sqrt{\frac{f_{cd}}{MPa}} \cdot MPa \cdot (0.6 \cdot t_w) & \text{if } N_y \leq 0 \\ 0 & \text{if } N_y > 0 \end{cases}$

$$\phi_{vf} \cdot V_{cyz} = 475.9 \cdot \frac{kN}{m}$$

$$A_{vyz} = \begin{cases} \frac{|V_{cyz}| - \phi_{vf} \frac{V_{cyz}}{2}}{\phi_{vf} f_y} & \text{if } |V_{yz}| \geq \phi_{vf} V_{cyz} \\ 0 & \text{otherwise} \end{cases} = 18.51 \cdot \frac{cm^2}{m}$$

$$THSR_{yz} = \begin{cases} \text{"No THSR Required"} & \text{if } A_{vyz} \leq 0 \\ \text{"Inc tw or THSR is Required"} & \text{otherwise} \end{cases} = \text{"Inc tw or THSR is Required"}$$

Estimation of the reinforcement Areas ( $A_s$ ) required by flexion in the faces subjected to tension

$$\text{Quadratic Equation for No axial Load} \quad a(a_x) = a_x^2 - 2 \cdot d \cdot a_x + \frac{2 \cdot |M_{cx}|}{\phi_b \cdot 0.85 \cdot f_{cd}}$$

$$a_x := \min(a_x) = 49.5 \cdot \text{mm}$$

$$\text{Quadratic Equation for axial Load} \quad n(a_{xN}) = a_{xN}^2 - 2 \cdot d \cdot a_{xN} + \frac{|N_x| \cdot (2 \cdot d - t_w) + 2 \cdot |M_{cx}|}{\phi_b \cdot 0.85 \cdot f_{cd}}$$

$$a_{xN} := \min(a_{xN}) = 100 \cdot \text{mm}$$

Required Reinforcement Area due to the  $M_x$ .

$$A_{sfx} := \begin{cases} \frac{(0.85 \cdot f_{cd} \cdot a_x)}{\phi_b \cdot f_y} & \text{if } N_x \geq 0 \\ \frac{0.85 \cdot f_{cd} \cdot a_{xN} - |N_x|}{\phi_b \cdot f_y} & \text{if } 0.85 \cdot f_{cd} \cdot a_{xN} - |N_x| \geq 0 \\ 0 & \text{otherwise} \end{cases} = 0 \cdot \frac{\text{cm}^2}{\text{m}}$$

Required Reinforcement Area due to the  $M_y$ .

$$\text{Quadratic Equation for No axial Load} \quad h(a_y) = a_y^2 - 2 \cdot d \cdot a_y + \frac{2 \cdot |M_{cy}|}{\phi_b \cdot 0.85 \cdot f_{cd}}$$

$$a_y := \min(a_y) = 48.2 \cdot \text{mm}$$

$$\text{Quadratic Equation for axial Load} \quad f(a_{yN}) = a_{yN}^2 - 2 \cdot d \cdot a_{yN} + \frac{|N_y| \cdot (2 \cdot d - t_w) + 2 \cdot |M_{cy}|}{\phi_b \cdot 0.85 \cdot f_{cd}}$$

$$a_{yN} := \min(a_{yN}) = 105 \cdot \text{mm}$$

Required Reinforcement Area due to the  $M_y$ .

$$A_{sfy} := \begin{cases} \frac{(0.85 \cdot f_{cd} \cdot a_y)}{\phi_b \cdot f_y} & \text{if } N_y \geq 0 \\ \frac{0.85 \cdot f_{cd} \cdot a_{yN} - |N_y|}{\phi_b \cdot f_y} & \text{if } 0.85 \cdot f_{cd} \cdot a_{yN} - |N_y| \geq 0 \\ 0 & \text{otherwise} \end{cases} = 0 \cdot \frac{\text{cm}^2}{\text{m}}$$

## Estimation of reinforcement areas per layer (or face)

### Bottom Layer along the x-direction (Asxb)

$$\text{Reinforcement area required by } A_{sTxb} \text{ tension} \approx \begin{cases} \frac{1}{2} \cdot \frac{N_x}{\phi_t \cdot f_y} & \text{if } N_x > 0 \\ 0.0 & \text{otherwise} \end{cases} = 0 \cdot \frac{cm^2}{m}$$

$$\text{Reinforcement area required for bending } A_{sFxb} \approx \begin{cases} A_{sfx} & \text{if } M_{cx} < 0 \\ 0 & \text{if } M_{cx} \geq 0 \\ 0 & \text{if } M_x = 0 \wedge M_y = 0 \wedge M_{xy} \neq 0 \end{cases} = 0 \cdot \frac{cm^2}{m}$$

Reinforcement area required by shear

$$\text{Shear force to be resisted by the in-plane reinforcement } V_{ubxy} \approx \frac{N_{xy}}{2} + \frac{M_{xy}}{(0.8 \cdot t_w)} = 1410 \cdot \frac{kN}{m}$$

$$\text{Ultimate design shear affected the strength reduction factor } V_{sxb} \approx \frac{|V_{ubxy}|}{\phi_v} = 1410 \cdot \frac{kN}{m}$$

$$\text{Area of reinforcement required by shear } A_{sVxb} \approx \frac{1}{f_y} \cdot V_{sxb} = 28.198 \cdot \frac{cm^2}{m}$$

Total Required Area

$$A_{sBx\_req} \approx \begin{cases} (A_{sTxb} + A_{sFxb} + A_{sVxb}) & \text{if } V_{xz} < V_{cxz} \\ \left( A_{sTxb} + A_{sFxb} + A_{sVxb} + \frac{1.25 V_{xz}^2}{\phi_{Edo} \cdot f_y} \right) & \text{otherwise} \end{cases} = 28.2 \cdot \frac{cm^2}{m}$$

### Top layer along the x-direction (Asxt)

$$\text{Reinforcement area required by tension } A_{sTxt} \approx \begin{cases} \frac{1}{2} \cdot \frac{N_x}{\phi_t \cdot f_y} & \text{if } N_x > 0 \\ 0 & \text{otherwise} \end{cases} = 0 \cdot \frac{cm^2}{m}$$

$$\text{Reinforcement area required for bending } A_{sFxt} \approx \begin{cases} A_{sfx} & \text{if } M_{cx} > 0 \\ 0 & \text{if } M_{cx} \leq 0 \\ 0 & \text{if } M_x = 0 \wedge M_y = 0 \wedge M_{xy} \neq 0 \end{cases} = 0 \cdot \frac{cm^2}{m}$$

Reinforcement required by shear

Shear force to be resisted by the in-plane reinforcement

$$V_{utxy} = \frac{N_{xy}}{2} - \frac{M_{xy}}{(0.8 \cdot t_w)} = 1539 \cdot \frac{kN}{m}$$

Ultimate design shear affected the strength reduction factor

$$V_{sxt} = \frac{|V_{utxy}|}{\phi_v} = 1539 \cdot \frac{kN}{m}$$

Area of reinforcement required by Shear

$$A_{sVxt} = \frac{V_{sxt}}{f_y} = 30.782 \cdot \frac{cm^2}{m}$$

Total required reinforcement area

$$A_{sTx\_req} = \begin{cases} (A_{sFxt} + A_{sVxt} + A_{sTxt}) & \text{if } V_{xz} < V_{cxz} \\ \left( A_{sFxt} + A_{sVxt} + A_{sTxt} + \frac{1.25 V_{xz}^2}{\sqrt{E_{do}} \cdot f_y} \right) & \text{otherwise} \end{cases} = 30.8 \cdot \frac{cm^2}{m}$$

Bottom layer along the y-direction ( $A_{syb}$ )

Reinforcement area required by tension  $A_{sTyb} = \begin{cases} \frac{1}{2} \cdot \frac{N_y}{\phi_t \cdot f_y} & \text{if } N_y > 0 \\ 0.0 & \text{otherwise} \end{cases} = 0 \cdot \frac{cm^2}{m}$

Reinforcement area required for bending  $A_{sFyb} = \begin{cases} A_{sfy} & \text{if } M_{\sigma y} > 0 \\ 0 & \text{if } M_{\sigma y} \leq 0 \\ 0 & \text{if } M_x = 0 \wedge M_y = 0 \wedge M_{xy} \neq 0 \end{cases} = 0 \cdot \frac{cm^2}{m}$

Shear force to be resisted by the in-plane reinforcement

$$V_{ubyx} = \frac{N_{xy}}{2} + \frac{M_{xy}}{(0.8 \cdot t_w)} = 1410 \cdot \frac{kN}{m}$$

Ultimate design shear affected the strength reduction factor

$$V_{syb} = \frac{|V_{ubyx}|}{\phi_v} = 1410 \cdot \frac{kN}{m}$$

Area of Reinforcement required by Shear

$$A_{sVyb} = \frac{V_{syb}}{f_y} = 28.198 \cdot \frac{cm^2}{m}$$

Total required reinforcement area

$$A_{sBy\_req} \cong \begin{cases} (A_s T_{yb} + A_s F_{yb} + A_s V_{yb}) & \text{if } V_{xz} < V_{cxz} \\ \left( A_s T_{yb} + A_s F_{yb} + A_s V_{yb} + \frac{1.25 V_{yz}^2}{\nu_{Edo} f_y} \right) & \text{otherwise} \end{cases} = 28.2 \cdot \frac{cm^2}{m}$$

Top layer along the y-direction (Asyt)

Reinforcement area required by tension  $A_{sTyt} \cong \begin{cases} \frac{1}{2} \cdot \frac{N_y}{\phi_t f_y} & \text{if } N_y > 0 \\ 0.0 & \text{otherwise} \end{cases} = 0 \cdot \frac{cm^2}{m}$

Reinforcement area required for bending  $A_{sFyt} \cong \begin{cases} A_s f_y & \text{if } M_{\sigma y} < 0 \\ 0 & \text{if } M_{\sigma y} \geq 0 \\ 0 & \text{if } M_x = 0 \wedge M_y = 0 \wedge M_{xy} \neq 0 \end{cases} = 0 \cdot \frac{cm^2}{m}$

Reinforcement area required by shear

Shear force to be resisted by the in-plane reinforcement  $V_{utyx} \cong \frac{N_{xy}}{2} - \frac{M_{xy}}{(0.8 \cdot t_w)} = 1539 \cdot \frac{kN}{m}$

Ultimate design shear affected the strength reduction factor  $V_{syt} \cong \frac{|V_{utyx}|}{\phi_v} = 1539 \cdot \frac{kN}{m}$

Area of Reinforcement required by Shear  $A_{sVyt} \cong \frac{V_{syt}}{f_y} = 30.782 \cdot \frac{cm^2}{m}$

Total required reinforcement area

$$A_{sTy\_req} \cong \begin{cases} (A_s T_{yt} + A_s F_{yt} + A_s V_{yt}) & \text{if } V_{yz} < V_{cyz} \\ \left( A_s T_{yt} + A_s F_{yt} + A_s V_{yt} + \frac{V_{yz}^2}{\nu_{Edo} f_y} \right) & \text{otherwise} \end{cases} = 45.6 \cdot \frac{cm^2}{m}$$

### Corroborating Flexure and Axial Interaction

Max Concrete Deformation

$$\varepsilon_u \approx 0.003$$

$$\varepsilon_y \approx \frac{f_y}{E_s} = 0.0025$$

Effective Depth

$$d_v = 1125 \cdot \text{mm}$$

Neutral Axis for Balanced Condition

$$c_{bal} \approx \frac{\varepsilon_u}{\varepsilon_u + \varepsilon_y} \cdot d_v = 614 \cdot \text{mm}$$

Balanced Force in Y Direction

$$a_{ybal} \approx 0.85 \cdot c_{bal} = 522 \cdot \text{mm}$$

$$\frac{c_{bal}}{d_v} = 0.545$$

$$C_{cy} \approx 0.85 \cdot f_{cd} \cdot a_{ybal} = 18621 \cdot \frac{\text{kN}}{\text{m}}$$

$$A_{sy} \approx \max(A_{sBy\_req}, A_{sTy\_req})$$

$$N_{bal\_y} \approx C_{cy} - A_{sy} \cdot f_y = 16341 \cdot \frac{\text{kN}}{\text{m}}$$

$$Check\_NbalY\_Limit \approx \begin{cases} \text{"Ok\_Ny < Nbal"} & \text{if } |N_y| \leq N_{bal\_y} \\ \text{"NG\_Compression\_Control"} & \text{otherwise} \end{cases} = \text{"Ok\_Ny < Nbal"}$$

Balanced Force in X Direction

$$a_{xbal} \approx 0.85 \cdot c_{bal} = 522 \cdot \text{mm}$$

$$\frac{a_{xbal}}{t_w} = 0.435$$

$$C_{cx} \approx 0.85 \cdot f_{cd} \cdot a_{ybal} = 18621 \cdot \frac{\text{kN}}{\text{m}}$$

$$A_{sx} \approx \max(A_{sBx\_req}, A_{sTx\_req})$$

$$N_{bal\_x} \approx C_{cx} - A_{sx} \cdot f_y = 17082 \cdot \frac{\text{kN}}{\text{m}}$$

$$Check\_NbalX\_Limit \approx \begin{cases} \text{"Ok\_Nx < Nbal"} & \text{if } |N_x| \leq N_{bal\_x} \\ \text{"NG\_Compression\_Control"} & \text{otherwise} \end{cases} = \text{"Ok\_Nx < Nbal"}$$

**COMPARISSON OF THE REQUIRED AREAS USING THE ACI AND THE EC2**

$$A_{req\_ACI} \approx (A_{sTx\_req} \quad A_{sTy\_req} \quad A_{sBx\_req} \quad A_{sBy\_req})$$

$$\begin{matrix} & \text{Top} & & \text{Bottom} \\ & x & y & x & y \end{matrix}$$

$$A_{req\_ACI} = (30.8 \quad 45.6 \quad 28.2 \quad 28.2) \cdot \frac{cm^2}{m}$$

$$A_{sTot\_ACI} \approx \sum A_{req\_ACI} = 133 \cdot \frac{cm^2}{m}$$

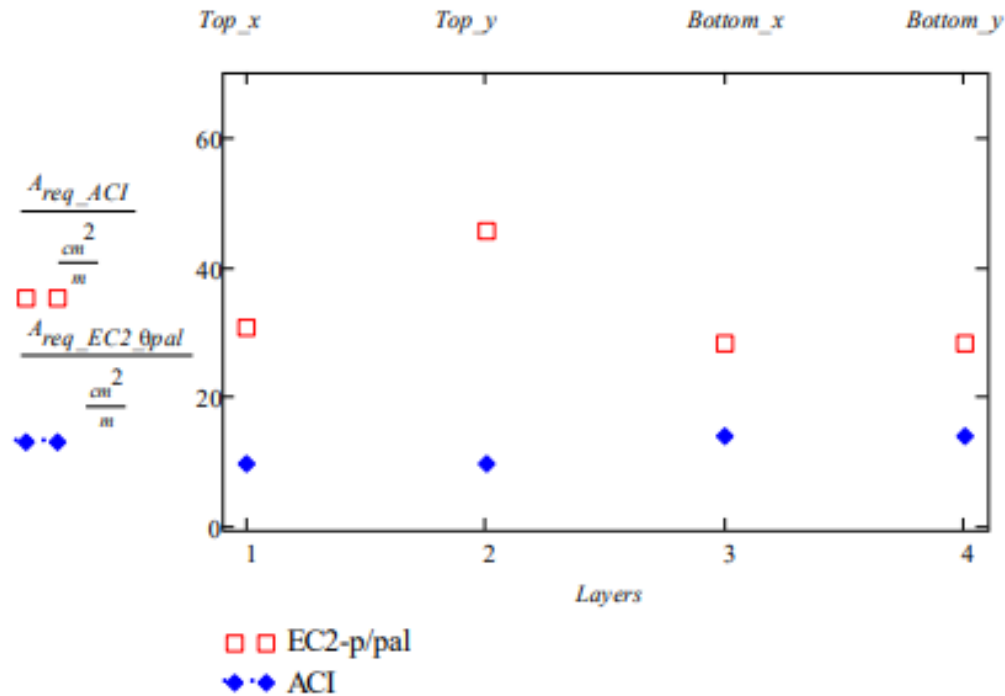
$$A_{req\_EC2\_0pal} = (9.42 \quad 9.42 \quad 13.92 \quad 13.92) \cdot \frac{cm^2}{m}$$

$$A_{sTot\_EC20pal} \approx \sum A_{req\_EC2\_0pal} = 47 \cdot \frac{cm^2}{m}$$

$$A_{req\_EC2\_045} = (25.7 \quad 0 \quad 0 \quad 30.4) \cdot \frac{cm^2}{m}$$

$$A_{sTot\_EC2045} \approx \sum A_{req\_EC2\_045} = 56 \cdot \frac{cm^2}{m}$$

Layers  $\approx$  (1 2 3 4)



$$\frac{A_{sTot\_ACI}}{A_{sTot\_EC20pal}} = 284. \%$$

## Drawing Details and summary Design

Assumed Bar Diameter  $d_{bar} := \frac{7}{8} in = 22.2 \cdot mm$

Area of the Assumed Bar  $A_{bar} := \frac{\pi \cdot d_{bar}^2}{4} = 3.88 \cdot cm^2$

### EC2 Summary Design

$$A_{reqEC2}^T = (24 \ 24 \ 24 \ 24) \cdot \frac{cm^2}{m}$$

Rebar Ratio Required from the EC2  $\rho_{EC2\_total} := \frac{A_{reqEC2}^T}{t_w} = (0.2 \ 0.2 \ 0.2 \ 0.2) \cdot \%$

$$\begin{matrix} & Top & & Bottom \\ & x & y & x & y \end{matrix}$$

**Minimum spacing for the assumed bar**  $S_{EC2} := \frac{A_{bar}}{A_{reqEC2}^T} = (161.6 \ 161.6 \ 161.6 \ 161.6) \cdot mm$

$$\rho_{z\_EC2} := \rho_z = 0.083 \cdot \%$$

Required reinforcement Area from the EC2

$$A_{reqACI}^T = (30.8 \ 45.6 \ 28.2 \ 28.2) \cdot \frac{cm^2}{m}$$

### PACI Summary Design

$$\rho_{ACI} := \frac{A_{reqACI}^T}{t_w} = (0.26 \ 0.38 \ 0.23 \ 0.23) \cdot \%$$

Required reinforcement area from the ACI

$$\begin{matrix} & Top & & Bottom \\ & x & y & x & y \end{matrix}$$

**Minimum Spacing for the assumed bar**  $S_{ACI} := \frac{A_{bar}}{A_{reqACI}^T} = (126 \ 85.1 \ 137.6 \ 137.6) \cdot mm$

Rebar ratio required from the ACI

$$\rho_{z\_ACI} := \frac{A_{vxz} + A_{vyz}}{l_m} = 0.185 \cdot \%$$

## PUBLICATIONS

**Conference Paper.** “Design of RC Wall Panels following the Eurocode Procedure (EC2) along with Linear Elastic FEM Analysis Results” ACI Convention, Spring 2018, Design of Concrete Structures: Relating FEM Analysis and RC Design Using Codes/Standards. UTAH-US, 2018.

**Conference Paper.** “Design Optimization of RC panels for Nuclear Structures: The Eurocode based (Sandwich Model) Approach”. International Conference on Technological Innovations in Nuclear Civil Engineering, 29th-31st August, 2018. Paris-Saclay, France